UNDERSTANDING THE INHIBITION OF THE ALZHEIMER'S Aβ PEPTIDE FIBRILLIZATION BY HUMAN SERUM ALBUMIN

UNDERSTANDING THE INHIBITION OF THE ALZHEIMER'S Aβ PEPTIDE FIBRILLIZATION BY HUMAN SERUM ALBUMIN

By

JULIJANA MILOJEVIC

BSc. Honours Chemistry, McMaster University

A Thesis

Submitted to the School of Graduate Studies

in Partial Fulfillment of the Requirements

for the Degree

Doctor of Philosophy

McMaster University

Doctor of Philosophy (2011) McMaster University

(Department of Chemistry and Chemical Biology) Hamilton, Ontario

TITLE: Understanding the Inhibition of the Alzheimer's Aβ Peptide Fibrillization by Human Serum Albumin

AUTHOR: Julijana Milojevic

SUPERVISOR: Dr. Giuseppe Melacini

NUMBER OF PAGES: 256, CCLVI

ABSTRACT

Aggregation of the Alzheimer's Aβ peptide in the brain and blood plasma is controlled by endogenous Aβ binding proteins. The structural basis for the interaction between the Aβ peptide and the Aβ binding proteins is critical not only to understand how Aβ amyloids are controlled in vivo, but also to guide the design of novel Aβ-self association inhibitors. However, the current knowledge of the structures of the Aβ/Aβ binding protein complexes is still sparse. This thesis focuses mainly on the interaction of the Aβ peptide with Human Serum Albumin (HSA). It is known that HSA binds ~90% of the Aβ in human plasma and prevents the Aβ self-association into amyloid fibrils. However, the mechanism of Aβ self-association inhibition by albumin was not understood prior to our work. We have shown that albumin preferentially binds toxic Aβ oligomers and fibrils inhibiting their growth into larger Aβ assemblies through a "monomer competitor" mechanism. Using a combination of NMR, domain deletion mutants, dynamic light scattering and ultrafiltration we have investigated the stoichiomery and affinity of the Aβ oligomer: HSA complexes. Our results indicate that all three domains of HSA bind Aβ oligomers and fibrils with an affinity in the 1-100 nM range. Such binding site degeneracy explains how albumin minimizes competition by other ligands such as fatty acids and drugs. Moreover we have used the soluble and NMR suitable domain 3 of albumin to dissect further the determinants of the Aβ oligomer binding to albumin at subdomain and peptide resolution. We show that both subdomains of the HSA domain 3 (*i.e.* 3A and 3B) bind the Aβ oligomers. In addition, we identified a

peptide sequence within subdomain 3B that displays significant potency in the inhibition of Aβ self-association.

THESIS SUMMARY

The conformational features associated with toxicity of different Aβ species (*i.e.* monomers, oligomers, fibrils) are not well understood. The currently available structures for the Aβ peptide either in isolation or in complex with inhibitory proteins are surveyed in *Chapter 1* for the purpose of defining common structural features for the inhibition of the Aβ self association.

This thesis focuses mainly on the interaction of the Aβ peptide with Human Serum Albumin (HSA). Several open questions about the albumin: Aβ interactions have been addressed in this thesis. *The first open question pertains to the Aβ species recognized by albumin: does HSA bind Aβ monomers or Aβ assemblies such as oligomers and fibrils?* Prior attempts to address this question relied on several methods such as ThT fluorescence, circular dichroism (CD) spectroscopy, electron microscopy (EM), cell based assays, Western blots and dynamic light scattering (DLS)(1, 2, 3, 4). However, these techniques are not as sensitive to the interactions involving Aβ monomers as solution NMR and therefore cannot reliably be used to differentiate interactions of albumin with different Aβ species. *Therefore our initial aim was to develop solution*

NMR methods required to differentiate the interactions of Aβ oligomers and monomers with inhibitory proteins. This methodological work is discussed in Chapter 2and was published in Milojevic et al. J.Phys.Chem.B 2007.

The NMR methods developed in Chapter 2 were then used to probe the differential interactions of HSA with Aβ monomers and Aβ assemblies, as reported in *Chapters 3 and 4, that were published in Milojevic et al. JACS 2007 and Milojevic et al. Biophys. J. 2009*. Chapter 3 focuses on the application of NMR methods to the Aβ deletion mutant Aβ (12-28), which provides a stable model system for the Aβ monomers/oligomer equilibrium, while Chapter 4 extends the results of Chapter 3 to longer and more physiologically relevant Aβ peptides (*i.e.* Aβ (1-40) and (1-42)), taking advantage of a combined experimental design based on NMR and fluorescence spectroscopies.

Together Chapters 3 and 4 provide solid evidence that albumin preferentially binds Aβ oligomers and fibrils rather than Aβ monomers. The next basic question was then what is the stoichiometry and what are the affinities for the HSA: Aβ assemblies complexes? This question was addressed in *Chapter 5, published in Milojevic et al. Biophys. J. 2011, in which we used a combination of NMR, domain deletion mutants, dynamic light scattering and ultrafiltration to show that all three domains of HSA bind Aβ oligomers and fibrils with an affinity in the 1-100 nM range.*

The results of Chapter 5 explain how albumin minimizes competition by other ligands such as FAs and drugs for *Aβ* binding through binding site degeneracy. In addition, the conclusions of Chapter 5 imply that each domain of albumin can be used as

a model system to further probe the HSA/*Aβ* interactions. In Chapter 6 we therefore focused on the soluble and NMR suitable domain 3 of albumin to dissect further the determinants of the *Aβ* oligomer binding to albumin at subdomain and peptide resolution.

In Chapter 6 we show that both subdomains of the HSA domain 3 (*i.e.* 3A and 3B) bind the *Aβ* oligomers. In addition, we identified a peptide sequence within subdomain 3B that displays significant potency in the inhibition of *Aβ* self-association. Finally, in Chapter 7 we summarize the main outcomes of the thesis and provide an overview of future questions, related hypotheses and experimental design for the continuation of the HSA/*Aβ* project.

ACKNOWLEDGMENTS

With great sense of gratitude I want to acknowledge and thank several individuals without whom this thesis would not be possible.

First, I want to thank my supervisor, Dr. Giuseppe Melacini. Dr. Melacini, thank you for all the encouragements, patience, understanding, respect and the excitement you showed towards my research, results and even the smallest achievements. You have been a great mentor and have inspired and helped me learn and develop in many ways. I will always be very grateful to you and have deepest respect toward you. I also would like to thank my committee members Dr. Ortega and Dr. Bain for their advices and encouragements.

Thanks to the previous and current, Melacini lab group members: Rahul, Hao, Veronica, Federica, Somenath, Soumita, Mona, Tyler, Bryan, Elle, Emy, William, Madoka, Rajeevan, Amir, Geeta. Especially, I want to thank Veronica and Rahul who helped me and influenced me at the beginning of my graduate carrier. Rajeevan and Amir, kids, I will miss our lunches and laughter's at Bridges – I almost became vegetarian☺. You have been great friends and great support to me in the last year. Thank you!

Finally, the biggest thanks are for my family, my niece, my sisters, my parents, my husband, my grandparents and Bojana for always encouraging me and looking out for me. Mom and dad you trusted me, supported and encouraged me in every possible way from the very beginning to the end -Thank you family!

TABLE OF CONTENTS

ABSTRACT iv

THESIS SUMMARY v

ACKNOWLEDGMENTS viii

LIST OF FIGURES xiii

LIST OF TABLES xvi

LIST OF ABBREVIATIONS xvii

CHAPTER 1 1

Introduction

1.1 Alzheimer's Disease 2

1.2 Processing of the Amyloid Precursor Protein (APP) 3

1.3 The Amyloid Cascade Hypothesis 5

1.4 Nucleation Dependent Polymerization 6

1.5. Structures and Size Distributions of Aβ Assemblies 7

1.5.1 Structures of the Aβ Monomers 7

1.5.2 Size Distributions and Structures of Aβ oligomers 9

1.5.3 Structures of the Aβ protofibirls 13

1.6 The Peripheral Sink Hypothesis 14

1.6.1. Proteins in Plasma and CSF Regulate the Equilibrium of Soluble Aβ Partitioning between the Brain and the Periphery 17

1.6.1.1 Interactions of Human Serum Albumin with Aβ 17

1.6.1.2 Interactions of the Apolipoproteins with Aβ 19

1.6.1.3 Interactions of the Low Density Lipoproteins with Aβ. 21

1.6.1.4 Interactions of the Serapins with Aβ. 21
1.6.1.5 Interactions of Human Macroglobulin with Aβ. 22
1.6.1.6 Interactions of Alcohol Dehydrogenase with Aβ. 23
1.6.1.7 Interactions of Affibody Protein $Z_{A\beta3}$ with Aβ. 24
1.6.2. Common Features of the Aβ Binding Proteins 25
1.7 Human Serum Albumin: Structure and Functions 29
1.7.1 Fatty Acid Binding Sites in HSA 30
1.7.2 Drug Binding Sites in HSA 33
1.8 Biomolecular NMR Spectroscopy 34
1.9 Thesis Overview 36
References 41

CHAPTER 2 51

Analysis and Parametric Optimization of ^{1}H Off-Resonance Relaxation NMR Experiments Designed to Map Polypeptide Self-Recognition and Other Non-Covalent Interactions

Abstract 53
Introduction 54
Materials and Methods 56
Theoretical Treatment 59
Results and Discussion 63
Conclusions 75
Acknowledgments 76
References 76

CHAPTER 3.....79

Understanding the Molecular Basis for the Inhibition of the Alzheimer's Aβ-Peptide Oligomerization by Human Serum Albumin Using Saturation Transfer Difference and Off-Resonance Relaxation NMR Spectroscopy

Abstract.....81
Introduction.....82
Materials and Methods.....84
Results and Discussion.....88
Conclusions.....104
Acknowledgements:.....104
References.....105
Supplementary Material.....109

CHAPTER 4.....116

Human Serum Albumin Inhibits Aβ Fibrillization through a 'Monomer-Competitor' Mechanism

Abstract.....118
Introduction.....119
Material and Methods.....125
Results.....127
Discussion.....141
Conclusions.....145
Acknowledgements:.....146
Suplementary information.....147
References.....156

CHAPTER 5 159

Stoichiometry and Affinity of the Human Serum Albumin – Alzheimer's Aβ Peptide Interactions

Abstract 161
Introduction 162
Results 166
Discussion 183
Acknowledgements 188
References 188
Supporting Information 191
Material and Methods 192
References for suplemetary material 205

CHAPTER 6 206

Investigating the Determinants of the Alzheimer's Aβ Peptide Biding to Human Serum Albumin:

NMR Study of the HSA Domain 3: Aβ Interactions

Abstract 207
Introduction 208
Materials and Methods 211
Results 217
Discussion 231
References: 234
Supporting Information: 238

CHAPTER 7 240

Concluding Remarks and Outlook on Future Developments

References 254

LIST OF FIGURES

CHAPTER 1

Figure 1. Processing pathways of the amyloid precursor protein (APP). 5
Figure 2. A general model for the Aβ self-association..... 7
Figure 3. Current structures of the Aβ 9
Figure 4. Comparison of the Aβ protofibril structural models.....13
Figure 5. Mechanisms of Aβ clearance across the blood brain barrier (BBB).....16
Figure 6. Structures of the proteins interacting with Aβ.. 27
Figure 7. Domain organization of HSA. 32
Figure 8: Comparison between STD experiments as applied to Protein /Ligand (a) and (b) Aβ Oligomer/Aβ Monomer systems.....35

CHAPTER 2

Figure 1. Pulse sequences for the measurement of non-selective off-resonance relaxation rates with one- (a) and two- (b) dimensional detection.....54
Figure 2. Static magnetic field (Bo) dependence of relaxation rates vs. the correlation time (τc) for a model two spin system. 64
Figure 3. Plots of relaxation rates *vs.* static magnetic field (B_o) for selected values of the correlation time τ_c. 66
Figure 4. Tilt angle (θ) dependence of the relaxation rates *vs*. the correlation time (τ_c) for a model two spin system at 700 MHz. 68
Figure 5. Inter-scan delay (T_c) dependence of the relaxation rates *vs*. the correlation time (τ_c) plots for a model two spin system. 71
Figure 6. Plot of the relative $R_{35.5^o,ns}$ relaxation rates *vs.* residue number in Aβ (12-28) 74

CHAPTER 3

Figure 1. Effect of HSA addition and of 30 kDa-cut off filtration on the ^{1}H 1D-WG spectra of 1 mM Aβ(12-28).....90
Figure 2. Effect of HSA addition and filtration on 2D saturation transfer difference and reference TOCSY spectra 91
Figure 3**.** Effect of HSA addition and filtration on the saturation transfer H_α-H_N ratios 93
Figure 4. Saturation transfer titration curves for representative residues 95
Figure 5. Effect of HSA on the non-selective off-resonance Hα relaxation rates.....99
Figure 6. Proposed schematic model for the interactions between HSA and the oligomers of the Aβ peptide.....100

Figure S1. Control spectra to monitor the stability over time of the unfiltered (left panels) and filtered (right panels) Aβ(12-28) NMR samples. 111
Figure S2. Effect of filtration and retentate re-suspension on the ^{1}H 1D-WG spectra of Aβ(12-28) 111
Figure S3. Effect of salt addition on the ^{1}H 1D-WG spectra of filtrated Aβ(12-28). 112
Figure S4. 2D-Saturation transfer difference evidence that HSA does not interact with the monomers....112
Figure S5. Quantitative comparison between the Hα-STD intensities measured for the filtered Aβ(12-28) sample in the presence and absence of HSA. 113
Figure S6. 1D-Saturation transfer difference evidence that HSA does not interact with the monomers. 114
Figure S7. 1D-Line-width evidence that HSA does not interact with the monomers....114
Figure S8. Representative decay plots for the non-selective off-resonance relaxation rates of the H_{α} protons in Aβ(12-28)....115

CHAPTER 4

Figure 1. Possible hypothetical models for the mechanism of oligomerization inhibition by a generic inhibitory protein P 123
Figure 2. Probing the interaction of the Aβ (12-28) and aspirin with HSA....129
Figure 3. Effect of HSA on the saturation transfer reference (STR) and saturation transfer difference (STD) spectra of Aβ (1-40) and Aβ (1-42) samples. 131
Figure 4. Probing Aβ assemblies using Thioflavin T (ThT) fluorescence and interactions with the HSA using the tryptophan fluorescence....134
Figure 5.Time-dependent aggregation of 90 μM Aβ(1-42) in the absence and presence of 5 μM HSA....137
Figure 6. Effect of a delayed addition of HSA on the aggregation profile of Aβ (1-42)....140

Figure S1. Effect of saturation frequency on the saturation transfer difference (STD) spectra of a 0.5 mM HSA sample 152
Figure S2**.** Effect of HSA on the saturation transfer reference (STR) and saturation transfer difference (STD) spectra of aspirin, L-tryptophan.. 153
Figure S3. Effect of pH on the maximum emission wavelength of the HSA tryptophan fluorescence as a monitor of the structural transitions of albumin....154
Figure S4. Albumin interacts with Thioflavin T....154
Figure S5. Effect of HSA on the 1D–NMR spectra of the Aβ (12-28) peptide 155
Figure S6. Effects of salt on the Aβ signal intensity and probe performance....155

CHAPTER 5

Figure 1. Domain organization of HSA and design of the HSA constructs....164
Figure 2. Effect of wt HSA and its deletion mutants on the 1D–NMR spectra of the Aβ (12-28) peptide. 167
Figure 3. Dose-response STD-based profiles for the inhibition of the Aβ (12-28) self-association by HSA and its deletion mutants....171
Figure 4. Correlations between the non-selective off-resonance relaxation data of full length HSA and those measured for the four HSA deletion mutants 173

Figure 5. Intensity *vs.* size distribution obtained from dynamic light scattering (DLS) measurements of 0.1 mM Aβ (1-42) in the presence and absence of 200 μM of HSA.. 182
Figure 6. Schematic model to summarize the prevailing stoichiometries and affinities for the complexes between HSA and the Aβ protofibrils.....184

Figure S1. CD spectra of all albumin constructs.....202
Figure S2. Effect of insulin and lysozyme on the aggregated 1 mM Aβ (12-28) sample.....202
Figure S3. Effect of HSA and of the HSA deletion mutants on the early aggregation of the Aβ (1-42) peptide.....203
Figure S4. 1D-WG NMR spectra comparisons to show that the HSA deletion mutants do not interact with the monomeric Aβ(1-42) peptide.....203
Figure S5. Effect of domain 3 on the relative I_{STD}/I_{STR} ratios measured for the filtered 0.65 mM Aβ (12-28) peptide aggregated through addition of 40 mM NaCl.....204
Figure S6. 1D –STR NMR spectra of the Aβ(12-28) peptide in the absence and presence of HSA domain 3. 204

CHAPTER 6

Figure 1. Distribution of the ligand binding sites within human serum albumin 210
Figure 2. Effect of domain 3 mutants on the relative I_{STD}/I_{STR} ratios measured for filtered 1 mM Aβ (12-28) peptide aggregated through the addition of 40 mM NaCl. 219
Figure 3. Interaction of domain 3 and its point mutants with Aβ (1-42) probed by 1D-NMR. 220
Figure 4. Dose-response STD-based profiles for the inhibition of the Aβ (12-28) self-association by domain 3 and its sub-domain deletion mutants.....222
Figure 5. Interaction of domain 3 and its sub-domain deletion mutants with Aβ (1-42) probed by 1D-NMR. 223
Figure 6. Overlap between the NMR detection window and the albumin/Domain 3 binding competent window.....226
Figure 7. Probing the interactions of Domian 3 with the Aβ (1-40) 228
Figure 8. Probing the interactions of the Aβ and albumin peptides 230

Figure S1. The NMR derived structure probabilitie obtained by PECAN analysis 238
Figure S2**.** Estimating TFA concentration in the Aβ samples.....238
Figure S3. Preparation protocol of the Domain 3: Aβ complexes 239
Figure S4. ^{1}H-^{15}N compound chemical shifts of 0.1 mM domain 3 caused by 1 mM TFA.....239

CHAPTER 7

Figure 1. Chemometrics and NMR analysis of the Domain 3: Aβ interactions.....243

Figure 2. Effect of the lipid addition on the 1D-WG spectra of the apo albumin 246
Figure 3. Dose-response STD-based profiles for the inhibition of the Aβ (12-28) self-association by apo albumin and albumin saturated with linoleic acid.....246
Figure 4. Plot of backbone ^{15}N relaxation rates of HSA domain 3 *vs* residue number.....249
Figure 5. Proposed scheme to identify the Aβ binding sequence within the Aβ inhibitory proteins 251
Figure 6. Sequence alignment of the Aβ CHC pentapeptide inhibitory sequence and the Aβ binding sites within ABAD 252
Figure 7. Identifying Aβ binding sequence within the $Z_{Aβ3}$. 252
Figure 8. ^{1}H 1D-NMR spectra of 1 mM Ttr (105-115).....254
Figure 9. ^{1}H 1D-NMR spectra of 1 mM Ttr (105-115) in the presence of 100 μM HSA.....254

LIST OF TABLES

CHAPTER 1

Table 1**.** Comparison of protein functions, Aβ affinties (K_D), Aβ binding mechanisms and Aβ binding site structures.....28
Table 2**.** Comparison of the protein sequences involved in Aβ binding.....28

CHAPTER 5

Table S1. Comparison of α-Helical Content in Different HSA Constructs.....201

LIST OF ABBREVIATIONS

Aβ:	Amyloid-beta peptide
AT:	Antitrypsin
ABAD:	Alcohol Dehydrogenase
ACT:	α1- Antichymotrypsin
AD:	Alzheimer's disease
ApoE:	ApolipoproteinE
α2M:	α2-Macroglobulin
APP:	Amyloid Precursor Protein
BBB:	Blood Brain Barrier
CCS:	Compound Chemical Shifts
CD:	Circular Dichroism
CHC:	Central Hydrophobic Core
CNS:	Central Nervous System
CSF:	Cerebrospinal Fluid
EM:	Electron Microscopy
FA:	Fatty Acid
HSA:	Human Serum Albumin
HSQC:	Heteronuclear Single Quantum Coherence
Hsp:	Heat Shock Protein
IR:	Inversion Recovery
LPR:	Low-density Lipoprotein Receptor Related Protein
MD	Molecular Dynamics
MW:	Molecular Weight

NAD:	Nicotinamide Adenine Dinucleotide
NMR:	Nuclear Magnetic Resonance
NOE:	Nuclear Overhauser Effect
OD:	Optical Density
ORR:	Off Resonance Relaxation
PECAN:	Protein Energetic Conformational Analysis from NMR Chemical Shifts
PICUP:	Photo-Induced Cross-Linking
RAGE:	Receptor for Advanced Glycation End Products
ROE:	Rotating Frame Overhauser Enhancement
SL:	Spin Lock
ST:	Saturation Transfer
STD:	Saturation Transfer Difference
STR:	Saturation Transfer Reference
SPR:	Surface Plasmon Resonance
sLRP:	Soluble Low-Density Lipoprotein Receptor Protein
ThT:	Thyoflavin T
TOCSY:	Total Correlation Spectroscopy
WG:	Water Suppression by Gradient-Tailored Excitation

CHAPTER 1

INTRODUCTION

1.1 ALZHEIMER'S DISEASE

Alzheimer's disease (AD) is one of the most common age related neurodegenerative disorders. It is an irreversible brain disease clinically characterized by a progression from episodic memory problems to a global decline of cognitive function, with death occurring on average 9 years after onset of the disease symptoms (5, 6). Currently ~ 25 million people have been diagnosed with Alzheimer's disease, however this number is expected to exceed 42 million by 2020 (7). Despite extensive scientific efforts no treatment is currently available to either stop or slow the deterioration of brain cells in Alzheimer's disease.

The anatomic pathology of Alzheimer's disease includes neurofibrilary tangles (NFTs), senile plaques (SPs), and cerebrocortical atrophy (8). Neurofibrils tangles and senile plaques were first described by Alois Alzheimer more than 100 years ago (1907) (7) and are now universally accepted as a hallmark of the disease. Extracellular senile plaques mainly consist of the β-sheet structured aggregates of the amyloid–β (Aβ) peptide, while intracellular neurofibrillar tangles consist mainly of aggregates of the hyperphosphorylated tau protein (7). As a result, the Alzheimer research field has two competing hypotheses regarding the molecular pathology of the disease: abnormal Aβ metabolism in the brain and abnormal tau protein processing. Genetic studies have

however clearly confirmed that Aβ is crucial in AD pathogenesis. Mapping of genes that segregate within families that develop early onset AD dementia (<65 years of age) led to the identification of mutations in the amyloid precursor protein (APP) gene on chromosome 21 (9, 10). These mutations result mainly in increased production of Aβ.

1.2 Processing of the Amyloid Precursor Protein (APP)

Aβ is a 40-42 amino acid long polypeptide chain produced by a sequential cleavage of the type-I transmembrane glycoprotein termed amyloid precursor protein (APP) (11). The amyloid precursor protein (APP) is ubiquitously expressed throughout the body in three major isoforms consisting of 695, 751 and 770 amino acids (12, 13). Although all isoforms contain the Aβ sequence, the APP 695 is mainly expressed in neurons and is thought to play a major role in neurite outgrowth and axonal sprouting (14). Longer isoforms contain the Kunith protease inhibition sequence, which inactivates proteins involved in blood coagulation (15).

APP processing can be divided into two pathways: non-amyloidogenic and an amyloidogenic pathway. In the prevalent non-amyloidogenic pathway APP is cleaved by α secretases that clip within the Aβ region (*i.e.* at K_{16}-L_{17} in Aβ or residues 612 and 613 in APP), thus precluding Aβ formation while producing a ~100 kDa N-terminal fragment (sAPPα) (Figure 1A). sAPPα is involved in the regulation of neuronal growth, excitability and neuron plasticity (16). The retained 83 a.a. membrane C-terminal

fragment (C83) is cleaved by γ secretase to produce a short 3kDa fragment termed p3 and the APP intracellular domain (AICD). AICD can form multiprotein complexes, which are transported to the nucleus and may be involved in intracellular signaling events and gene transcription (16). Although it was initially thought that p3 is not toxic, recent studies show that this fragment interacts with the membrane and forms Zn-dependent channels (17).

The amyloidogenic APP processing pathway involves β- and γ- secretases. First, cleavage by β-secretase at residues 671 and 672 of APP results in the release of sAPPβ into the extracelular space (18). The 99 a.a. C terminal fragment that remains bound to the membrane is cleaved by γ-secretese to generate AICD and Aβ. Owing to a somewhat imprecise γ-secretase-mediated intramembrane cleavage, the Aβ peptides have heterogeneous C-termini with varying tendencies to aggregate and seed amyloid deposits (16). Most of the Aβ is 40 a.a. long, while 10 % is 42 a.a. long. Aβ (1-42) being more hydrophobic is more prone to aggregation and is therefore mainly found in cerebral plaques (19). While it is known that the APP protein is expressed and sequestered not only in the cell membrane but also in the intracellular membranes (13), insoluble Aβ plaques are found mainly in the extracellular space. The trafficking and role of the intracellular Aβ is still not fully understood.

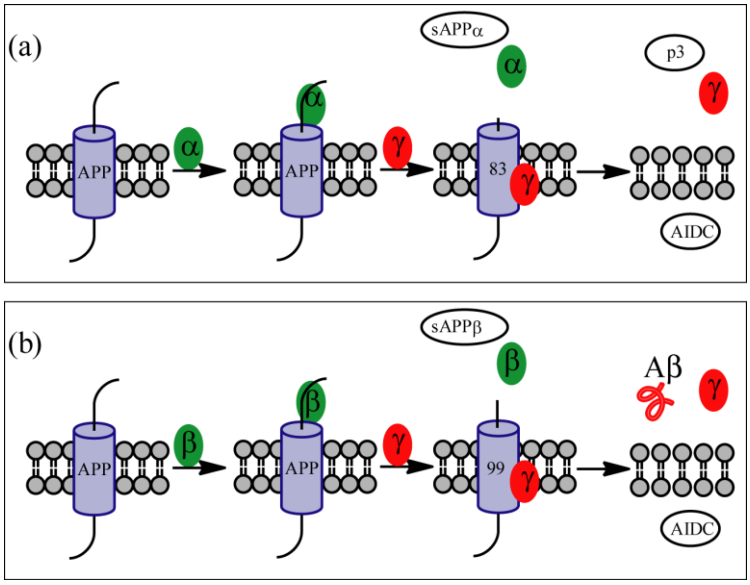

Figure 1. Processing pathways of the amyloid precursor protein (APP). Panel (a) depicts the non amyloidogenic APP processing pathway, which involves the α and γ secretases. This cleavage results in the extracellular release of the p3 fragment, which does not produce amyloid fibrils. Panel (b) reports the amyloidogenic pathway, which involves the β and γ secretases and results in the extracellular release of the Aβ peptide.

1.3 The Amyloid Cascade Hypothesis

The "amyloid cascade" hypothesis proposes that the pathogenesis of AD is triggered by changes in the steady-state levels of the Aβ in the brain. There is evidence for three mechanisms of Aβ accumulation: overproduction of Aβ, production of longer forms of Aβ (which are more prone to aggregation) and impaired clearance of Aβ. All these mechanisms result in the increased concentration of the Aβ within the brain and its subsequent deposition into Aβ plaques. It is understood that during the conversion of the Aβ monomers into the Aβ fibrils and plaques, several Aβ intermediates, such as low and

high molecular weight oligomers and protofibrils, form. Initially, the amyloid cascade hypothesis proposed the insoluble Aβ fibrils and plaques as the main toxic peptide moiety. However Aβ fibrils and plaques are not specific to AD and have been observed in older patients free from AD symptoms (20). This finding was explained by showing that Aβ oligomers and protofibrils are more toxic than Aβ fibrils (21, 22), while plaques have been proposed to be inert. Indeed, the formation of plaques has been suggested as a neuroprotective pathway for sequestering toxic oligomers.

The Aβ oligomers have been proven to be neurotoxic by a variety of mechanisms, including permeabilization of the cell membranes, disruption of the cytosolic Ca^{2+} ion homeostasis and formation of reactive oxygen species (20, 23). In addition, binding of Aβ oligomers to a variety of proteins, such as mitochondrial alcohol dehydrogenase, causes their dysfunction (24). At synapses, the oligomers close neuronal insulin receptors and mirror the effects of Type II diabetes (25). Oligomer interaction with tau and several kinases results in the hyperphosphorylation of the tau, which affects its role in maintaining axon structure and eventually results in the death of neurons (25).

1.4 Nucleation Dependent Polymerization

Considerable efforts were invested to understand the mechanism leading to Aβ self-association and deposition. Now it is understood that amyloidogenic peptides self-assemble to fibrils by a nucleated polymerization mechanism (26). Accordingly to the

nucleation dependent mechanism, the overall rate of amyloid formation is limited by a slow nucleation or lag phase during which partially folded Aβ intermediates (i.e. oligomers) are generated. Once formed oligomers self associate into protofibrils that rapidly grow by monomer addition (elongation phase) into Aβ fibrils.

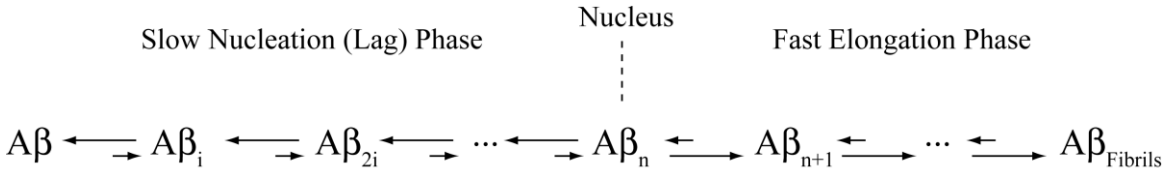

Figure 2. A general model for the Aβ self-association showing formation of the nucleus as a rapid, reversible, unfavorable equilibrium occurring during the nucleation phase. Self-association of the early oligomers ($A\beta_i$) and their rearrangement into the nucleus ($A\beta_n$) also occurs during the nucleation phase. The size or structure of the nucleus is currently not known, but it is suggested to grow by monomer addition into larger fibril assemblies.

1.5. Structures and Size Distributions of Aβ Assemblies

Given the pathological significance of Aβ, elucidating the structures of Aβ species is crucial to understand the molecular forces that drive the Aβ conversion into amyloid structures and to understand the different toxicities associated with different Aβ species.

1.5.1 Structures of the Aβ Monomers

The structure of the Aβ monomers was investigated in both membrane mimicking environments and in aqueous solutions. Figure 3 (a) and (b) compares the Aβ (1-42)

structures determined by solution NMR in 80% and 30 % HFIP solutions, respectively (27, 28). The Aβ (1-42) structures show two helical domains separated by a turn region between residues 23 and 27. Although these conformations were determined using a mixture of organic solvents and water, similar structural components were found in recent molecular dynamic simulations of Aβ in a membrane bilayer (29). Moreover, comparison of the two structures in Figure 3 (a) and (b) indicates that a decrease in the solution hydrophobicity results in the unfolding of the Aβ helices. However, this observation still does not explain how Aβ monomers convert into Aβ fibrils in water. Detailed structural studies of the Aβ peptides in aqueous solution are complicated by the peptide hydrophobicity and its tendency to precipitate. Therefore, the determination of the monomeric Aβ structures in aqueous solution has greatly relied on the molecular dynamic (MD) simulations (Figure 3 (c)) (30). As indicated in Figure 3 (c), MD simulations suggest that in aqueous solution instead of being completely unfolded, Aβ folds into a heterogeneous ensemble of compact collapsed coil structures, in which the central hydrophobic residues (CHC: L17-F20) are shielded from unfavorable interactions with the solvent (30, 31, 32). This is consistent with the structure of the Aβ (1-40) monomer in 100% H_2O solution recently solved by NMR (Figure 3 (d)) (33). As shown in Figure 3 (d), the central hydrophobic core region (L17-A21) of the peptide remains in mostly helical, while hydrophobic residues of the N and C–termini collapse against the CHC helix resulting in a cluster of hydrophobic residues (33). This structure does not appear to be in agreement with the proposed Aβ extended random coil conformation suggested by Hou *et al*. (34). However, as discussed in a recent study by Ball *et al.*, no single structure

is expected to fully capture the complexity of the highly degenerate free energy landscape of monomeric Aβ (35). Specifically, Ball *et al.* has argued that monomeric Aβ exists as a heterogeneous ensemble of isoenergetic peptide conformations, however it is not clear which monomeric Aβ conformations drive the Aβ self-assembly into oligomers (35).

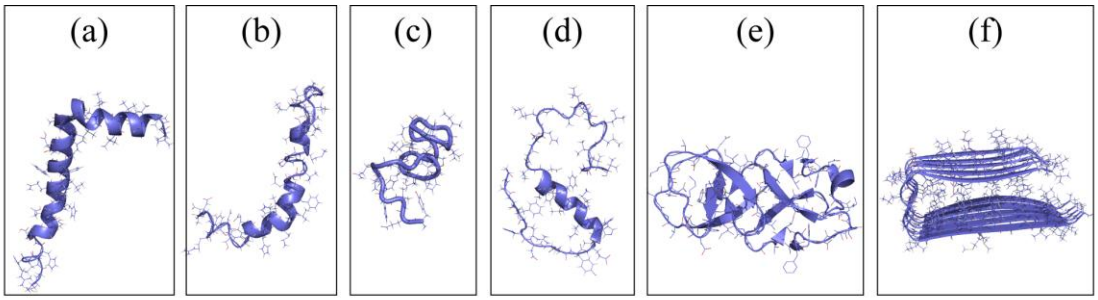

Figure 3. Current structures of the Aβ available on the protein data bank**.** (a) NMR derived structure for monomeric Aβ (1-42) in 20% water, 80 % HFIP (pdb: 1IYT)(27). (b) Aβ (1-42) monomer structure in 70% H_2O, 30% HFIP solution (pdb:1Z0Q (28)). (c) Structure obtained by MD simulation for the monomeric Aβ (10-35) in 100% H_2O (pdb:1HZ3) (30). Panel (d) reports a recent NMR derived structure of the Aβ (1-40) monomers in aqueous solution by Vivekanandan *et al.* (pdb: 2LFM) (33). Panel (e) reports the structure of the Aβ-p3 oligomer (tetramer), stabilized in the IgNAR cage (pdb: 3M0Q) (IgNAR domains are not included for clarity) (38). Panel (f) displays the structure of the Aβ (1-42) protofibrils from Luhrs *et al.* (pdb: 2BEG) (43).

1.5.2 Size Distributions and Structures of Aβ oligomers

The combination of size exclusion chromatography, SDS-page analysis and photo-induced cross-linking (PICUP) identified that the two main Aβ alloforms, Aβ (1-42) and Aβ (1-40), oligomerize through two distinct oligomerization pathways (36). Aβ (1-40) forms mainly dimers, trimers and tetramers, in the equilibrium with Aβ monomers,

while Aβ (1-42) assembles into pentamers and hexamers, as well in higher molecular weight oligomers such as nonamers through dodecamers (36). Larger oligomeric structures are also termed as Aβ derived diffusible ligands (ADDL) and were reported *in vivo*. Aβ 12mers (~56 kDa), termed Aβ*56 were isolated in transgenic mice and were shown to be toxic to neuronal cells (37).

Aβ (1-42) pentamers have been recently described as disc-shaped structures with a width of 10-15 nm and a height of ~2 nm, which are stabilized at low-temperature and low-salt conditions (21). Mahiuddin *et al.* showed that neurotoxic oligomers similarly to the Aβ fibrils contain a β strand-turn-β strand conformation, which promotes extensive intra-molecular interactions between hydrophobic residues of the CHC and of the C-terminus (21). However Aβ oligomers as opposed to the fibrils do not form an extended inter-molecular β-sheet structure, but are composed of loosely aggregated parallel β-strands (21).

Using solid-state NMR and electron microscopy, Chimon *et al*. showed that before fibrilization, Aβ (1–40) forms spherical amyloid intermediates of 15–35 nm in diameter. These intermediates have a molecular weight of 650 kDa (150 monomers or more) and have demonstrated higher toxicity than Aβ fibrils (21). Moreover, using solid state NMR Chimon *et al*. showed that V12, V18, V24 and A30 contain multiple NMR resonances, suggesting that the isolated intermediates coexist as multiple conformers or poly-morphologies (21). While the major conformer appears to contain β-sheets as observed in the Aβ fibrils, the minor conformers are α-helical and this has been proposed to be a unique feature of amyloid intermediates (21).

In an effort to correlate structural features of the Aβ oligomers to their toxicity, recently the more detailed structure of the Aβ oligomers formed by the p3 peptide (Aβ(18-42)) was reported by Streltsov *et al.* (Figure 3(e)) (38). The authors created an Aβ (18-41) - IgNAR fusion construct that effectively prevented uncontrolled amyloid formation and stabilized the Aβ tetramers within the cage of IgNAR domains (pdb:3MOQ) (38). This caging approach cleverly circumvents the problems associated with inhomogeneous Aβ oligomers, which have traditionally presented a challenge for high-resolution structural studies.

As indicated in Figure 3 (e), the reported tetramer has an ellipsoidal shape with a ~27x39 Å equatorial dimension (interface of the dimers) and a ~18Å polar dimension structurally characterized by three β strands formed by CHC residues (V18-A21) and C- terminal residues (30-35 and 38-40). While the C-terminal β-strands (30-35 and 38-40) are connected in an antiparallel manner by a loop formed by residues 36-39 into a hairpin structure, the CHC β- strand (V18-A21) is connected to the C-terminus either by a long loop formed by residues 22-29 or by a short 3_{10} helix formed by residues 24-26. Interestingly it was proposed that changes in the stability of this turn segment spanning residues 24-26 nucleate Aβ folding (38). The stability of the loop region (residues 22-29) is mainly determined by the conformations of the Lys28 side chain, which in the 3_{10} helix structure is directed out of the loop plane and is stabilized by intramolecular contacts with main chain carbonyls of Val24 and Asn27. In the loop structure Lys28 is instead directed internally to form intramolecular contacts with the carbonyl oxygen of Asp23 and Ser26 and intermolecular contacts with Gly29 and Asn27. Moreover, the

current structure (Figure 3e) indicates that the tetramers are mainly stabilized through hydrophobic interactions within the oligomer core. These interactions involve the Leu34 side chains that form a hydrophobic clamp holding dimers in the tetrameric structure. Consequently, a Leu34Cys mutant did not form tetramers, but selectively formed dimers. Phe 19 was also present in the core of the tetramer and its mutations severely affected Aβ aggregation. Extensive hydrophobic contacts of Phe19 and Leu 34 were also suggested by independent solution NMR data of Aβ oligomers (21). Aβ42 dimers stabilized by 0.2% SDS (39) indicate intramolecular hydrophobic contacts between CHC residues and C terminus. Liping *et al.* proposes Aβ dimers consist of the interchain in-register parallel β-sheet formed by residues 34-40, while CHC residues (V18-A21) form antiparallel β-sheet through intramolecular contacts with the β strand spanning residues K28-G33 (39). Similarly to Streltsov *et al*., Liping *et al*., proposes that a bend / turn formation between residues 23 and 30 dictates intramolecular contacts within Aβ and is a trait that determines oligomer stabilization. To understand how amyloid formation can be inhibited it is first necessary to decipher how oligomers grow into larger assemblies. Initially it was suggested that oligomers grow through addition of monomers to protofibrils and fibrils, however recent molecular dynamics (MD) simulations propose that Aβ (1-42) oligomers self–associate and then rearrange into Aβ protofibrils (40). Urbanc *et al.* using discrete molecular dynamics investigated key peptide regions involved in oligomer formation. They show that hydrophobic interactions drive the initial formation of Aβ (1-42) oligomers up to hexamers, however electrostatic interactions

drive the self-association of hexamers into elongated high MW aggregates, termed paranuclei, which are precursors to Aβ protofibrils.

1.5.3 STRUCTURES OF THE Aβ PROTOFIBIRLS

Protofibrils, as opposed to oligomers, are characterized by very well defined cross-β structures, in which hydrogen bonded β-strands align perpendicularly to the protofibril's axis with the backbone hydrogen bonds parallel to the protofibrils axis (41). Two models of the detailed three-dimensional structures of Aβ(1-42) and Aβ(1-40) protofibrils have been proposed and verified experimentally (the Ma-Nussinov-Tycko model and the Luhrs *et al.* model) (42, 43). Both models suggest similar intermolecular arrangements for the protofilaments with stacked, parallel and in-register β-sheets. However the intra-molecular interactions proposed by two models are significantly different (Figure 4).

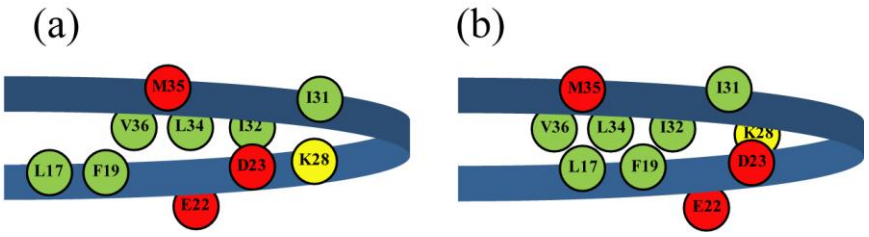

Figure 4. Comparison of the Aβ protofibril structural models. Panel (a) depicts Luhrs (43) while panel (b) depicts Ma-Nussinov-Tycko model (42). In both models only key residues from the first strand are highlighted.

The Ma-Nussinov-Tycko model (Figure 4(b)) proposes residues 10-22 and 30-40 form β-strands and residues 23-29 bend or loop to allow the two strands to interact. Luhrs *et al*. model (Figure 4(a)) suggests that residues 1-16 are structurally disordered, while residues 17-26 and 31-42 form two β-strands, connected by a U-turn spanning residues 27-30 (Figure 4 (a)). In both models the loop region is stabilized though the formation of a salt bridge between D23 and K28, however the different number of residues involved in the U-turns of the two models results in differences in the packing of the two β–strands as indicated in Figure 4. More extensive hydrophobic packing between the C-terminus and the CHC β-stands in the Ma-Nussinov-Tycko model results in a more narrow turn, compared to the loop reported in the Luhrs model. Although these models were derived using different Aβ peptides, *i.e.* Aβ (1-42) and Aβ (1-40), respectively, different intramolecular interactions between the two β-strands could be used to explain the polymorphism often observed in Aβ fibrils. Moreover, Luhrs proposed that protofibril growth occurs only at the odd protofibril end which opposed to the even end contains exposed hydrophobic residues. The exposed hydrophobic residues are proposed to bind the oncoming Aβ monomers and also to be recognition site for the Aβ fibrilization inhibitors.

1.6 The Peripheral Sink Hypothesis

The APP is ubiquitously expressed throughout the body and it is not clear why amyloid deposition occurs only in the brain. Recent studies show that late-onset AD is

associated with a 30% impairment in the clearance of both Aβ (1-42) and Aβ (1-40) from the brain, indicating that Aβ clearance mechanisms may be critically important in the development of AD (44). Aβ can be removed from the brain in two ways, either through protease degradation or through shift of the soluble Aβ from the brain toward the peripheral blood stream (45) (Figure 5). Significant Aβ degradation occurs in the plasma, but a negligible Aβ fraction is degraded within the brain (45), where active transport across the blood brain barrier (BBB) is the main Aβ clearance pathway (45). Two main membrane protein receptors are associated with Aβ transport across the BBB: the low-density lipoprotein receptor-related protein (LRP), which regulates efflux of Aβ from the brain towards the periphery, and the RAGE protein, which serves as an Aβ influx receptor (45) (Figure 5).

In healthy individuals Aβ is effectively cleared from the brain across the BBB, however in AD patients, the Aβ accumulation in the brain is promoted by three mechanisms. First, disrupted BBB allows diffusion of Aβ from the periphery toward the brain (3). Second, in the AD, RAGE receptor is up-regulated (45) promoting the shift of soluble Aβ from the periphery towards the brain. Third, the LRP receptor is down regulated (46), which inhibits clearance of the Aβ from the brain.

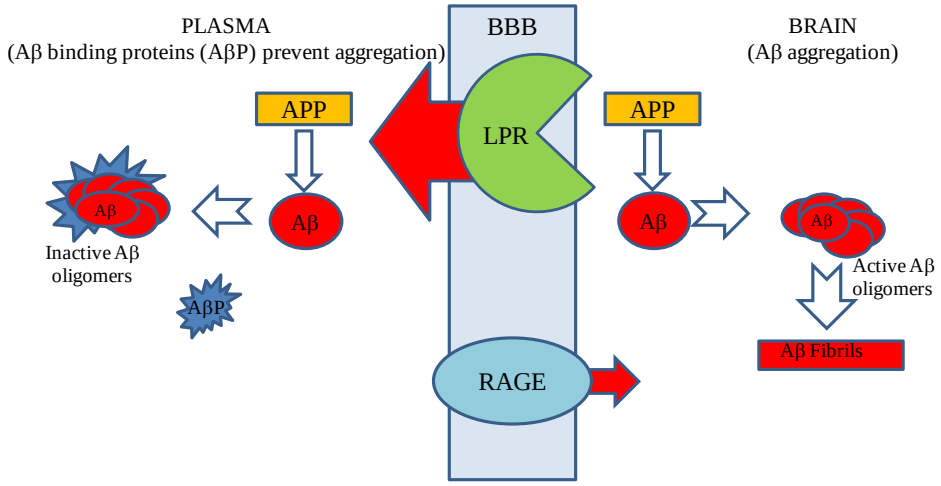

Figure 5. Mechanisms of Aβ clearance across the blood brain barrier (BBB). The steady-state level of Aβ depends on the balance between production and clearance. The transport of Aβ across the blood–brain barrier (BBB) is mainly mediated by receptors [*i.e.* receptor for advanced glycation end products (RAGE) and lipoprotein receptor-related protein (LRP)] on endothelial cells. In the plasma, Aβ carrier proteins (AβP) bind Aβ and prevent its aggregation. Moreover this interaction promotes an equilibrium shift of the free soluble Aβ from the brain toward peripheral plasma.

The peripheral sink hypothesis proposes that binding of soluble Aβ to peripheral agents that cannot cross the BBB prevents Aβ deposition in the brain in two ways. First, it prevents reflux of Aβ toward the brain. Second, it promotes an equilibrium shift of the soluble Aβ from the brain toward the periphery. A proof of principle for the peripheral sink hypothesis was provided by an Aβ-specific monoclonal antibody which was administered directly into the blood of transgenic mice expressing human amyloid precursor protein (47). The antibody increased plasma levels of Aβ by 1000-fold and decreased the Aβ burden in the brain (47).

1.6.1. Proteins in Plasma and CSF Regulate the Equilibrium of Soluble Aβ Partitioning between the Brain and the Periphery

The structural background (*i.e.* structures of Aβ oligomers in complex with inhibitory proteins) that could potentially help understand key determinants for binding of Aβ to different inhibitory proteins and guide design of potent Aβ-self association inhibitors is still sparse. Here we will review interaction of several proteins with Aβ to understand common protein structures and sequences that drive interaction with Aβ. Proteins reviewed are mainly selected from the list of the proteins interacting with Aβ in plasma, published by Bohrmann in 1999 (4). However, other Aβ–binding proteins for which either the interacting sequence or the structure is available were used to help us understand key requirements of the effective Aβ fibrilization inhibition.

1.6.1.1 Interactions of Human Serum Albumin with Aβ

High concentrations of inhibitory proteins in plasma, as opposed to CSF, prevent Aβ amyloid formation in the peripheral tissues (4). At physiological Aβ concentrations (0.5-0.7 nM) about 90% of Aβ is bound to albumin (3). Albumin represents about 60% of the plasma inhibitory activity followed by α1-antitrypsin and immunoglobins A and G. The critical role of albumin in Aβ regulation is supported by recent investigations, which show that low plasma concentrations of albumin are associated with cognitive impairment (48). Moreover Boada *et al.* demonstrated that albumin replacement through plasma dialysis is a promising strategy for the treatment of mild AD (49). The Aβ binding sites

within albumin were investigated by Bohrmann *et al.* (4) through competition with the anti-diabetic drug tolbutamide. Since tolbutamide increases aggregation of the Aβ peptide in the presence, but not in the absence of HSA, authors argued that Aβ and tolbutamide compete for a common binding site on albumin. However tolbutamide binding sites on albumin are not well characterized, and therefore location of Aβ binding sites is not known. Furthermore, Barcelo *et al.* (2) demonstrated that bovine serum albumin is capable of inhibiting in a dose-dependent manner both the formation of Aβ (1-40) aggregates from monomeric peptide and the ongoing growth of Aβ (1-40) fibrils. It was also suggested that high albumin concentrations are neuroprotective, although lower albumin concentrations promote a shift of the Aβ equilibrium towards small MW aggregates and trap soluble and possibly toxic Aβ oligomers (2). Rozga *et al.* (1) investigated the mechanism of albumin Aβ interactions using CD spectroscopy and suggested that albumin binds Aβ monomers with a K_D of 10 μM. However, the proposed binding mode is not in agreement with the binding mechanism of Bohrmann *et al.*, who proposed albumin selectively recognizes fibrilized as opposed to the monomeric Aβ. Moreover the proposed binding constant by Rozga *et al*. does not explain how albumin inhibits Aβ oligomerization at physiological conditions (*i.e*. nM Aβ concentrations).

As a first step towards understanding the interactions between HSA and Aβ, in the following sections we survey several other Aβ binding proteins. Although the structural information available for these Aβ complexes is still sparse, the comparative analysis of

Aβ binding proteins is likely to reveal common features relevant for Aβ binding and for generating initial hypotheses on the Aβ–HSA interactions as well.

1.6.1.2 INTERACTIONS OF THE APOLIPOPROTEINS WITH Aβ

Other lipid binding proteins besides albumin interact with Aβ. For instance, proteins in the apolipoprotein family, such as ApoE and ApoJ (clusterin), are expressed in both, brain and plasma, and bind Aβ with high affinity. ApoE has three isoforms, ApoE2, ApoE3, and ApoE4 that differ in the amino acids at positions 112 and 158 (50) and bind Aβ with slightly different affinities. ApoE4 (pdb: 1B68) is considered a risk factor for the development of AD, since it has lower affinity for Aβ then other isoforms (the apparent K_D values for ApoE3 and ApoE4 are 21 and 27 nM, respectively (51) and leads to higher circulating Aβ levels in plasma (52). ApoE is a helical 35 kDa protein (299a.a.) that contains an N-terminal and a C-terminal (216-299) domain, separated by a long loop. The C-terminal domain is composed of three α-helices, while the N-terminal domain is a four α-helix bundle (Figure 6d). Both N and C terminal domains were proposed to be involved in Aβ binding (53, 54). Moreover the dynamics of the C-terminus are suggested to be crucial for Aβ binding (51). For instance, ApoE3, which contains a dynamic C-terminus, has higher affinity for the Aβ oligomers than ApoE4, with a less dynamic C-terminus stabilized through interactions with the N-terminal helices (51). MD simulations suggest that Aβ binding to the N-terminal domain results in a large unfolding

of ApoE as a result of salt bridge reorganization, mainly driven by formation of a salt bridge between Aβ Asp 23 and ApoE Arg 38 (53).

Clusterin (ApoJ) is a lipid-binding protein recently proposed as an AD biomarker. Thambisetty and colleagues showed that increased plasma ApoJ concentration is correlated with the development, severity and progression of Alzheimer's disease (55). Clusterin is a disulfide–linked hetero dimeric glycoprotein (~40kDa), expressed in all mammalian tissues that binds Aβ with high affinity (K_D ~ 2nM) (56, 57). In the plasma this protein is present at 0.44-1.35 μM, while in the CSF it is present in the 15-45 nM concentration range (56). This protein is mainly involved in lipid transport and membrane recycling. However, it also binds amyloid deposits irrespective of the protein sequence constituting the amyloid deposits (57, 58). The detailed mechanism of ApoJ: Aβ interaction is unknown, but recent results indicate that the effects of ApoJ on the cytotoxicity of aggregates depends on both the stage of amyloid formation and on the clusterin: Aβ ratio (58). At high (1:10) stoichiometric Aβ: clusterin ratios, clusterin inhibits Aβ aggregation, while at low concentrations it promotes formation of neurotoxic Aβ oligomers (59). Additionally, ApoJ has a higher affinity for freshly prepared samples, suggesting it possibly preferentially interacts with early Aβ oligomers or monomers as opposed to slow-forming fibrils. The clusterin structure is still not available, but recently it was suggested to contain a high number of amphipathic helices at the C- terminus (60). These are potential Aβ binding sites, since it was recently shown that a short 10 a.a. peptide derived from ApoJ (a.a. 113–122) inhibits amyloid formation (61).

1.6.1.3 INTERACTIONS OF THE LOW DENSITY LIPOPROTEINS WITH Aβ.

Sagare *et al.* (62) has suggested that the soluble circulating low-density lipoprotein receptor protein (sLRP) is the key endogenous peripheral regulator of Aβ in humans. Using co-immunoprecipitation it was found that about 70-90% of Aβ was bound to sLRP in the plasma of healthy individuals. Although this study is not in agreement with the initial study done by Biere *et al.*, (1996) (3), it was shown that in individuals with Alzheimer's disease there was a 30–35% drop in sLRP-bound Aβ resulting in a 300–400% increase in free, protein-unbound Aβ. sLPR binds Aβ (1-40) and Aβ (1-42) with dissociation constants (K_D) of 1.9 and 5.1 nM, respectively, however the structural or sequence details for such high affinity interaction between sLRP and Aβ are still not available.

1.6.1.4 INTERACTIONS OF THE SERAPINS WITH Aβ.

Antitrypsin (AT) and α1- antichymotrypsin (ACT) are serine protease inhibitors ("serapins") that also bind Aβ (4,63). These proteins are found in association with Aβ amyloid plaques and also have elevated expression in AD patients (64). In plasma AT and ATC are present at 25 μM and 8.6 μM concentrations, while in brain they are present at 120 nM and 38 nM concentrations, respectively (4). The mechanism of interactions of serapin with Aβ is concentration dependent. At low concentrations ATC promotes Aβ fibrilization while at high concentration it promotes disaggregation of fibrils (64, 65) into

soluble toxic Aβ forms (65). It is interesting to note that serapins themselves self-associate to form fibrils. This self-association is mediated by the reactive protease binding loops (RL) (Figure 6 (c)), which readily form β-strand structures and have also been suggested to be involved in the interaction of serapines with Aβ peptides (66). An additional mechanism in which Aβ inserts its N-terminus into the serapin and completes a serapin β–sheet has also been proposed (67). Although the two proposed mechanisms are significantly different, as one involves incorporation of the reactive loop into Aβ, while other involves incorporation of Aβ within serapin structure, both mechanisms involve formation of a β-sheet. This suggests that both hydrophobic interactions and H-bonding are required for binding Aβ.

1.6.1.5 INTERACTIONS OF HUMAN MACROGLOBULIN WITH Aβ.

Human α2M (α2-macroglobulin) is a large homotetrameric plasma glycoprotein (1451 a.a.) and a major circulating endoproteinase inhibitor. It is found in plasma at concentrations of 12-20 μM and also in AD senile plaques. Fraser *et al.* reported that human α2M binds ^{125}I-Aβ (1-42) in a 1:1 ratio with an apparent dissociation constant of 380 pM (68). This dissociation constant value is significantly different from the dissociation constant of 290 +/- 20 nM obtained for the interaction with the Aβ (1-40) (69). Although at the first sight these two K_D values seam significantly different they do

not necessarily contradict each other but might correspond to the interaction processes occurring during different Aβ aggregation stages.

α2M binds different proteinases, within its central cavity, and undergoes conformational change to an "active" state with a ten-fold higher affinity for Aβ (69). *α*2M saturated with Aβ is still capable of binding its substrate trypsin within its cavity, suggesting that Aβ does bind not within the protein cavity. The complete structure of α2M is not available, however it was suggested that conformational changes upon activation result in the exposure of residues 1314-1365, which were suggested as key Aβ binding determinants (70). It was proposed that this protein region is largely unstructured, as denatured *α*2M retained Aβ binding activity (71).

1.6.1.6 Interactions of Alcohol Dehydrogenase with Aβ.

While albumin, ApoE, ApoJ, ATC,AT, *α*2M, represent some of the proteins that interact with Aβ in the extracellular space in both plasma and brain, Aβ is found within the intracellular space as well, where it has major effects on tau phosphorylation and it also causes mitochondrial abnormalities (72). Lustbader *et al*. (73) investigated the interaction with the Aβ of ABAD, an alcohol dehydrogenase found in the mitochondria. This interaction is critical for cellular toxicity of Aβ, since the Aβ: ABAD interactions promote neuronal production of free radicals and are proved to aggravate memory loss in APP transgenic mice (73). ABAD is the only short-chain dehydrogenase/reductase

(SDR) superfamily protein that binds Aβ. This interaction excludes nicotinamide adenine dinucleotide (NAD), an ABAD cofactor, and occurs with a K_D of 38+/- 5 nM at 306 K (73, 74). Unlike other SDR proteins, ABAD contains a loop (*i.e.* loop D or L_D), which was identified as the Aβ binding motif (Figure 6(b)). Synthetic peptides spanning the sequence of the L_D loop inhibited binding of Aβ (1-40) and Aβ (1-42) to immobilized ABAD with inhibitory constants of 4.9 and 1.7 μM, respectively (73). Based on these results, L_D was proposed as a major mediator in Aβ binding. In addition, site directed mutagenesis identified polar residues (*e.g.* tyrosine, threonine, serine and histidine) within the L_D loop as key Aβ binding determinants. However, when the ABAD crystal structure was solved in the presence of the Aβ peptide (73), no electron density was observed for Aβ or the L_D loop suggesting that both the Aβ and the L_D loop are at least partially disordered in the complex (73) (Figure 5(b)). ABAD specifically binds Aβ residues in the N terminus and CHC, as Aβ (23-35) did not bind ABAD (73). Moreover ABAD mainly recognizes aggregated Aβ, while immobilized monomeric Aβ (1–40) did not bind ABAD.

1.6.1.7 Interactions of Affibody Protein $Z_{Aβ3}$ with Aβ.

Recently solution structure of the monomeric Aβ (1–40) bound to the phage display affibody protein $Z_{Aβ3}$ was determined (75) (Figure 6(a)). This was the first and so far the only available complete structure of the Aβ bound to its protein inhibitor. The Aβ

(1-40) bound to $Z_{A\beta3}$ is in a hairpin conformation, with the β strands spanning residues 17-23 and 30-36. Monomeric Aβ structure bound to $Z_{A\beta3}$ resembles the structure of the Aβ within the protofibril, however while in the Aβ protofibril hydrogen bonds are intermolecular, in the $Z_{A\beta3}$ bound structure Aβ hydrogen bonds are intramolecular. $Z_{A\beta3}$ consists of 3 helices, that are linked by a sulfide bridge and that dimerize to form an hydrophobic tunnel interacting with the hydrophobic faces of the Aβ sheet (76). Extensive hydrophobic interactions within the $Z_{A\beta3}$ dimer are required for high Aβ affinity (K_D of 17 nM) as the $Z_{A\beta3}$ mutant $(Z_{A\beta3}C28S)_2$, which does not form dimers binds Aβ with a K_D of 520 nM. Binding of Aβ to $Z_{A\beta3}$ is coupled to folding of both Aβ and the $Z_{A\beta3}$. Helix 1 of the $Z_{A\beta3}$ unfolds and forms a β-strand that extensively hydrogen bonds with the β-strands of the Aβ. Moreover unfolding of helix 1 opens a large hydrophobic cavity, whose interior mainly contains hydrophobic leucine residues. However Tyr 18 in helix 1 forms hydrogen bonds with the E22 of the Aβ and stabilizes it within the hydrophobic cavity.

1.6.2. Common Features of the Aβ Binding Proteins

Although the Aβ–binding proteins surveyed here represent just a very small fraction of all the Aβ interacting proteins, several common features possibly relevant for Aβ binding were identified. First, all inhibitory proteins bind Aβ with high affinity. Dissociation constant values are in the low nM range, close to the physiological Aβ

concentrations. Second, the majority of the proteins involved in Aβ binding bind also endogenous hydrophobic compounds as indicated in Table 1, suggesting Aβ binding might be driven by hydrophobic interactions. This conclusion is supported by the observation that Aβ binding by the ABAD protein is mainly driven by a favorable entropic change (74). Therefore the Aβ: inhibitory protein interactions are reminiscent of the early Aβ self-association steps, which are also driven by the hydrophobic interactions (42). Third, the comparison of the protein structures interacting with Aβ in Figure 6 suggests that exposed protein loops might be involved in Aβ binding. Unfolded protein segments and loops typically preserve the conformational flexibility required to adapt to different Aβ structures. Such Aβ interacting loops are inherently present in fibrilization inhibitory proteins such as ABAD, ATC, TC or are produced through protein unfolding or structural changes such as those observed for ApoE, $Z_{A\beta}$ and α_2M. This might indicate that protein dynamics might play an important role in Aβ binding, as unstructured dynamic protein regions can easily convert into β-strands and compete with Aβ fibril growth. Interestingly, some of the proteins reviewed here, such as ApoE (77), albumin (78), ATC and AT, are themselves capable under specific experimental conditions of forming amyloid–like fibrils. For ATC and AT, the regions involved in fibril formation are also involved in Aβ self-association inhibition. Therefore it could be speculated that protein regions prone to amyloid formation are also involved in the Aβ amyloid inhibition.

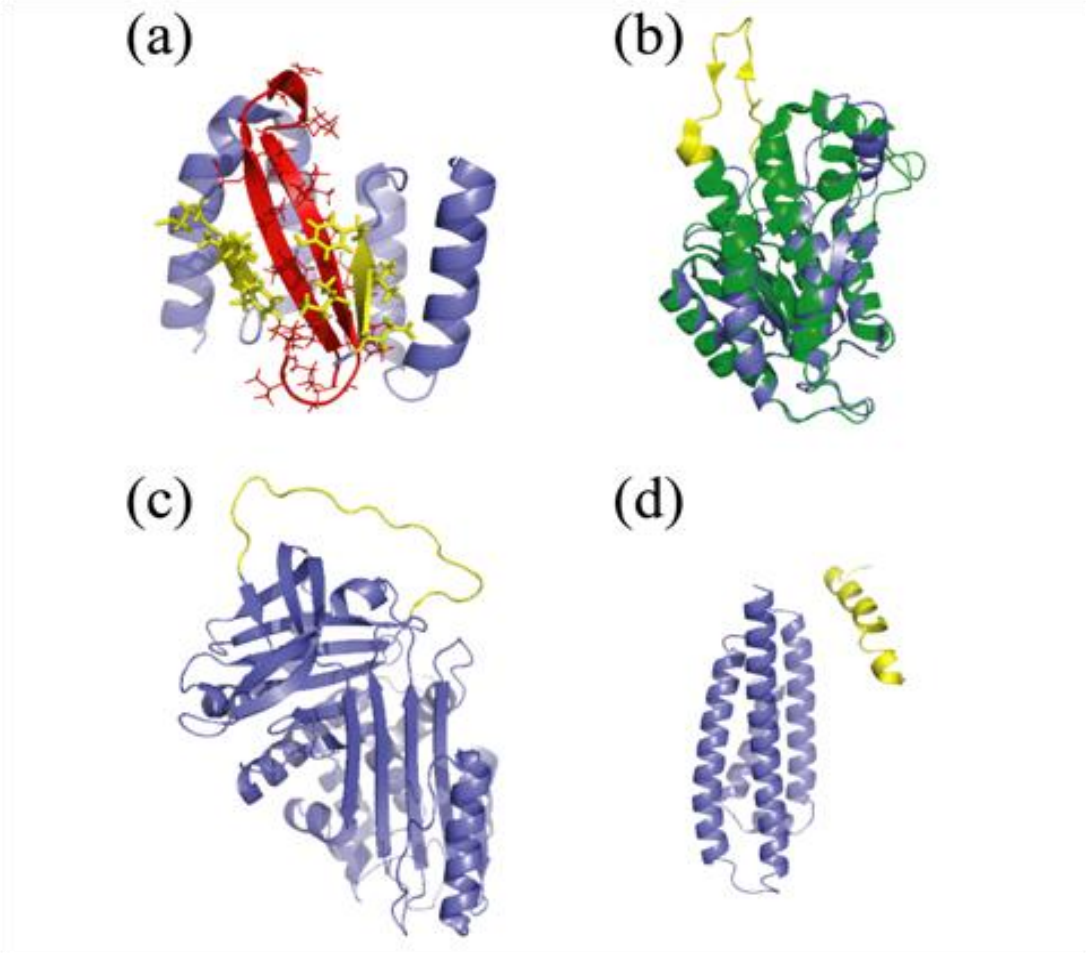

Figure 6. Structures of the proteins interacting with Aβ. Panel (a) depicts structure of $Z_{Aβ3}$ bound to Aβ (1-40) (pdb: 2OTK) (75). Helix 1 of the $Z_{Aβ3}$ adapts to β-strand which forms H-bonds with Aβ monomers. Panel (b) reports overlap of two human ABAD structures. Structure depicted in blue represents structure of human ABAD bound to Aβ (1-40) (pdb file: 1SO8) (73) while structure in green corresponds to the structure of human ABAD bound to the cofactor NAD^+ and NAD^+ inhibitor (pdb: 1U7T) (79). L_D loop which interacts with Aβ is depicted in the cofactor bound structure in yellow color. This loop region is however absent in the Aβ bound structure. Panel (c) depicts structure of the alpha 1antitrypsin (pdb: 1HP7) (80). Reactive loop shown in red was proposed to be involved in Aβ binding. This loop is also involved in AT self association. Panel (d) presents ApoE4 N (pdb: 1B68)(81) and C terminal (pdb: 1OEG) (82). Long loop connecting two helices is absent in the structure. C-terminus is shown in yellow is proposed to be crucial for ApoE self-association, but also for Aβ binding.

Table 1. Comparison of protein functions, Aβ affinities (K_D), Aβ binding mechanisms and Aβ binding site structures

Protein	Protein Function	K_D	Aβ binding mechanism	Aβ binding site Structure
sLRP1	Lipid carrier protein	~15 nM	Not available	N/A
HSA	Hydrophobic ligand carrier protein	70-100 nM	Selectively binds Aβ oligomers	N/A
ApoJ	Lipid transport, membrane recycling	2 nM	Not available	Helix
ApoE	Lipid carrier protein	~ 20 nM	Selectively binds Aβ oligomers	Helix
ABAD	Alcohol dehydrogenase	38+/- 5 nM	Selectively binds Aβ oligomers	Loop
α2M	Chaperone	380 pM - 290 nM	Not available	Loop
$Z_{Aβ3}$	Aβ fibrilization inhibitor	15 nM	Selectively binds Aβ monomers	Helix-Loop

Table 2. Comparison of the protein sequences involved in Aβ binding

Protein	Protein Sequence Interacting with Aβ
$Z_{Aβ3}$	VDNKFNKEMASAGGEIVYLPNLNPDQLCAFIHSLHDDPSQSANLLAEAKKLNDAQAPK
ABAD (92-113)	AGIAVASKTYNLKKGQTHTLED
AT (344-361)	GTEAAGAMFLEAIPMSIPP
ATC	GTEASAATAVKITLLSALV
ApoE (269-289)	PLVEDMQRQWAGLVEKVQAAVGT
α2M (1314-1365)	QVTIQSSGTFSTKFQVENSNRLLLQQVSLPEVPGEYSMSVTGEGCVY
ApoJ (113–122)	LVGRQLEEFL

1.7 HUMAN SERUM ALBUMIN: STRUCTURE AND FUNCTIONS

Human serum albumin is a highly abundant extracellular protein, present in the plasma at concentration of ~0.6 mM. It is a versatile carrier protein, responsible for trafficking and disposal of many metabolites, such as saturated and nonsaturated fatty acids, tyroxine, hemin, bilirubin. Fatty acids represent its primary physiological ligands, but albumin is able to bind diverse cationic and anionic exogenous hydrophobic ligands and therefore has attracted a long standing pharmaceutical interest and has been one of the most extensively studied proteins.

The first crystal structure of this 585 amino acid (66 kDa) protein was obtained in 1992 to show a hearth shaped structure with approximate overall dimensions in the apo state of 80 x 30 x 30 Å and consisting of three structurally similar helical domains (Figure 7) (83). Each domain consists of two sub-domains, named A and B, connected by a flexible loop. The A sub-domains contain six helices, while the B-subdomains contain only four helices.

The structure of each sub-domain is stabilized by a large number of disulfide bonds. Three disulfide bonds are formed in the 1A sub-domain, while the 2A and 3A sub-domains contain four disulfide bonds each. Each B sub-domain contains two disulfide bonds. The absence of disulfide bonds between sub-domains or domains allows a high degree inter-domain and inter-subdomain flexibility, manifested for example in ligand induced domain rotations (84). While sub-domains are connected by loops, domains are not joined by loops but by shared helices. Domain 1 and 2 share a continuous 9-turn helix

formed by residue 173-205, while domains 2 and 3 share a helix formed by residues 366-398. Although different domains are structurally similar, the orientation of domains with respect to each other is different resulting in an asymmetric distribution of binding sites (*e.g.* fatty acid and drug binding sites).

1.7.1 Fatty Acid Binding Sites in HSA

There are in total seven binding sites proposed for medium and long chain fatty acids as depicted in Figure 6. Binding to albumin involves mainly unsaturated fatty acid, such as oleic acid (cis-9-octadecenoic acid), linoleic acid (cis 9, 12, octadecadienoic acid, C18:2) and arachidonic acid (84). Under normal physiological conditions, between 0.1-2 moles of fatty acids are complexed with one mole of HSA (85). The fatty acid binding affinities range from ~2 nM to 1 μM (84, 85) and are modulated by a combination of hydrophobic and electrostatic interactions as well as by the conformation of fatty acids within binding sites. For instance, an extended conformation is more favorable than a constrained curved fatty acid conformation (85).

Fatty acid binding sites 1-5 (FA 1-5, Figure 6) have highest affinity for fatty acids since they contain conserved amino acids that form salt-bridges with to the fatty acid carboxylate group and stabilize it within the FA binding pocket (85). Low affinity binding sites (FA6-7) involve mainly hydrophobic interactions.

The fatty acid binding site 1 (FA1, Figure 6) is located within the hydrophobic cavity of the 1B sub-domain. This hydrophobic cavity spans a width of ~17Å (85), and binds fatty acids in the extended conformation which maximizes hydrophobic interactions

and contributes to high affinity for long chain fatty acids at this site. Furthermore, the carboxylate moiety of the fatty acid in sub-domains 1B is stabilized through interactions with arginine 117.

The fatty acid binding site 2 (FA2) is unique in that it is located at the interface of three sub-domains, 1A, 1B and 2A. Fatty acid binding to this site induces a rotation of domain 1 with respect to domain 2 to form hydrophobic cavity, while the fatty acid carboxylate moiety is anchored by Arg 257 and Ser 287 from sub-domain 3A and Tyr 150 from sub-domain 1B. Fatty acid binding sites 3 and 4 (FA3 and FA4) form a T-shaped cavity in the 3A sub-domain. This cavity contains two hydrophylic openings separated by 10 Å. Myristate in the FA3 binding site is stabilized by Ser342 and Arg 348 from 2B and by Arg 485 from 3A sub-domain, while the myristate molecule in the FA4 binding site is stabilized by interactions with Arg410, Tyr411, and Ser489. Myristate in FA4 binds in an extended conformation and is parallel to helices 3 and 4, while myristate in FA3 is perpendicular to these helices. Two fatty acids in the 3A subdomain are in hydrophobic contact with each other suggesting they might bind cooperatively. The fatty acid 5 binding site (FA5) is located in the 3B sub-domain. This cavity is very similar to the FA1 hydrophobic cavity located in the 1B sub-domain and similarly to FA1, the fatty acid in FA5 binds in the extended conformation and is stabilized within this cavity through interactions with lysine 525.

Unlike the 1B and 3B sub-domains, the 2B sub-domain contains no fatty acid binding sites since this sub-domain is confined by the presence of adjacent bulky side chains, such as those of Phe 309, Phe 330 and Tyr 353. Moreover the entrance to this site

is hindered by a short helix (residue 305-311) formed by the 2A-2B linker, which further inhibits binding to this site. However, an additional fatty acid binding site (FA6) is formed at the 2A and 2B sub-domain interface. The FA7 binding site is contained entirely within the sub-domain 2A (also known as drug site I). Both FA6 and FA7 are weak FA binding sites, since they contain no amino acid side-chain residues that can make salt-bridges to the fatty acid carboxylate group.

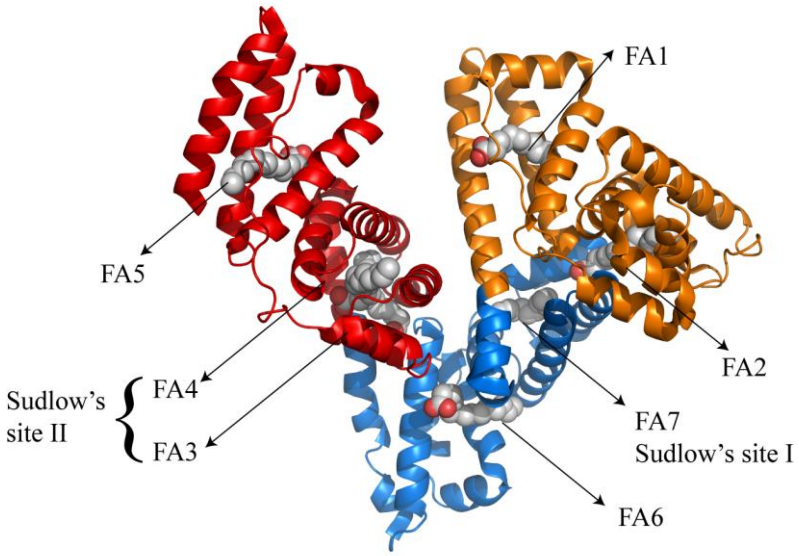

Figure 7. Domain organization of HSA (PDB file1E7H) (86). The HSA domains 1, 2 and 3 are colored orange, blue and red, respectively. Palmitate molecules are shown in space-filling representation to indicate fatty acid binding sites and are colored by atom: carbon (gray), oxygen (red). Drug binding sites are indicated as Sudlow's sites 1 and 2. High affinity fatty acid binding sites are located in 3B, 3A and 1A hydrophobic cavities and are labeled as FA5, FA4, and FA2, respectively.

1.7.2 Drug Binding Sites in HSA

Unlike the fatty acid binding sites, which are distributed throughout the albumin multi-domain structure, exogenous ligands bind mainly in domain 2 (*i.e.* Sudlow's site I) and domain 3 (*i.e.* Sudlow's site II). Both binding sites are located in the A sub-domains and therefore share a common structural motif composed of six helices arranged to form a hydrophobic cavity with distinct polar features defined by helices 1, 2 and 6. The 1A sub-domain cavity is enclosed by the 2A sub-domain and therefore does not contain any drug binding site. The opening of the sub-domain 3A cavity is exposed to solvent, while the 2A subdomain binding site faces the 3A sub-domain and is therefore more constricted. In addition, while Sudlow's site II is confined mainly within domain 3, Sudlow's site I is formed by residues from 1B, 2B and 3A. Typical site I ligands are bulky heterocyclic anions with a charge situated in a central position of the molecule, whereas drugs that are bound in site II are generally aromatic carboxylic acids with an extended conformation and the negative charge located at one end of the molecule. The diversity of the ligands that bind site II and the ability of this site to bind more than one ligand at the same time have been interpreted as the result of flexibility in this region and/or of the presence of different but overlapping sub-sites within site I. Albumin mainly binds hydrophobic drugs, however the selectivity of the biding sites is mainly dictated by the charged/polar albumin residues present in the vicinity of the hydrophobic cavities that similarly to FA stabilize exogenous ligands within the binding pockets.

1.8 BIOMOLECULAR NMR SPECTROSCOPY

In order to investigate the interactions between the Aβ peptide and inhibitory proteins such as human serum albumin we have used saturation transfer difference (STD) (88-91) and off-resonance relaxation (ORR) NMR experiments (92). While ORR NMR experiments are discussed in more detail in Chapter 2, here we will mainly focus on the STD experiments. Although the STD experiments were initially developed to screen binding of small molecules to proteins, they are an efficient tool to probe Aβ self-association as well (91). The main strength of STD experiments is the high sensitivity to weak binding (88-90). Weak binding occurs also in the initial lag Aβ self-association phase and therefore STD experiments are ideally suited to study early self-association processes. The STD experiments rely on the selective RF saturation of the protein resonances, as indicated in Figure 8(a). When probing protein: ligand interactions, selective protein saturation is easily achievable through a train of Gaussian pulses applied outside of the spectral region of and the ligand and selectively at the protein resonances (*i.e.* ~0 ppm) (88-90). From the point of saturation, saturation then transfers to the whole protein through spin-diffusion and then to the interacting ligands through chemical exchange, resulting in a decreased ligand signal. The extent of ligand signal loss depends on the protein: ligand proximity and therefore saturation transfer experiments can be used to map ligand binding epitopes.

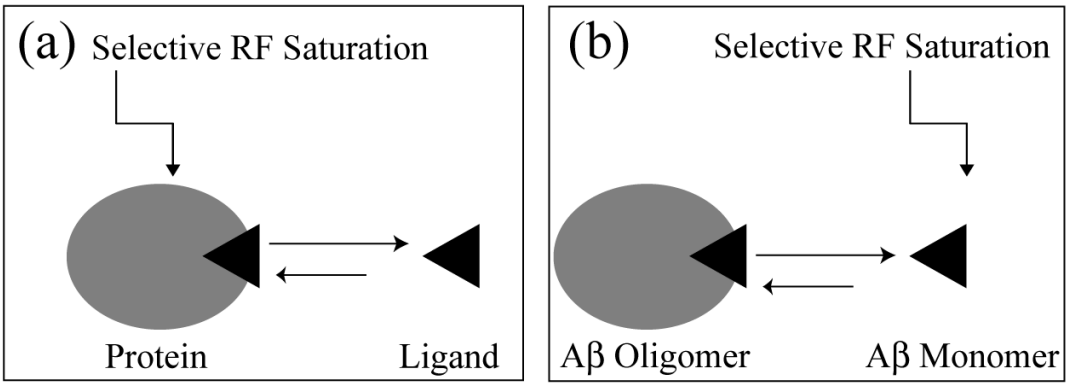

Figure 8: Comparison between STD experiments as applied to Protein /Ligand (a) and Aβ Oligomer/Aβ Monomer (b) systems.

When probing Aβ self-association selective oligomer saturation is not possible. This is mainly due to the oligomer signals not being directly observable by solution NMR and also due to the possible overlap of the monomeric and oligomeric Aβ signals. Therefore, as indicated in Figure 8(b), saturation is introduced mainly through RF irradiation of the monomeric Aβ signal, followed by magnetization transfer via chemical exchange to the interacting Aβ oligomers (91). Fast magnetization diffusion though oligomers provides efficient Aβ oligomer saturation, after which saturation is transferred back to the Aβ monomers, which are directly NMR observable. Since Aβ monomers serve a double purpose, *i.e.* to introduce and to detect magnetization, artifacts can be introduced via offset effects (*i.e.* saturation of spectral regions close to the saturation frequencies), monomer intra-molecular cross-relaxation and incomplete oligomer saturation (91). Huang *et al.* demonstrated that offset effect extend 350 Hz outside the saturated frequency and are therefore effectively eliminated by quantifying the STD

effect through spectral regions that are far from the saturation ppm values. Biases due to cross-relaxation and incomplete oligomer saturation can be evaluated by averaging the results measured at different saturation frequencies (91).

1.9 THESIS OVERVIEW

Chapter 2: Analysis and Parametric Optimization of ^{1}H Off-Resonance Relaxation NMR Experiments Designed to Map Polypeptide Self-Recognition and Other Non-Covalent Interactions (Milojevic et al. J. Phys. Chem. B, 2006)

The initial goal of the project involved the optimization of non selective off-resonance ^{1}H relaxation experiments designed to probe sparsely populated Aβ oligomeric states. As explained in *Chapter 2* this experiment was designed to map at residue resolution polypeptide self-recognition during the early stages of oligomerization. The key feature of this experiment is the initial application of the off-resonance spin lock pulse at the angle of 35.5^{o}, which ensures cancelation of cross-relaxation. The resulting self-relaxation rates are increase monotonically with the correlation times and therefore with the molecular size. The efficiency of the nonselective off-resonance ^{1}H relaxation NMR experiment was demonstrated on the Aβ (12-28) peptide in acetate buffer (pH 4.7). Three key parameters, *i.e.* the static magnetic field ($B0$), the tilt angle (θ) of the effective field and the interscan relaxation delay that precedes the spin-lock at the beginning of the

pulse sequence, were optimized and a general guideline for the optimal setup of this experiment was proposed.

Chapter 3: Understanding the Molecular Basis for the Inhibition of the Alzheimer's Aβ-Peptide Oligomerization by Human Serum Albumin Using Saturation Transfer Difference and Off-Resonance Relaxation NMR Spectroscopy (Milojevic et al. JACS, 2007)

NMR is ideally suited to probe interactions involving small MW solutes. Therefore we have used NMR to investigate the Aβ species interacting with albumin through the comparative analysis of Aβ in its albumin inhibited and oligomer filtrated states, as explained in *Chapter 3*. Specifically, the perturbations in the Aβ samples were monitored through saturation transfer difference and nonselective off-resonance relaxation experiments. This combined NMR strategy reveals a mechanism for the oligomerization inhibitory function of HSA, according to which HSA targets preferentially the soluble oligomers of Aβ (12-28). Moreover we show that albumin selectively interacts with the high MW aggregates as opposed to low MW aggregates and monomers at pH 4.7. We propose a model according to which HSA specifically caps the exposed hydrophobic patches located at the growing and/or transiently exposed sites of the Aβ oligomers, thereby blocking the addition of further monomers and the growth of the prefibrilar assemblies.

Chapter 4: Human Serum Albumin Inhibits Aβ Fibrillization through a 'Monomer-Competitor' Mechanism (Milojevic et al. Biophys. J., 2009)

We have investigated the Aβ-HSA interactions using a combined experimental strategy based on saturation transfer difference (STD) NMR, intrinsic albumin fluorescence and thyoflavin T fluorescence experiments. Several models such as ''monomer competitor'', ''monomer stabilizer'' or a ''dissociation catalyst'' were considered for the Aβ:HSA interactions. Our data consistently show that albumin selectively binds to cross-β-structured Aβ as opposed to Aβ monomers through a "monomer competitor" model. We show that the proposed "monomer competitor" model applies not only for the albumin interactions involving Aβ (12–28) peptide at pH 4.7 but also applies to the physiological Aβ (1–40), and Aβ (1–42) peptides at physiological pH values.

Chapter 5 Stoichiometry and Affinity of the Human Serum Albumin – Alzheimer's Aβ Peptide Interactions (Milojevic et al. Biophys. J., 2011)

For the purposed of identifying the HSA domains involved in Aβ binding, we sub-cloned the HSA gene, isolated individual albumin domains and tested them against Aβ as described in *Chapter 5*. The Aβ oligomer-albumin complexes were investigated through a

generally applicable experimental strategy which combined saturation transfer and off-resonance relaxation NMR experiments with ultrafiltration, domain deletions, and dynamic light scattering. Our results show that the Aβ oligomers are recognized by albumin through largely independent binding sites that are evenly partitioned across the three albumin domains and that bind the Aβ oligomers with similar dissociation constants in the 1–100 nM range, as assessed based on a Scatchard-like model of the albumin inhibition isotherms. Our data not only explain why albumin is able to inhibit amyloid formation at physiological nM Aβ concentrations, but are also consistent with the presence of a single high affinity albumin-binding site per Aβ protofibril, which avoids the formation of extended insoluble aggregates.

Chapter 6: Investigating the Determinants of the Alzheimer's Aβ Peptide Biding to Human Serum Albumin: NMR Study of the HSA Domain 3: Aβ Interactions

Although in chapter 5 we have identified the Aβ oligomers binding domains, each domain contains in turn two sub-domains, A and B, separated by a flexible loop. We wanted to know if both or only one of the sub-domains contributed to Aβ binding. Therefore the individual sub-domains (3A and 3B) were subcloned, expressed and purified and tested against Aβ to show that both sub-domains are involved in Aβ binding. In addition, several domain 3 mutants known to disrupt fatty acid and affect ligand

binding, such as R410AY411A, S489A, R485A, S489AR485A, were also tested for Aβ binding as well (87), revealing that the determinants for Aβ binding are different from those for FA binding. Furthermore, we have monitored changes in the domain 3 ^{15}N-^{1}H HSQC spectrum induced by Aβ binding and identified a peptide region of albumin that displays significant inhibitory potency towards Aβ self-association. Interestingly, the identified Aβ binding region matches with a peptide region of HSA that is prone to self-associate into amyloid fibrils.

Chapter 7: Concluding Remarks and Outlook on Future Developments

In this chapter we will summarize the key results achieved in this thesis and we then proceed to outline the key questions that we believe should be addressed in future studies of Aβ-HSA interactions.

REFERENCES

1. Rozga, M., M. Kloniecki, A. Jablonowska, M. Dandlez and W. Bal 2007. The binding constant for amyloid A beta 40 peptide interaction with human serum albumin. Biochem. Biophys. Res. Commun. 364, 714-718.

2. Reyes Barcelo, A. A., F.J. Gonzalez-Velasquez and M.A. Moss 2009. Soluble aggregates of the amyloid-beta peptide are trapped by serum albumin to enhance amyloid-beta activation of endothelial cells. Journal of Biological Engineering. 3, 5.

3. Biere, A. L., B. Ostaszewski, E.R. Stimson, B.T. Hyman, J.E. Maggio and D.J. Selkoe 1996. Amyloid beta-peptide is transported on lipoproteins and albumin in human plasma. J. Biol. Chem. 271, 32916-32922.

4. Bohrmann, B., L. Tjernberg, P. Kuner, S. Poli, B. Levet-Trafit, J. Naslund, G. Richards, W. Huber, H. Dobeli and C. Nordstedt 1999. Endogenous proteins controlling amyloid beta-peptide polymerization - possible implications for beta-amyloid formation in the central nervous system and in peripheral tissues. J. Biol. Chem. 274, 15990-15995.

5. Bruinsma, I. B., A. Karawajczyk, G. Schaftenaar, R.M.W. de Waal, M.M. Verbeek and F.L. van Delft 2011. A rational design to create hybrid beta-sheet breaker peptides to inhibit aggregation and toxicity of amyloid-beta. Med.chem.comm. 2, 60-64.

6. Querfurth, H. W. and F.M. LaFerla 2010. MECHANISMS OF DISEASE alzheimer's disease. N. Engl. J. Med. 362, 329-344.

7. Gebhardt, F. M.andP. R. Dodd 2009. Metabolic Abnormalities in Alzheimer Disease. Metabolic Encephalopathy, 483-530

8. Bell, R. D. and B.V. Zlokovic 2009. Neurovascular mechanisms and blood-brain barrier disorder in alzheimer's disease. Acta Neuropathol. 118, 103-113.

9. Cai, X. D., T.E. Golde and S.G. Younkin 1993. Release of excess amyloid beta-protein from a mutant amyloid beta-protein precursor. Science. 259, 514-516.

10. Suzuki, N., T.T. Cheung, X.D. Cai, A. Odaka, L. Otvos, C. Eckman, T.E. Golde and S.G. Younkin 1994. An increased percentage of long amyloid-beta protein secreted by familial amyloid-beta protein-precursor (beta-app(717)) mutants. Science. 264, 1336-1340.

11. Glenner, G. G. and C.W. Wong 1984. Alzheimers-disease - initial report of the purification and characterization of a novel cerebrovascular amyloid protein. Biochem. Biophys. Res. Commun. 120, 885-890.

12. Haass, C., E.H. Koo, A. Mellon, A.Y. Hung and D.J. Selkoe 1992. Targeting of cell-surface beta-amyloid precursor protein to lysosomes - alternative processing into amyloid-bearing fragments. Nature. 357, 500-503.

13. Thinakaran, G. and E.H. Koo 2008. Amyloid precursor protein trafficking, processing, and function. J. Biol. Chem. 283, 29615-29619.

14. Cam, J. A. and G. Bu 2006. Modulation of beta-amyloid precursor protein trafficking and processing by the low density lipoprotein receptor family. Molecular Neurodegeneration. 1, 8.

15. del Zoppo, G. J. 2009. Bleeding in the brain amyloid-beta may keep clots away. Nat. Med. 15, 1132-1133.

16. De Strooper, B. and W. Annaert 2000. Proteolytic processing and cell biological functions of the amyloid precursor protein. J. Cell. Sci. 113, 1857-1870.

17. Jang, H., F.T. Arce, S. Ramachandran, R. Capone, R. Azimova, B.L. Kagan, R. Nussinov and R. Lal 2010. Truncated beta-amyloid peptide channels provide an alternative mechanism for alzheimer's disease and down syndrome. Proc. Natl. Acad. Sci. U. S. A. 107, 6538-6543.

18. Kaether, C. and C. Haass 2004. A lipid boundary separates APP and secretases and limits amyloid beta-peptide generation. J. Cell Biol. 167, 809-812.

19. Dong, J., K. Lu, A. Lakdawala, A.K. Mehta and D.G. Lynn 2006. Controlling amyloid growth in multiple dimensions. Amyloid-Journal of Protein Folding Disorders. 13, 206-215.

20. Strodel, B., J.W.L. Lee, C.S. Whittleston and D.J. Wales 2010. Transmembrane structures for alzheimer's A beta(1-42) oligomers. J. Am. Chem. Soc. 132, 13300-13312.

21. (a) Ahmed, M., J. Davis, D. Aucoin, T. Sato, S. Ahuja, S. Aimoto, J.I. Elliott, W.E. Van Nostrand and S.O. Smith 2010. Structural conversion of neurotoxic amyloid-beta(1-42) oligomers to fibrils. Nature Structural & Molecular Biology. 17, 561-568. (b) Chimon, S., M.A. Shaibat, C.R. Jones, D.C. Calero, B. Aizezi and Y. Ishii 2007. Evidence of fibril-like beta-sheet structures in a neurotoxic amyloid intermediate of alzheimer's beta-amyloid. Nature Structural & Molecular Biology. 14, 1157-1164.

22. Haass, C. and D.J. Selkoe 2007. Soluble protein oligomers in neurodegeneration: Lessons from the alzheimer's amyloid beta-peptide. Nature Reviews Molecular Cell Biology. 8, 101-112.

23. Varadarajan, S., S. Yatin, M. Aksenova and D.A. Butterfield 2000. Review: Alzheimer's amyloid beta-peptide-associated free radical oxidative stress and neurotoxicity. J. Struct. Biol. 130, 184-208.

24. Gable, C.C., 2009, The Oligomer Structures and Toxicity, The Open Biology Journal, 222-227

25. Rauk, A. 2008. Why is the amyloid beta peptide of alzheimer's disease neurotoxic? Dalton Transactions., 1273-1282.

26. Hortschansky, P., V. Schroeckh, T. Christopeit, G. Zandomeneghi and M. Fandrich 2005. The aggregation kinetics of alzheimer's beta-amyloid peptide is controlled by stochastic nucleation. Protein Science. 14, 1753-1759.

27. Crescenzi, O., S. Tomaselli, R. Guerrini, S. Salvadori, A.M. D'Ursi, P.A. Temussi and D. Picone 2002. Solution structure of the alzheimer amyloid beta-peptide (1-42) in an apolar microenvironment - similarity with a virus fusion domain. European Journal of Biochemistry. 269, 5642-5648.

28. Tomaselli, S., V. Esposito, P. Vangone, N.A.J. van Nuland, A.M.J.J. Bonvin, R. Guerrini, T. Tancredi, P.A. Temussi and D. Picone 2006. The alpha-to-beta conformational transition of alzheimer's A beta-(1-42) peptide in aqueous media is reversible: A step by step conformational analysis suggests the location of beta conformation seeding. Chembiochem. 7, 257-267.

29. Miyashita, N., J.E. Straub and D. Thirumalai 2009. Structures of beta-amyloid peptide 1-40, 1-42, and 1-55-the 672-726 fragment of APP-in a membrane environment with implications for interactions with gamma-secretase. J. Am. Chem. Soc. 131, 17843-17852.

30. Zhang, S., K. Iwata, M.J. Lachenmann, J.W. Peng, S. Li, E.R. Stimson, Y. Lu, A.M. Felix, J.E. Maggio and J.P. Lee 2000. The alzheimer's peptide A beta adopts a collapsed coil structure in water. J. Struct. Biol. 130, 130-141.

31. Triguero, L., R. Singh and R. Prabhakar 2008. Comparative molecular dynamics studies of wild-type and oxidized forms of full-length alzheimer amyloid beta-peptides A beta(1-40) and A beta(1-42). J Phys Chem B. 112, 7123-7131.

32. Vitalis, A. and A. Caflisch 2010. Micelle-like architecture of the monomer ensemble of alzheimer's amyloid-beta peptide in aqueous solution and its implications for A beta aggregation. J. Mol. Biol. 403, 148-165.

33. Vivekanandan, S., J.R. Brender, S.Y. Lee and A. Ramamoorthy 2011. A partially folded structure of amyloid-beta(1-40) in an aqueous environment. Biochem. Biophys. Res. Commun. 411, 312-316.

34. Hou, L. M., H.Y. Shao, Y.B. Zhang, H. Li, N.K. Menon, E.B. Neuhaus, J.M. Brewer, I.J.L. Byeon, D.G. Ray, M.P. Vitek, T. Iwashita, R.A. Makula, A.B. Przybyla and M.G. Zagorski 2004. Solution NMR studies of the A beta(1-40) and A beta(1-42) peptides establish that the met35 oxidation state affects the mechanism of amyloid formation. J. Am. Chem. Soc. 126, 1992-2005.

35. Ball, K. A., A.H. Phillips, P.S. Nerenberg, N.L. Fawzi, D.E. Wemmer and T. Head-Gordon 2011. Homogeneous and heterogeneous tertiary structure ensembles of amyloid-beta peptides. Biochemistry (N. Y.). 50, 7612-7628.

36. Bitan, G., M.D. Kirkitadze, A. Lomakin, S.S. Vollers, G.B. Benedek and D.B. Teplow 2003. Amyloid beta-protein (A beta) assembly: A beta 40 and A beta 42 oligomerize through distinct pathways. Proc. Natl. Acad. Sci. U. S. A. 100, 330-335.

37. Lesne, S., M.T. Koh, L. Kotilinek, R. Kayed, C.G. Glabe, A. Yang, M. Gallagher and K.H. Ashe 2006. A specific amyloid-beta protein assembly in the brain impairs memory. Nature. 440, 352-357.

38. Streltsov, V. A., J.N. Varghese, C.L. Masters and S.D. Nuttall 2011. Crystal structure of the amyloid-beta p3 fragment provides a model for oligomer formation in alzheimer's disease. Journal of Neuroscience. 31, 1419-1426.

39. Yu, L., R. Edalji, J.E. Harlan, T.F. Holzman, A.P. Lopez, B. Labkovsky, H. Hillen, S. Barghorn, U. Ebert, P.L. Richardson, L. Miesbauer, L. Solomon, D. Bartley, K. Walter, R.W. Johnson, P.J. Hajduk and E.T. Olejniczak 2009. Structural characterization of a soluble amyloid beta-peptide oligomer. Biochemistry (N. Y.). 48, 1870-1877.

40. Urbanc, B., M. Betnel, L. Cruz, G. Bitan and D.B. Teplow 2010. Elucidation of amyloid beta-protein oligomerization mechanisms: Discrete molecular dynamics study. J. Am. Chem. Soc. 132, 4266-4280.

41. Serpell, L. C. 2000. Alzheimer's amyloid fibrils: Structure and assembly. Biochimica Et Biophysica Acta-Molecular Basis of Disease. 1502, 16-30.

42. Ma, B. and R. Nussinov 2006. Simulations as analytical tools to understand protein aggregation and predict amyloid conformation. Curr. Opin. Chem. Biol. 10, 445-452.

43. Luhrs, T., C. Ritter, M. Adrian, D. Riek-Loher, B. Bohrmann, H. Doeli, D. Schubert and R. Riek 2005. 3D structure of alzheimer's amyloid-beta(1-42) fibrils. Proc. Natl. Acad. Sci. U. S. A. 102, 17342-17347.

44. Mawuenyega, K. G., W. Sigurdson, V. Ovod, L. Munsell, T. Kasten, J.C. Morris, K.E. Yarasheski and R.J. Bateman 2010. Decreased clearance of CNS beta-amyloid in alzheimer's disease. Science. 330, 1774-1774.

45. Zlokovic, B. V. 2004. Clearing amyloid through the blood-brain barrier. J. Neurochem. 89, 807-811.

46. Deane, R., Z.H. Wu and B.V. Zlokovic 2004. RAGE (yin) versus LRP (yang) balance regulates alzheimer amyloid beta-peptide clearance through transport across the blood-brain barrier. Stroke. 35, 2628-2631.

47. DeMattos, R. B., K.R. Bales, D. J. Cummins, J.-C. Dodart, S. M.Paul and D. M. Holtzman 2001. Peripheral anti-Aβ antibody alters CNS and plasma Aβ clearance and decreases brain Aβ burden in a mouse model of Alzheimer's disease. Proc. Natl. Acad. Sci. U. S. A. 98:8850–8855.

48. Llewellyn, D. J., K.M. Langa, R.P. Friedland and I.A. Lang 2010. Serum albumin concentration and cognitive impairment. Current Alzheimer Research. 7, 91-96.

49. Boada, M., P. Ortiz, F. Anaya, I. Hernandez, J. Munoz, L. Nunez, J. Olazaran, I. Roca, G. Cuberas, L. Tarraga, M. Buendia, R.P. Pla, I. Ferrer and A. Paez 2009. AMYLOID-TARGETED THERAPEUTICS IN ALZHEIMER'S DISEASE: USE OF HUMAN ALBUMIN IN PLASMA EXCHANGE AS A NOVEL APPROACH FOR A beta MOBILIZATION. Drug News & Perspectives. 22, 325-339.

50. Dong, J., C.A. Peters-Libeu, K.H. Weisgraber, B.W. Segelke, B. Rupp, I. Capila, M.J. Hernaiz, L.A. LeBrun and R.J. Linhardt 2001. Interaction of the N-terminal domain of apolipoprotein E4 with heparin. Biochemistry (N. Y.). 40, 2826-2834.

51. Petrlova, J., H. Hong, D.A. Bricarello, G. Harishchandra, G.A. Lorigan, L. Jin and J.C. Voss 2011. A differential association of apolipoprotein E isoforms with the amyloid-beta oligomer in solution. Proteins-Structure Function and Bioinformatics. 79, 402-416.

52. Sharman, M. J., M. Morici, E. Hone, T. Berger, K. Taddei, I.J. Martins, W.L.F. Lim, S. Singh, M.R. Wenk, J. Ghiso, J.D. Buxbaum, S. Gandy and R.N. Martins 2010.

APOE genotype results in differential effects on the peripheral clearance of amyloid-beta(42) in APOE knock-in and knock-out mice. Journal of Alzheimers Disease. 21, 403-409.

53. Luo, J., J. Marechal, S. Warmlander, A. Graslund and A. Peralvarez-Marin 2010. In silico analysis of the apolipoprotein E and the amyloid beta peptide interaction: Misfolding induced by frustration of the salt bridge network. Plos Computational Biology. 6, 1-7.

54. Tamamizu-Kato, S., J.K. Cohen, C.B. Drake, M.G. Kosaraju, J. Drury and V. Narayanaswami 2008. Interaction with amyloid peptide compromises the lipid binding function of apolipoprotein E. Biochemistry (N. Y.). 47, 5225-5234.

55. Thambisetty, M., A. Simmons, L. Velayudhan, A. Hye, J. Campbell, Y. Zhang, L. Wahlund, E. Westman, A. Kinsey, A. Guntert, P. Proitsi, J. Powell, M. Causevic, R. Killick, K. Lunnon, S. Lynham, M. Broadstock, F. Choudhry, D.R. Howlett, R.J. Williams, S.I. Sharp, C. Mitchelmore, C. Tunnard, R. Leung, C. Foy, D. O'Brien, G. Breen, S.J. Furney, M. Ward, I. Kloszewska, P. Mecocci, H. Soininen, M. Tsolaki, B. Vellas, A. Hodges, D.G.M. Murphy, S. Parkins, J.C. Richardson, S.M. Resnick, L. Ferrucci, D.F. Wong, Y. Zhou, S. Muehlboeck, A. Evans, P.T. Francis, C. Spenger and S. Lovestone 2010. Association of plasma clusterin concentration with severity, pathology, and progression in alzheimer disease. Arch. Gen. Psychiatry. 67, 739-748.

56. Matsubara, E., B. Frangione and J. Ghiso 1995. Characterization of apolipoprotein J-alzheimers A-beta interaction. J. Biol. Chem. 270, 7563-7567.

57. Calero, M., A. Rostagno, E. Matsubara, B. Zlokovic, B. Frangione and J. Ghiso 2000. Apolipoprotein J (clusterin) and alzheimer's disease. Microsc. Res. Tech. 50, 305-315.

58. Yerbury, J. J., S. Poon, S. Meehan, B. Thompson, J.R. Kumita, C.M. Dobson and M.R. Wilson 2007. The extracellular chaperone clusterin influences amyloid formation and toxicity by interacting with prefibrillar structures. Faseb Journal. 21, 2312-2322.

59. Oda, T., P. Wals, H.H. Osterburg, S.A. Johnson, G.M. Pasinetti, T.E. Morgan, I. Rozovsky, W.B. Stine, S.W. Snyder, T.F. Holzman, G.A. Krafft and C.E. Finch 1995. Clusterin (apoj) alters the aggregation of amyloid beta-peptide (A-beta(1-42)) and forms slowly sedimenting A-beta complexes that cause oxidative stress. Exp. Neurol. 136, 22-31.

60. Mishra, V. K., M.N. Palgunachari, J.S. Hudson, R. Shin, T.D. Keenum, N.R. Krishna and G.M. Anantharamaiah 2011. Structure and lipid interactions of an anti-

inflammatory and anti-atherogenic 10-residue class G* apolipoprotein J peptide using solution NMR. Biochimica Et Biophysica Acta-Biomembranes. 1808, 498-507.

61. Navab, M., G.M. Anantharamaiah, S.T. Reddy, B.J. Van Lenten, A.C. Wagner, S. Hama, G. Hough, E. Bachini, D.W. Garber, V.K. Mishra, M.N. Palgunachari and A.M. Fogelman 2005. An oral ApoJ peptide renders HDL antiinflammatory in mice and monkeys and dramatically reduces atherosclerosis in apolipoprotein E-null mice. Arteriosclerosis Thrombosis and Vascular Biology. 25, 1932-1937.

62. Sagare, A., R. Deane, R.D. Bell, B. Johnson, K. Hamm, R. Pendu, A. Marky, P.J. Lenting, Z. Wu, T. Zarcone, A. Goate, K. Mayo, D. Perlmutter, M. Coma, Z. Zhong and B.V. Zlokovic 2007. Clearance of amyloid-beta by circulating lipoprotein receptors. Nat. Med. 13, 1029-1031.

63. Giunta, S., R. Galeazzi, M. Marcellini, E.H. Corder and L. Galeazzi 2007. The inflammation-sensitive protein alpha 1-anti-chymotrypsin neutralizes fibrillar aggregation and cytotoxicity of the beta-amyloid peptide more effectively than alpha 1-antitrypsin. Clin. Biochem. 40, 887-892.

64. Powers, G. A., C.L.L. Pham, M.C. Pearce, G.J. Howlett and S.P. Bottomley 2007. Serpin acceleration of amyloid fibril formation: A role for accessory proteins. J. Mol. Biol. 366, 666-676.

65. Aksenov, M. Y., M.V. Aksenova, J.M. Carney and D.A. Butterfield 1996. Alpha 1-antichymotrypsin interaction with A beta(1-42) does not inhibit fibril formation but attenuates the peptide toxicity. Neurosci. Lett. 217, 117-120.

66. Elliott, P. R., D.A. Lomas, R.W. Carrell and J.P. Abrahams 1996. Inhibitory conformation of the reactive loop of alpha(1)-antitrypsin. Nat. Struct. Biol. 3, 676-681.

67. Kinghorn, K. J., D.C. Crowther, L.K. Sharp, C. Nerelius, R.L. Davis, H.T. Chang, C. Green, D.C. Gubb, J. Johansson and D.A. Lomas 2006. Neuroserpin binds A beta and is a neuroprotective component of amyloid plaques in alzheimer disease. J. Biol. Chem. 281, 29268-29277.

68. Du, Y. S., B.H. Ni, M. Glinn, R.C. Dodel, K.R. Bales, Z.Y. Zhang, P.A. Hyslop and S.M. Paul 1997. Alpha(2)-macroglobulin as a beta-amyloid peptide-binding plasma protein. J. Neurochem. 69, 299-305

69. Mettenburg, J. M., S. Arandjelovic and S.L. Gonias 2005. A chemically modified preparation of alpha 2-macroglobulin binds beta-amyloid peptide with increased affinity and inhibits A beta cytotoxicity. J. Neurochem. 93, 53-62.

70. Mettenburg, J. M., D.J. Webb and S.L. Gonias 2002. Distinct binding sites in the structure of alpha(2)-macroglobulin mediate the interaction with beta-amyloid peptide and growth factors. J. Biol. Chem. 277, 13338-13345.

71. Mettenburg, J. M. and S.L. Gonias 2005. Beta-amyloid peptide binds equivalently to binary and ternary alpha(2)-macroglobulin-protease complexes. Protein Journal. 24, 89-93.

72. Morais, V. A. and B. De Strooper 2010. Mitochondria dysfunction and neurodegenerative disorders: Cause or consequence. Journal of Alzheimers Disease. 20, S255-S263.

73. Lustbader, J. W., M. Cirilli, C. Lin, H.W. Xu, K. Takuma, N. Wang, C. Caspersen, X. Chen, S. Pollak, M. Chaney, F. Trinchese, S.M. Liu, F. Gunn-Moore, L.F. Lue, D.G. Walker, P. Kuppusamy, Z.L. Zewier, O. Arancio, D. Stern, S.S.D. Yan and H. Wu 2004. ABAD directly links A beta to mitochondrial toxicity in alzheimer's disease. Science. 304, 448-452.

74. Yan, Y. L., Y.Z. Liu, M. Sorci, G. Belfort, J.W. Lustbader, S.S. Yan and C.Y. Wang 2007. Surface plasmon resonance and nuclear magnetic resonance studies of ABAD-A beta interaction. Biochemistry (N. Y.). 46, 1724-1731.

75. Hoyer, W., C. Gronwall, A. Jonsson, S. Stahl and T. Hard 2008. Stabilization of a beta-hairpin in monomeric alzheimer's amyloid-beta peptide inhibits amyloid formation. Proc. Natl. Acad. Sci. U. S. A. 105, 5099-5104.

76. Hoyer, W. and T. Hard 2008. Interaction of alzheimer's A beta peptide with an engineered binding protein - thermodynamics and kinetics of coupled folding-binding. J. Mol. Biol. 378, 398-411.

77. Hatters, D. M., N. Zhong, E. Rutenber and K.H. Weisgraber 2006. Amino-terminal domain stability mediates apolipoprotein E aggregation into neurotoxic fibrils. J. Mol. Biol. 361, 932-944.

78. Taboada, P., S. Barbosa, E. Castro and V. Mosquera 2006. Amyloid fibril formation and other aggregate species formed by human serum albumin association. J Phys Chem B. 110, 20733-20736.

79. Kissinger, C. R., P.A. Rejto, L.A. Pelletier, J.A. Thomson, R.E. Showalter, M.A. Abreo, C.S. Agree, S. Margosiak, J.J. Meng, R.M.A.D. Vanderpool, B. Li, A.

Tempczyk-Russell and J.E. Villafranca 2004. Crystal structure of human ABAD/HSD10 with a bound inhibitor: Implications for design of alzheimer's disease therapeutics. J. Mol. Biol. 342, 943-952.

80. Kim, S. J., J.R. Woo, E.J. Seo, M.H. Yu and S.E. Ryu 2001. A 2.1 angstrom resolution structure of an uncleaved alpha(1)-antitrypsin shows variability of the reactive center and other loops. J. Mol. Biol. 306, 109-119.

81. Dong, J., C.A. Peters-Libeu, K.H. Weisgraber, B.W. Segelke, B. Rupp, I. Capila, M.J. Hernaiz, L.A. LeBrun and R.J. Linhardt 2001. Interaction of the N-terminal domain of apolipoprotein E4 with heparin. Biochemistry (N. Y.). 40, 2826-2834.

82. Wang, G. S., G.K. Pierens, W.D. Treleaven, J.T. Sparrow and R.J. Cushley 1996. Conformations of human apolipoprotein E(263-286) and E(267-289) in aqueous solutions of sodium dodecyl sulfate by CD and H-1 NMR. Biochemistry (N. Y.). 35, 10358-10366.

83. Sugio, S., A. Kashima, S. Mochizuki, M. Noda and K. Kobayashi 1999. Crystal structure of human serum albumin at 2.5 angstrom resolution. Protein Eng. 12, 439-446.

84. Petitpas, I., T. Grune, A.A. Bhattacharya and S. Curry 2001. Crystal structures of human serum albumin complexed with monounsaturated and polyunsaturated fatty acids. J. Mol. Biol. 314, 955-960.

85. Curry, S., H. Mandelkow, P. Brick and N. Franks 1998. Crystal structure of human serum albumin complexed with fatty acid reveals an asymmetric distribution of binding sites. Nat. Struct. Biol. 5, 827-835.

86. Bhattacharya, A. A., T. Grune and S. Curry 2000. Crystallographic analysis reveals common modes of binding of medium and long-chain fatty acids to human serum albumin. J. Mol. Biol. 303, 721-732.

87. Simard, J. R., P.A. Zunszain, C.E. Ha, J.S. Yang, N.V. Bhagavan, I. Petitpas, S. Curry and J.A. Hamilton 2005. Locating high-affinity fatty acid-binding sites on albumin by x-ray crystallography and NMR spectroscopy. Proc. Natl. Acad. Sci. U. S. A. 102, 17958-17963.

88. Mayer, M. and B. Meyer 1999. Characterization of ligand binding by saturation transfer difference NMR spectroscopy RID A-8828-2008. Angewandte Chemie-International Edition. 38, 1784-1788.

89. Angulo, J. and P.M. Nieto 2011. STD-NMR: Application to transient interactions between biomolecules-a quantitative approach. European Biophysics Journal with Biophysics Letters. 40, 1357-1369.

90. Mayer, M. and T. James 2002. Detecting ligand binding to a small RNA target via saturation transfer difference NMR experiments in D2O and H2O. J. Am. Chem. Soc. 124, 13376-13377.

91. Huang, H., J. Milojevic and G. Melacini 2008. Analysis and optimization of saturation transfer difference NMR experiments designed to map early self-association events in amyloidogenic peptides. J Phys Chem B. 112, 5795-5802.

92. Milojevic, J., V. Esposito, R. Das and G. Melacini 2006. Analysis and parametric optimization of H-1 off-resonance relaxation NMR experiments designed to map polypeptide self-recognition and other noncovalent interactions. J Phys Chem B. 110, 20664-20670

ANALYSIS AND PARAMETRIC OPTIMIZATION OF ^{1}H OFF-RESONANCE RELAXATION NMR EXPERIMENTS DESIGNED TO MAP POLYPEPTIDE SELF-RECOGNITION AND OTHER NON-COVALENT INTERACTIONS

CHAPTER 2

Chapter Two Preface

This work has been published in:

Milojevic, J., V. Esposito, R. Das and G. Melacini 2006. Analysis and parametric optimization of H-1 off-resonance relaxation NMR experiments designed to map polypeptide self-recognition and other noncovalent interactions. J Phys Chem B. 110, 20664-20670

Permission has been granted by the publisher to reproduce the material here.

I conducted all the experiments and data analysis described in this chapter.

G. Melacini conducted theoretical treatments. V. Esposito provided assistance in the data analysis.

ANALYSIS AND PARAMETRIC OPTIMIZATION OF ^{1}H OFF-RESONANCE RELAXATION NMR EXPERIMENTS DESIGNED TO MAP POLYPEPTIDE SELF-RECOGNITION AND OTHER NON-COVALENT INTERACTIONS

Milojevic, J., V. Esposito, R. Das and G. Melacini 2006 J Phys Chem B. 110, 20664-20670

ABSTRACT: The measurement of ^{1}H off-resonance non-selective relaxation rates ($R_{\theta,ns}$) has been recently proposed as an effective method to probe peptide self-recognition, opening new perspectives in the understanding of the pre-fibrillization oligomerization processes in amyloidogenesis. However, a full analysis and parametric optimization of the NMR experiments designed to measure $R_{\theta,ns}$ relaxation rates is still missing. Here we analyze the dependence of the $R_{\theta,ns}$ rates upon three critical parameters: the tilt angle of the effective field during the spin lock, the static magnetic field and finally the repetition delay. Our analysis reveals that the tilt angle $\theta = 35.5^{o}$ not only minimizes spin-diffusion, but also avoids experimental artifacts such as J-transfer and poor adiabaticity. In addition, we found that when the dominant relaxation mechanism is caused by uncorrelated pair-wise ^{1}H dipole - ^{1}H dipole interactions the $R_{35.5^{o},ns}$ rate is not significantly affected by static field variations, suggesting a wide applicability of the ^{1}H off-resonance non-selective relaxation experiment. Finally, we show that the self-recognition maps based on the comparative analysis of the $R_{35.5^{o},ns}$ rates can tolerate decreases in the inter-scan delays without significantly compromising the identification of critical self-association loci. These considerations provide not only a better

understanding of the ^{1}H off-resonance non-selective relaxation, but they also serve as guidelines for the optimal set up of this experiment.

INTRODUCTION

We have recently proposed (1) a non-selective off-resonance ^{1}H relaxation NMR experiment (Figure 1) designed to map at residue resolution polypeptide self-recognition during the early stages of oligomerization.

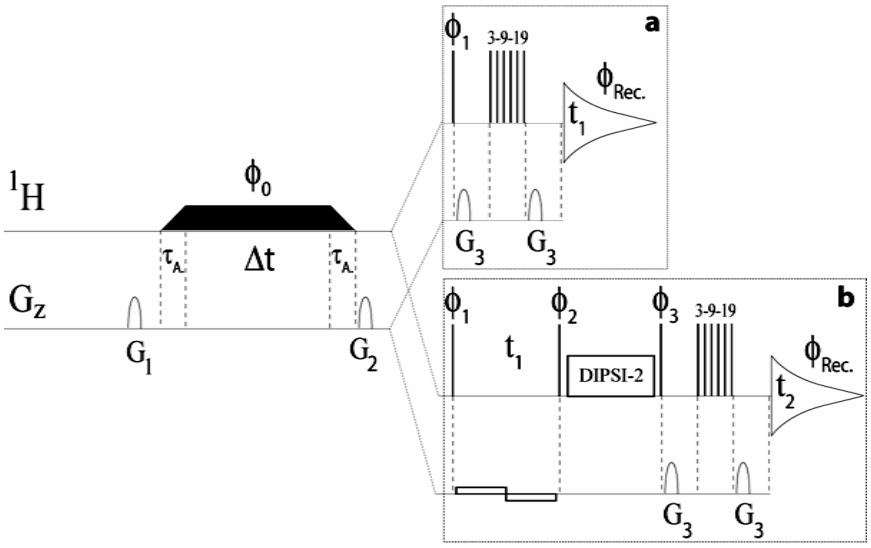

Figure 1. Pulse sequences for the measurement of non-selective off-resonance relaxation rates with one- (a) and two- (b) dimensional detection. The phases, gradients and other parameters for the pulse sequence in panel (b) are the same as those in Figure 2 of reference (1). For the 1D version of the experiment (*i.e.* 1a) $\phi_1 = (x)_2 (-x)_2$ and $\phi_{rec.} = (x)_2 (-x)_2$, while all the remaining parameters are as in panel (b).

The proposed non-selective off-resonance ^{1}H relaxation NMR pulse sequence (Figure 1) is obtained from the well-established 1D-Watergate (Figure 1a) or 2D-TOCSY (Figure 1b) experiments (2-5) inserting an adiabatic spin-lock (6-9) between the inter-scan delay and the first 90^o pulse of the 1D or 2D detection block (Figure 1). One of the most significant applications of these pulse sequences is to the growing class of amyloidogenic peptides related to several neurodegenerative diseases such as Alzheimer's and Parkinson's for which the reversible self-association preceding full fibrillization represents a promising target for the early pharmacological treatment (10-15). Other NMR experiments such the CPMG pulse train designed to measure spin-spin (R_2) relaxation rates and the selective R_1 ($R_{1,s}$) measurements can be used to probe self-recognition (16) because, when the main relaxation mechanism arises from ^{1}H-^{1}H dipolar-dipolar interactions, these rates are linearly proportional to the spectral density term evaluated at zero frequency, which in turn is linearly proportional to the correlation time (τ_c) (16-20). However, the implementation of both CPMG and $R_{1,s}$ NMR measurements is experimentally challenging due to concurrent scalar coupling (J) evolution during CPMG sequences and to the necessary selectivity for $R_{1,s}$ experiments that limits their application only to small molecules and requires multiple measurements for multiple resolved protons. All these limitations are overcome by the proposed non-selective off-resonance ^{1}H relaxation NMR experiment. The J evolution typical of the CPMG train is avoided by setting the relaxation spin-lock off-resonance (6-9, 21,22) and the selectivity requirements of $R_{1,s}$ experiments are effectively eliminated since the

relaxation of all protons is monitored simultaneously in the proposed off-resonance experiment (1).

The efficiency of the non-selective off-resonance ^{1}H relaxation NMR experiment[1] has been demonstrated by its application to the Aβ (12-28) peptide in acetate buffer (pH 4.7), which has been shown to be a good model for the early stages of the Aβ fibrillization (23). Specifically, the non-selective off-resonance ^{1}H relaxation NMR measurement identified the 16 ± 1 to 22 ± 1 segment as the main site of self-recognition in agreement with previous mutagenesis studies (24, 25). However, despite the promising potential of the non-selective off-resonance ^{1}H relaxation NMR experiments for mapping pre-fibrillization equilibria a full analysis and parametric optimization of this pulse sequence is still not available. Here we focus on the analysis of the non-selective off-resonance ^{1}H relaxation experiments with respect to three key parameters, *i.e.* the static magnetic field (B_o), the tilt angle (θ) of the effective field and finally the inter-scan relaxation delay that precedes the spin-lock influencing the initial spin polarization state at the beginning of the off-resonance relaxation. Based on these analyses we propose general guidelines for the optimal set up of this experiment.

MATERIALS AND METHODS

2D Non-selective Off-Resonance Experiment: All data were collected using an AV700 Bruker spectrometer operating at 700 MHz. Off-resonance relaxation data were acquired

using the recently published non-selective off-resonance relaxation 2D-TOCSY pulse sequence (1). The off-resonance spin lock with the trapezoidal shape including two adiabatic pulses of 4 ms duration was applied at the angle of 35.5^{o} for 5 ms, 23 ms, 42 ms, 60 ms and 80 ms. The relaxation delay between the end of the acquisition and the start of the first adiabatic pulse was 1 sec. The strength of the off-resonance spin lock was 8.23 kHz. For the detection a 45 ms long DIPSI-2 pulse train with strength of 10 kHz was used. 16 scans and 128 dummy scans were employed in each experiment; two replicas were collected for each data set both for 1mM Aβ (12-28) and for 0.1mM Aβ (12-28). The spectral widths for both dimensions were 8389.26 Hz with 256 and 1024 t_1 and t_2 complex points, respectively. Water suppression was achieved through a Watergate scheme implemented with the binomial 3-9-19 pulse train (2).

All 2D replica sets were added and processed using Xwinnmr (Bruker Inc.). The 2D cross-peak intensities were measured using Sparky 3.111 (26) by Gaussian line fitting and determination of fit heights (1). The fit heights error was estimated by calculating the standard deviation for the distribution of differences in intensities of identical peaks in duplicate spectra (27). After the addition of the replicate spectra the error was scaled up proportionally to the square root of the total number of scans. For residues [15-19], [21-24], and [26-28] the TOCSY $H_{\alpha,i}$-$H_{N,i}$ cross-peaks were used for data analysis, whereas for the N-terminal residues V_{12} and $H_{14,}$ the $H_{\alpha,12}$-$H_{Me,12}$ and the $H_{\alpha,14}$-$H_{\beta h,14}$ cross-peaks were used since the $H_{\alpha,i}$-$H_{N,i}$ cross-peaks were affected by the fast exchange with water. Similarly, the $H_{\alpha,20}$-$H_{N,20}$ and the $H_{\alpha,26}$-$H_{N,26}$ cross-peaks were partially overlapped and therefore required the use of the $H_{\alpha,20}$-$H_{\beta l,20}$ cross-peak as reporter of the signal decay

during the off-resonance spin-lock. Due to the overlap of its degenerate H_α protons, G25 was omitted from the analysis of the off- resonance relaxation rates (1). The initial rates of decay were obtained through the program Curvefit (28) that implements a Levenberg-Marquardt non-linear least squares exponential fitting of the fit height decay measured for each cross-peak. The related errors were obtained as previously published (1). The rates and errors obtained were normalized with respect to the largest measured rate and smoothed by an *i,i+1* moving window (1). No averaging was possible for V12, V24 and K28 due the lack of data at the following residues and actual values were used. In all analyses the previously established assignment (1, 23) was employed. The off-resonance relaxation data with a relaxation delay of 2 s were measured previously (1).

Non-selective T_1 Measurements: Non-selective T_1 values for the H_α protons of Aβ (12-28) were estimated using the inversion recovery (IR) experiment with delays of 100 ms, 300 ms, 450 ms, and 600 ms and an relaxation delay of 4 sec. 16 scans and 128 dummy scans were collected for each experiment. A composite (90_x 180_y 90_x) pulse was employed for the non-selective inversion to minimize pulse imperfections. For the detection of the inversion recovery, a 2D-TOCSY was used and set up as the previous 2D-TOCSY employed as detection block of the non-selective off-resonance measurements. Due to the long repetition delay necessary for inversion recovery experiments, the data acquisition for each IR point took on the average about ~10-12 hours. The data were processed using Xwinnmr (Bruker Inc.). The intensities of the TOCSY $H_{\alpha,i}$-$H_{N,i}$ cross-peaks were obtained using Sparky (26) fit heights and were plotted

as a function of the inversion recovery delay, τ. The estimated $T_{1,ns,eff.}$ values fell in the 0.5 s - 0.9 s range.

THEORETICAL TREATMENT

At first order approximation, the decay of the magnetization of a generic spin *i* (I_{iZ}) aligned along the off-resonance spin-lock axis (OZ) is:

$$I_{iZ,\Delta t} = I_{iZ,0} + \left(\frac{dI_{iZ}}{dt}\right)_0 \Delta t \qquad (1)$$

where $I_{iZ,0}$ and $I_{iZ,\Delta t}$ are the values of I_{iZ} at the start and at the end of the Δt delay (Figure 1), respectively, and $\left(\frac{dI_{iZ}}{dt}\right)_0$ is the value of $\frac{dI_{iZ}}{dt}$ at the start of the Δt delay. Assuming that the only non-negligible relaxation mechanism arises from uncorrelated pair-wise ^{1}H dipole-dipole interactions and that contributions from chemical exchange are negligible because weak binding affinities (K_D > high μM) such as those previously measured for the Aβ (12-28) peptide (23,29) fall within the fast exchange regime (16), $\left(\frac{dI_{iZ}}{dt}\right)_0$ can be computed through the Solomon equations for the multi-tilted rotating frame of *n* homo-nuclear spins I_i (6-9):

$$\frac{dI_{iZ}}{dt} = -\sum_j \rho_{ij}^{/} I_{iZ} - \sum_j \sigma_{ij}^{/} I_{jZ} + c\sum_j (\rho_{ij} + \sigma_{ij}) I_{eq.} \qquad (2)$$

with:

$$\rho_{ij}^{/} = c^2 \rho_{ij} + s^2 \lambda_{ij} \qquad (3)$$

$$\sigma_{ij}^{/} = c^2\sigma_{ij} + s^2\mu_{ij} \qquad (4)$$

where j is any spin different from spin i, c = cos(θ), s = sin(θ) (where θ is the tilt angle, *i.e.* the angle formed by the longitudinal axis of the laboratory frame and the effective spin-lock axis), ρ_{ij} and σ_{ij} are the laboratory frame rates of longitudinal direct and cross relaxation, respectively, while λ_{ij} and μ_{ij} are the rotating frame rates of transverse direct and cross relaxation, respectively. ρ'_{ij} and σ'_{ij} are the respective effective rates of direct and cross relaxation along the direction of the effective field and $I_{eq.}$ is the equilibrium magnetization of spin i. At the beginning of the Δt delay, equation (2) becomes:

$$\left(\frac{dI_{iZ}}{dt}\right)_0 = -\sum_j \rho_{ij}^{/} I_{iZ,0} - \sum_j \sigma_{ij}^{/} I_{jZ,0} + c\sum_j (\rho_{ij} + \sigma_{ij}) I_{eq.} \qquad (5)$$

If the inter-scan delay is significantly longer than $1/R_{1,ns}$, then $I_{iZ,0} \cong I_{jZ,0} \cong I_{eq.}$ and equation (1) becomes:

$$I_{iZ,\Delta t} = I_{iZ,0}\left\{1 - \left[\sum_j \rho_{ij}^{/} + \sum_j \sigma_{ij}^{/} - c\sum_j (\rho_{ij} + \sigma_{ij})\right]\Delta t\right\} \qquad (6)$$

This means that the initial rate of decay for spin i in the non-selective off-resonance experiment (defined as $R_{\theta,ns}^{i}$) is:

$$R_{\theta,ns}^{i} = \sum_j \rho_{ij}^{/} + \sigma_{ij}^{/} - c\left(\rho_{ij} + \sigma_{ij}\right) \qquad (7)$$

Based on equations (3) and (4), equation (7) can be recast as:

$$R_{\theta,ns}^{i} = (c-1)c\sum_j \left(\rho_{ij} + \sigma_{ij}\right) + s^2\sum_j \left(\lambda_{ij} + \mu_{ij}\right) \quad (8a)$$

Considering that $R^i_{1,ns} = \sum_j \left(\rho_{ij} + \sigma_{ij}\right)$ and that $R^i_2 = \sum_j \left(\lambda_{ij} + \mu_{ij}\right)$, equation 8a can in turn be re-written as equation 8b (29, 30):

$$R^i_{\theta,ns} = (c-1)cR^i_{1,ns} + s^2 R^i_2 \qquad (8b)$$

Both equations 8a and 8b, can be evaluated using the spectral densities computed on the assumption that the relaxation is caused by the modulation of ^1H_i-^1H_j dipole-dipole interactions through isotropic Brownian rotations (31):

$$\begin{aligned}
\rho_{ij} &= J(0) + 3J(\omega_0) + 6J(2\omega_0) \\
\sigma_{ij} &= -J(0) + 6J(2\omega_0) \\
\lambda_{ij} &= \frac{5}{2}J(0) + \frac{9}{2}J(\omega_0) + 3J(2\omega_0) \\
\mu_{ij} &= 2J(0) + 3J(\omega_0)
\end{aligned} \qquad (9)$$

with ω_o being the proton Larmor frequency and $J(\omega)$ being the Lorentzian spectral density function:

$$J(\omega) = \frac{\gamma_H{}^4 h^2}{40\pi^2 r_{ij}^6} \frac{\tau_c}{1+\omega^2\tau_c^2} \qquad (10)$$

In equation (10) h is the Planck constant, γ_H is the proton gyromagnetic ratio, τ_c is the correlation time, and r_{ij} is the inter-nuclear distance between protons i and j (16).

In principle the θ values are in the range 0^o-90^o. However, the $\theta = 35.5^o$ value is particularly interesting because when $\theta = 35.5^o$ the off-resonance spin-lock effective

dipolar cross-relaxation rate approaches zero in the spin-diffusion limit ($\sigma_{ij}^{/} \cong 0$) due to NOE/ROE compensation (Figure 2b) (1). As a result the cross-talk between spins with different non-selective off-resonance relaxation rates is minimized. Furthermore, in the spin-diffusion limit $R_{1,ns}^{i}$ approaches zero as well (Figure 2a, b) and hence equation (7) simplifies to:

$$R_{35.5^o,ns}^{i} \cong \sum_{j} \rho_{ij}^{/} \quad \text{(in the spin-diffusion limit)} \qquad (11)$$

Since the term on the right is the selective self-relaxation rate along the spin-lock field tilted at 35.5°, equation (11) can be recast as:

$$R_{35.5^o,ns}^{i} \cong R_{35.5^o,s}^{i} \quad \text{(in the spin-diffusion limit)} \qquad (12)$$

In other words, for $\theta = 35.5^o$ the non-selective off-resonance relaxation rate in the spin-diffusion limit does not differ significantly from the selective off-resonance self-relaxation rate. In conclusion, in the spin diffusion limit and when $\theta = 35.5^o$ an easily implementable non-selective NMR experiment offers information similar to that provided by a more experimentally challenging selective measurement.

RESULTS AND DISCUSSION

Based on the theoretical framework described above we have analyzed how the static magnetic field (B_o), the effective field tilt angle (θ) and finally the inter-scan relaxation delay affect the non-selective off-resonance ^{1}H relaxation rates ($R^i_{\theta,ns}$). Given the importance of the 35.5° tilt angle as mentioned above, we will start the analysis assuming $\theta = 35.5^o$.

The Effect of the Static Magnetic Field B_o

The plots of the ^{1}H relaxation rates R_2, $R_{1,s}$, $R_{1,ns}$ and $R_{35.5^o,ns}$ *vs*. the logarithm of τ_c in seconds have been calculated at five static fields ranging from 300 MHz to 700 MHz using the model discussed above (Figure 2a). Figure 2a reveals that the effect of B_o on the τ_c dependence of the calculated ^{1}H relaxation rates follows three distinct patterns in different τ_c regions. First, for low τ_c values (*i.e.* $\log_{10}(\tau_c/\text{sec}) < \sim -10$) all ^{1}H relaxation rates (*i.e.* R_2, $R_{1,s}$, $R_{1,ns}$ and $R_{35.5^o,ns}$) are only minimally and almost negligibly dependent on B_o (Figure 2a). This result common to all the simulated ^{1}H relaxation rates is explained by the previous model considering that all spectral densities are computed through equation (10) in which the B_o dependence is formalized by the $(\omega\tau_c)^2$ term in the denominator. When $\log_{10}(\tau_c/\text{sec}) < \sim -10$, then the $(\omega\tau_c)^2$ term in equation (10) becomes less relevant explaining the absence of significant B_o dependence at low τ_c values (Figure 2a).

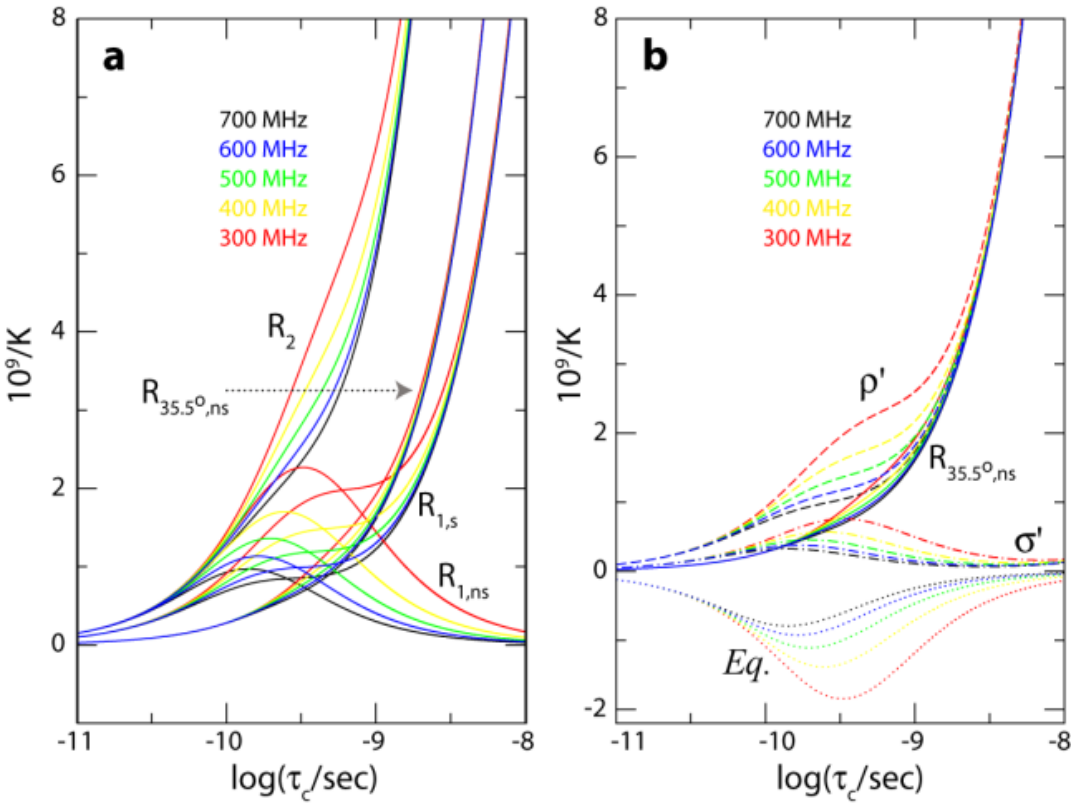

Figure 2. Static magnetic field (Bo) dependence of relaxation rates vs. the correlation time (τc) for a model two spin system where $K = \hbar^2\gamma H^4/10r_{ij}6$. (a) τc dependence of the non-selective ($R_{1,ns}$) and selective ($R_{1,s}$) longitudinal relaxation rates as well as of the transverse relaxation rate for in-phase magnetization (R2) and of the non-selective off-resonance relaxation rate at the tilt angle $\theta = 35.5^o$ ($R_{35.5^o,ns}$) at different Bo fields. The proton Larmor frequencies are color coded as indicated in the two panels. (b) τc dependence of the self- (ρ', dashed line), cross-relaxation (σ', dot-dashed line) and equilibrium ($-\cos(35.5^o)R_{1,ns}$, dotted line) components of $R_{35.5^o,ns}$ (solid line) at different Bo fields.

A similar quasi - B_o independent behavior is observed also at high τ_c values (i.e. $\log_{10}(\tau_c/\text{sec}) > \sim -8.5$), however with the exception of $R_{1,ns}$ which is still significantly affected by B_o even for $\log_{10}(\tau_c/\text{sec}) > \sim -8.5$ (Figure 2a). This observation is accounted for by the previous model considering that the R_2, $R_{1,s}$ and $R_{35.5^o,ns}$ rates but not the $R_{1,ns}$ rate contain a J(0) term which increases proportionally with τ_c and does not depend on the

static field as indicated by equation (10) explaining the absence of significant B_o dependence at high τ_c values for R_2, $R_{1,s}$ and $R_{35.5^o,ns}$. On the contrary, $R^i_{1,ns} = \sum_j \left(\rho_{ij} + \sigma_{ij}\right)$ and therefore based on equation (9) does not depend on J(0) terms. In the other spectral density functions that define $R_{1,ns}$ the $(\omega\tau_c)^2$ term in equation (10) introduces a significant B_o dependence on $R_{1,ns}$ due to the high τ_c values, accounting for the B_o effects on $R_{1,ns}$ observed at $\log_{10}(\tau_c/\text{sec}) > \sim -8.5$ in Figure 2a.

Finally, at intermediate τ_c values (*i.e.* $\sim -10 \leq \log_{10}(\tau_c/\text{sec}) \leq \sim -8.5$) a third distinct pattern is seen (Figure 2a). Unlike the previous low and high τ_c regions, at $-10 \leq \log_{10}(\tau_c/\text{sec}) \leq \sim -8.5$ all R_2, $R_{1,s}$, $R_{1,ns}$ and $R_{35.5^o,ns}$ relaxation rates are affected by B_o (Figure 2a). While for R_2, $R_{1,s}$ and $R_{1,ns}$ the B_o dependency is quite dramatic, for $R_{35.5^o,ns}$ the effect of B_o is only minimal at intermediate τ_c values (Figure 2a and 3ab). This unusual behavior specific of $R_{35.5^o,ns}$ is explained by Figure 2b showing the dissection of $R_{35.5^o,ns}$ in terms of self- (ρ'), cross-relaxation (σ') and equilibrium ($-\cos(35.5^o)R_{1,ns} = -c\left(\rho_{ij} + \sigma_{ij}\right)$) components as indicated by equation (7). Inspection of Figure 2b reveals that the absolute values of all three $R_{35.5^o,ns}$ components (*i.e.* ρ', σ' and $\cos(35.5^o)R_{1,ns}$) increase at lower B_o. However, due to the negative sign of the equilibrium term in equation (7) the effect of B_o on ρ' and σ' is compensated by that on $\cos(35.5^o)R_{1,ns}$ explaining the marginal dependence of $R_{35.5^o,ns}$ on B_o (Figure 2a,b). This compensatory mechanism explains also why the $R_{35.5^o,ns}$ rates are minimally affected by B_o increases above 700 MHz, up to static fields of at least 900 MHz as seen in Figure 3 showing how

$R_{35.5^o,ns}$ depends on B_o at two representative τ_c values. As a result for the remaining Figures and related discussion we will assume a static field of 700 MHz.

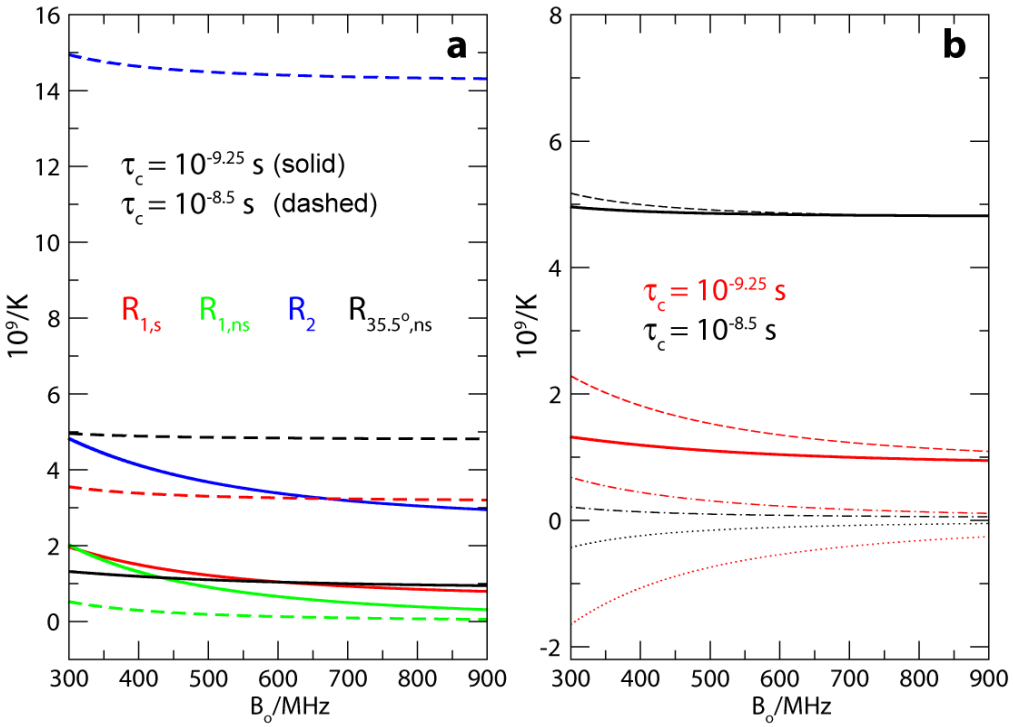

Figure 3. Plots of relaxation rates *vs.* static magnetic field (B_o) for selected values of the correlation time τ_c. (a) B_o dependence of $R_{1,ns}$, $R_{1,s}$, R_2 and $R_{35.5^o,ns}$ relaxation rates at the τ_c values $10^{-9.25}$ s and $10^{-8.5}$ s. The color and the solid/dashed line coding are as indicated in panel (a). (b) B_o dependence of the components of the $R_{35.5^o,ns}$ relaxation rate at the τ_c values $10^{-9.25}$ s (red) and $10^{-8.5}$ s (black). The coding for solid, dashed, dotted and dot-dashed lines is as explained in panel (b) of Figure 2.

The Tilt Angle (θ) Dependence

The tilt angle (θ) defines the orientation with respect to the laboratory frame z-axis of the effective field generated by the off-resonance spin-lock. The effect of the tilt angle on

the non-selective off-resonance relaxation rates ($R^i_{\theta,ns}$) is described by equation (8b), showing that $R^i_{\theta,ns}$ results essentially from a linear combination of $R^i_{1,ns}$ and R^i_2 with coefficients (c-1)c and s^2, respectively, where c = cos(θ) and s = sin(θ) with θ ranging in principle from 0^o to 90^o. If $\theta = 0^o$, which corresponds to a negligible spin-lock strength relative to its offset, then equation (8b) predicts that $R^i_{\theta,ns} = 0$ (Figure 4a) consistently with the absence of significant perturbations caused by the spin-lock (Figure 1). If $\theta = 90^o$, which corresponds to a negligible spin-lock offset relative to its strength, then equation (8b) predicts that $R^i_{\theta,ns} = R^i_2$ (Figure 4a) consistently with the effective field being essentially in the xy plane (Figure 1). As θ increases from 0^o to 90^o, the $R^i_{\theta,ns}$ rate increases monotonically from the τ_c independent zero value to R^i_2, with the $R^i_{\theta,ns}$ increments being more significant at lower θ values (Figure 4a).

Among the θ angles in the 0^o - 90^o range, the θ value 35.5^o is particularly interesting because, as mentioned above, at $\theta = 35.5^o$ and in the spin diffusion limit $\sigma'_{ij} \cong 0$ (Figure 4bc) due to NOE/ROE compensation thus minimizing the cross-talk between different spins during the relaxation. Furthermore, at $\theta = 35.5^o$ the non-selective and the selective off-resonance relaxation rates converge in the spin-diffusion limit (equation 12) (Figure 4bc).

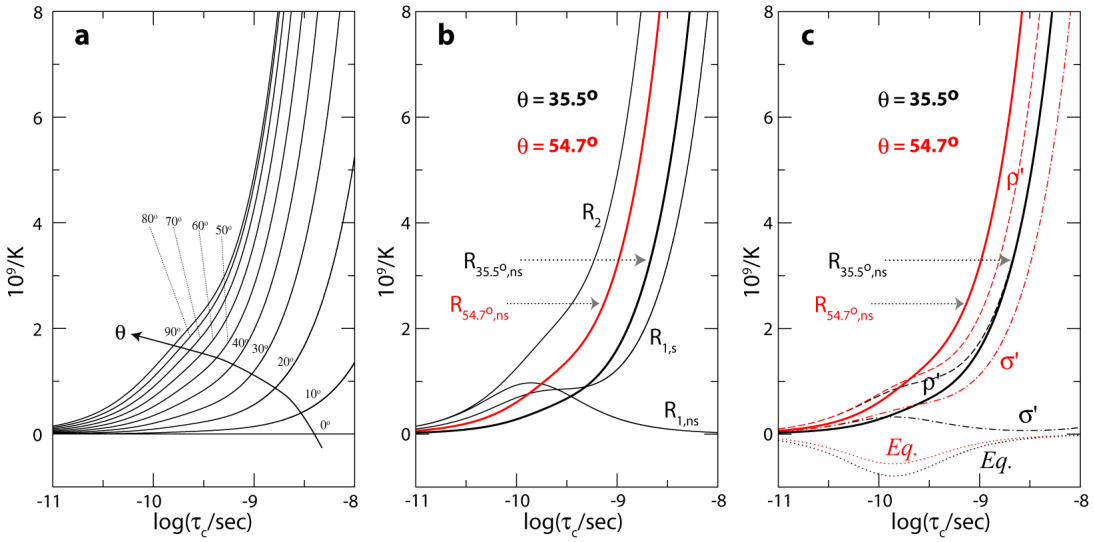

Figure 4. Tilt angle (θ) dependence of the relaxation rates *vs.* the correlation time (τ_c) for a model two spin system at 700 MHz. (a) Plots of $R_{\theta,ns}$ *vs.* τ_c for θ ranging from 0° to 90°. (b) τ_c dependence of the non-selective off-resonance relaxation rates at the tilt angles $\theta = 35.5°$ ($R_{35.5°,ns}$) and $\theta = 54.7°$ ($R_{54.7°,ns}$). For reference purposes the non-selective ($R_{1,ns}$) and selective ($R_{1,s}$) longitudinal relaxation rates as well as the transverse relaxation rate for in-phase magnetization (R_2) are shown. (c) τ_c dependence of the self- (ρ', dashed line), cross-relaxation (σ', dot-dashed line) and equilibrium ($-\cos(35.5°)R_{1,ns}$, dotted line) components of $R_{\theta,ns}$ (solid line) at the tilt angles $\theta = 35.5°$ and $\theta = 54.7°$. Other details are as in Figure 2. The data referring to $\theta = 35.5°$ is included in Figure 4bc as well for the purpose of facilitating the comparison between $\theta = 35.5°$ and $\theta = 54.7°$. The tilt angles are color coded as indicated in panels b and c.

Another tilt angle (θ) value at which the non-selective and the selective off-resonance relaxation rates are linearly proportional to each other in the spin-diffusion limit is $\theta = 54.7°$. At this θ value $\rho_{ij}^{/}$ is equal to $2\sigma_{ij}^{/}$ independently of the correlation time τ_c (6-9). Therefore, considering again that in the spin-diffusion limit $R_{1,ns}^{i}$ is negligible as compared to the effective dipolar self-relaxation rate $\rho_{ij}^{/}$, equation (8) leads to:

$$R_{54.7°,ns}^{i} \cong 1.5\sum_{j}\rho_{ij}^{/} \text{ (in the spin-diffusion limit)} \qquad (13)$$

Since $\sum_j \rho_{ij}^{/}$ is the selective self-relaxation rate along the spin-lock field tilted at 54.7°, we have:

$$R^i_{54.7^o,ns} \cong 1.5 R^i_{54.7^o,s} \text{ (spin-diffusion limit)} \quad (14)$$

as can also be seen in Figure 4c. In other words, in the spin-diffusion limit the non-selective off-resonance relaxation rate is linearly related to the selective self-relaxation rate both for $\theta = 35.5^o$ and for $\theta = 54.7^o$ (Figure 4bc). When $\theta = 35.5^o$ there is the added advantage that the effective cross-relaxation rate is negligible ($\sigma_{ij}^{/} \cong 0$), as mentioned above, thus minimizing the cross-talk between different spins that is particularly efficient in the spin-diffusion limit. When $\theta = 54.7^o$ the effective cross-relaxation rate is not negligible any more and the non selective off-resonance relaxation at $\theta = 54.7^o$ is faster than at $\theta = 35.5^o$ (Figure 4bc) increasing the probability that the peaks generated by the NMR pulse sequences displayed in Figure 1 decay under the noise for long Δt relaxation delays. This problem could be avoided by using very short Δt delays, however when the Δt duration approaches that of the adiabatic pulses (Figure 1), the θ angle is ill defined. Based on these considerations, the 35.5° value for the tilt angle θ is still preferred to $\theta =$ 54.7°. Values of the θ angle significantly higher than 54.7° are not recommended as J-transfer effects and poor adiabaticity may compromise the off-resonance experiments described in Figure 1. Values of the θ angle significantly lower than 35.5° are not advisable because at $\theta < 35.5^o$ the sensitivity of $R^i_{\theta,ns}$ to τ_c increases is only minimal and again the cross-talk between different relaxing spins is active. In conclusion, 35.5° is still

the preferred optimal value for the tilt angle θ and the remaining part of the discussion will assume $\theta = 35.5^{o}$.

The Repetition Delay Dependence

The time between the first digitized point and the beginning of the trapezoidal spin-lock in the pulse sequences of Figure 1 defines the inter-scan repetition delay denoted as T_c (*i.e.* T_c = relaxation delay + acquisition time). The main effect of T_c is on the initial polarization at the start of the off-resonance relaxation spin-lock (Figure 1). If T_c is significantly (i.e. ~five-fold) longer than the effective time-constant for the longitudinal relaxation during the inter-scan delay ($1/R_{1,ns,eff}$) then the initial polarization at the start of the off-resonance relaxation spin-lock is similar to its equilibrium value: $I_{iZ,0} \cong I_{jZ,0} \cong I_{eq.}$ as assumed before to derive equation (6) from equation (5). However, if T_c is reduced to speed up the non-selective off-resonance measurement then the $I_{iZ,0} \cong I_{jZ,0} \cong I_{eq.}$ assumption doesn't apply any more. A better approximation is:

$$I_{iZ,0} \cong I_{jZ,0} \cong I_{eq.}\varepsilon \quad (14)$$

where: $\varepsilon \approx 1 - e^{-T_c R_{1,ns,eff}}$ (15) based on the Ernst angle theory (5). As a result, equation (7) above has to be modified to:

$$R^{i}_{\theta,ns} = \varepsilon\left(\sum_{j}\rho^{/}_{ij} + \sigma^{/}_{ij}\right) - c\left(\rho_{ij} + \sigma_{ij}\right) \quad (16)$$

Using this equation the $R_{35.5^o,ns}$ *vs.* $\log(\tau_c/\text{sec})$ plots were re-computed for three different scenarios corresponding to $T_c = 1.122$ sec and increasing values of $1/R_{1,ns,eff.}$ (i.e. $1/R_{1,ns,eff.} = 0.5$ sec and $1/R_{1,ns,eff.} = 0.9$ sec) (Figure 5a).

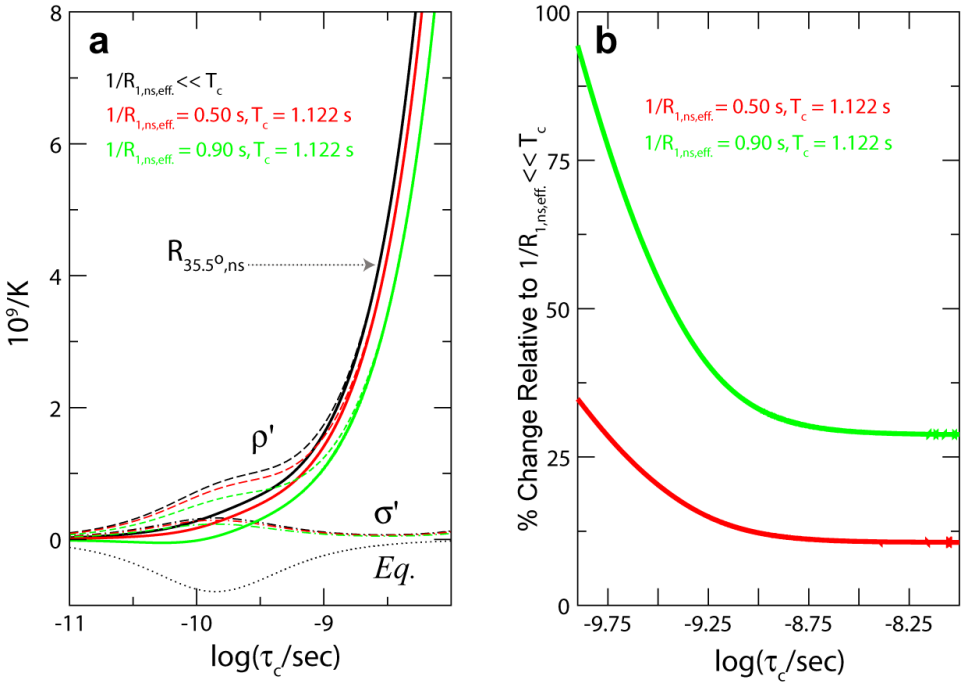

Figure 5. Inter-scan delay (T_c) dependence of the relaxation rates *vs.* the correlation time (τ_c) plots for a model two spin system. (a) Three different representative scenarios for the inter-scan delay (T_c) dependence are shown and color coded as indicated in the Figure. The τ_c dependence of the self- (ρ'), cross-relaxation (σ') and equilibrium ($-\cos(35.5^o)R_{1,ns}$) components of $R_{35.5^o,ns}$ are reported for each scenario at a static field of 700 MHz. Other details are as in the Figure describing the tilt angle dependence (Figure 4). The effective time-constant for the longitudinal relaxation during the inter-scan delay is $1/R_{1,ns,eff.}$. (b) Percent change of $R_{35.5^o,ns}$ *vs.* τ_c at $1/R_{1,ns,eff} = 0.5$ s (red) and 0.9 s (green) relative to the $1/R_{1,ns,eff.} << T_c$ scenario.

These $R_{1,ns,eff}$ values are representative for the range spanned by the H_α protons of the Aβ (12-28) peptide as indicated by our inversion recovery measurements. Figure 5a shows that in all three scenarios considered ($1/R_{1,ns,eff.} << T_c$; $1/R_{1,ns,eff.} = 0.5$ sec; $1/R_{1,ns,eff.} = 0.9$ sec) the $R_{35.5^o,ns}$ rate is monotonically increasing with $\log(\tau_c/sec)$ when τ_c is > sub-ns. In other words, it is possible that $R_{35.5^o,ns}$ is still able to probe self-recognition even when the condition $1/R_{1,ns,eff.} << T_c$ is not fully fulfilled. Figure 5a also shows that as $R_{1,ns,eff.}$ decreases a negative offset is introduced in the $R_{35.5^o,ns}$ *vs*. $\log(\tau_c/sec)$ plots. The main cause of the negative offset is the modulation of the $\left(\sum_j \rho_{ij}^{/} + \sigma_{ij}^{/}\right)$ term in equation (16) above by the factor $\varepsilon < 1$ in equation (15). If this negative offset is expressed in terms of percentage change relative to the reference case of $1/R_{1,ns,eff.} << T_c$ (Figure 5b), then the effect of decreasing $R_{1,ns,eff.}$ rates is more significant at shorter τ_c values rather then when the spin diffusion limit is approached (Figure 5b). This is true for both scenarios with $1/R_{1,ns,eff.} = 0.5$ sec and $1/R_{1,ns,eff.} = 0.9$ sec (Figure 5b). However, as the $1/R_{1,ns,eff}$ values increase the percentage change becomes more and more significant (Figure 5b).

The theoretical predictions illustrated by Figure 5 are supported by the observed non-selective $R_{35.5^o,ns}$ rates at $T_c = 1.122$ sec and by the comparison with the experimental $R_{35.5^o,ns}$ rates at $T_c = 2.122$ sec (Figure 6). Figure 6a displays the plots of $R_{35.5^o,ns}$ *vs*. residue number measured at $T_c = 1.122$ sec for both 1 mM (circles) and 0.1 mM (squares) Aβ (12-28). The trend seen in both Figure 6a plots is similar to that previously observed

for the $R_{35.5^o,ns}$ measurements at T_c = 2.122 sec:[1] at mM concentrations the oligomers in equilibrium with the monomer enhance the $R_{35.5^o,ns}$ rates especially for the central hydrophobic core which is known to be one of the key sites of Aβ self-recognition; at sub-mM concentrations the oligomers dissociate decreasing the $R_{35.5^o,ns}$ rates to values that are to good approximation residue-independent. These results are consistent with our theoretical prediction that even after reducing T_c the $R_{35.5^o,ns}$ rates are still monotonically increasing with τ_c. In addition, the Figure 6a plot measured at 1 mM concentrations (circles) is not significant different from the related plot previously measured for longer T_c values (*i.e.* 2.122 sec) (1), as shown in Figure 6b. However, a different scenario is observed at 0.1 mM concentrations. In the dilute sample the variation of T_c from 1.122 sec to 2.122 sec causes a significant change in the measured $R_{35.5^o,ns}$ rates (Figure 6c). These observations are fully consistent with our simulations (Figure 5b) predicting that T_c variations affect more significantly the $R_{35.5^o,ns}$ rates at lower τ_c values.

The difference plot (Figure 6d) between the two sets of measurements at T_c = 1.122 sec (Figure 6a) is qualitatively similar to that previously observed at T_c = 2.122 sec (1). Both measurements of $R_{35.5^o,ns}$ rates at T_c = 1.122 sec and at T_c = 2.122 sec (1) provide similar results for the identification of the residue segment responsible for self-recognition: residues (16 ± 1, 22 ± 1) for T_c = 2.122 sec and residues (15 ± 1, 22 ± 1) for T_c = 1.122 sec (Figure d), which are within error from each other. We therefore conclude that decreases in the inter-scan repetition delays (T_c) do not necessarily lead to significantly different self-recognition maps. However, despite the time-saving achieved by lowering

the T_c value, at lower T_c values the signal-to-noise ratio obviously decreases and the probe and sample heating caused by the spin-lock is less efficiently dissipated.

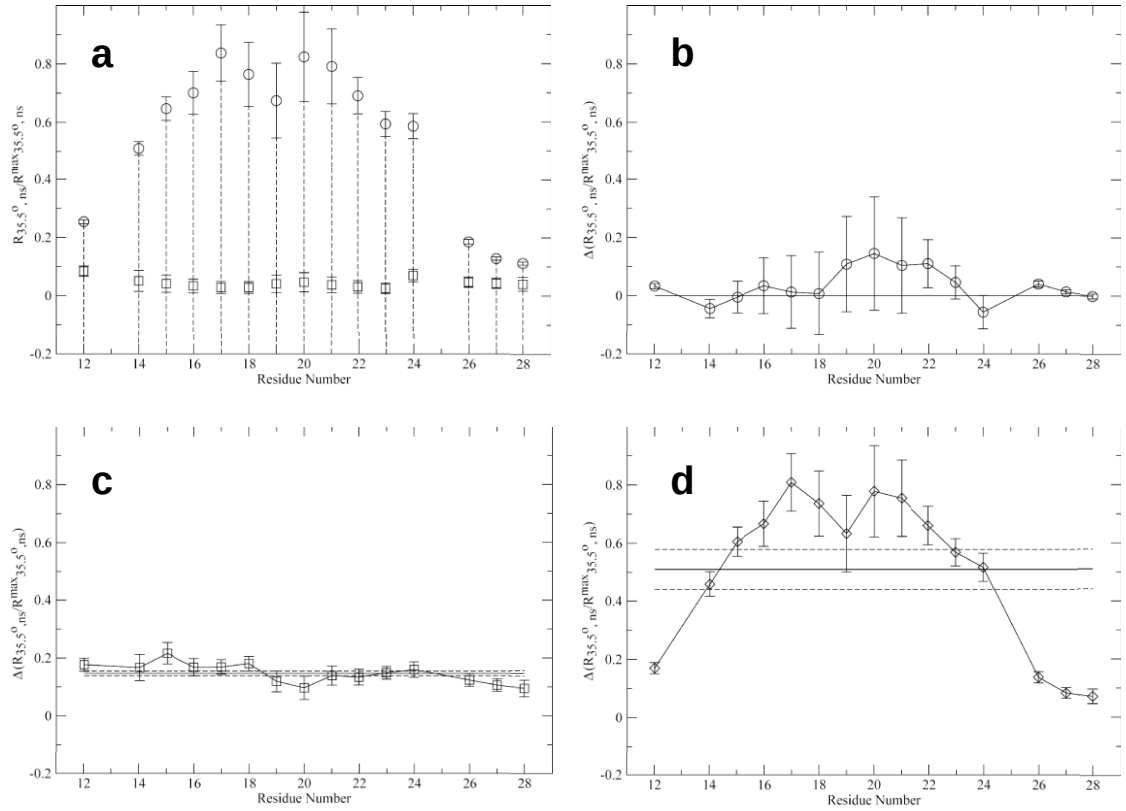

Figure 6. Plot of the relative $R_{35.5^o,ns}$ relaxation rates *vs.* residue number in Aβ (12-28) with sequence H_3N^+-VHHQ$_{15}$KLVFF$_{20}$AEDVG$_{25}$SNK-COO–. All rates were measured at 20 ^{o}C in 50 mM d_4-acetate buffer at pH 4.7 and at 700 MHz. (a) Relative relaxation rates acquired at 1 mM (circles) and 0.1 mM (squares) Aβ(12-28) concentrations with a 1.122 s inter-scan delay (T_c). (b) Difference between the relative $R_{35.5^o,ns}$ relaxation rates of the 1 mM Aβ(12-28) sample acquired with 2.122 s and 1.122 s inter-scan delays. (c) Difference between the relative $R_{35.5^o,ns}$ relaxation rates of the 0.1 mM Aβ (12-28) sample acquired with the 2.122 s and 1.122 s inter-scan delays. Solid and dashed lines indicate mean ± the standard error, respectively. (d) Refers to the difference between the two plots shown in panel (a). The horizontal solid and dashed lines indicate the mean ± the standard error, respectively. All rates and the related errors were computed as previously explained (1).

CONCLUSIONS

In summary, we have analyzed how the ^{1}H off-resonance non-selective relaxation rates ($R_{\theta,ns}$) depend on three key parameters: the tilt angle for the effective field during the off-resonance spin-lock, the static magnetic field and the inter-scan delay. We have found that the tilt angle $\theta = 35.5^o$ is optimal not only for the suppression of spin-diffusion effects but also for the preservation of good adiabaticity, the J-transfer suppression and the sensitivity to peptide self-recognition. Our analysis also revealed that the effect of the static magnetic field on $R_{35.5^o,ns}$ is minimal as compared to other typical ^{1}H relaxation rates (i.e. $R_{1,ns}$, $R_{1,s}$ and R_2) due to the compensation between the equilibrium ($\cos(35.5^o)$ $R_{1,ns}$) term and the self- (ρ') and cross-relaxation (σ') terms. As a result, the proposed ^{1}H off-resonance non-selective $R_{35.5^o,ns}$ experiment is applicable over a wide range of magnetic fields (*i.e.* 300-900 MHz) as the sensitivity and resolution allow. Finally, we show that short inter-scan delays are expected to preserve the monotonic increase of $R_{35.5^o,ns}$ *vs.* τ_c within a wide range of τ_c values. However as the inter-scan delay decreases with respect to $1/R_{1,ns}$ a negative offset is introduced mainly due to the down-scaling of the self- and cross-relaxation rates ρ' and σ'. In relative terms the effect of this negative offset is more significant at short τ_c values, but the proposed experiment is still able to provide reliable self-recognition maps. Overall the ^{1}H off-resonance non-selective $R_{35.5^o,ns}$ measurement emerges as a robust NMR method suitable to probe a variety of non-covalent interactions.

ACKNOWLEDGMENTS: We are grateful to NSERC for financial support and to Hao Huang and Dr. Alex Bain for helpful discussions. VE was supported by a fellowship from the University Federico II of Naples.

REFERENCES:

1. Esposito, V., R. Das and G. Melacini 2005. Mapping polypeptide self-recognition through H-1 off-resonance relaxation. J. Am. Chem. Soc. 127, 9358-9359.

2. Sklenar, V., M. Piotto, R. Leppik and V. Saudek 1993. Gradient-tailored water suppression for H-1-N-15 hsqc experiments optimized to retain full sensitivity. Journal of Magnetic Resonance Series a. 102, 241-245.

3. Messerle, B. A., G. Wider, G. Otting, C. Weber and K. Wuthrich 1989. Solvent suppression using a spin lock in 2d and 3d nmr-spectroscopy with H2O solutions. Journal of Magnetic Resonance. 85, 608-613.

4. Ramamoorthy, A. and N. Chandrakumar 1992. Comparison of the coherence-transfer efficiencies of laboratory-frame and rotating-frame experiments. Journal of Magnetic Resonance. 100, 60-68.

5. Cavanagh, J.,W. J. Fairbrother,A. G. Palmer III and N. J. Skelton 1996. Protein NMR spectroscopy: Principles and practice.

6. Desvaux, H. and P. Berthault 1999. Study of dynamic processes in liquids using off-resonance rf irradiation. Prog Nucl Magn Reson Spectrosc. 35, 295-340.

7. Desvaux, H., P. Berthault, N. Birlirakis and M. Goldman 1994. Off-resonance roesy for the study of dynamic processes. Journal of Magnetic Resonance Series a. 108, 219-229.

8. Bain, A. D. and G.J. Duns 1994. Simultaneous determination of spin-lattice and spin-spin relaxation-times in nmr - a robust and facile method for measuring T-2 - optimization and data-analysis of the offset-saturation experiment. Journal of Magnetic Resonance Series a. 109, 56-64.

9. Desvaux, H., Berthault, P., Birlirakis, N., Goldman, M., Desvaux, H., Goldman, M. 1996. A simple solution to decrease angular dispersion in off-resonance experiments. J. Magn. Reson. B110, 198–201.

10. Miranker, A. D. 2004. Unzipping the mysteries of amyloid fiber formation. Proc. Natl. Acad. Sci. U. S. A. 101, 4335-4336.

11. Stefani, M. and C.M. Dobson 2003. Protein aggregation and aggregate toxicity: New insights into protein folding, misfolding diseases and biological evolution. Journal of Molecular Medicine-Jmm. 81, 678-699.

12. Zagorski, M. G., J. Yang, H.Y. Shao, K. Ma, H. Zeng and A. Hong 1999. Methodological and chemical factors affecting amyloid beta peptide amyloidogenicity. Amyloid, Prions, and Other Protein Aggregates. 309, 189-204.

13. Merlini, G. and P. Westermark 2004. The systemic amyloidoses: Clearer understanding of the molecular mechanisms offers hope for more effective therapies. J. Intern. Med. 255, 159-178.

14. Temussi, P. A., L. Masino and A. Pastore 2003. From alzheimer to huntington: Why is a structural understanding so difficult? EMBO J. 22, 355-361.

15. Gorman, P. M. and A. Chakrabartty 2001. Alzheimer beta-amyloid peptides: Structures of amyloid fibrils and alternate aggregation products. Biopolymers. 60, 381-394.

16. Stockman, B. J. and C. Dalvit 2002. NMR screening techniques in drug discovery and drug design. Prog Nucl Magn Reson Spectrosc. 41, 187-231.

17. (a) Palmer, A. G. 2004. NMR characterization of the dynamics of biomacromolecules. Chem. Rev. 104, 3623-3640. (b) Palmer, A. G., M.J. Grey and C.Y. Wang 2005. Solution NMR spin relaxation methods for characterizing chemical exchange in high-molecular-weight systems. Nuclear Magnetic Resonance of Biological Macromolecules, Part C. 394, 430-465.

18. (a) Kay, L. E. 1998. Protein dynamics from NMR. Biochemistry and Cell Biology-Biochimie Et Biologie Cellulaire. 76, 145-152. (b) Kay, L. E. 2005. NMR studies of protein structure and dynamics. Journal of Magnetic Resonance. 173, 193-207.

19. Hajduk, P. J., E.T. Olejniczak and S.W. Fesik 1997. One-dimensional relaxation- and diffusion-edited NMR methods for screening compounds that bind to macromolecules. J. Am. Chem. Soc. 119, 12257-12261.

20. Valensin, G., T. Kushnir and G. Navon 1982. Selective and non-selective proton spin-lattice relaxation studies of enzyme-substrate interactions. Journal of Magnetic Resonance. 46, 23-29.

21. Bruschweiler, R., C. Griesinger and R.R. Ernst 1989. Correlated motion monitored by nmr relaxation in the rotating frame - a source of structural and dynamic information on macromolecules. J. Am. Chem. Soc. 111, 8034-8035.

22. Eichmuller, C. and N.R. Skrynnikov 2005. A new amide proton R-1 rho experiment permits accurate characterization of microsecond time-scale conformational exchange. J. Biomol. NMR. 32, 281-293.

23. Jarvet, J., P. Damberg, K. Bodell, L.E.G. Eriksson and A. Graslund 2000. Reversible random coil to beta-sheet transition and the early stage of aggregation of the A beta(12-28) fragment from the alzheimer peptide. J. Am. Chem. Soc. 122, 4261-4268.

24. (a) Tjernberg, L. O., J. Naslund, F. Lindqvist, J. Johansson, A.R. Karlstrom, J. Thyberg, L. Terenius and C. Nordstedt 1996. Arrest of beta-amyloid fibril formation by a pentapeptide ligand. J. Biol. Chem. 271, 8545-8548. (b) Wurth, C., N.K. Guimard and M.H. Hecht 2002. Mutations that reduce aggregation of the alzheimer's A beta 42 peptide: An unbiased search for the sequence determinants of A beta amyloidogenesis. J. Mol. Biol. 319, 1279-1290.

25. Paivio, A., J. Jarvet, A. Graslund, L. Lannfelt and A. Westlind-Danielsson 2004. Unique physicochemical profile of alpha-amyloid peptide variant A beta 1-40E22G protofibrils: Conceivable neuropathogen in arctic mutant carriers. J. Mol. Biol. 339, 145-159.

26. Kneller, D. G. and I.D. Kuntz 1993. Ucsf sparky - an nmr display, annotation and assignment tool. J. Cell. Biochem., 254-254.

27. Farrow, N. A., R. Muhandiram, A.U. Singer, S.M. Pascal, C.M. Kay, G. Gish, S.E. Shoelson, T. Pawson, J.D. Formankay and L.E. Kay 1994. Backbone dynamics of a free and a phosphopeptide-complexed src homology-2 domain studied by N-15 nmr relaxation. Biochemistry (N. Y.). 33, 5984-6003.

28. Palmer, A. G. 1998, Curvefit Copyright (C), Department of Biochemistry and Molecular Biophysics, Columbia University, 630 West 168th Street, New York, NY 10032.

29. Mansfield, S. L., D.A. Jayawickrama, J.S. Timmons and C.K. Larive 1998. Measurement of peptide aggregation with pulsed-field gradient nuclear magnetic resonance spectroscopy. Biochimica Et Biophysica Acta-Protein Structure and Molecular Enzymology. 1382, 257-265.

30. Van de Ven, F. J. M. 1955, Multidimensional NMR in Liquids - Basic Principles and Experimental Methods, VCH Publishers Inc., (New York).

31. Goldman, M. 1988, *Quantum Description of High-Resolution NMR in Liquids*, Clarendon Press, (Oxford).

UNDERSTANDING THE MOLECULAR BASIS FOR THE INHIBITION OF THE ALZHEIMER'S Aβ-PEPTIDE OLIGOMERIZATION BY HUMAN SERUM ALBUMIN USING SATURATION TRANSFER DIFFERENCE AND OFF-RESONANCE RELAXATION NMR SPECTROSCOPY

CHAPTER 3

Chapter Three Preface

This work has been published:

Milojevic, J., V. Esposito, R. Das and G. Melacini 2007. Understanding the molecular basis for the inhibition of the alzheimer's A beta-peptide oligomerization by human serum albumin using saturation transfer difference and off-resonance relaxation NMR spectroscopy. J. Am. Chem. Soc. 129, 4282-4290.

Permission has been granted by the publisher to reproduce the material here.

I conducted all the experimental work and data analysis described in this chapter.

UNDERSTANDING THE MOLECULAR BASIS FOR THE INHIBITION OF THE ALZHEIMER'S Aβ-PEPTIDE OLIGOMERIZATION BY HUMAN SERUM ALBUMIN USING SATURATION TRANSFER DIFFERENCE AND OFF-RESONANCE RELAXATION NMR SPECTROSCOPY

Milojevic, J., V. Esposito, R. Das and G. Melacini 2007. J. Am. Chem. Soc. 129, 4282-4290.

ABSTRACT: Human serum albumin (HSA) inhibits the formation of amyloid beta-peptide (Aβ) fibrils in human plasma. However, currently it is not known how HSA affects the formation of the highly toxic soluble diffusible oligomers that occur in the initial stages of Aβ fibrillization. We have therefore investigated by solution NMR the interaction of HSA with the Aβ (12-28) peptide, which has been previously shown to provide a reliable and stable model for the early pre-fibrillar oligomers as well as to contain key determinants for the recognition by albumin. For this purpose we propose a novel NMR approach based on the comparative analysis of Aβ in its inhibited and filtrated states monitored through both saturation transfer difference and recently developed non-selective off-resonance relaxation experiments. This combined NMR strategy reveals a mechanism for the oligomerization inhibitory function of HSA, according to which HSA targets preferentially the soluble oligomers of Aβ (12-28) rather than its monomeric state. Specifically, HSA caps the exposed hydrophobic patches located at the growing and/or transiently exposed sites of the Aβ oligomers, thereby blocking the addition of further monomers and the growth of the pre-fibrillar assemblies. The proposed model has implications not only for the pharmacological treatment of Alzheimer's disease specifically, but also for the inhibition of oligomerization in amyloid-related diseases in general. In addition, the proposed NMR approach is expected

to be useful for the investigation of the mechanism of action of other oligomerization inhibitors as well as of other amyloidogenic systems.

INTRODUCTION

A hallmark of Alzheimer's disease (AD)[1] is the deposition of amyloid plaques in the brain parenchyma and in the meningocerebral blood vessels (1-4). The primary component of AD amyloid deposits is the 40-42 amino acid β-peptide (Aβ) resulting from the proteolytic processing of the ubiquitous transmembrane β-amyloid precursor protein (5-7). Most nucleated cells in the body secrete the Aβ polypeptide, but Aβ aggregates into amyloid fibrils exclusively in the central nervous system (CNS) and not in peripheral tissues (7, 8). The absence of Aβ fibril depositions in such tissues is the result of the presence of Aβ-carrier plasma proteins that are able to inhibit Aβ–amyloid deposition (9, 10). Essentially the same carrier proteins are present in the cerebrospinal fluid (CSF) as well but at about a 1000-fold lower concentration (11) thus significantly reducing their inhibitory effect on amyloid formation in CSF as compared to plasma. Most of the amyloid-inhibitory activity of plasma is accounted for by human serum albumin (HSA) (10), which is the most abundant protein in both plasma and CSF (9,12). The IC_{50} value (10 μM) for the inhibition by albumin of Aβ (1-40) incorporation into existing β-amyloid fibrils is significantly lower than the concentration of HSA in plasma (644 μM) but higher than the concentration of HSA in the CSF (3 μM), explaining why amyloid fibrils are found selectively in the CNS but not in peripheral tissues (10).

Despite the physiological relevance of the HSA-Aβ peptide interaction, the current understanding of the molecular basis for the recognition of Aβ by HSA is still limited and several key questions about the amyloid-inhibitory mechanism of HSA remain unanswered. For instance, a growing body of evidence points to soluble diffusible oligomers formed early in the fibrillization pathways as the main toxic species responsible for AD (13, 14). However, it is not known how albumin affects the initial steps of Aβ oligomerization. Hence we have investigated using solution NMR the interaction between HSA and the Aβ (12-28) peptide, which spans the central hydrophobic core of Aβ ($L_{17}VFFA_{20}$) (15-17) and it has been previously shown to provide a reliable and stable model for the early pre-fibrillization oligomerization equilibria of Aβ (15). Furthermore, this peptide is also suitable to investigate the effect of albumin because key binding sites for HSA are confined to the Aβ (1-28) segment (18), but the first eleven, mostly hydrophilic, N-terminal residues are not significantly involved in self-recognition (19).

Solution NMR experiments have the ability to probe at residue and atomic resolution not only the monomeric state of Aβ (12-28) (20), but also its self-assembled forms including the soluble oligomers (21-24). Specifically, 2D-saturation transfer difference (STD) (22, 23) and recently developed off-resonance relaxation (ORR) (24) experiments measure cross- and self-relaxation rates, respectively, which are very sensitive to the presence of soluble high molecular weight (MW) species in fast dynamic exchange with the monomers and are therefore excellent probes for the reversible pre-nuclear self-association equilibria (24). Here, we have employed a combined STD/ORR approach to

monitor the effect of both albumin addition and filtration on the peptide under investigation. The comparative analysis of the STD/ORR data for the inhibited and filtered states reveals that HSA not only interacts preferentially with the pre-fibrillar oligomeric species, but also targets and caps the exposed hydrophobic sites within the oligomers thus preventing further monomer addition and exchange. The resulting model rationalizes the Aβ oligomerization inhibition function of HSA.

MATERIALS AND METHODS

Sample Preparation - The Alzheimer peptide fragment Aβ (12-28) ($^{+}H_3N$-$V_{12}HHQKLVFFAEDVGSNK_{28}$-$COO^{-}$) with a purity of 98.6 % was purchased from Genscript Corp., Piscataway, NJ, USA. 1mM Aβ (12-28) samples for NMR analysis were prepared by dissolving a weighed amount of lyophilized peptide in 50 mM deuterated (d_4) sodium acetate buffer, pH 4.7 (uncorrected for isotope effects), containing 90 % doubly distilled H_2O and 10 % D_2O (Cambridge Isotope Laboratories). After dissolving the peptide in the buffer, solutions were centrifuged for five minutes at 2,000 rpm and 4 ^{o}C. The stability over time of the samples prepared according to this protocol was monitored by 1D spectra as shown in Figure S1 (left panels). HSA (Sigma) was 99% pure, fatty acid free and essentially globulin free. For the titration experiments aliquots from concentrated stock HSA solutions (0.2 mM, 1.5 mM and 3 mM HSA) were added to the 1mM Aβ (12-28) NMR sample. 1.5 mM and 0.2 mM HSA stock solutions were obtained by dilution of the 3 mM HSA solution. Addition from different stock solutions was

performed to minimize volumetric errors (the smallest volume added was 1 μL) and also to reduce dilution effects. The total volume added was less then 20 μl and therefore the dilution effects were negligible (< 4%). The NMR spectra were recorded immediately after addition of HSA and the samples were stable after each HSA addition. This was confirmed by 1D experiment recorded before and after each titration point.

Filtration Protocol – Ultrafree-MC Millipore 30 kDa cut-off filters were used. Glycerol was removed from the filters by washing with 50 mM deuterated (d_4) sodium acetate buffer for at least five times. Filtration was performed at room temperature by centrifugation at 5 min intervals and 5,000 rpm. Due to the heating in the centrifuge, samples were held in ice for 2 minutes after every 5 min filtration cycle. The centrifugation cycles were repeated until a total of 500 μL of the filtered solution was collected. The stability over time of the filtered samples prepared according to this protocol was monitored by 1D spectra as shown in Figure S1 (right panels).

NMR Spectroscopy - All experiments were performed at 293 K using a Bruker Avance 700 NMR spectrometer. 2D saturation transfer difference and 1D-WG experiments were acquired with a 5 mm TCI CryoProbe, while 2D non-selective off-resonance relaxation experiments (24) were acquired with a TXI probe. For all experiments water suppression was achieved through a Watergate (WG) scheme implemented with the binomial 3-9-19 pulse train as explained before (24). All 1D ^{1}H NMR spectra were recorded with 128 scans, 32 dummy scans and spectral widths of 8389.26 Hz sampled with at least 4096

complex points. The repetition delay for all 1D experiments was 2 s. The peptide ^{1}H NMR signals were assigned using standard procedures (25).

2D Non-Selective Off-Resonance Relaxation (ORR) Experiments - Off-resonance relaxation data were acquired using the non-selective off-resonance relaxation 2D-TOCSY experiments (24). The off-resonance spin lock with the trapezoidal shape was applied at the angle of 35.5^{o} for 5 ms, 23 ms, 42 ms, 60 ms and 80 ms with a strength of 8.23 kHz. For the TOCSY mixing a 45 ms long 10 kHz DIPSI-2 pulse train was used. The inter-scan delay was 2 s and for each sample two replicate experiments were acquired at each relaxation time. Eight scans and 128 dummy scans were employed in each experiment. The spectral widths for both dimensions were 8389.26 Hz with 256 t_1 and 1024 t_2 complex points.

2D Saturation Transfer Difference (STD) Experiments - The pulse sequence used for the 2D-STD NMR experiments (23) was implemented without the 30 ms spin-lock pulse to enhance the sensitivity, as the TOCSY spin-lock effectively serves already as an implicit relaxation filter. A train of 40 Gaussian–shaped pulses of 50 ms each separated by 1 ms inter-pulse delay was applied to introduce selective saturation. The strength of each Gaussian pulse was 119 Hz with a 1 % truncation and 1000 digitization points. The train of Gaussian pulses was preceded by a 100 ms delay in all STD experiments. The spectral widths for both dimensions were 8389.26 Hz and were digitized by 200 t_1 and 1024 t_2 complex points. The on-resonance irradiation was performed at the high field pro-

R γ V_{18} methyl resonance (~0.7 ppm). As a result signals in the methyl region of the STD spectra do not reflect true STD effects but rather simply direct saturation by the selective RF. Our STD measurements therefore focused on the Hα protons, which are not directly affected by the RF field of the Gaussian train used to introduce saturation. The off-resonance control irradiation was performed at 30 ppm. The saturation transfer difference (STD) spectrum was obtained by phase cycling subtraction of the on-resonance and off-resonance data acquired in interleaved mode. The number of scans and dummy scans in the 2D-STD experiments were 16 and 128, respectively. Separate reference ST experiments were also acquired with eight scans and 128 dummy scans.

Data analysis - All 2D replicate data sets were added and processed using Xwinnmr (Bruker Inc.). Data was analyzed as previously published (23, 24). Briefly, the 2D cross-peak intensities were measured using Sparky 3.111 (26) by Gaussian line fitting and determination of fit heights (24). The corresponding fit height error was estimated by calculating the standard deviation for the distribution of the differences in the intensities of identical peaks in duplicate spectra. After the addition of the duplicate spectra, the error was scaled up proportionally to the square root of the total number of scans. The TOCSY $H_{\alpha,i}$-$H_{N,i}$ cross-peaks for residues [15-19], [21-24], and [26-28] were used for data analysis. For residues V_{12}, H_{14} and F_{20}, the $H_{\alpha,12}$-$H_{Me,12}$, $H_{\alpha,14}$-$H_{\beta h,14}$ and $H_{\alpha,20}$-$H_{\beta l,20}$ cross-peaks were used to avoid overlap and water exchange artifacts. G_{25} was omitted from the analysis of the off- resonance relaxation rates due to the degeneracy between its two H_{α} protons (24). The non-selective off-resonance relaxation rates of decay were

obtained through mono-exponential fitting using the Curvefit program (27) and errors in the fitted decay rates were obtained as previously explained (24). The rates obtained through the nonlinear fitting and the related errors were normalized with respect to the largest measured rate.

The saturation transfer ratios (I_{STD}/I_{STR}) were computed starting from the Sparky fit heights, correcting for the differences in the number of scans. The errors in the fit heights were evaluated as for the non-selective off-resonance experiments and then were propagated to the (I_{STD}/I_{STR}) ratios. In the interpretation of these ratios, it should be considered that the saturation starts from the pro-R γ methyl of V_{18} and concurrently diffuses through both intra- and inter-molecular pathways. While the contributions due to the inter-molecular diffusion usually prevail over those caused by the intra-molecular pathways, the latter may not be fully negligible for the directly saturated residue (*i.e.* V_{18}) and the adjacent amino acids (22).

RESULTS AND DISCUSSION

The Aβ (12-28) Peptide Includes Key Determinants of the Aβ - HSA Interactions - As a first step towards the understanding of how human serum albumin (HSA) affects the pre-fibrillization oligomerization equilibria of Aβ (12-28) we acquired 1D NMR spectra of this peptide in the absence and presence of HSA (Figure 1 A, B). The spectrum of 1 mM Aβ (12-28) without HSA (Figure 1A) is line-broadened beyond the line-width typically expected for single chain short 17-amino acid peptides, indicating that monomeric Aβ

(12-28) is in a dynamic equilibrium with its pre-nuclear oligomers (15,16,28). Such oligomers are not an artifact of the peptide manufacturing process as previously shown (15) and as also confirmed here in Figure S2 A-C and in Figure S3 A, B. These Figures show that when oligomers are formed through different pathways, such as the addition of retentate or of salt to the filtered sample, a line-broadening similar to that observed for the unfiltered sample is obtained. Upon addition of sub-stoichiometric amounts (~1:100) of HSA to the Aβ (12-28) peptide a dramatic line-width reduction is observed (Figure 1B), similarly to the effect of filtration (Figure 1C). Analogous significant line-sharpening effects upon HSA addition are also observed when the oligomers are prepared through alternative methods (Figure S2 D and Figure S3 C). These observations are consistent with the hypothesis that HSA preferentially interacts with the line-broadening inducing Aβ (12-28) oligomers rather than with the Aβ (12-28) monomers, which would otherwise be line-broadened by HSA. In addition, the reduced line-width occurring upon addition of HSA suggests also that the interaction of HSA with the Aβ (12-28) oligomers interferes with the monomer-oligomer exchange, which causes the increased line-widths observed in the absence of albumin (Figure 1A) (15,28). While these considerations clearly indicate that the Aβ (12-28) peptide under our experimental conditions includes key determinants for the Aβ - HSA interaction, the hypothesis on the preferential interaction of HSA with oligomeric rather than with monomeric Aβ (12-28) is somewhat counterintuitive. This is because the largely unstructured Aβ (12-28) peptide contains a central hydrophobic core (CHC) that drives its oligomerization (15-17, 24) and HSA is known to bind hydrophobic ligands such as fatty acids. Therefore, before fully ruling out

the interaction of HSA with the Aβ (12-28) monomers, we further investigated the HSA / Aβ (12-28) system using more advanced methods, such as 2D-saturation transfer difference (22, 23) and 2D-non-selective off-resonance relaxation experiments (24), which probe self-recognition with high sensitivity and resolution.

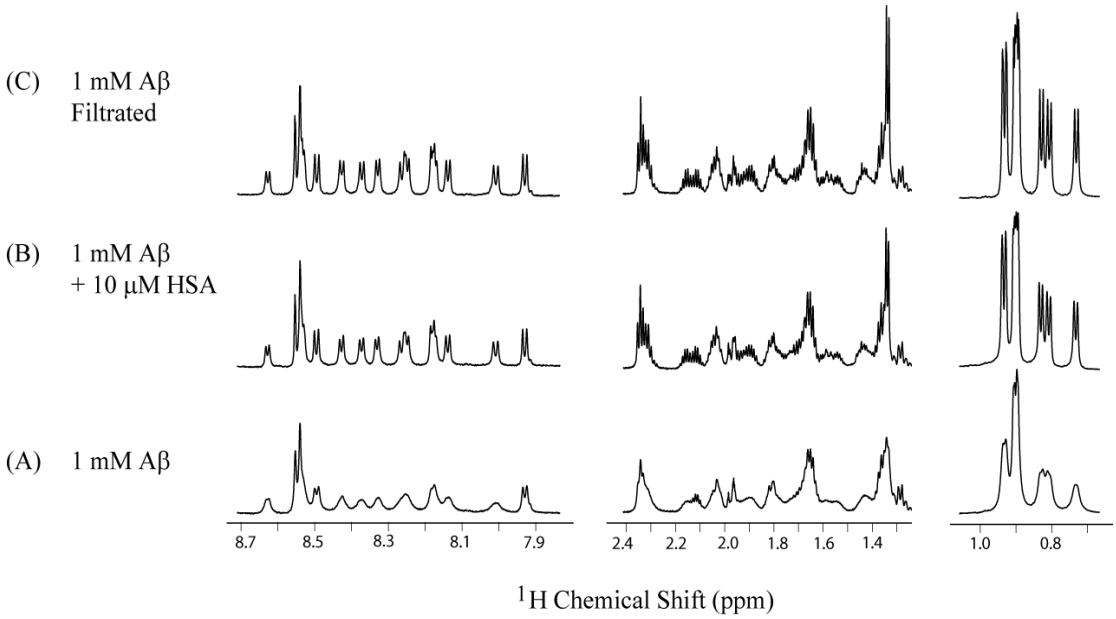

Figure 1. Effect of HSA addition and of 30 kDa-cut off filtration on the ^{1}H 1D-WG spectra of 1 mM Aβ(12-28). (A) Unfiltered 1 mM Aβ(12-28) before HSA addition. (B) Unfiltered sample after addition of 10 μM HSA. (C) 1 mM Aβ(12-28) after 30 kDa filtration. All spectra were recorded at 700 MHz using a TCI CryoProbe and at 293 K with a 50 mM sodium acetate buffer-d_4 (pH 4.7). Different spectral regions are vertically scaled to optimally fit into the stacking space.

HSA does not interact with the Aβ (12-28) monomers - Saturation transfer experiments have been used in the past to detect weak binding of small ligands to proteins with high sensitivity (23). In addition, more recently STD experiments have been applied to amyloidogenic peptides proving that saturation transfer is very sensitive to oligomerization (22, 28). We therefore acquired 2D-saturation transfer difference

TOCSY experiments for the Aβ (12-28) peptide under several conditions with the purpose of investigating the effect of HSA on both monomers and oligomers. Figure 2 shows the H_N-H_α fingerprint regions of the saturation transfer difference TOCSY spectra (STD) (red) and the corresponding reference spectra (STR) (black) for a 1 mM Aβ(12-28) sample without and with HSA (panels A and C, respectively).

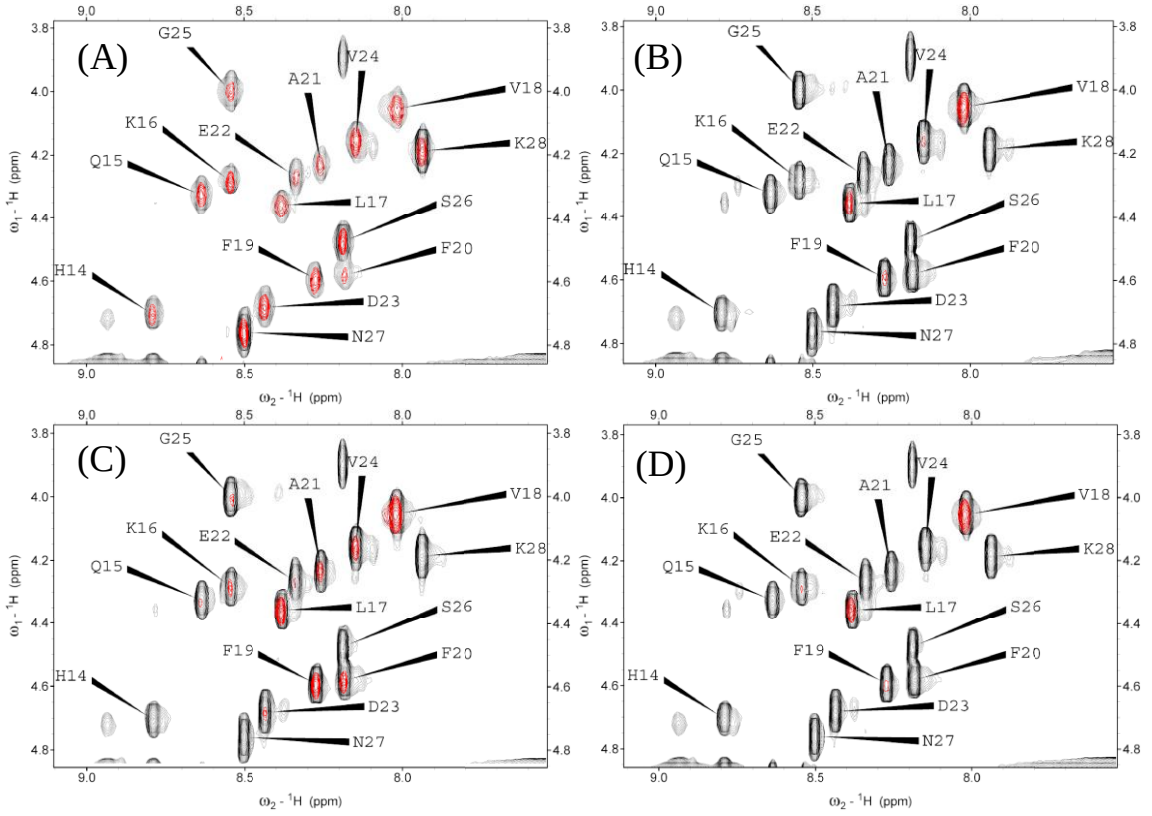

Figure 2. Effect of HSA addition and filtration on 2D saturation transfer difference and reference TOCSY spectra. In all panels the superimposition of the H_α-H_N finger print regions of the 2D-saturation transfer difference (red) and reference (black) spectra is shown. Panels (A) and (B) correspond to 1 mM Aβ(12-28) before and after 30 kDa-cutoff filtration, respectively. Panels (C) and (D) refer to the unfiltered and filtrated 1 mM Aβ(12-28), respectively, both after addition of 10 μM HSA. The lowest contour level for all spectra was set at ten times the estimated noise. Spectra shown at lower contour levels are available in Figure S4. All spectra were measured at 700 MHz , 293 K in 50 mM sodium acetate buffer-d_4 (pH 4.7).

In the absence of HSA an intense STD signal arising from the monomer-oligomer exchange is observed (Figure 2A). After addition of HSA the intensity of the STR cross-peaks increases due to the slower transverse relaxation but the intensity of the STD signal decreases relative to that of the STR spectrum (Figure 2C).

This is also shown more quantitatively in Figure 3A where the normalized I_{STD}/I_{STR} ratios obtained for the H_N-H_α fingerprint regions are plotted *vs*. the Aβ (12-28) sequence. Figure 3A clearly illustrates that the I_{STD}/I_{STR} ratios decrease after HSA addition for all residues in agreement with the line-sharpening observed in the 1D spectra (Figure 1). These observations are consistent with the absence of interactions between HSA and the monomeric peptide as hypothesized above. However, an alternative and more trivial explanation is also possible, *i.e.* the small 1:100 sub-stoichiometric amount of added HSA could be saturated by the Aβ (12-28) oligomers and therefore not be able to interact with the peptide monomers. In order to rule out this possibility, we acquired additional saturation transfer difference data. First, we performed STD experiments where HSA was added to a filtered sample, devoid of most line-broadening inducing oligomers. As a second control, we have also acquired STD spectra for 1 mM Aβ (12-28) with increasing HSA concentrations (*i.e.* we performed an HSA titration).

For the control filtration STD experiments, a 1 mM Aβ (12-28) sample was passed through a 30 kDa filter and the resulting ST spectra and normalized I_{STD}/I_{STR} ratios are shown in Figures 2B and 3B, respectively. The comparison between panels 2A and 2B as well as Figure 3B clearly indicates that the 30 kDa filtration removed most of the

oligomers generating the STD effect, with the residual STD signal observed for residues 17 and 18 likely being an artifact of the selected saturation frequency, as discussed in the Material and Methods section. Therefore the filtered sample is devoid of the potentially HSA saturating peptide oligomers. Additionally, the absence of 'seed' oligomers that may nucleate further oligomerization makes the filtered samples stable (15, 29).

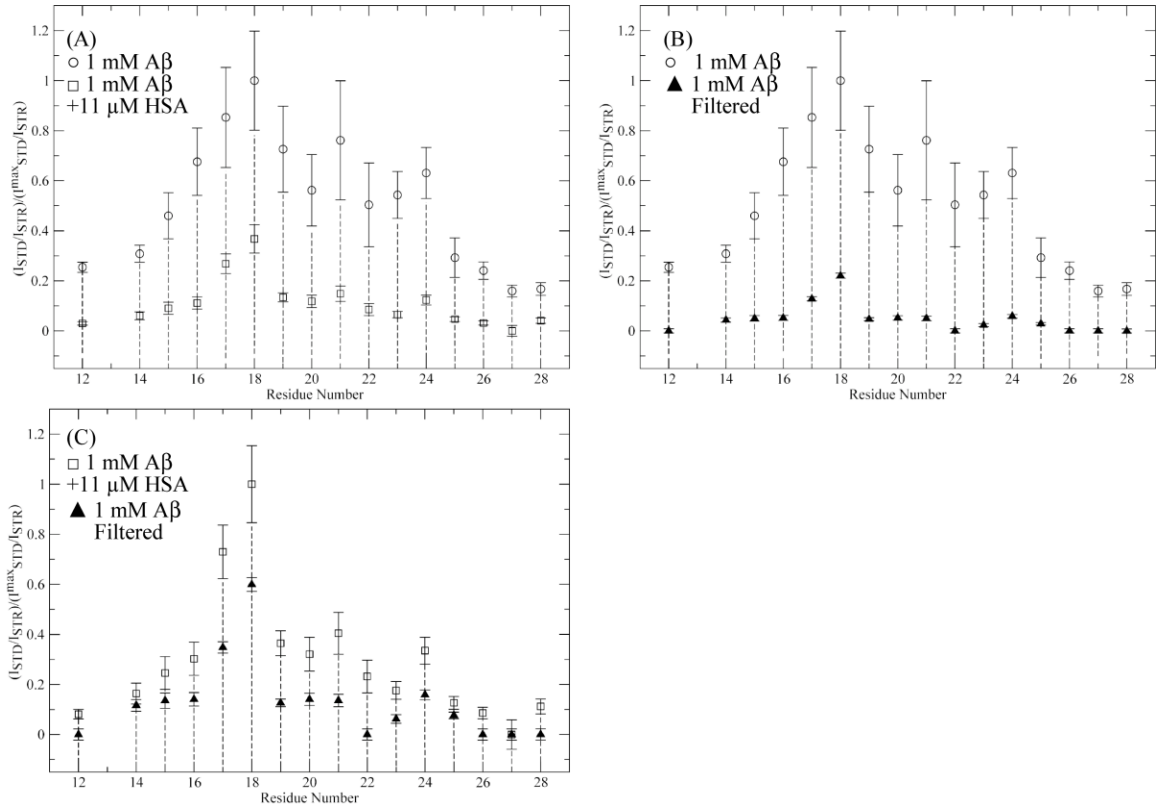

Figure 3**.** Effect of HSA addition and filtration on the saturation transfer H_α-H_N ratios. (A) Effect of HSA on the saturation transfer ratios of unfiltered 1 mM Aβ(12-28). Circles and squares correspond to unfiltered 1 mM Aβ(12-28) before and after 11 μM HSA addition, respectively. All ratios were normalized to the maximum saturation transfer ratio measured in the absence of HSA. (B) Effect of filtration on the saturation transfer ratios of 1 mM Aβ(12-28). Circles and filled triangles correspond to 1 mM Aβ(12-28) before and after filtration, respectively. All ratios were normalized to the maximum saturation transfer ratio measured before filtration. (C) Comparison of the effects of HSA and filtration. Full triangles and squares correspond to 1 mM Aβ(12-28) after filtration and to unfiltered 1 mM Aβ(12-28) after 11 μM HSA addition, respectively. All ratios were normalized to the highest ratio measured for 1 mM Aβ(12-28) in the presence of the HSA. Each set of saturation transfer ratios appears twice in this figure in order to facilitate comparisons among different experimental conditions.

The origin of such stability may not be only kinetic but also thermodynamic due to possible dilution effects occurring upon filtration. Upon addition of 10 μM HSA to the filtered sample no significant changes were detected by STD, as shown in Figure 2D and confirmed by Figures S4-S7. The similarity between the 2D-spectra shown in panels 2B and 2D strongly suggests that HSA does not interact with the Aβ (12-28) monomers and possibly nor with residual unfiltered low MW oligomers, even after the potentially HSA-saturating oligomers have been removed by filtration. It should however be noticed that the interactions with oligomers characterized by MW < 10 kDa may possibly escape detection by the STD method.

The lack of Aβ monomer – albumin interactions is also independently supported by our HSA titration study monitored by STD experiments (Figure 4). As expected, the titration plots reveal that the I_{STD}/I_{STR} ratios decrease as the HSA concentration is increased (Figure 4) until an asymptotic behavior is reached for all residues at HSA concentrations in the ~8-10 μM range. Further addition of HSA above 8-10 μM does not significantly affect the I_{STD}/I_{STR} ratios, consistently with the absence of HSA-monomeric Aβ (12-28) interactions. In summary, based on the above analysis we have conclusively demonstrated that HSA does not recognize the monomeric Aβ (12-28) peptide. This result leads therefore to the still open question of defining which Aβ (12-28) oligomerization states are able to recognize HSA.

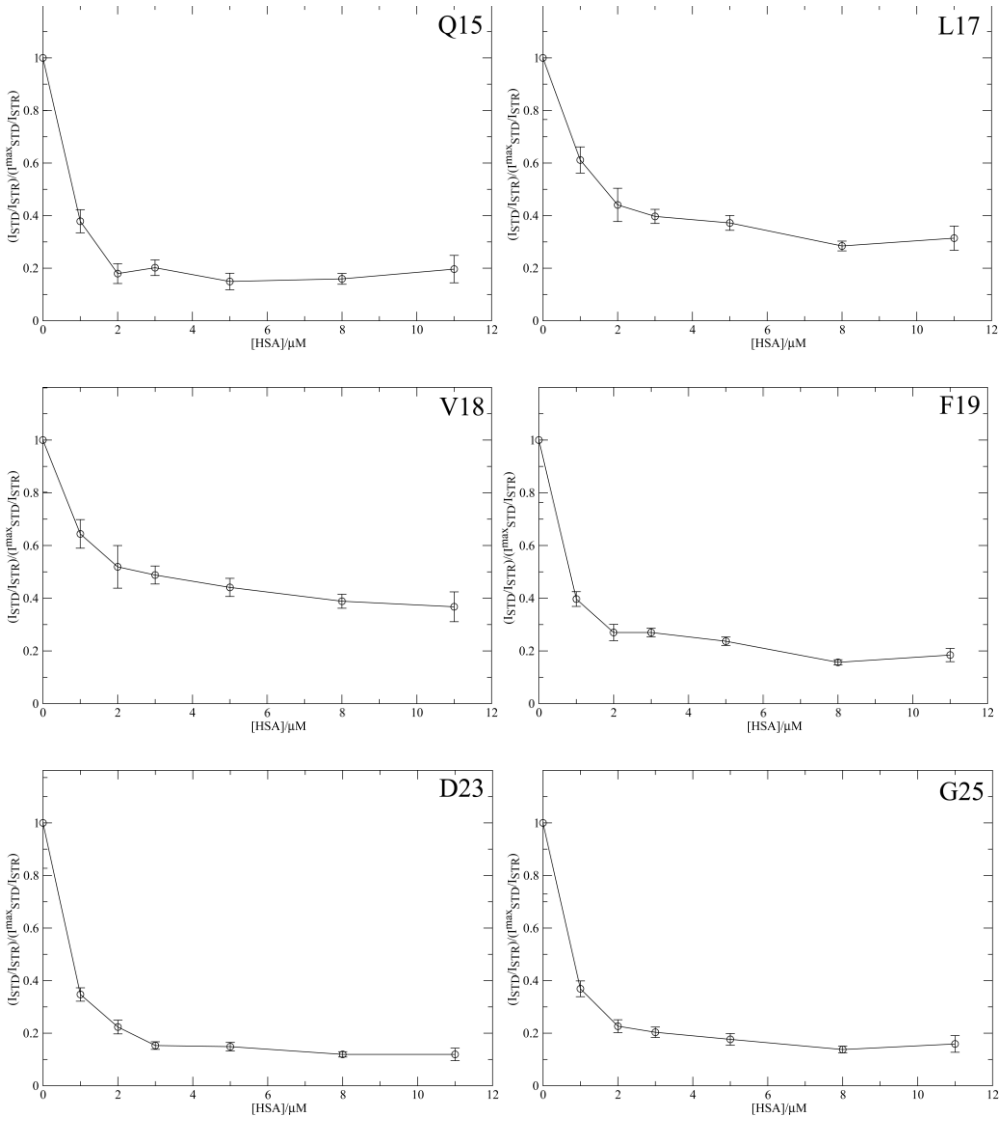

Figure 4. Saturation transfer titration curves for representative residues. Decreases in the I_{STD}/I_{STR} ratio of the H_α-H_N cross peaks are observed as the HSA concentration increases until an asymptotic regime is reached. All ratios were normalized to their maximum value measured before adding HSA.

The HSA recognition competent states - In order to establish the molecular weight range for the oligomers that are able to interact with HSA the results from the STD experiments in the presence of HSA were compared to the results obtained after 30 kDa

cut-off filtration (Figures 2B, 2C and 3C). Both Figure 2C and Figure 3C show that upon addition of HSA the I_{STD}/I_{STR} ratios decrease but not to the extent observed upon filtration (Figure 2B). This observation suggests that the addition of HSA does not completely prevent monomer-oligomer exchange. In other words the oligomers interacting with HSA are only a subset of those eliminated by filtration. When HSA interacts with Aβ (12-28) oligomers with MW larger than a critical value, the residues of monomeric Aβ (12-28) become shielded from these oligomers, explaining the line-sharpening (Figure 1) and the reduced I_{STD}/I_{STR} ratios observed upon HSA addition (Figure 3A).

Accounting for the observed selectivity of albumin for the high MW Aβ oligomers - Our integrated NMR analysis conclusively reveals that under our experimental conditions HSA recognizes preferentially the high MW oligomers of Aβ(12-28), while no interactions were detected with the low MW assemblies or with the monomers. This result is quite intriguing because HSA is known to bind hydrophobic ligands and therefore it is reasonable to think that HSA would target the highly hydrophobic core of the primarily unstructured monomeric Aβ (12-28) peptide (15). However, this scenario is clearly inconsistent with our experimental data. Furthermore, no binding could be detected by surface plasmon resonance between immobilized biotinlated Aβ (1-40) peptides and albumin (10), in full agreement with our solution results on the lack of interactions between albumin and monomeric Aβ (12-28).

A possible explanation for this apparent paradox is that, despite the Aβ (12-28) is largely unstructured (15), residual local structure is still present in the monomeric peptide.

For instance, small populations of structures with turn-like or helical conformational preferences have been proposed for Aβ peptides (30) and the upfield shift at ~0.7 ppm of the pro-R methyl of V_{18} observed for Aβ (12-28) has been accounted for in terms of intra-molecular contacts between $F_{19}F_{20}$ and V_{18} (17). It is therefore possible that these local interactions present in monomeric Aβ prevent HSA from recognizing the single Aβ (12-28) peptide chains. It is also possible that the interaction of HSA with monomeric Aβ (12-28) is entropically unfavorable. For instance, we can assume that monomers are significantly more flexible than oligomers, and therefore binding would cause large entropy losses making this process thermodynamically unfavorable. Oligomers, on the other hand, are expected to be more structured as a result of self-association and therefore the entropy losses that occur upon binding are not as significant as for the monomers.

In the low MW oligomers the HSA recognition motif may not yet be fully stabilized explaining why HSA is not able to bind small oligomers. Similar results were obtained with an antibody designed to target higher molecular weight oligomers. It was observed that the antibody did not cross-react with the low MW assemblies (14) suggesting that there is a significant structural difference between lower and higher molecular weight oligomers. Finally, it should also be considered that another possible explanation for the selectivity of HSA towards the high MW oligomers is that the multiple polypeptide chains in each oligomer may provide additional recognition motifs absent in the monomers; *i.e.* oligomers might behave as a multivalent ligand and this mutivalency may be required for binding to HSA. The next question to address is whether the shielding of

monomeric Aβ (12-28) caused by HSA binding to the oligomers is selective for a specific sub-set of Aβ (12-28) residues or it is a global effect involving all residues in Aβ (12-28).

HSA prevents all residues of monomeric Aβ(12-28) from interacting with oligomeric Aβ(12-28) - A careful analysis of the STD and of the 1D spectra (Supplementary Material, p. S2) indicates that these experiments cannot provide reliable information about the shielding selectivity. These limitations can be overcome by using a recently published non-selective off-resonance relaxation experiment (24). Specifically, Figure S8 and 5A show the observed non-selective off-resonance relaxation decays and the corresponding rates, respectively, before and after HSA addition. As expected, a significant decrease of H_{α}-$R_{35.5}^{o}{}_{,ns}$ relaxation rates measured for the 1 mM Aβ (12-28) sample is observed upon addition of 10 μM HSA for most residues (Figure S8 and 5A). In addition, the changes in relaxation rates caused by HSA (Figure 5A) correlate well with those caused by filtration (Figure 5B, correlation coefficient of 0.96). Considering that filtration physically removes the oligomers from the solution without any residue-specificity, the good correlation observed in Figure 5B suggests that, as a result of HSA addition, *all* residues of monomeric Aβ (12-28) are equally shielded from the oligomers.

Towards a model of Aβ oligomerization inhibition by HSA - Another question that is still open is how albumin can recognize the hydrophobic patches of the oligomers since the oligomerization is driven by the shielding of the central hydrophobic core of the Aβ(12-28) peptide (16, 17) and therefore the hydrophobic core of the oligomers is expected to be significantly more shielded relative to the monomers.

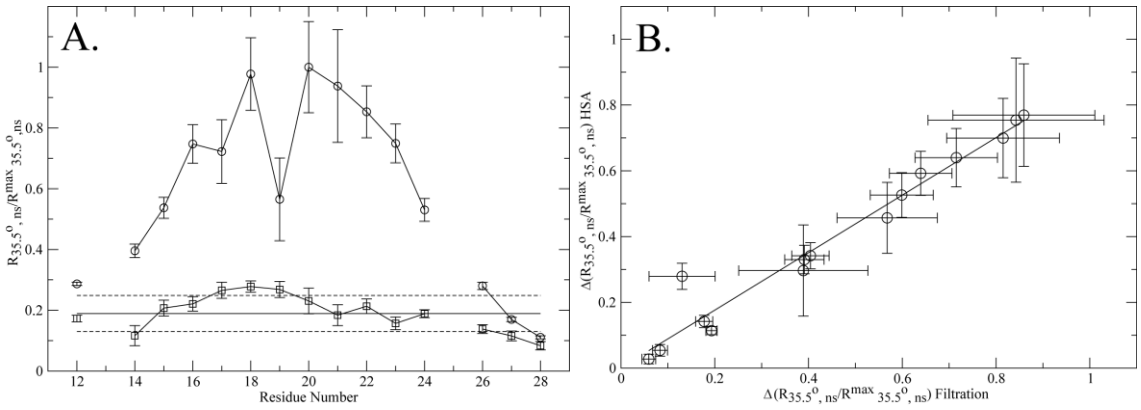

Figure 5. Effect of HSA on the non-selective off-resonance Hα relaxation rates. (A) Plot of relative $R_{35.5}{}^{o}{}_{,ns}$ relaxation rates *vs.* residue number in Aβ (12-28). Circles correspond to 1 mM Aβ(12-28) in the absence of HAS, while squares correspond to 1 mM Aβ(12-28) in the presence of 10 μM HSA. All rates were normalized to the maximum rate of the two sets ($R^{max}{}_{35.5}{}^{o}{}_{,ns}$), as explained before.[24] All rates were measured at 293K in 50 mM d_4-Sodium Acetate buffer at pH 4.7 and 700 MHz. Solid and dashed lines indicate the mean +/– the standard deviation of the $R_{35.5}{}^{o}{}_{,ns}$ rates measured for the sample containing 10 μM HSA. (B) Linear correlation between the variations in $R_{35.5}{}^{o}{}_{,ns}$ rates caused by filtration and by HSA addition. The horizontal axis refers to the difference between the normalized $R_{35.5}{}^{o}{}_{,ns}$ relaxation rates measured for 1 mM Aβ(12-28) before and after filtration, while the vertical axis refers to the difference between the normalized $R_{35.5}{}^{o}{}_{,ns}$ relaxation rates measured for 1 mM Aβ(12-28) in the absence and presence of 10 μM HSA.

A possible explanation is that HSA targets the Aβ (12-28) oligomers at sites where new monomers bind during the growth of the peptide assembly ("growing loci") and possibly also at sites transiently exposed to the solvent during the monomer/oligomer exchange process ("exchange loci"). At these sites hydrophobic residues are available for HSA recognition. The binding of HSA to a range of soluble Aβ (12-28) oligomers (Figure 6) would then block the further monomer addition and/or the monomer exchange with the peptide assemblies.

This model not only accounts for the known oligomerization inhibitory function of HSA, but also for the marked reductions in ORR-rates and I_{STD}/I_{STR} ratios observed in our 2D experiments upon HSA addition (Figures 3 and 5).

Furthermore, the shielding by HSA of the hydrophobic "growing or exchange loci" recognition motives can also explain why all residues of the monomer are equally blocked from the interaction with the oligomers.

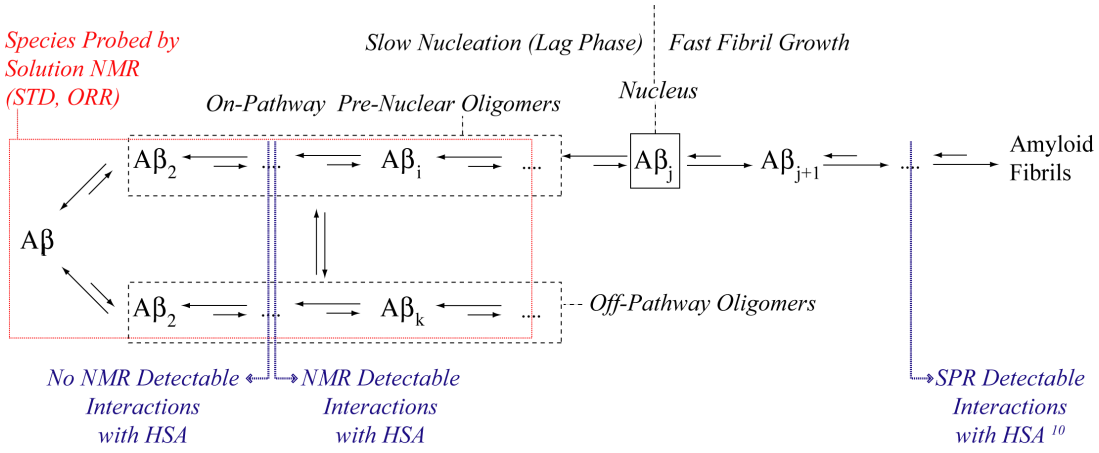

Figure 6. Proposed schematic model for the interactions between HSA and the oligomers of the Aβ peptide. The notation $A\beta_n$ refers to an assembly of n polypeptide chains with the value of n increasing from left to right. Soluble off- and pre-nuclear on-pathway oligomers are denoted with black dashed boxes to differentiate them from other states involved in the general nucleation / growth mechanism (41, 42). The red dotted box indicates the Aβ assemblies that are probed by solution NMR through saturation transfer difference (STD) and non-selective off-resonance relaxation (ORR) experiments. In blue we specify which species are human serum albumin (HSA)-binding competent. Further details about the nature of the interactions between HSA and the soluble oligomers are provided in the text. The NMR data presented here cannot differentiate between on- and off-pathway oligomers and are not relevant for the interactions with the post-nuclear oligomers or with the fibrils. However, previous surface plasmon resonance (SPR) investigations did report binding interactions between Aβ fibrils and HSA (10).

Some general considerations can be drawn about the nature of the oligomer binding sites for HSA, *i.e.* the hypothesized "growing loci" and "exchange loci", based on the possible symmetries of the oligomer overall morphology. Two main groups of Aβ oligomeric assemblies have been proposed so far: oligomers with translational symmetry and oligomers with spherical symmetry (31). For the former class, including unit-protofibrils and disc-shaped assemblies (32), growing or exchange loci can be envisaged at the tips of the oligomers similarly to what has been proposed for the fibrillar growth through monomer attachment at the end of existing fibrils, where exposed hydrophobic patches (*e.g.* residues 17-21) remain available (33). For the latter class of oligomers with spherical symmetry (34), including micellar aggregates (31), ADDLs (*i.e.* Aβ-derived diffusible ligands) (35), amylospheroids (36) and β-amy balls (34.37), the identification of exposed hydrophobic stretches is less obvious. Nevertheless, it is possible that monomer addition to these oligomers occurs through a two-step 'dock-lock' mechanism previously proposed for the Aβ deposition onto amyloid templates (38). According to the 'dock-lock' hypothesis, monomers in solution would first only loosely bind ('dock') the pre-existing Aβ assemblies and the incorporation into the core of the oligomer ('locking') with full burial of the central hydrophobic core of Aβ would occur only later, when the subsequent Aβ monomer docks. Therefore, if albumin recognizes partly exposed hydrophobic residues at the docking site of the oligomer, further growth of the Aβ assembly would be halted according to the 'dock-lock' mechanism.

One possible alternative model for the inhibition by HSA of the Aβ monomer-oligomer association might also be the disruption of Aβ oligomers by albumin. A possible

mechanism for such oligomer disruption is through their destabilization relative to the monomers, *i.e.* through monomer stabilization. However, we did not observe any interaction between HSA and the monomers, which could potentially account for such monomer stabilization. On the contrary, we did observe a preferential interaction of HSA with the oligomers. Therefore, while oligomer disruption cannot be fully ruled out at the present stage, it is possible that the oligomers are still present in solution. In addition, the decay/plateau trend observed for the STD-monitored titration plots (Figure 4) is fully consistent with HSA binding to the existing oligomers, causing the decay, until all binding sites in the oligomers are saturated with HSA, causing the plateau. Furthermore, other proteins with fibrillogenesis inhibitory functions such as ApoE3 and Hsp70 have been shown to target and bind pre-fibrillar oligomers, as discussed below (39, 40).

Comparison with other Aβ oligomerization inhibitory systems - The model proposed here for the inhibitory function of HSA with respect to Aβ oligomerization (Figure 6) may also apply to other systems. For instance, the apolipoprotein ApoE3 represents another endogenous inhibitor of amyloid formation and it is known that ApoE3 specifically targets pre-nuclear oligomers, thus interfering with the nucleation process required for fibril formation (39). Furthermore, it has been recently found (40) that the fibrillization of α-synuclein is inhibited by the chaperone Hsp70 using a mechanism in which Hsp70 selectively recognizes pre-fibrillar oligomeric rather than monomeric α-synuclein. Upon binding the α-synuclein oligomers, this chaperone caps available hydrophobic patches thus inhibiting the progression of α-synuclein assemblies toward amyloid fibrils.

The similarity between the oligomerization inhibitory mechanism proposed for the HSA / Aβ system and those reported for other systems, suggests that the model put forward for HSA (Figure 6) may represent a more general paradigm defining a shared cellular defense strategy against amyloid-related diseases. This conclusion is supported by the recent discovery that different amyloidogenic protein sequences lead to pre-fibrillar soluble oligomers with a common structure and a common pathogenic mechanism (14, 40) despite their sequence variability.

Pharmacological relevance - The model of Figure 6 is also pharmacologically relevant. First, the hydrophobic capping mechanism may be used as a general therapeutic strategy to trap the early soluble oligomers and block further oligomerization. Second, considering that under physiological conditions plasma Aβ is mainly bound to HSA, it is clear that the HSA - Aβ interactions may play a central role in the pathology of AD. The presence of these interactions has therefore to be taken into account when designing drug therapies. For instance, the administration of drugs competing with the Aβ oligomers for the same HSA binding sites, as was previously reported for the anti-diabetic medication tolbutamide (10), can cause the displacement of the Aβ oligomers from albumin thus enhancing β-amyloid formation and therefore possibly promoting the development of AD. This means that the effective target for amyloid treatments is not simply the Aβ-peptide but the complex system composed of both albumin and the Aβ-peptide.

CONCLUSIONS

The comparative NMR analysis of 1D and 2D STD and ORR experiments of filtered and inhibited states of Aβ (12-28) has revealed that HSA inhibits Aβ oligomerization by selectively recognizing a distribution of soluble high MW pre-fibrillar oligomers and targeting their exposed hydrophobic loci. As a result of albumin capping these hydrophobic patches, the addition of further monomers is blocked and the growth of the oligomers inhibited. This oligomerization inhibition strategy may represent a general cellular defense scheme and it may also open new perspectives in the design of anti-amyloid therapies. Furthermore, the filtration based ORR/STD NMR approach employed here to investigate the inhibitory mechanism of albumin is generally applicable to other oligomerization inhibitors as well as to other amyloidogenic systems.

ACKNOWLEDGEMENTS: We thank NSERC, the Alzheimer Society of Canada and the Canadian Institutes of Health Research (CIHR) for financial support to GM. GM is also grateful to the Heart and Stroke Foundation of Canada for a Maureen Andrew New Investigator award and VE to the Federico II University of Naples for a graduate fellowship. We thank Hao Huang for helpful discussions.

REFERENCES

1. SEUBERT, P., C. VIGOPELFREY, F. ESCH, M. LEE, H. DOVEY, D. DAVIS, S. SINHA, M. SCHLOSSMACHER, J. WHALEY, C. SWINDLEHURST, R. MCCORMACK, R. WOLFERT, D. SELKOE, I. LIEBERBURG and D. SCHENK 1992. Isolation and quantification of soluble alzheimers beta-peptide from biological-fluids. Nature. 359, 325-327.

2. VANGOOL, W., M. KUIPER, G. WALSTRA, E. WOLTERS and P. BOLHUIS 1995. Concentrations of amyloid-beta protein in cerebrospinal-fluid of patients with alzheimers-disease. Ann. Neurol. 37, 277-279.

3. MOTTER, R., C. VIGOPELFREY, D. KHOLODENKO, R. BARBOUR, K. JOHNSONWOOD, D. GALASKO, L. CHANG, B. MILLER, C. CLARK, R. GREEN, D. OLSON, P. SOUTHWICK, R. WOLFERT, B. MUNROE, I. LIEBERBURG, P. SEUBERT and D. SCHENK 1995. Reduction of beta-amyloid peptide(42), in the cerebrospinal-fluid of patients with alzheimers-disease. Ann. Neurol. 38, 643-648.

4. Scheuner, D., C. Eckman, M. Jensen, X. Song, M. Citron, N. Suzuki, T. Bird, J. Hardy, M. Hutton, W. Kukull, E. Larson, E. LevyLahad, M. Viitanen, E. Peskind, P. Poorkaj, G. Schellenberg, R. Tanzi, W. Wasco, L. Lannfelt, D. Selkoe and S. Younkin 1996. Secreted amyloid beta-protein similar to that in the senile plaques of alzheimer's disease is increased in vivo by the presenilin 1 and 2 and APP mutations linked to familial alzheimer's disease RID C-2451-2009. Nat. Med. 2, 864-870.

5. TANZI, R., J. GUSELLA, P. WATKINS, G. BRUNS, P. STGEORGEHYSLOP, M. VANKEUREN, D. PATTERSON, S. PAGAN, D. KURNIT and R. NEVE 1987. Amyloid beta-protein gene - cdna, messenger-rna distribution, and genetic-linkage near the alzheimer locus. Science. 235, 880-884.

6. KANG, J., H. LEMAIRE, A. UNTERBECK, J. SALBAUM, C. MASTERS, K. GRZESCHIK, G. MULTHAUP, K. BEYREUTHER and B. MULLERHILL 1987. The precursor of alzheimers-disease amyloid-A4 protein resembles a cell-surface receptor. Nature. 325, 733-736.

7. HAASS, C. and D. SELKOE 1993. Cellular processing of beta-amyloid precursor protein and the genesis of amyloid beta-peptide. Cell. 75, 1039-1042.

8. HAASS, C., A. HUNG, M. SCHLOSSMACHER, T. OLTERSDORF, D. TEPLOW and D. SELKOE 1993. Normal cellular processing of the beta-amyloid precursor protein results in the secretion of the amyloid-beta peptide and related molecules. Alzheimers Disease: Amyloid Precusor Proteins, Signal Transduction, and Neuronal Transplantation. 695, 109-116.

9. Biere, A. L.,B. Ostaszewski, E.R. Stimson, B.T. Hyman, J.E. Maggio, and D.J. Selkoe. 1996, Amyloid β -peptide is transported on lipoproteins and albumin in human plasma, J. Biol. Chem. 271: 32916–32922.

10. Bohrmann, B., L. Tjernberg, P. Kuner, S. Poli, B. Levet-Trafit, J. Naslund, G. Richards, W. Huber, H. Dobeli, C. Nordstedt. 1999. Endogenous Proteins Controlling Amyloid β -Peptide Polymerization. J. Biol. Chem. 274: 15990–15995.

11. Hardman, J. G., Limbird, L. E., Molinoff, P. B., Ruddon, R. W., and Gilman, A. G. (1996) *Goodman & Gilman's The Pharmacological Basis of Therapeutics,* 9th Ed., McGraw-Hill,New York

12. Kuo, Y.M., T.A. Kokjohn, W. Kalback, D. Luehrs, D.R. Galasko, N. Chevallier, E.H. Koo, M.R. Emmerling, A.E. Roher. 2000. Amyloid- β Peptides Interact with Plasma Proteins and Erythrocytes: Implications for Their Quantitation in Plasma. Biochemical and Biophysical Research Communications. 268: 750-756.

13. Klein, W., W. Stine and D. Teplow 2004. Small assemblies of unmodified amyloid beta-protein are the proximate neurotoxin in alzheimer's disease. Neurobiol. Aging. 25, 569-580.

14. Kayed, R., E. Head, J. Thompson, T. McIntire, S. Milton, C. Cotman and C. Glabe 2003. Common structure of soluble amyloid oligomers implies common mechanism of pathogenesis. Science. 300, 486-489.

15. Jarvet, J., P. Damberg, K. Bodell, L.E.G. Erksson, A. Graslund. 2000. Reversible random coil to beta-sheet transition and the early stage of aggregation of the A beta(12-28) fragment from the Alzheimer peptide. J. Am. Chem. Soc. 122: 4261-4268.

16. Mansfield, S. L., D.A. Jayawickrama, J.S. Timmons and C.K. Larive 1998. Measurement of peptide aggregation with pulsed-field gradient nuclear magnetic resonance spectroscopy. Biochimica Et Biophysica Acta-Protein Structure and Molecular Enzymology. 1382, 257-265.

17. Zhang, S. S., N. Casey and J.P. Lee 1998. Residual structure in the alzheimer's disease peptide: Probing the origin of a central hydrophobic cluster. Fold. Des. 3, 413-422.

18. McLaurin, J., D. Yang, C. Yip and P. Fraser 2000. Review: Modulating factors in amyloid-beta fibril formation. J. Struct. Biol. 130, 259-270.

19. Tycko, R. 2003. Applications of solid state NMR to the structural characterization of amyloid fibrils: Methods and results. Prog Nucl Magn Reson Spectrosc. 42, 53-68.

20. Zagorski, M., J. Yang, H. Shao, K. Ma, H. Zeng and A. Hong 1999. Methodological and chemical factors affecting amyloid beta peptide amyloidogenicity. Amyloid, Prions, and Other Protein Aggregates. 309, 189-204.

21. Ippel, J., A. Olofsson, J. Schleucher, E. Lundgren and S. Wijmenga 2002. Probing solvent accessibility of amyloid fibrils by solution NMR spectroscopy. Proc. Natl. Acad. Sci. U. S. A. 99, 8648-8653.

22. Narayanan, S., B. Bosl, S. Walter, B. Reif. 2003 Importance of low-oligomeric-weight species for prion propagation in the yeast prion system Sup35/Hsp104. Proc. Natl. Acad. Sci. U.S.A. 100: 9286-9291.

23. (a) Mayer, M., B. Mayer. 2001. Group epitope mapping by saturation transfer difference NMR to identify segments of a ligand in direct contact with a protein receptor. J. Am. Chem. Soc. 123: 6108-6117. (b) Mayer, M. and T. James 2002. Detecting ligand binding to a small RNA target via saturation transfer difference NMR experiments in D2O and H2O. J. Am. Chem. Soc. 124, 13376-13377

24. (a) Esposito, V., R. Das, G. Melacini. 2005. Mapping polypeptide self-recognition through ^{1}H off-resonance relaxation. J. Am. Chem. Soc. 127: 9358-9359. (b) Milojevic, J., V. Esposito, R. Das and G. Melacini 2006. Analysis and parametric optimization of H-1 off-resonance relaxation NMR experiments designed to map polypeptide self-recognition and other noncovalent interactions. J Phys Chem B. 110, 20664-20670.

25. Wuthrich, K. 1986 NMR of Proteins and Nucleic Acids, Wiley, John &Sons, Inc.

26. Sparky 3.111 Goddard, T. D. and Kneller, D. G., SPARKY 3, University of California, San Francisco.

27. Curvefit Copyright (C) 1998 Arthur G. Palmer, Department of Biochemistry and Molecular Biophysics, Columbia University, 630 West 168th Street, New York, NY 10032.

28. Narayanan, S., B. Bosl, S. Walter, B. Reif. 2003 Importance of low-oligomeric-weight species for prion propagation in the yeast prion system Sup35/Hsp104. Proc. Natl. Acad. Sci. U.S.A. 100: 9286-9291.

29. Bernstein, S., T. Wyttenbach, A. Baumketner, J. Shea, G. Bitan, D. Teplow and M. Bowers 2005. Amyloid beta-protein: Monomer structure and early aggregation states of A beta 42 and its pro(19) alloform. J. Am. Chem. Soc. 127, 2075-2084.

30. (a) Riek, R., P. Guntert, H. Dobeli, B. Wipf and K. Wuthrich 2001. NMR studies in aqueous solution fail to identify significant conformational differences between the monomeric forms of two alzheimer peptides with widely different plaque-competence, A beta(1-40)(ox) and A beta(1-42)(ox). European Journal of Biochemistry. 268, 5930-5936. (b) Zhang, S., K. Iwata, M.J. Lachenmann, J.W. Peng, S. Li, E.R. Stimson, Y. Lu, A.M. Felix, J.E. Maggio and J.P. Lee 2000. The alzheimer's peptide A beta adopts a collapsed coil structure in water. J. Struct. Biol. 130, 130-141.

31. Tiana, G., F. Simona, R. Brogliaa and G. Colombo 2004. Thermodynamics of beta-amyloid fibril formation. J. Chem. Phys. 120, 8307-8317.

32. Mastrangelo, I., M. Ahmed, T. Sato, W. Liu, C. Wang, P. Hough and S. Smith 2006. High-resolution atomic force microscopy of soluble A beta 42 oligomers. J. Mol. Biol. 358, 106-119.

33. Luhrs, T., C. Ritter, M. Adrian, D. Riek-Loher, B. Bohrmann, H. Doeli, D. Schubert and R. Riek 2005. 3D structure of alzheimer's amyloid-beta(1-42) fibrils. Proc. Natl. Acad. Sci. U. S. A. 102, 17342-17347.

34. Chimon, S. and Y. Ishii 2005. Capturing intermediate structures of alzheimer's beta-amyloid, A beta(1-40), by solid-state NMR spectroscopy. J. Am. Chem. Soc. 127, 13472-13473.

35. Chromy, B., R. Nowak, M. Lambert, K. Viola, L. Chang, P. Velasco, B. Jones, S. Fernandez, P. Lacor, P. Horowitz, C. Finch, G. Krafft and W. Klein 2003. Self-assembly of A beta(1-42) into globular neurotoxins. Biochemistry (N. Y.). 42, 12749-12760.

36. Hoshi, M., M. Sato, S. Matsumoto, A. Noguchi, K. Yasutake, N. Yoshida and K. Sato 2003. Spherical aggregates of beta-amyloid (amylospheroid) show high neurotoxicity and activate tau protein kinase I/glycogen synthase kinase-3 beta. Proc. Natl. Acad. Sci. U. S. A. 100, 6370-6375.

37. Westlind-Danielsson, A. and G. Arnerup 2001. Spontaneous in vitro formation of supramolecular beta-amyloid structures, "beta amy balls", by beta-amyloid 1-40 peptide. Biochemistry (N. Y.). 40, 14736-14743.

38. Esler, W., E. Stimson, J. Jennings, H. Vinters, J. Ghilardi, J. Lee, P. Mantyh and J. Maggio 2000. Alzheimer's disease amyloid propagation by a template-dependent dock-lock mechanism. Biochemistry (N. Y.). 39, 6288-6295.

39. Evans, K.C., E.P. Berger, C.G. Cho, K.H. Weisgraber, P.T. Lansbury. 1995. Apolipoprotein E is a kinetic but not a thermodynamic inhibitor of amyloid formation: implications for the pathogenesis and treatment of Alzheimer disease. Proc. Natl. Acad. Sci. U.S.A. 92: 763-767.

40. Dedmon, M., J. Christodoulou, M. Wilson and C. Dobson 2005. Heat shock protein 70 inhibits alpha-synuclein fibril formation via preferential binding to prefibrillar species. J. Biol. Chem. 280, 14733-14740.

41. COME, J., P. FRASER and P. LANSBURY 1993. A kinetic-model for amyloid formation in the prion diseases - importance of seeding. Proc. Natl. Acad. Sci. U. S. A. 90, 5959-5963.

42. JARRETT, J. and P. LANSBURY 1993. Seeding one-dimensional crystallization of amyloid - a pathogenic mechanism in alzheimers-disease and scrapie. Cell. 73, 1055-1058.

SUPPLEMENTARY MATERIAL

Limitations of the STD and of the 1D spectra in the assessment of the Aβ oligomer shielding selectivity. The plots in Figure 3 indicate that the I_{STD}/I_{STR} ratio of the H_N-H_α cross peaks corresponding to residues L_{17} and V_{18} are larger then the average value measured for the other residues. Despite this observation may suggest that the oligomer-shielding effect of HSA is residue-specific, it is also possible that the observed enhanced I_{STD}/I_{STR} ratios for L_{17} and V_{18} are simply an artifactual result of intra-molecular spin diffusion that propagates through the monomers, as explained before in the Materials and

Methods section. Similarly, the 1D-WG spectra (Figure 1) clearly indicate that the extent of line sharpening upon addition of HSA is not the same for all residues. For instance, H_{14} remains broad (Figure 1) even after addition of HSA. This could be a result of specific interactions of HSA with particular side chains in the Aβ sequence, but it could also be an artifact arising from intermediate proton exchange with water. These ambiguities can be solved by using a recently published non-selective off-resonance relaxation experiment (24). The advantage of this technique is that it applies a strong off-resonance adiabatic spin-lock that affects equally all residues and therefore it avoids the residue-specific effects which are observed in the saturation transfer and in the 1D experiments.

Full author list for reference 4:

Scheuner, D., Eckman, C., Jensen, M., Song, X., Citron, M., Suzuki, N., Bird, T. D., Hardy, J., Hutton, M., Kukull, W., Larson, E., Levy-Lahad, E.,Viitanen, M., Peskind, E., Poorkaj, P., Schellenberg, G., Tanzi, R., Wasco, W., Lannfelt, L., Selkoe, D. J., and Younkin,S. G. (1996) *Nat. Med.* **2**, 864–870

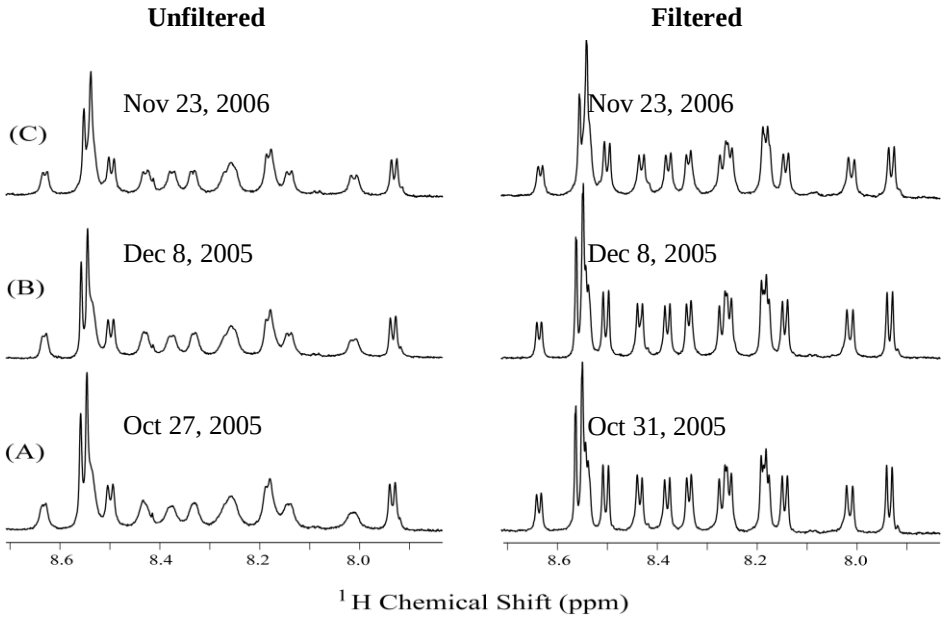

Figure S1. *Control spectra to monitor the stability over time of the unfiltered (left panels) and filtered (right panels) Aβ(12-28) NMR samples*. Dates of acquisition are reported in each panel. Spectra in (A) were recorded at the beginning of the NMR sessions for both unfiltered and filtered samples, while spectra in (B) were acquired at the end of the NMR sessions, *i.e.* after more than one month. Spectra in (C) were collected after more than 11 months. All spectra were measured at 700 MHz using a TCI CryoProbe and at 293 K in 50 mM sodium acetate buffer-d_4 (pH 4.7). Between the experiments the samples were held at room temperature. Samples were prepared as indicated in the Materials and Methods section.

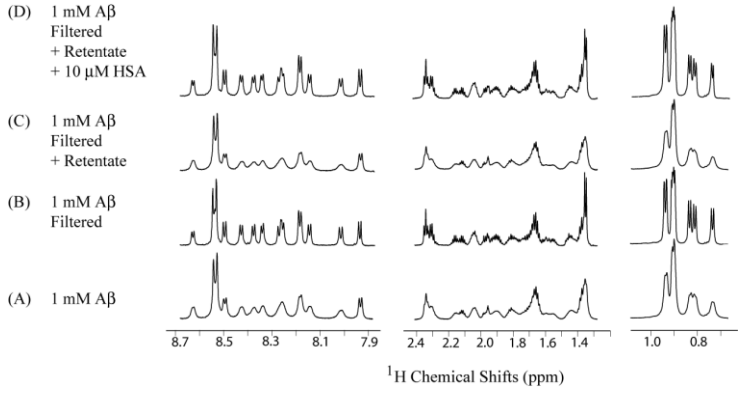

Figure S2. *Effect of filtration and retentate re-suspension on the ^{1}H 1D-WG spectra of Aβ(12-28).* 1D-WG spectra of 1 mM Aβ(12-28) before (A) and after (B) 30 kDa cut-off filtration. (C) Effect of the retentate re-suspension to the filtered Aβ(12-28) sample and (D) effect of the addition of 10 µM HSA to the re-suspended sample. All spectra were recorded at 700 MHz using a TCI CryoProbe and at 293 K in 50 mM sodium acetate buffer-d_4 (pH 4.7). Different spectral regions are vertically scaled to optimally fit into the stacking space.

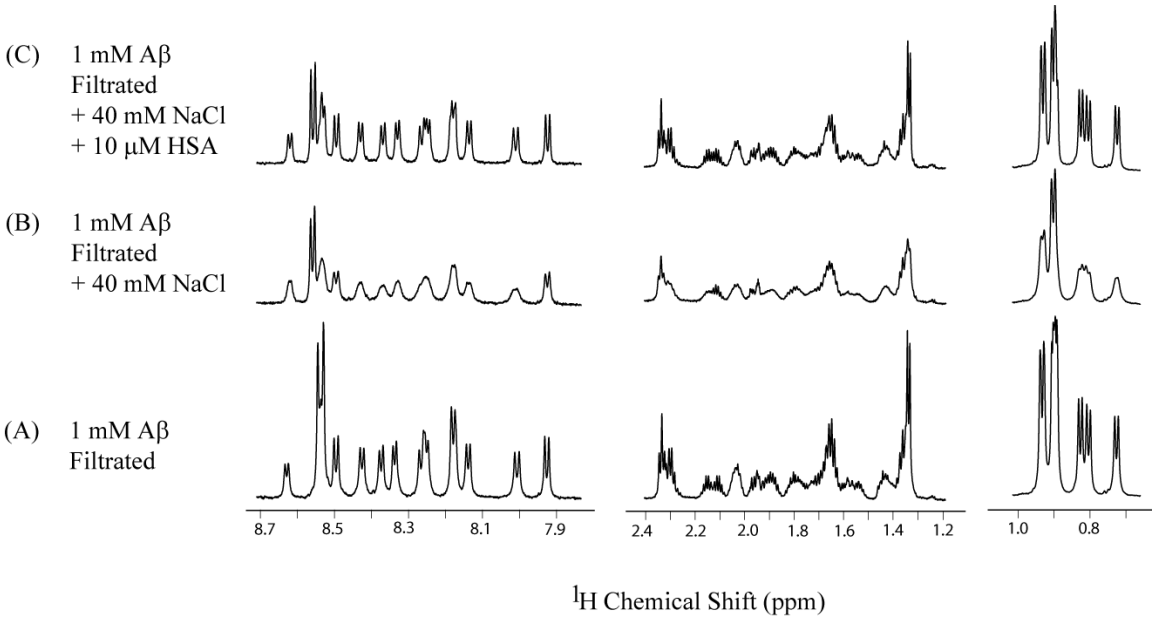

Figure S3. *Effect of salt addition on the ^{1}H 1D-WG spectra of filtrated Aβ(12-28).* Filtrated Aβ(12-28) sample before (A) and after (B) addition of 40 mM NaCl. Salt was added as a 20 μL aliquot of a 1 M NaCl solution. (C) Effect of the addition of 10 μM HSA to the sample corresponding to the spectrum shown in panel (B). All spectra were collected at 700 MHz using a TCI CryoProbe and at 293 K with a 50 mM sodium acetate buffer-d_4 (pH 4.7). Different spectral regions are vertically scaled to optimally fit into the stacking space.

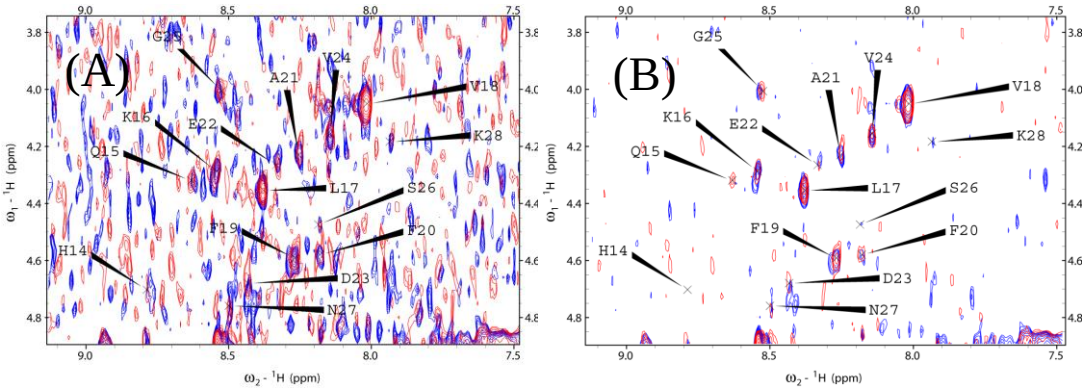

Figure S4. *2D-Saturation transfer difference evidence that HSA does not interact with the monomers*. Superimposition of the Hα-HN fingerprint region of the 2D saturation transfer difference spectra of the filtered Aβ(12-28) sample in the presence (blue) and in the absence (red) of 10 μM HSA. The contour levels where set at two and four times the estimated noise level in (A) and (B), respectively. No significant difference is observed upon HSA addition. All spectra were measured at 700 MHz using a TCI CryoProbe and at 293 K in 50 mM sodium acetate buffer-d_4 (pH 4.7).

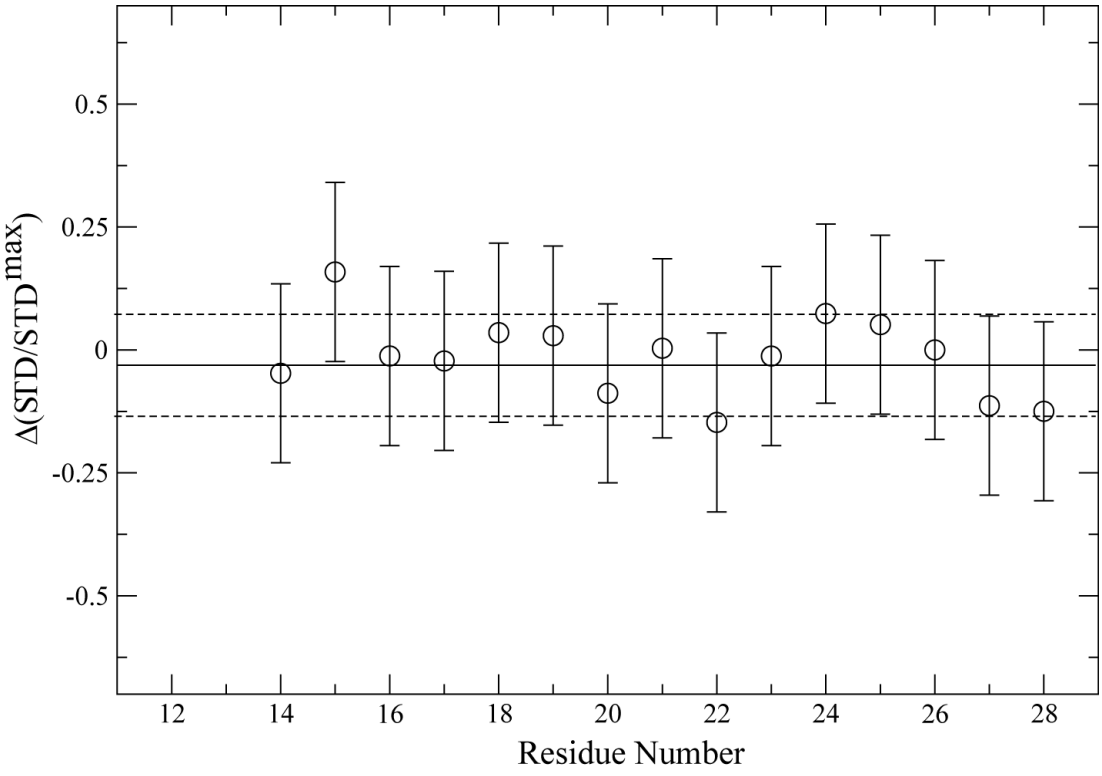

Figure S5. *Quantitative comparison between the Hα-STD intensities measured for the filtered Aβ(12-28) sample in the presence and absence of HSA.* Differences between the red and blue spectra shown in Figure S4 plotted *vs.* residue number. For each sample two copies of the experiment were obtained and the error was estimated as the standard deviation of the differences between the individual spectra. After addition of the spectra the STD intensities and their corresponding errors were normalized with respect to the highest STD intensity value (*i.e.* V_{18} of the filtered sample). Only residues for which STD Hα-HN or Hα-Hβ cross-peaks could be observed (*i.e.* residues 14-28) are reported. The solid and dashed lines indicate the average value ± one standard deviation, respectively.

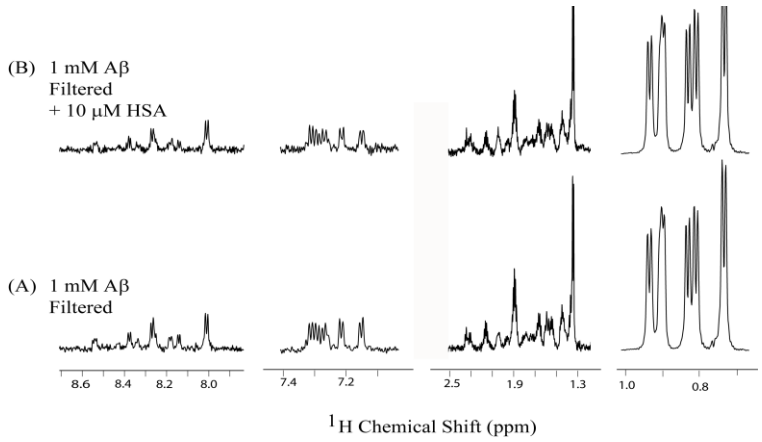

Figure S6.1*D-Saturation transfer difference evidence that HSA does not interact with the monomers.* 1D-STD spectra of the filtered Aβ(12-28) sample in the absence (A) and the presence (B) of 10 μM HSA. In the three spectral regions shown (*i.e.* amide region, aromatic and aliphatic region) a residual STD signal was observed. Such signal does not appear to be significantly affected by HSA. A 30 ms spin-lock was employed to suppress the background HSA signal (23). All spectra were measured at 700 MHz using a TCI CryoProbe and at 293 K in 50 mM sodium acetate buffer-d_4 (pH 4.7).

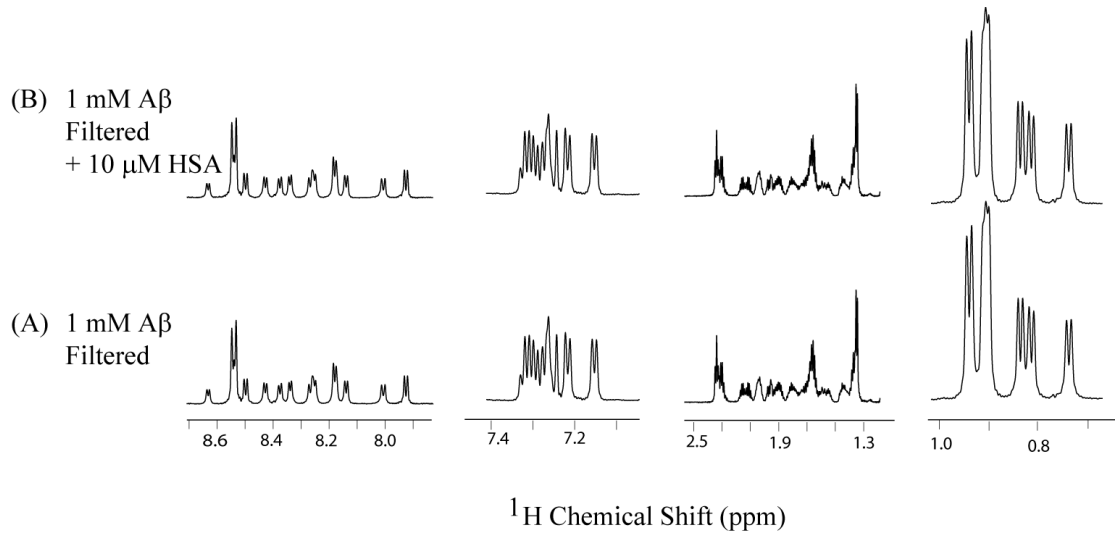

Figure S7. *1D-Line-width evidence that HSA does not interact with the monomers*. Reference spectra for the Aβ(12-28) filtered sample in the absence (A) and presence (B) of 10 μM HSA. No appreciable line-width change is observed upon HSA addition. A 30 ms spin-lock was employed to suppress the background HSA signal (23). All spectra were measured at 700 MHz using a TCI CryoProbe and at 293 K in 50 mM sodium

acetate buffer-d_4 (pH 4.7). Different spectral regions are vertically scaled to optimally fit into the stacking space.

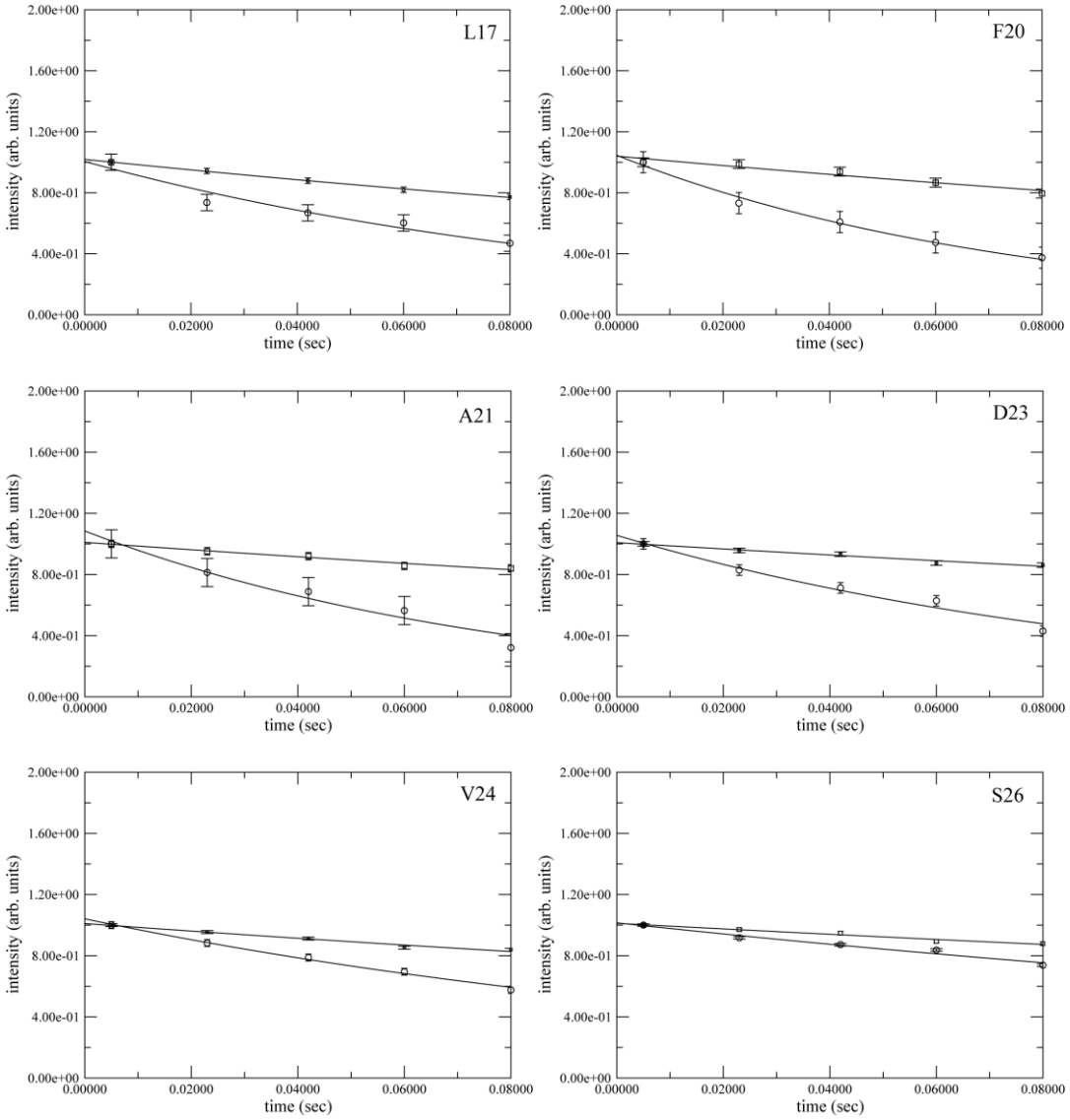

Figure S8. *Representative decay plots for the non-selective off-resonance relaxation rates of the H_α protons in Aβ(12-28).* The horizontal axis refers to the different relaxation times, while the vertical axis reports the cross-peak fit heights normalized with respect to the value measured for the 5 ms relaxation time. Circles refer to the decay in the 1 mM Aβ(12-28) sample without HSA, while squares refer to the slower decay observed after the addition of 10 μM HSA. Solid lines indicate best fit mono-exponentials. All rates were measured at 293 K in 50 mM sodium acetate buffer-d_4 (pH 4.7) and at 700 MHz. All spectra were measured at 700 MHz using a TXI Probe and at 293 K in 50 mM sodium acetate buffer-d_4 (pH 4.7).

HUMAN SERUM ALBUMIN INHIBITS Aβ FIBRILLIZATION THROUGH A 'MONOMER-COMPETITOR' MECHANISM

CHAPTER 4

Chapter Four Preface

This work has been published:

Milojevic, J., A. Raditsis and G. Melacini 2009. Human serum albumin inhibits A beta fibrillization through a "monomer-competitor" mechanism. Biophys. J. 97, 2585-2594.

Permission has been granted by the publisher to reproduce the material here.

I conducted all the experiment and data analysis described in this chapter. A. Raditsis provided assistance in the data acquisition.

HUMAN SERUM ALBUMIN INHIBITS Aβ FIBRILLIZATION THROUGH A 'MONOMER-COMPETITOR' MECHANISM

Milojevic, J., A. Raditsis and G. Melacini 2009, Biophys. J. 97, 2585-2594.

ABSTRACT: Human serum albumin (HSA) is not only a fatty acid and drug carrier protein, but it is also a potent inhibitor of Aβ self-association in plasma. However, the mechanism underlying the inhibition of Aβ fibrillization by HSA is still not fully understood. We have therefore investigated the Aβ - HSA system using a combined experimental strategy based on saturation transfer difference (STD) NMR and intrinsic albumin fluorescence experiments on three Aβ peptides with different aggregation propensities (*i.e.* Aβ (12-28), Aβ (1-40) and Aβ (1-42)). Our data consistently show that albumin selectively binds to cross-β structured Aβ oligomers as opposed to Aβ monomers. The HSA/Aβ oligomer complexes have K_D values in the μM or sub- μM range and compete with the further addition of Aβ monomers to the Aβ assemblies, thus inhibiting fibril growth ('monomer competitor' model). Other putative mechanisms, according to which albumin acts as a 'monomer stabilizer' or a 'dissociation catalyst', are not supported by our data, thus clearing previous discrepancies in the literature of Aβ-HSA interactions. In addition, the model and the experimental approaches proposed here are anticipated to be of broad relevance for the characterization of other systems that involve amyloidogenic peptides and oligomerization inhibitors.

INTRODUCTION

A distinctive hallmark of Alzheimer's disease (AD) is the deposition of amyloid plaques in the brain (1). Two major components of these amyloid deposits are the amyloid-β (Aβ) peptides Aβ (1-40) and Aβ (1-42) (2). The Aβ peptides are produced through the proteolytic cleavage of the amyloid precursor protein (APP) (2-4) and are distributed in both the cerebrospinal fluid (CSF) and blood (5). The brain/blood Aβ equilibrium is shifted towards the bloodstream by agents in the peripheral serum that do not penetrate the blood brain barrier (BBB) but bind the Aβ peptide (5). Such agents have been proposed to act like a 'peripheral sink' which lowers the risk of amyloid plaque deposition in the brain and of AD (5). One of the most potent Aβ 'sequestering' systems is human serum albumin (HSA), which under physiological conditions binds more than 90 % of Aβ (1-40) and Aβ (1-42) in blood serum (6, 7). Furthermore, HSA is one of the most potent endogenous inhibitors of Aβ fibrillization (6, 7). The interactions between the Aβ peptides and HSA represent therefore a critical component of the transport and metabolism of the Aβ system and their investigation may provide clues for possible therapeutic strategies against AD.

In spite of the physiological and pharmacological relevance of the Aβ/HSA system, the mechanism underlying the inhibition of Aβ fibrillization by HSA is still not fully understood. At least three main types of models have been proposed for proteins known to prevent peptide amyloidogenesis (Fig. 1a-c) (8-10). According to model (I)

(Fig. 1a) the inhibitory protein (P) selectively binds and stabilizes the monomeric form of the amyloidogenic peptide preventing its self-association. An example of a protein recently found to act according to such a "monomer stabilizer" mechanism is the phage-display selected affibody $Z_{A\beta3}$, which binds monomeric Aβ (1-40) with nanomolar affinity, effectively preventing its fibrillization (8). Another possible mechanism to explain fibrillization inhibition (model II, Fig. 1b) assumes that the oligomers which serve as seeds for rapid aggregation are kinetically but not thermodynamically stable (9). In this case, the inhibitory protein P rather than selectively binding to the monomeric peptide acts as a catalyst that accelerates the dissociation of the oligomers into monomers (model II, Fig. 1a). An example of a system previously shown to function according to such a dissociation catalyst mechanism is the molecular chaperone Hsp104, which dissociates the oligomeric Sup35 prion-peptide into monomeric species unable to interact with Hsp104 (9). An additional model that does not involve any peptide monomer-inhibitory protein interactions, is the "monomer competitor" model (Fig. 1c, III) in which the inhibitory protein selectively binds to the oligomers preventing the further addition of peptides and growth into larger oligomer assemblies. An example of such a mechanism is provided by the apolipoprotein E3 (ApoE3), which inhibits fibrillogenesis by binding soluble oligomers (10). From these examples it is clear that different proteins with fibrillization inhibitory functions often adopt different inhibition mechanisms.

In the case of HSA, based on the data published so far (6, 7, 11-14), it is not possible to establish consistently and conclusively which model best describes its interactions with the Aβ system and the consequent inhibition of Aβ fibrillization. The

monomer stabilizer model (I, Fig. 1a) is apparently supported by immunoassays (12) and by circular dichroism (CD) binding studies (13) that have been interpreted in terms of an Aβ monomer:HSA complex with a 1:1 stoichiometry and a dissociation constant in the μM range ($K_D = 5 \pm 1$ μM) (12, 13). However, these results do not agree with surface plasmon resonance (SPR) data (7), showing that albumin interferes with the incorporation of biotin-Aβ (1-40) into amyloid fibrils by selectively binding polymeric but not monomeric derivatized Aβ (1-40). The SPR evidence therefore does not support model I. Although similar conclusions have also been obtained through preliminary NMR HSA binding studies on a short Aβ fragment (11), these early SPR/NMR results were later dismissed by others (13) on the basis of the extensive use of derivatization or fragmentation of the Aβ peptides.

Considering the discrepancies currently present in the literature of Aβ – HSA interactions (6, 7, 11-14), it is important to obtain more direct and conclusive evidence to reliably establish which model (Fig. 1a-c) best explains the inhibitory action of HSA with respect to Aβ fibrillization. In an attempt to solve these inconsistencies, dynamic light scattering (DLS) has been recently employed to map the effect of bovine serum albumin (BSA) on the oligomer size distribution of Aβ (1-40), revealing that albumin shifts the Aβ oligomer distribution towards low molecular weight oligomers and possibly monomers (14). However, based on this DLS investigation a conclusive model selection (Fig. 1a-c) was still not possible, as interactions of albumin with monomeric Aβ could not be ruled out (14).

Given the incongruities among the previous reports (6, 7, 11-14), the main goal of this manuscript is to differentiate and clarify which of the three hypothetical mechanisms (Fig. 1a-c) applies to the inhibitory function of Aβ fibrillization by HSA. For this purpose, we have investigated the HSA/Aβ system using NMR and tryptophan fluorescence, as illustrated in Fig. 1d. These two spectroscopic techniques were chosen because they probe the multiple interactions of the HSA/Aβ system in complementary ways. NMR is ideal to sense interactions involving small molecular weight species, *i.e.* mainly the Aβ monomer / HSA and the Aβ monomer / Aβ oligomer interactions (Fig. 1d), while fluorescence takes advantage of the presence of a tryptophan residue in HSA (*i.e.* W214) but not in the Aβ peptide. As a result, tryptophan fluorescence probes only the interactions involving HSA, *i.e.* the Aβ monomer / HSA and Aβ oligomer / HSA interactions (Fig. 1d). Thus all possible interactions of the HSA/Aβ system are detected by this integrated experimental design and specifically the putative binding of Aβ monomers by HSA is characterized by two independent methods, providing a solid experimental basis for the selection of the hypothetical models outlined in Fig. 1a-c.

The experimental scheme illustrated in Fig. 1d was applied to three different Aβ peptides with increasing length and propensity to oligomerize: Aβ (12-28), Aβ (1-40) and Aβ (1-42). The Aβ (12-28) fragment was chosen because it spans the central hydrophobic core of the Aβ peptide and it contains key residues necessary for the interactions with HSA (11).

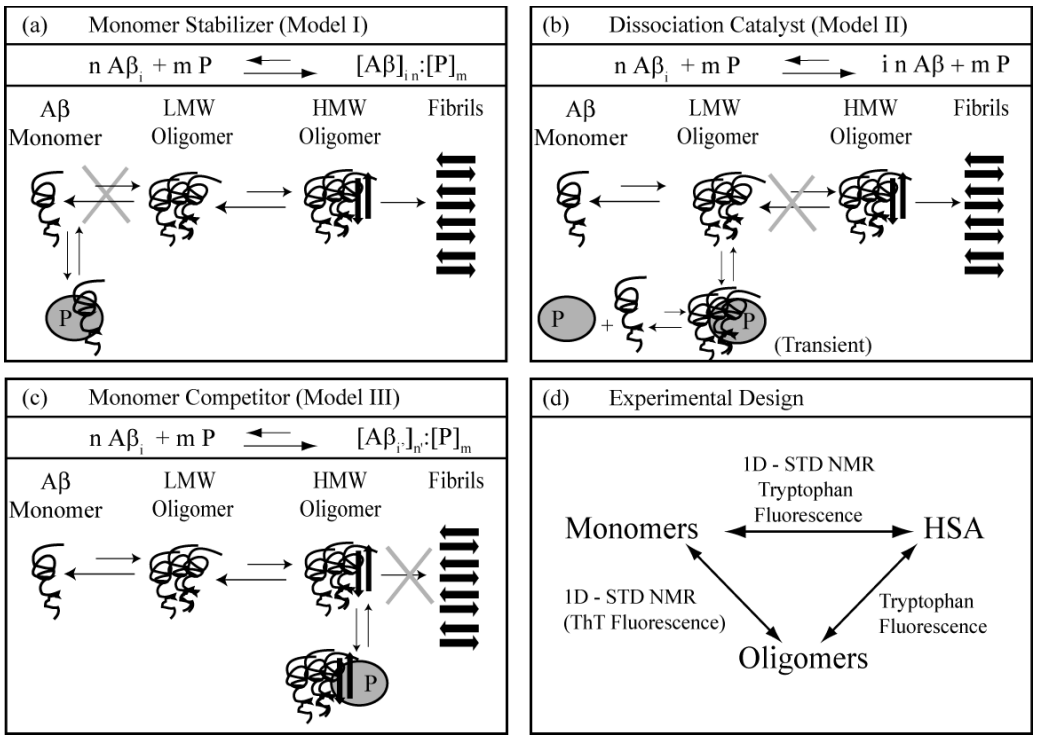

Figure 1. Panels **(a-c)** depict possible hypothetical models for the mechanism of oligomerization inhibition by a generic inhibitory protein P. Aβ denotes the Aβ peptide in its monomeric state, while $A\beta_i$ and $A\beta_{i'}$ indicate Aβ oligomers. LMW and HMW Aβ refer to low and high molecular weight Aβ oligomers, respectively. The letters n, m and n' refer to integer numbers that define the stoichiometry of the non-covalent complexes involving the Aβ peptide and the P protein. In both models (I) and (II), oligomers are disrupted (*i.e.* "cleared") by P. While an Aβ oligomer – HSA complex in model (II) forms only transiently, in model (III) does not clear the oligomers and binds stably to them preventing their further growth into larger assemblies. In order to include the possibility that the inhibitory binding protein partially converts large oligomers into a higher number of smaller oligomers the subscripts i and n were replaced by i' and n' for the P bound oligomers in model (III). In any case, such oligomers must remain larger than the critical size required to interact with the inhibitory protein (denoted as i_{cs} in panel c), *i.e.* i n = i' n' and $i_{cs} < i' < i$. The cartoon representation of the models was used for clarity but it does not imply a specific pathway for fibril formation nor it assigns specific structures or stoichiometries for Aβ in different oligomerization or HSA bound states. Panel **(d)** summarizes the experimental design to test models I-III. While STD NMR experiments probe mainly interactions with the low molecular weight components of the system (*i.e.* Aβ monomers) and give no direct information on the interactions of HSA with the oligomers, tryptophan fluorescence can probe HSA interactions with both, Aβ monomers and oligomers. Due to HSA / Thioflavin T (ThT) interactions, ThT fluorescence can be used to reliably probe cross-β-structured oligomers only in the absence of HSA.

The Aβ (12-28) peptide can be easily stabilized for weeks or months in its monomeric state at high concentrations suitable for NMR (11, 15). Furthermore, once Aβ (12-28) oligomers form, their exchange with the monomeric state is sufficiently fast to be detected by saturation transfer difference (STD) NMR experiments with high sensitivity (11,16). However, Aβ (12-28) is only a fragment of the Aβ peptide most commonly found in amyloid plaques in vivo. We therefore complemented our Aβ (12-28) studies with a parallel investigation on the more biologically relevant Aβ (1-40), for which the monomer to oligomer transition is sufficiently slow under conditions suitable for NMR to allow the acquisition of NMR data for the monomeric state. Finally, the Aβ (1-42) was selected for its high propensity to self-associate thus facilitating the detection and characterization of interactions involving the Aβ oligomers. For each Aβ system the presence of oligomers was independently monitored through STD NMR and ThT fluorescence experiments, thus providing a solid foundation for the selection of the inhibitory model (Fig. 1a-c).

Our results consistently support for all three tested peptides a selective interactions of HSA with Aβ oligomers rather than monomers, thus firmly disproving that HSA acts as a "monomer stabilizer", *i.e.* model I in Fig. 1a is excluded. Additionally, our data conclusively rule out the oligomer "dissociation catalyst" model (Fig. 1b, II) and confirm the "monomer competitor" mechanism (Fig. 1c, III). According to this model, HSA binds Aβ oligomers without causing their full dissociation into monomers and

competes with the addition of further Aβ monomers, effectively preventing the growth of the Aβ oligomers into larger assemblies.

MATERIAL AND METHODS

Sample Preparation. Details about the sample preparation protocols (11, 16, 17) are available as Supplementary Material (page S2).

NMR Spectroscopy. The frequency for the saturation of HSA was optimized using a 0.5 mM HSA solution prepared in 50 mM acetic acid–d_4 at pH 4.7, 10% D_2O and by setting the carrier frequency of the saturating Gaussian pulse train at -0.26, 0.57, 0.66, and 7.05 ppm, while the off-resonance saturation frequency was kept constant at 30 ppm. All saturation transfer difference (STD) experiments were acquired using previously described pulse sequences (16,18) and a Bruker Avance 700 MHz spectrometer equipped with 5 mm TCI Cyroprobe at 20 ^{o}C, unless otherwise specified. Selective saturation was achieved using a train of 40 Gaussian-shaped pulses of 50 ms each and separated by a 1 ms inter pulse delay, resulting in total saturation time of ~2 seconds which was preceded by a 100 ms inter-scan delay. The strength of each saturating Gaussian pulse was 110 Hz with a 1 % truncation and 1000 digitization points. The saturation transfer difference spectra were obtained by subtracting on-resonance and off-resonance spectra through phase cycling, while the off-resonance spectra were recorded as reference. A 0.1 ms or 30 ms spin lock (SL) was used prior to signal detection to maximize or to suppress HSA signal, respectively. For all STR and STD spectra acquired in the presence of an Aβ

peptide, the spin-lock duration was set to 30 ms. In all experiments the water magnetization was suppressed using the 3-9-19 Watergate gradient spin-echo (19). For all STD experiments 64 scans and 16 dummy scans were acquired, except for Aβ (1-40) and Aβ (1-42) for which 512 scans were accumulated. For the more sensitive saturation transfer reference (STR) experiments 32 scans and 32 dummy scans were acquired. The spectral processing parameters are included in the figure captions. The methyl spectral region (0.6 – 1.1 ppm) was integrated and measured as a function of time to monitor the aggregation profile of the Aβ peptides. The error was estimated from the spectral noise to be ~5 %. The 1D intensity loss was modeled through an offset-exponential: $a*e^{-bt} + c$, where the a-c parameters were obtained through non-linear curve fitting.

Fluorescence Spectroscopy. Tryptophan fluorescence spectra were acquired using a Varian Cary Eclipse spectrophotometer and were recorded in a 0.5 x 1-cm cell (0.5 cm at the emission and 1 cm at the excitation side) with the excitation and the emission slit width set to 5 nm. An excitation wavelength of 295 nm was used to excite the single tryptophan residue of HSA, Trp 214 (20, 21, 22). When fluorescence measurements were used to investigate ligand interactions, ligand solution without HSA (blank solutions) were acquired first and were then subtracted from the spectra in the presence of the HSA. All spectra were recorded three times and were smoothed using a 10 point average. ThT fluorescence spectra were recorded using a Tecan Safire fluorescence spectrometer and 96 well plates with 50 μL sample volumes. In this case excitation and emission wavelengths were set at 450 and 490 nm, respectively (23). Spectra measured prior to the addition of 20 μM of ThT were subtracted to correct for the blank fluorescence

contribution. For each sample at least four measurements were performed and the resulting averaged values are reported. The error was calculated as the standard deviation of all measurements.

RESULTS

Optimization and Controls of STD Experiments. A critical step to obtain a reliable selection among the models outlined in Fig. 1a-c is to test whether monomeric Aβ peptides interact with albumin. For this purpose we have used 1D saturation transfer difference (STD) and reference (STR) NMR spectra, which are ideal to probe interactions with K_D values in the μM range (24), such as those previously reported between Aβ and HSA (13). Unlike previous investigations (11), the STD experiments used here were specifically optimized to probe Aβ / HSA interactions. Details about the optimization of the STD experiments and the related controls using known HSA ligands such as aspirin and L-tryptophan (25, 26) are available as Supplementary Material (p. S2, Figs. S1-S3).

HSA Does not Interact with the Monomeric Aβ(12-28) Peptide. As an initial step to test model I (Fig. 1a) we have characterized the interactions between HSA and monomeric Aβ (12-28) through STD NMR experiments. Specifically, we recorded STD data for the Aβ (12–28) peptide (Fig. 2a-d) using the same acetate buffer and concentrations as in the control spectra with aspirin and L-tryptophan (Fig. S2). Under these experimental conditions, Aβ (12-28) is stable as a monomeric species due to the

combination of 30 kDa-cutoff filtration and the subsequent dilution to sub-mM levels included in our sample preparation protocols (11, 15-17). The absence of oligomers in the Aβ (12-28) solutions used for the STD experiments is also independently confirmed by the lack of STD signal observed in the absence of HSA (Fig. 2a), because the 0.66 ppm saturation frequency employed for albumin causes saturation of the methyls of Aβ(12-28) as well (16). Therefore if Aβ (12-28) oligomers were present, they would give rise to a detectable STD signal in Fig. 2a, as the monomer/oligomer exchange in acetate buffer has been shown to be sufficiently fast to provide excellent saturation transfer (11, 16).

It should also be noticed that HSA is known to undergo several pH – dependent inter-domain re-orientations (22), which possibly affect its ligand interactions (25). The different HSA conformers can be probed using the maximum fluorescence emission wavelength (λ_{max}), as shown in Figure S3. Figure S3 indicates that even at pH 4.7 albumin exists mainly in the physiological N-state. The STD data of Fig. 2 are therefore relevant for the N-form of albumin.

The STD and STR data of Fig. 2b-d show no significant STD signal or STR line-broadening for Aβ (12–28) at any HSA concentration tested. The absence of STD signal and of STR line-broadening in Fig. 2b-d clearly rules out the possibility that the N-state of HSA interacts with the monomeric Aβ (12–28) peptide with a K_D in the μM-mM range. It is also highly unlikely that monomeric Aβ (12–28) binds HSA with a lower K_D value (*i.e.* K_D ~ nM) as these high affinity interactions would result in significant signal losses and/or chemical shift changes in the reference spectrum of Fig. 2d.

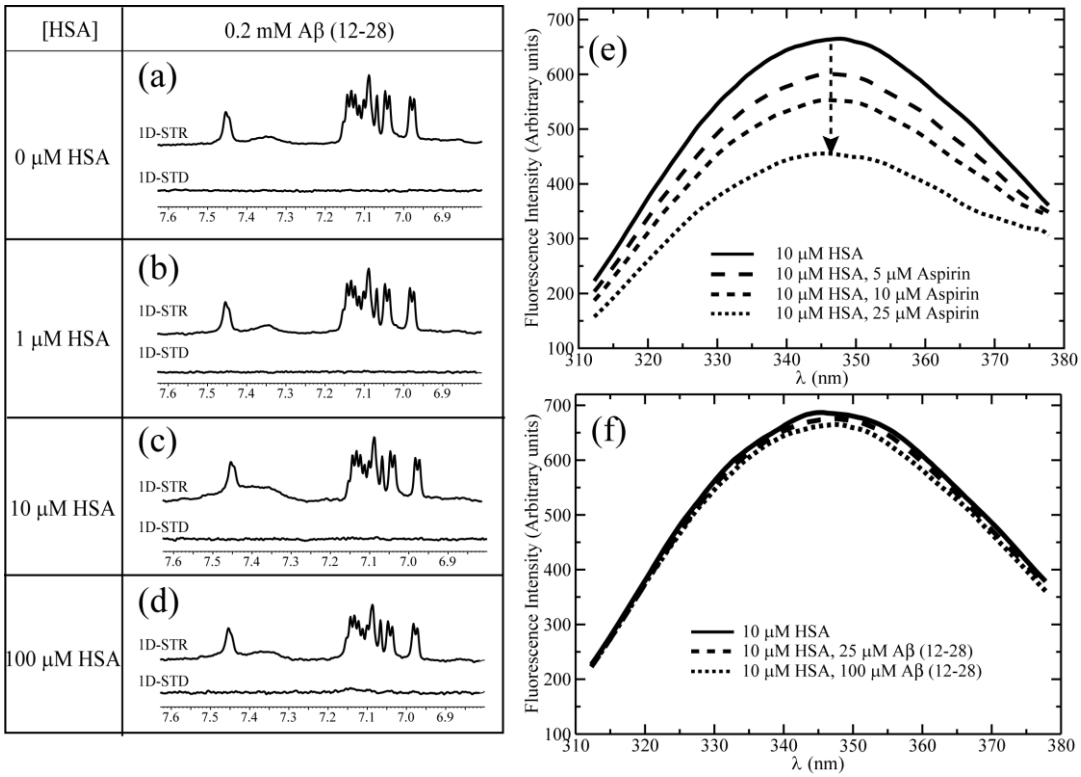

Figure 2. (a-d) Effects of HSA on the saturation transfer reference (STR) and saturation transfer difference (STD) spectra of 0.2 mM Aβ (12-28) in 50 mM acetic acid-d_4, pH 4.7, 10 % D_2O. The STR and STD spectra of 10 and 100 μM HSA solutions were subtracted from the protein peptide mixture spectra to remove residual HSA signal. All spectra were acquired at 700 MHz using a TCI CryoProbe and at 20 ^oC. A 30 ms long spin lock (SL) was used to minimize the residual HSA signal. All spectra were processed using a line broadening factor of 3 Hz. Panels **(e, f)** depict the effects of aspirin and Aβ (12-28), respectively, on the emission intrinsic fluorescence spectra of HSA.

The NMR results for the Aβ (12-28) / HSA system were further supported using independent HSA tryptophan fluorescence experiments. While wt Aβ peptides do not contain Trp residues, a single tryptophan is present in HSA (*i.e.* Trp 214) and is located in the proximity of Sudlow site I in subdomain IIA (26). Quenching of the intrinsic Trp 214 fluorescence has been previously used to probe binding to HSA for several ligands (26).

In general, ligand-dependent intrinsic tryptophan fluorescence quenching is either due to direct energy transfer from the albumin fluorophore to the bound ligand fluorophores or due to ligand-induced variations in the local Trp environment (20, 21, 26). For instance, Fig. 2e indicates that a significant dose-dependent quenching of the HSA Trp 214 fluorescence occurs upon addition of aspirin in the 5 to 25 μM concentration range. Considering that aspirin, similarly to the Aβ peptide, does not absorb at the HSA emission wavelength region around 340 nm (27), the data of Fig. 2e suggest that aspirin perturbs the albumin structure around Trp 214, as also expected since aspirin binds to Sudlow site I in the proximity of Trp 214. However, when similar fluorescence experiments were performed with the Aβ (12–28) peptide prepared in the monomeric state, no Trp fluorescence quenching was observed (Fig. 2f) indicating that monomeric Aβ (12–28) does not affect the environment of Trp 214 in HSA, consistently with the absence of binding as supported by the previous NMR data (Fig. 2e-d).

HSA Does not Interact with the Monomeric Aβ (1-40) Peptide. For the purpose of verifying that the absence of interactions between HSA and Aβ (12-28) is not due to the fragmentation of the Aβ peptide, a similar combined NMR and fluorescence-based experimental strategy was further extended to the biologically relevant Aβ (1-40) peptide prepared under conditions that favour the monomeric state (Fig. 3a-c, Fig. 4a,b). Specifically, Aβ (1-40) samples with concentrations ≤ 100 μM and freshly prepared according to the protocols described in the Supplementary Material (p. S2) are largely monomeric due to the lag time of the nucleation phase in the aggregation of Aβ(1-40)

(28). This is also independently confirmed by ThT fluorescence, which does not detect any significant concentration of cross-β aggregates for 25 or 100 μM Aβ(1-40) (Fig. 4a), and by the lack of detectable STD signal for Aβ(1-40) alone (Fig. 3a).

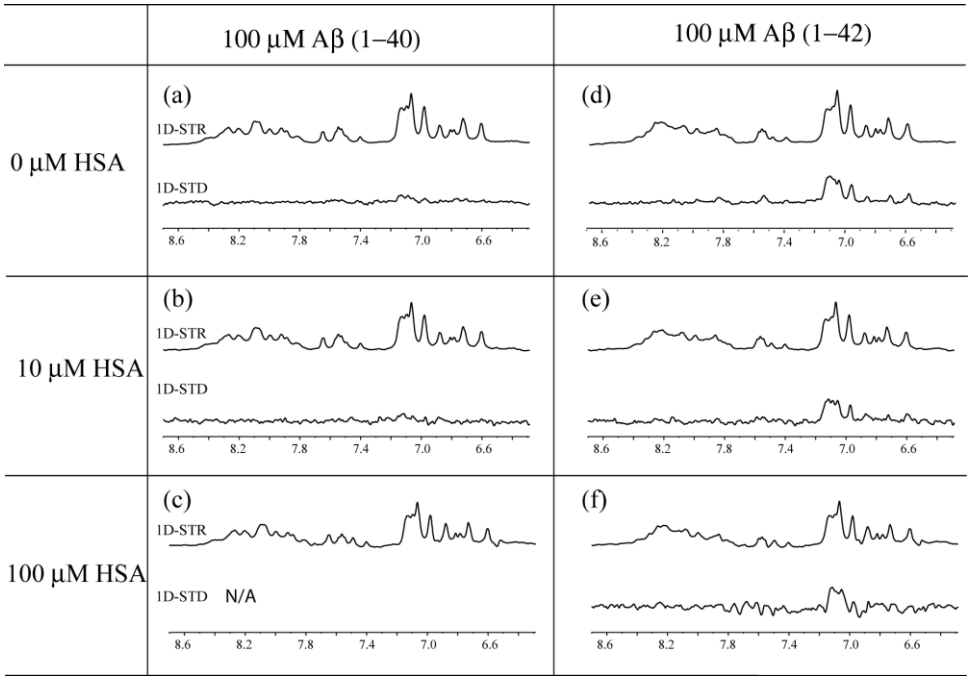

Figure 3. Effect of HSA on the saturation transfer reference (STR) and saturation transfer difference (STD) spectra of Aβ (1-40) and Aβ (1-42) samples. All peptide solutions were prepared at a 0.1 mM concentration in 20 mM potassium phosphate buffer, pH 7.4, 10 % D_2O. A 30 ms long spin lock (SL) was used to minimize the HSA signal. The STR and STD spectra of the 10 and 100 μM HSA solutions were collected and were subtracted from the protein peptide mixture spectra. While this subtraction was possible for the 100 μM Aβ (1-42) sample, this subtraction was not viable for the Aβ (1-40) sample due to the neglible STD effect arising from this peptide as compared to that originating from albumin. All spectra were acquired at 700 MHz using a TCI CryoProbe and at 20 ^{o}C. The STR and STD spectra were processed using a line broadening factor of 10 Hz. In panel (f), at a 100 μM albumin concentration the 30 ms spin-lock becomes less effective in completely removing the protein signal resulting in residual difference artifacts at 7.4-7.8 ppm range.

Considering, as discussed above, that the 0.66 ppm irradiation frequency causes saturation of the Aβ methyls as well, the observation of no significant STD signal in Fig. 3a points to the absence of Aβ(1-40) oligomers for which the peptide exchange with the monomeric state occurs sufficiently fast to give rise to saturation transfer (16), confirming the monomeric nature of our 100 μM Aβ(1-40) sample.

he lack of detectable STD signal for Aβ(1-40) in Fig. 3a also indicates that the Aβ(1-40) monomers are sufficiently unstructured to quench possible intra-monomer cross-saturation effects (16).

The STR spectra of freshly prepared 100 μM Aβ(1-40) in the absence and presence of different concentrations of HSA (Fig. 3a-c) show no significant changes in line broadening, chemical shift or intensity upon addition of HSA to the peptide solution pointing to the absence of HSA – monomeric Aβ (1-40) interactions in the μM K_D range. This conclusion is further confirmed by the lack of signal in the STD spectrum of Fig. 3b and by the absence of significant variations in the HSA Trp fluorescence spectra acquired even with 10-fold excess of Aβ (1–40) (Fig. 4b), further confirming the absence of interactions in the μM affinity range between HSA and monomeric Aβ(1-40).

HSA Selectively Interacts with the Oligomeric but not the Monomeric Aβ(1-42). At a peptide concentration of 25 μM and using sample preparation protocols that minimize self-association (28), it is possible to obtain Aβ (1-42) solutions for which the

ThT fluorescence is reduced close to basal levels (Fig. 4a), suggesting the absence of significant amounts of cross-β structured aggregates (29). Under these conditions no appreciable quenching of the intrinsic albumin fluorescence is observed upon addition of Aβ (1-42) (Fig. 4c) consistently with the absence of interactions between HSA and monomeric Aβ (1-42) with a K_D in the μM range.

However, when the self-assembly of Aβ (1-42) is promoted by increasing its concentration to 100 μM, not only significant thioflavin-T binding is observed (Fig. 4a), pointing to the presence of assemblies with cross-β structure (29), but also the intrinsic albumin fluorescence is quenched (Fig. 4c), suggesting that albumin selectively binds oligomeric Aβ (1-42) species. A positive control of these results is provided by a 100 μM Aβ (1-42) sample that was further aggregated for 3 hours at 37 ^{o}C prior to ThT measurements and HSA addition. This sample showed increased ThT fluorescence (Fig. 4a) and also resulted in an additional quenching of the HSA intrinsic fluorescence (Fig. 4c), consistently confirming that HSA selectively targets oligomers with cross-β structures as opposed to monomers.

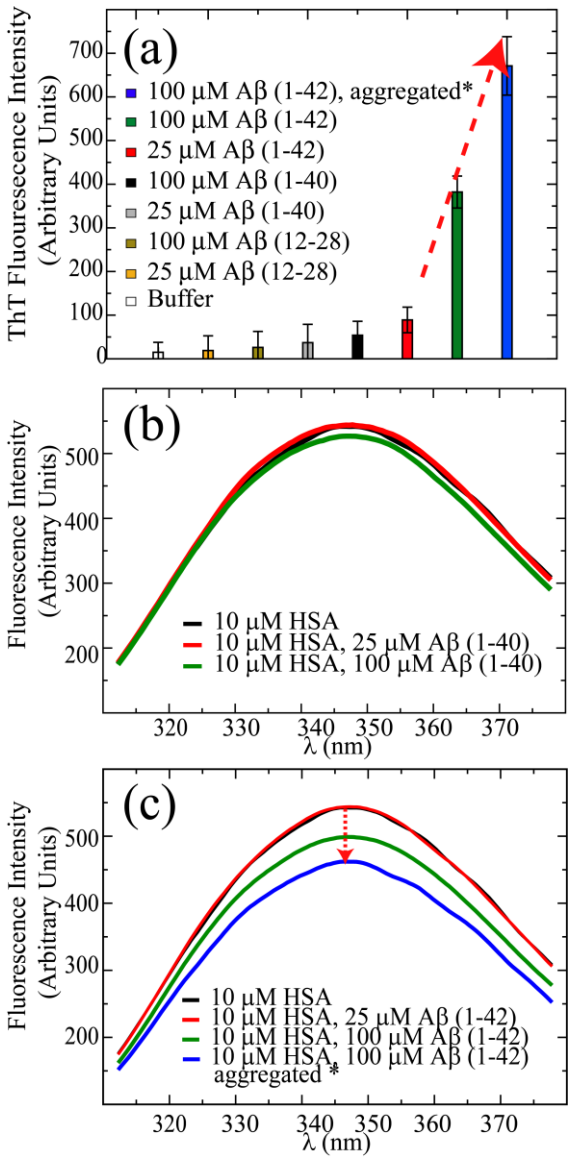

Figure 4. **(a)** Probing Aβ assemblies using Thioflavin T (ThT) fluorescence. All samples were freshly prepared, with the exception of one 100 μM Aβ (1-42) sample (blue bar) that was aggregated for 3 h at 37 ^{o}C prior to ThT fluorescence measurements. This sample is denoted by an asterisk (*). ThT was present in all samples at a 20 μM concentration. For each sample at least 4 measurements were collected and the average values are reported. The error was calculated as standard deviation of all measurements. **(b)** Interactions of HSA with Aβ (1-40) as probed by tryptophan fluorescence. **(c)** Interaction of HSA with Aβ (1-42) probed by HSA tryptophan fluorescence quenching at increasing Aβ (1-42) concentrations.

As a further control for the absence of HSA-Aβ (1-42) interactions, the STD and STR spectra of freshly prepared 100 μM Aβ(1-42) were acquired both in the absence and presence of increasing concentration of albumin (Fig. 3d-f). As shown in Fig. 3d-f, no significant change is observed in the STR spectra of Aβ(1-42) upon addition of HSA up to a 1:1 stoichiometric ratio, confirming that albumin does not bind monomeric Aβ(1-42) in the μM or sub-mM range. In addition, it is interesting to note that, unlike Aβ(1-40) (Fig. 3a), Aβ(1-42) gives rise to a significant STD signal even in the absence of albumin (Fig. 3d). This observation is consistent with intra-monomer cross-saturation caused by at least partial structuring of the monomeric Aβ(1-42) peptide and/or with the presence of oligomers which are sufficiently small to give rise to a detectable NMR signal or are in fast/intermediate exchange with the monomeric state. In either case, these oligomers are likely occurring early in the fibrillization pathways. The absence of STD changes upon albumin addition (Fig. 3d-f) is therefore consistent with a selective interactions of HSA with larger assemblies, such as those detected by ThT fluorescence but not STD, as their exchange with the monomeric state is too slow and/or their concentration is too low to be sensed by STR/STD NMR. However, when comparing ThT and STD as oligomer detection methods, it should also be considered that, unlike STD, the usefulness of ThT fluorescence measurements to probe the presence of assemblies with cross-β structure is mainly limited to Aβ solutions without any albumin. This is because ThT interacts with albumin as proven by the STD spectra of Fig. S4. In addition, independent recent studies also report that ThT binds albumin with a K_D of ~10 μM (30). Such ThT-albumin interactions may therefore affect and bias experiments in which ThT fluorescence is

employed to monitor Aβ aggregation in the presence of albumin, as previously attempted (14).

Albumin Inhibits Aβ(1-42) Fibril Growth at Sub-Stoichiometric Concentrations. While the analysis presented above clearly shows that HSA targets Aβ oligomers rather than monomers as entailed by models II and III (Fig. 1a-c), a better differentiation between these two remaining putative mechanisms requires additional experiments. For this purpose, we have measured the effect of HSA on the self-association of the Aβ (1-42) peptide at 37 ^{o}C, as monitored through 1D NMR signal losses over a period of 23 hours (Fig. 5a). Figure 5a shows that in the absence of oligomerization inhibitors more that 50 % of the original 1D signal is lost already after 3 hours from the acquisition of the first 1D NMR spectrum. After this rapid initial NMR signal loss, a slower decay is observed that levels off at a plateau of ~22 – 25 % of the original 1D intensity (Fig. 5a). No detectable line-broadening was observed in the NMR spectra of Aβ (1-42) during the course of its aggregation (Fig. 6), indicating that the exchange between NMR detectable and NMR undetectable species of Aβ (1-42) is slow in the chemical shift time scale (> ms). The absence of line-broadening over time also indicates that the observed NMR signal loss is due to the sequestration of Aβ (1-42) monomers into NMR undetectable oligomers, protofibrils and fibrils.

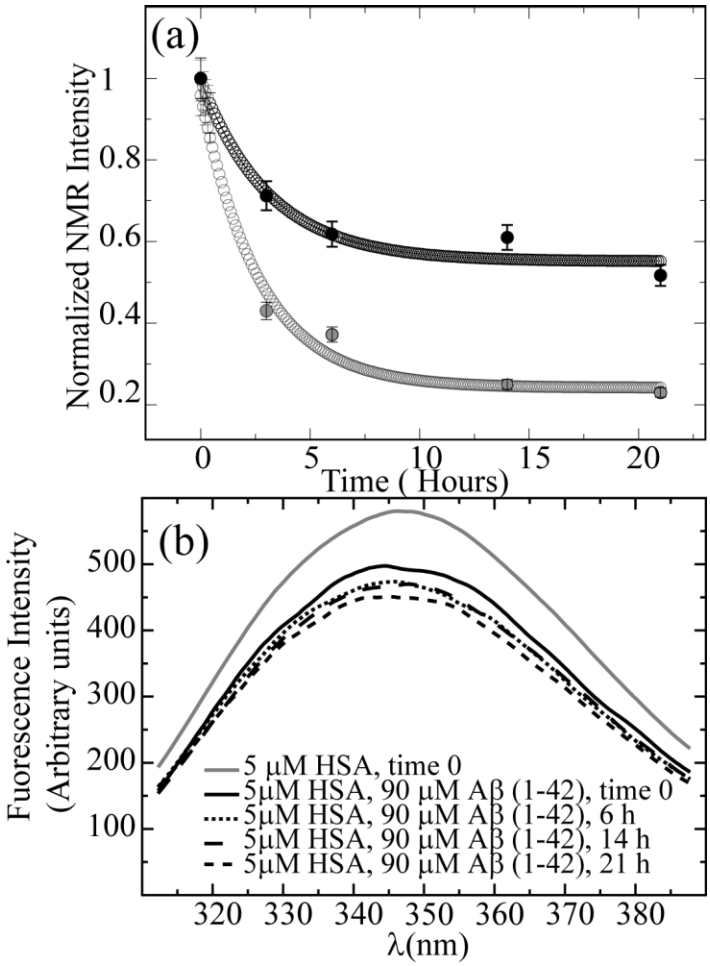

Figure 5.Time-dependent aggregation of 90 μM Aβ(1-42) in the absence (gray curve) and presence (black curve) of 5 μM HSA as monitored by NMR 1D NMR spectra with a 30 ms spin-lock filter **(a)** and by intrinsic HSA tryptophan fluorescence **(b)**. The experimental data were fitted using the offset decaying exponential: $a*e^{-bt} + c$, where t is in hours and the a-c parameters were obtained through non-linear curve fitting. The actual experimental data are plotted in solid circles, while the fitted values are shown in empty circles. Between the readings, samples were incubated in a water bath at 37 ^{o}C. The NMR intensities reported in panel (a) are normalized intensities of the methyl spectral region (0.6 – 1.1 ppm) measured as a function of time. The error was estimated from the spectral noise to be ~5%. NMR experiments were acquired at 700 MHz at 37 ^{o}C in 20 mM potassium phosphate, pH 7.4, 10% D_2O, 0.02% NaN_3.

In the presence of HSA at sub-stoichiometric ratios (*i.e.* 18/1 = [Aβ (1-42)]/[HSA]), the overall loss of the peptide NMR signal over time is significantly reduced

relative to what was observed for Aβ (1-42) alone (Fig. 5a). In the presence of albumin, the plateau value reached after the initial rapid decay stabilizes at about 50-60 % of the original NMR intensity, *i.e.* at ~twice the NMR signal detected in the absence of albumin. Since no direct contribution from the NMR resonances of albumin is expected in these spectra due to the low protein concentration and also due to the 30 ms spin-lock filter employed for these 1D spectra, the NMR data in Fig. 5a demonstrate that sub-stoichiometric concentrations of albumin are sufficient to inhibit the transition of Aβ (1-42) from NMR detectable monomeric into large NMR undetectable assemblies. Interestingly, line fitting with an offset-exponential decay function (Fig. 5a) shows that, unlike the plateau value, the initial rate of decay is not dramatically affected by albumin (*i.e.*-0.37 $hour^{-1}$ and -0.32 $hour^{-1}$ in the absence and presence of HSA, respectively). Assuming that the initial decay rate senses mostly the pre-nuclear early-oligomer seeded self-association, while the plateau height mainly probes the residual monomers or NMR detectable oligomers in equilibrium with fibrils, proto-fibrils and large oligomers, the data of Fig. 5a support the conclusion that HSA targets mainly larger oligomers, in line with our fluorescence and STD results (Figs. 3 and 4).

The partial aggregation of Aβ (1-42) in the presence of HSA was also monitored through albumin intrinsic Trp fluorescence spectra (Fig. 5b) acquired in parallel with the NMR data of Fig. 5a and under experimental conditions similar to those used for the NMR experiments. The fluorescence data of Fig. 5b show that a significant quenching occurs for all time points sampled after the addition of 90 μM Aβ (1-42). This is because at these concentrations samples of freshly prepared Aβ (1-42) peptide contain already

significant amounts of aggregates with cross-β structure, as indicated by the previous ThT fluorescence data (Fig. 4a). Overall, Fig. 5 shows that albumin is able to inhibit the time-dependent shift of the Aβ (1-42) oligomer distribution towards high molecular weight assemblies (Fig. 5a) by binding to cross-β structured aggregates (Fig. 5b). This figure also illustrates the complementarity of NMR and fluorescence experiments. NMR reports mainly on the low MW Aβ species in solution, which are unlikely to interact directly with albumin and therefore the intensity of the first point in Fig. 5a is not affected by the addition of HSA. Conversely, the intrinsic albumin fluorescence senses also interactions with high MW Aβ oligomers that would otherwise escape detection by NMR. This is why in Fig. 5b, the major variation of Trp fluorescence is observed for the very first time point, unlike what observed for the NMR time profile of Fig. 5a.

Albumin Does not Cause the Dissociation of Aβ Oligomers into Monomers. The picture emerging from the data presented above appears to be consistent with model III (Fig. 1c) as opposed to model II (Fig. 1b). However, model II (Fig. 1b), according to which albumin promotes the dissociation of pre-existing oligomers, is still able to explain the observed inhibition of Aβ fibrillization at substoichiometric amounts of HSA (Fig. 5a). Therefore, before conclusively ruling out model II we carried out additional experiments in which albumin is added to solutions in which significant populations of Aβ oligomers are pre-formed. For instance, Figure 6 illustrates that already three hours after preparation of the Aβ (1-42) samples, a significant loss of 1D signal intensity is

observed (Fig. 6a, b), pointing to the initial formation of assemblies with sizes beyond the NMR detection limit. If self-association continues after three hours in the absence of inhibitory protein, most of the NMR signal is lost already after 2 days (Fig. 6c).

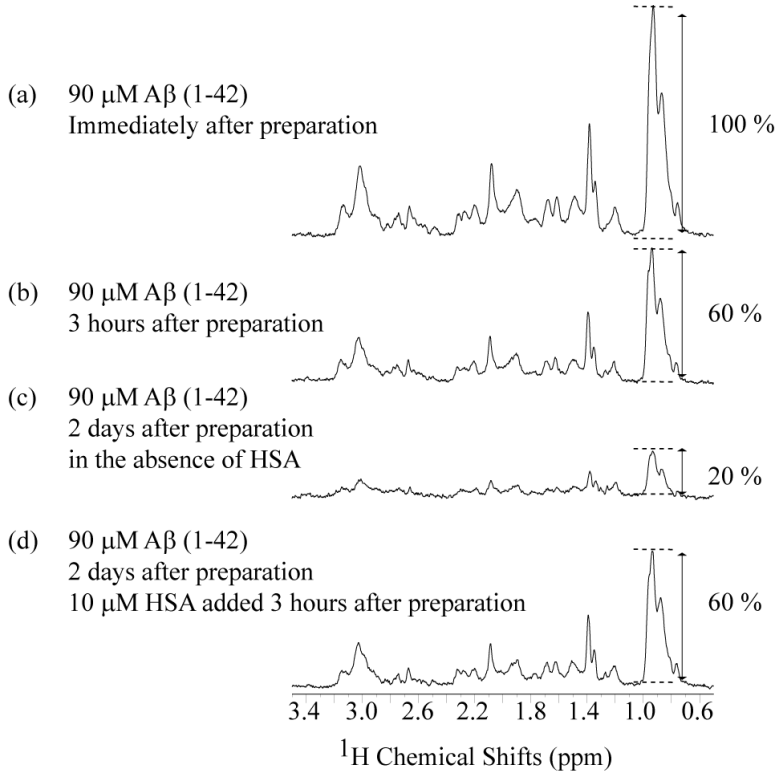

Figure 6. Effect of a delayed addition of HSA on the aggregation profile of Aβ (1-42). Panels **(a)** and **(b)** show the 1D NMR spectra of 90 μM Aβ(1-42) immediately after preparation and after 3 hours, respectively. In the absence of HSA, two days after the sample was prepared about 80 % of the initial NMR signal is lost as shown in panel **(c)**. However, if 10 μM of HSA is added 3 hours after sample preparation, no NMR signal losses are observed even after two days **(d)**. These spectra were recorded at 600 MHz and 37 ^{o}C. In between acquisition sessions, samples were stored in a water bath at 37 ^{o}C. Note that the Aβ (1-42) samples used in this and in the previous figure come from different stock solutions.

However, if HSA is added three hours after preparation, the intensity of the NMR intensity remains comparable to that measured prior to the addition of albumin (Fig. 6b,d), without the signal losses observed in the absence of HSA over the same time span

(Fig. 6c) but also without regaining the signal measured immediately after sample preparation (Fig. 6a). These observations therefore support the notion that HSA does not cause the Aβ (1-42) oligomers to dissociate into monomers. Similar results were obtained for the Aβ (12-28) peptide as indicated in Figs. S5, S6 and explained in the Supplementary Material section p. S3.

DISCUSSION

The data presented here (Figs. 2-5) consistently support the notion that albumin does not bind Aβ peptides which are predominantly in the monomeric or in the low molecular weight oligomeric states, lacking ThT-binding competent cross-β structure. This conclusion applies not only to the Aβ (12-28) fragment model system (Fig. 2) but also to the longer Aβ (1-40) and Aβ (1-42) peptides (Figs. 3-5) and is supported by both NMR data and independent HSA intrinsic Trp fluorescence experiments with an extensive series of positive and negative controls (Figs. 2-5; Figs. S1-S4). On this basis, it is therefore possible to rule out that albumin inhibits Aβ fibrillization though a 'monomer stabilizer' mechanism (*i.e.* model I, Fig. 1a), whereas at this stage the 'dissociation catalyst' and the 'monomer competitor' models (II and III, Fig. 1b,c respectively), which involve interactions with Aβ oligomers, appear more plausible. Indeed, interactions between albumin and the Aβ peptide oligomers with a K_D in the μM or sub-μM range are fully supported by the quenching observed in the HSA intrinsic fluorescence spectra (Fig. 4c and Fig. 5b), whenever cross-β structured Aβ aggregates are

present as indicated by detectable levels of ThT fluorescence (Fig. 4a). Overall, the quenching of the HSA intrinsic fluorescence observed upon addition of HSA appears strikingly well correlated with the intensity of the ThT fluorescence detected prior to HSA addition (Fig. 4), as expected if the HSA binding-competent forms of the Aβ peptides are assemblies with cross-β structure.

Our NMR data for experiments in which albumin was added to pre-formed Aβ assemblies (Fig. 6 and S5) show that the interactions between albumin and the Aβ oligomers does not cause the dissociation of Aβ into monomers, as predicted by the 'dissociation catalyst' (model II, Fig. 1b), but it kinetically inhibits the transition of the Aβ oligomer distribution from monomeric or low-molecular weight species into larger NMR-undetectable fibril-like assemblies that would otherwise occur in the absence of albumin (Fig. 5a) (31). This HSA-dependent accumulation of monomeric and low-molecular weight Aβ oligomers is observed even at sub-stoichiometric (*i.e.* 18:1) concentrations of albumin (Fig. 5a) and it is fully accounted for by the 'monomer competitor' model (III, Fig. 1c) assuming that HSA interacts with larger Aβ oligomers at the sites where further monomers would otherwise bind. The number of such sites of monomer addition is typically significantly lower than the number of polypeptide chains in an oligomer or fibril and therefore the binding of sub-stoichiometric amounts of HSA to cross-β structured oligomers is in principle sufficient to inhibit further addition of the monomers to the growing aggregates, thus preventing the consequent loss of NMR signal

as observed in Fig. 5a. For further details about the effect of HSA on the mechanism of homogenous nucleation-growth see supplementary material pg. S3-S4.

The 'monomer competitor' model (III, Fig. 1c) supported by our data is consistent with previously published dynamic light scattering (DLS) (14) and surface plasmon resonance (SPR) (7) experiments. DLS profiles indicate that when Aβ (1-40) aggregates in the presence of the HSA homolog bovine serum albumin (BSA), the population of large oligomers (*i.e.* Stokes radius ~ 140 nm) decreases and that of smaller assemblies (*i.e.* Stokes radius ≤ 34 nm) increases, consistently with the accumulation of low-molecular weight species in the presence of HSA (Fig. 5a). However, the DLS experiments alone are not sufficient to rule out possible Aβ monomer – HSA interactions (14). In this respect SPR is complementary to DLS. SPR does not map the oligomer re-distribution of the Aβ peptide, but it can probe direct albumin - Aβ monomer interactions. Specifically, SPR did not detect any interactions with HSA or BSA when monomeric biotin-Aβ (1-40) was immobilized on the sensor chip, while when the SPR experiment was repeated with pre-formed polymers of Aβ (1-42) deposited through a monoclonal antibody, clear evidence for binding with a μM or higher affinity was obtained (7). These SPR results are fully consistent with the selectivity reported here of HSA for large cross-β structured Aβ assemblies as opposed to Aβ monomers, indicating that the SPR data were not biased by the derivatization of the Aβ peptide with biotin and/or by the type of chip anchoring technique used, as previously speculated (13).

While consistent with and supported by previous DLS and SPR results, our conclusions on the 'monomer competitor' model (III, Fig. 1c) do not agree with previous investigations based on CD spectra (13) and immunoassays which have been interpreted in terms of binary 1:1 complexes between Aβ monomers and HSA (12). A possible explanation for this discrepancy may lie in the presence of undetected Aβ oligomers in equilibrium with Aβ monomers in the samples used for the CD and immunoassays experiments. Indeed, the Hill coefficients reported for the binding of Aβ (1-40) to HSA are in the 1.4-1.5 range (13), pointing to a higher cooperativity than that anticipated based on the formation of 1:1 complexes between Aβ monomers and HSA. Another challenge encountered when CD experiments are used to monitor Aβ - HSA interactions is the deconvolution of the contributions to the CD spectra from these two interacting components due to the poor selectivity of CD for Aβ and HSA. This problem is effectively circumvented using either intrinsic Trp fluorescence, since Trp is present only in HSA but not in the Aβ peptides, or T1ρ-filtered NMR experiments, where the long (*i.e.* 30 ms) spin-lock filters out most contributions from albumin, while preserving the signal of the low molecular weight Aβ peptides.

CONCLUSIONS

We have characterized the Aβ - HSA interactions using a combined experimental strategy based on NMR and intrinsic albumin fluorescence and we have applied it to a family of Aβ peptides (*i.e.* Aβ (12-28), Aβ (1-40) and Aβ (1-42)), for which the oligomeric state was independently assessed by ThT fluorescence and STD NMR experiments. Based on our NMR and fluorescence data and on an extensive series of positive and negative controls, we have shown that albumin selectively binds cross-β structured Aβ assemblies as opposed to Aβ monomers. This binding occurs with a K_D in the μM or lower range and competes with the further growth of the HSA-bound Aβ oligomers through monomer addition. Overall, our data clearly support a 'monomer competitor' model for the Aβ fibrillization inhibitor function of HSA, clearing previous discrepancies in the literature about Aβ - HSA interactions. Other putative mechanisms, according to which albumin acts as a 'monomer stabilizer' or a 'dissociation catalyst', are not supported by our data.

The proposed model for the Aβ/HSA interactions explains not only how albumin is able to affect fibrillization, but it will also help understand how inhibitory proteins affect the distribution of toxic soluble oligomers of amyloidogenic peptides in general, such as the inslet amyloid polypeptide (IAPP) (32). Furthermore, the combined STD NMR/fluorescence approach presented here is likely to be generally suitable for the

investigation of other systems involving the interactions of amyloidogenic peptides with fibrillization-inhibitory proteins.

ACKNOWLEDGEMENTS: We thank NSERC and the Alzheimer Society of Canada for financial support to G.M. G.M. is also grateful to the Heart and Stroke Foundation of Canada for a Maureen Andrew New Investigator award. J.M. is funded by an NSERC graduate fellowship. We thank Tyler E. McNicholl, Elle Dunitz, Rajeevan Selvaratnam, Dr. J. Ortega, Dr. A. Bain, Dr. Rahul Das and Dr. Somenath Chowdhury for helpful discussions. We thank Dr. J. Brennan for access to fluorescence facilities.

SUPLEMENTARY INFORMATION

Sample Preparation Protocols:

Aβ (12-28) Samples. The Aβ (12-28) peptide used in this investigation was purchased from EZBiolab Inc., with a purity greater than 95 %. 1 mM and 0.7 mM Aβ (12-28) solutions were prepared by dissolving the peptide as a lyophilized powder in 50 mM acetate buffer–d_4 at pH 4.7, with 10% D_2O. This buffer composition was used because it has been previously shown to stabilize the monomeric and early oligomeric forms of the Aβ (12-28) peptide (11, 16, 17). In order to remove aggregates formed during the peptide lyophilization and dissolution processes, the peptide solution was filtered through a Ultrafree-MC Millipore 30 kDa cutoff filter in 5 min intervals at 3,000 rpm. To maximize and stabilize the monomeric form of the peptide, the filtered 0.7 mM Aβ (12-28) sample was diluted to 0.2, 0.1 and 0.025 mM concentrations with 50 mM acetate buffer–d_4 at pH 4.7 and 10% D_2O and was used in the NMR and fluorescence measurements.

Aβ (1-40) and Aβ (1-42) Samples. The Alzheimer's peptides Aβ (1-40) and Aβ (1-42) were purchased from EZBiolab Inc., with a purity greater than 95 %. 1 mg of either Aβ peptide was initially dissolved in 500 µL of ice cold 10 mM NaOH. After dissolution, the sample was sonicated for 2 min and then it was placed on ice for 2 min. This sonication/cooling cycle was repeated twice. Aliquots taken from this stock solution were diluted in 20 mM potassium phosphate buffer at pH 7.4, 10 % D_2O and 0.02 %

NaN_3 resulting in 100, 90 and 25 μM peptide solutions. Aggregated 100 and 90 μM Aβ(1-42) peptide samples were prepared by incubating the Aβ (1-42) solution in a water bath at 37 ^oC for 3 hours without mixing.

Other Samples. L-Tryptophan and aspirin were purchased from Sigma-Aldrich. A 0.2 mM aspirin solution was prepared through serial dilutions of a 2 M aspirin stock DMSO solution with 50 mM acetate buffer–d_4 at pH 4.7, with 10 % D_2O. In the final solution DMSO was present at a residual concentration of 0.01 %. A 0.2 mM tryptophan solution was prepared through direct dissolution of the dry powder in acetate buffer. Fatty acid free and essentially globulin free HSA was purchased from Sigma with a 99 % purity. 1 mM stock solutions were prepared by dissolving HSA in the buffers used for the spectroscopic analyses.

Optimization and Controls for STD Experiments

In order to maximize the sensitivity of the STD experiments, we have first optimized the on-resonance frequency of the STD Gaussian pulse train for maximal HSA saturation. To monitor the degree of HSA saturation as a function of selective irradiation frequency, STD spectra were acquired for a concentrated HSA solution (*i.e.* 0.5 mM) using a short spin-lock (*i.e.* 100 μs) and setting the carrier frequency of the saturating Gaussian pulse train at offsets of -0.26, 0.57, 0.66, and 7.05 ppm (Fig. S1). Figure S1 indicates that saturation in the -0.26 – 0.66 ppm range results in optimal and thorough saturation, with STD spectra resembling the reference spectra (STR) acquired under the

same experimental conditions. Figure S1 also reveals that saturation of the aromatic region results in less efficient spin diffusion as shown by a lower STD signal of the methyl region relative to the saturated spectral region. We therefore selected a 0.66 ppm saturation frequency for all subsequent STD experiments.

Before applying the STD experiments to the Aβ systems, we tested the sensitivity of our STD experiments to interactions in the μM – mM range using known control HSA ligands, *i.e.* aspirin and L-tryptophan. Aspirin binds with an overall dissociation constant (K_D) of ~70 μM to Sudlow sites I and II, located in the HSA subdomains IIA and IIIA, respectively (26), while L–tryptophan binds with a ~mM K_D to Sudlow site II under our experimental conditions (25). We therefore acquired saturation transfer difference (STD) and reference (STR) spectra for both aspirin and L-tryptophan in the absence (Fig. S2a, e) and in the presence of HSA at different concentrations (Fig. 2b-d and 2f-h). Without HSA no STD signal is observed (Fig. S2a, e) proving that the STD signal is a result of protein- ligand interactions only. As 1 μM HSA is added, a detectable STD signal is apparent for aspirin with μM affinity (Fig. S2b) but not for L-tryptophan with mM affinity (Fig. S2f). As the concentration of HSA increases to 10 μM the STD signal of aspirin builds up (Fig. S2c) but further addition of HSA causes line-broadening for the aspirin resonances with consequent loss of signal (Fig. S2d). Unlike aspirin, the STD signal of L-tryptophan is detected only at 100 μM but not at 10 μM HSA, due to the lower affinity for HSA of L-tryptophan (Fig. S2g, h). Overall, the control experiments of Fig. S2a-h prove that the STD spectra acquired under our experimental conditions are

efficient at probing HSA interactions within a wide K_D range, provided that the STD and STR data are acquired at several HSA concentrations.

Test of the Model II ("Dissociation Catalyst" Model) using Aβ (12-28)

The 1D-NMR spectrum of monomeric Aβ (12-28) prepared through filtration (Fig. S5a) was acquired first as a reference. This 1D trace is characterized by narrow line-widths as expected for a 17 amino acid peptide in which the self-association equilibria are largely shifted towards the monomeric form. However, upon addition of 25 mM NaCl to the filtered Aβ (12-28) sample a marked increase in linewidths is observed for most resonances after an equilibration time of seven days (Fig. S5b). The salt-induced line-broadening is a result of the hydrophobic-collapse driven oligomerization promoted by the higher ionic strength, which weakens electrostatic inter-molecular repulsions (15). For the Aβ (12-28) system the NMR line-width is therefore a convenient qualitative indicator of self-association (11, 15-17). Upon addition of 10 μM HSA to the Aβ (12-28) sample with 25 mM NaCl a marked overall line-narrowing is detected (Fig. S5c), as previously observed (11), confirming that HSA interferes with the exchange of polypeptide chains between the monomeric and the oligomeric states of Aβ (12-28). However, while albumin addition sharpens several peaks to line-widths comparable with those of the filtered sample (Fig. S5a, c), it does not restore the NMR signal intensities to those observed for the original filtered Aβ (12-28) sample before the salt-induced oligomer formation (Fig. S5a). Similar conclusions are reached even with different window function-induced line broadening (Fig. S6a), proving that the intensity

differences between panels a and c of Fig. S5 are not an artifact of the specific apodization shape used. Furthermore, the intensity loss observed in the presence of protein (Fig. S5c) cannot be explained by direct salt effects on the sensitivity of the cryoprobe as the residual glycerol signal from the filter does not change significantly in the presence of salt (Fig. S6b). These experiments therefore show that although albumin prevents monomer/oligomer exchange it does not dissociate oligomers into monomers. The significantly lower population of the monomeric state in the samples with HSA (Fig. S5c) relative to the control solution (Fig. S5a) is therefore in agreement with the conclusion reached for Aβ (1-42) (Fig. 6).

Effect of HSA on the mechanism of homogenous nucleation – growth

A better appreciation of how HSA kinetically controls the Aβ fibrilization can also be obtained in light of a previously proposed model for the homogeneous nucleation/growth of Aβ fibrils (31). Accordingly to this model, nuclei are first formed through the reversible self-association of monomeric peptides into micellar aggregates. These peptidic micellar nuclei serve as seeds for the growth of fibrils through the largely irreversible addition of monomeric peptides. Based on this fibrillization mechanism, the main source of depletion of monomeric and low MW peptide aggregates is therefore the actual fibril growth. Albumin acts on the growth phase preventing the addition of monomeric peptide to the initially formed high MW oligomers and growing fibrils. The Aβ peptide remains then kinetically trapped in the thermodynamically unfavorable

nucleation phase, where it exists in the monomeric form in equilibrium with low MW aggregates.

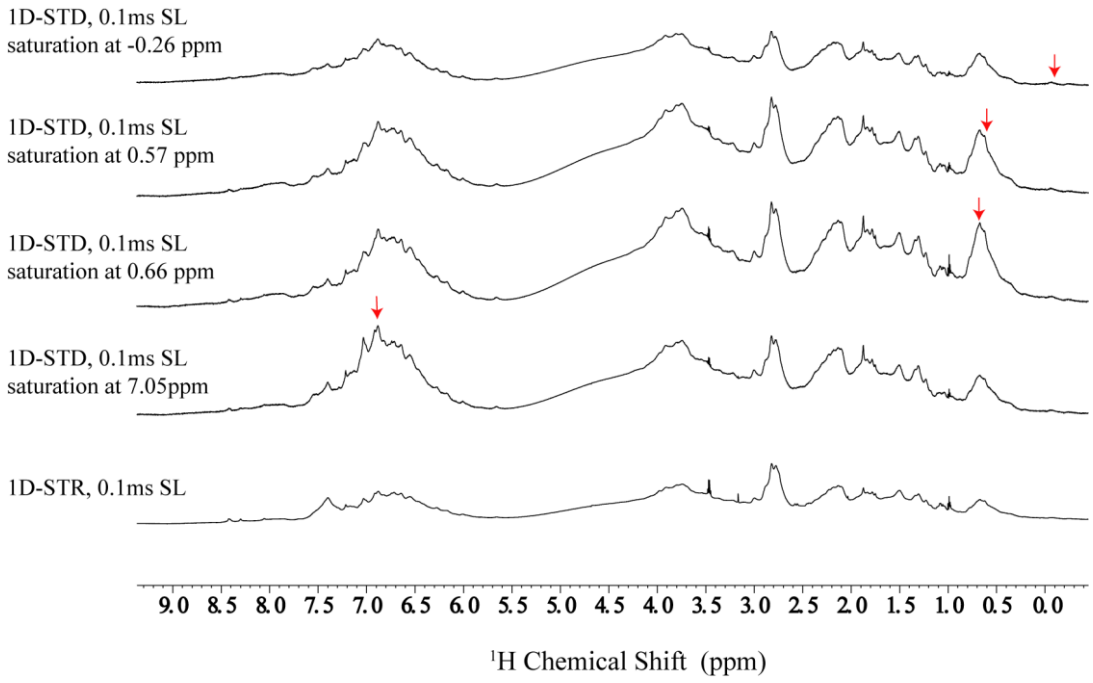

Figure S1. Effect of saturation frequency on the saturation transfer difference (STD) spectra of a 0.5 mM HSA sample. The bottom panel reports the reference spectrum (1D-STR) of the 0.5 mM HSA sample obtained with off resonance saturation at -30 ppm. Selective HSA saturation at 0.57, 0.66 and -0.26 ppm results in STD spectra similar to the reference STR spectra indicating complete saturation of the HSA at those frequencies. Saturation of the aromatic residues at 7.05 ppm does not provide complete saturation of the HSA molecule, resulting in higher signal intensity in the saturated aromatic region relative to other spectral regions. 0.5 mM HSA was prepared in 50 mM acetic acid–d_4 at pH 4.7. All spectra were recorded at 700 MHz using a TCI CryoProbe and at 20 ^{o}C. A short 0.1 ms spin lock (SL) was used to maximize the HSA signal and spectra were processed using a line broadening factor of 3 Hz. Red arrows indicate the selective saturation frequency offsets.

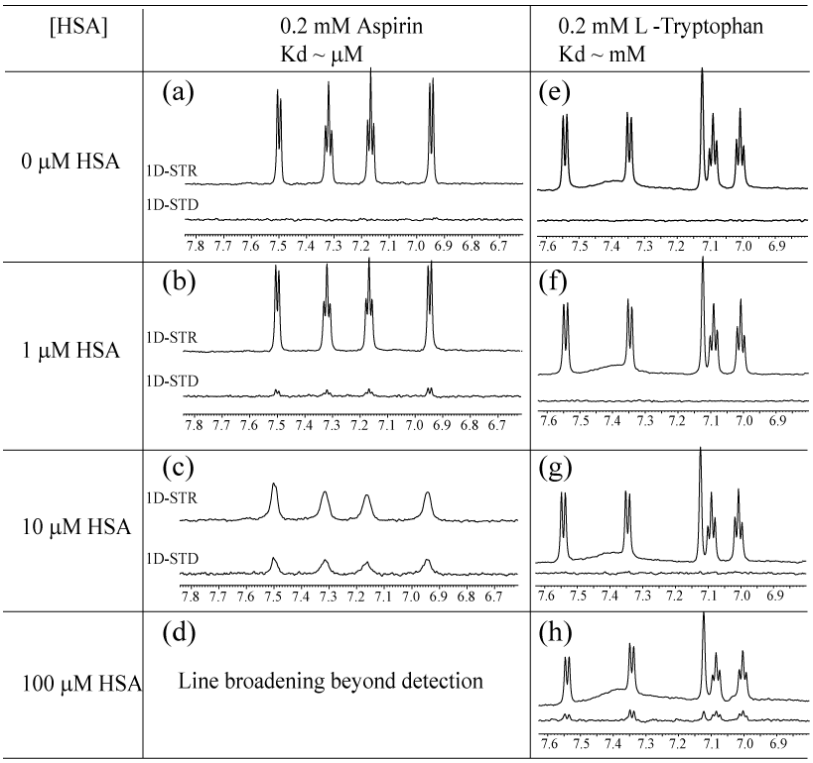

Figure S2**.** Effect of HSA on the saturation transfer reference (STR) and saturation transfer difference (STD) spectra of aspirin, L-tryptophan. All ligand solutions were prepared at 0.2 mM concentration in 50 mM acetic acid-d_4, pH 4.7, 10% D_2O. The STR and STD spectra of 10 and 100 μM HSA solutions were subtracted from the protein ligand mixture spectra to remove potential residual HSA signal. In addition, a 30 ms long spin lock (SL) was used to minimize the residual HSA signal. Aspirin was used to probe HSA interactions in the μM range, while L-Tryptophan at pH 4.7 is used to model HSA interactions with a K_D in the mM range. All spectra were acquired at 700 MHz using a TCI CryoProbe and at 20 ^oC. All spectra were processed using a line broadening factor of 3 Hz.

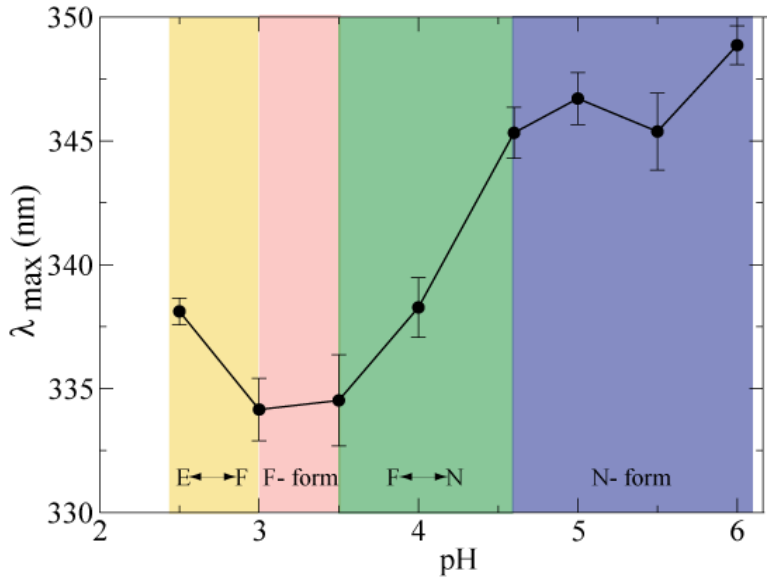

Figure S3. Effect of pH on the maximum emission wavelength of the HSA tryptophan fluorescence as a monitor of the structural transitions of albumin (22). Experiments were performed at 20 °C with a 5 μM HSA concentration in 50 mM sodium acetate buffer. Different pH values were obtained by adding 0.1 M NaOH or HCl solutions. Each spectrum was recorded at least three times and the average maximum wavelength (λ_{max}) values were plotted against pH. The error was calculated as the standard deviation of all λ_{max} values at each pH. pH ranges assigned to different inter-domain orientations of albumin are marked in different colors.

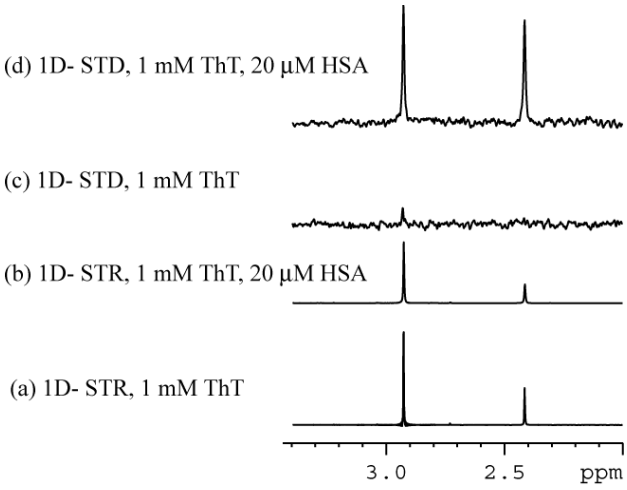

Figure S4. Albumin interacts with Thioflavin T. Panel (a) and (b) report the STR spectra of a 1 mM ThT solution in 50 mM sodium acetate buffer, pH 4.7, 10% D_2O in the absence and presence of 20 μM HSA, respectively. Panel (c) and (d) report the corresponding STD spectra for ThT in the absence and presence of 20 μM HSA, respectively. Experiments were acquired using a Bruker AV600 spectromete at 20 ^{o}C.

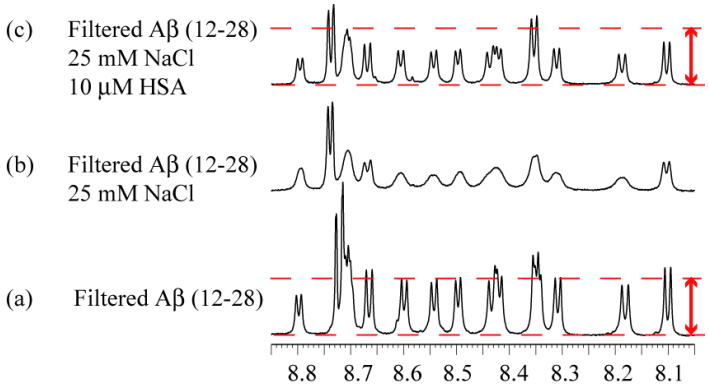

Figure S5. Effect of HSA on the 1D–NMR spectra of the Aβ (12-28) peptide. Panel **(a)** reports the spectrum of a 30 kDa filtered 1 mM Aβ (12-28) solution. Addition of 25 mM NaCl (panel **(b)**) causes significant aggregation as indicated by line broadening and intensity losses. Panel **(c)** shows the effect of the addition of HSA to the aggregated Aβ (12-28) sample. Red dotted lines and arrows were added to facilitate the comparison of the 1D intensities between different spectra and to show that although HSA addition results in line sharpening, it does not result in the restoration of the starting signal intensity. Experiments were recorded at 700 MHz using a TCI CryoProbe and at 20 ^{o}C. All spectra were processed using a line broadening factor of 0.3 Hz.

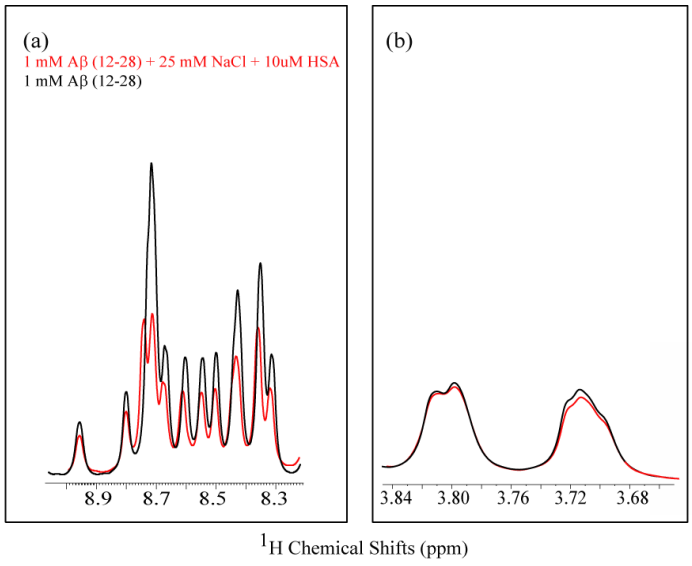

Figure S6. **(a)** The 1D NMR spectral expansion shown in black corresponds to the Aβ (12-28) filtered peptide solution without any salt or protein, while the trace in red shows the effect of the addition of 25 mM NaCl salt followed by the addition of 10 µM HSA. Both spectra were processed with a line broadening coefficient of 10 Hz. **(b)** The residual glycerol signal in the same spectra as in panel (a). The glycerol signal was used to test the probe performance under different salt conditions. No significant difference in the intensity of the glycerol signal was observed in the presence or absence of 25 mM NaCl, indicating that the salt addition did not compromise the probe performance.

REFERENCES

1. Cummings, J.L., 2004, Alzheimer's disease. N. Engl. J. Med. 351: 56–67.

2. Haass, C., D.J. Selkoe. 1993. Cellular processing of β- amyloid precursor protein and the genesis of amyloid β -peptide. Cell 73: 1039– 1042.

3. Walsh, D.M., I. Klyubin, J.V. Fadeeva, W.K. Cullen, R. Anwyl, M.S. Wolfe, M.H. Rowan, D. J. Selkoe. 2002. Naturally secreted oligomers of the Alzheimer amyloid β -protein potently inhibit hippocampal long-term potentiation in vivo. Nature. 416: 535–539.

4. Dahlgren, K. N., A. M, Manelli, W.K. Stine, L. K. Baker Jr., G.A. Krafft, M. J. LaDu. 2002, Oligomeric and fibrillar species of amyloid- β peptides differentially affect neuronal viability. J. Biol. Chem. 277: 32046–32053.

5. Zlokovic,B. V., Clearing amyloid through the blood–brain barrier. 2004. J. Neurochem. 89: 807–811

6. Biere, A. L.,B. Ostaszewski, E.R. Stimson, B.T. Hyman, J.E. Maggio, and D.J. Selkoe. 1996, Amyloid β -peptide is transported on lipoproteins and albumin in human plasma, J. Biol. Chem. 271: 32916–32922

7. Bohrmann, B., L. Tjernberg, P. Kuner, S. Poli, B. Levet-Trafit, J. Naslund, G. Richards, W. Huber, H. Dobeli, C. Nordstedt. 1999. Endogenous Proteins Controlling Amyloid β -Peptide Polymerization. J. Biol. Chem. 274: 15990–15995.

8. Hoyer, W., C. Gronwall, A. Jonsson, S. Stahl, T. Hard. 2008. Stabilization of a β -hairpin in monomeric Alzheimer's amyloid-β peptide inhibits amyloid formation. PNAS. 105 (13): 5099-5104

9. Narayanan, S., B. Bosl, S. Walter, B. Reif. 2003 Importance of low-oligomeric-weight species for prion propagation in the yeast prion system Sup35/Hsp104. Proc. Natl. Acad. Sci. U.S.A. 100: 9286-9291

10. Evans, K.C., E.P. Berger, C.G. Cho, K.H. Weisgraber, P.T. Lansbury. 1995. Apolipoprotein E is a kinetic but not a thermodynamic inhibitor of amyloid formation: implications for the pathogenesis and treatment of Alzheimer disease. Proc. Natl. Acad. Sci. U.S.A. 92: 763-767

11. Milojevic J., V. Esposito, R. Das, G. Melacini. 2007. Understanding the molecular basis for the inhibition of the Alzheimer's Aβ-peptide oligomerization by human serum albumin using saturation transfer difference and off-resonance relaxation NMR spectroscopy. J. Am. Chem. Soc.129 (14):4282 -4290

12. Kuo, Y.M., T.A. Kokjohn, W. Kalback, D. Luehrs, D.R. Galasko, N. Chevallier, E.H. Koo, M.R. Emmerling, A.E. Roher. 2000. Amyloid- β Peptides Interact with Plasma Proteins and Erythrocytes: Implications for Their Quantitation in Plasma. Biochemical and Biophysical Research Communications. 268: 750-756

13. Rozga, M.,M. Koniecki, M. Jabonowskaa, M. Dadlez, W. Bala. 2000. The binding constant for amyloid Aβ 40 peptide interaction with human serum albumin. Biochemical and Biophysical Research Communications. 364:714–718

14. Reyes Barcelo, A.A., F. J.Gonzalez-Velasquez, M.A. Moss. 2009. Soluble aggregates of the amyloid-β peptide are trapped by serum albumin to enhance amyloid-β activation of endothelial cells, Journal of Biological Engineering. 3:1-8

15. Jarvet, J., P. Damberg, K. Bodell, L.E.G. Erksson, A. Graslund. 2000. Reversible random coil to beta-sheet transition and the early stage of aggregation of the A beta(12-28) fragment from the Alzheimer peptide. J. Am. Chem. Soc. 122: 4261-4268.

16. Huang, H., J. Milojevic, G. Melacini. 2008. Analysis and Optimization of Saturation Transfer Difference NMR Experiments Designed to Map Early Self-Association Events in Amyloidogenic Peptides . J. Phys. Chem. B. 112: 5795-5802

17. Esposito, V., R. Das, G. Melacini. 2005. Mapping polypeptide self-recognition through ^{1}H off-resonance relaxation. J. Am. Chem. Soc. 127: 9358-9359.

18. Mayer, M., B. Mayer. 2001. Group epitope mapping by saturation transfer difference NMR to identify segments of a ligand in direct contact with a protein receptor. J. Am. Chem. Soc. 123: 6108-6117.

19. Piotta, M., V. Saudek, V. Sklenar. 1992. Gradient- tailored excitation for single-quantum NMR spectroscopy of aqueous solutions. J. Biomol. NMR. 2: 661-666

20. Thumser, A. E. A., A.G. Buckland, D.C. Wilton.1998. Monoacylglycerol binding to human serum albumin: Evidence that monooleoylglycerol binds at the dansylsarcosine site. Journal of Lipid Research. 39. 1033-1038.

21. Bojko, B., A. Sulkowska, M. Maciazek, J. Rownicka, F. Njau, W.W. Sulkowski. 2008. Changes of serum albumin affinity for aspirin induced by fatty acid. International Journal of Biological Macromolecules. 42: 314–323

22. Dockal, M., C.D. Carter, F. Ruker. 2000. Conformational Transitions of the Three Recombinant Domains of Human Serum Albumin Depending on pH, J. Bio.Chem. 275, (5): 3042–3050

23. Benseny-Cases,N., M. Cocera, J. Cladera. 2007. Conversion of non-fibrillar beta-sheet oligomers into amyloid fibrils in Alzheimer's disease amyloid peptide

aggregation. Biochemical and Biophysical Research Communications. 361: 916–921

24. Stockman B.J, C. Dalvit. 2002. NMR screening techniques in drug discovery and drug design. Progress in Nuclear Magnetic Resonance Spectroscopy. 41: 187–231

25. Yang, J.,D.S. Hage.1996. Role of binding capacity versus binding strength in the separation of chiral compounds on protein-based high-performance liquid chromatography columns Interactions of D- and L-tryptophan with human serum albumin Journal of Chromatography A.725: 273-285

26. Bocedi A., S. Notaril, P. Narciso, B. Alessandro, M. Fasano, P. Ascenzi.2004. Binding of anti-HIV drugs to human serum albumin. IUBMB Life. 56(10): 609–614

27. Miles I. C.,H.G. Schenk.1970. Fluorescence of acetylsalicylic acid in solution and its measurement in presence of salicylic acid, Anal. Chem., 42 (6): 656–659

28. Hou L., H. Shao, Y. Zhang, H. Li, N.K. Menon, E.B. Neuhaus, J. M. Brewer, I. L. Byeon, D.G. Ray, M. P. Vitek, T. Iwashita, R.A. Makula, A. B. Przybyla, M.G. Zagorski. 2004. Solution NMR Studies of the Aβ (1-40) and Aβ (1-42) Peptides Establish that the Met35 Oxidation State Affects the Mechanism of Amyloid Formation J. Am. Chem. Soc.. 126: 1992-2005

29. Walsh P., J. Yau, K. Simonetti, S. Sharpe. 2009. Morphology and secondary structure of stable beta-oligomers formed by amyloid peptide PrP(106-126). Biochemistry. 48(25):5779-81.

30. Priyankar S., F. Sadaf, A. Basir , H.K. Rizwan. 2009. Interactions of thioflavin T with serum albumins: Spectroscopic analyses. Spectrochimica Acta Part, ASAP in press.

31. Lomakin A, D.S. Chung, G.B. Benedek , D.A.Kirschner, D.B. Teplow. 1996. On the nucleation and growth of amyloid beta-protein fibrils: detection of nuclei and quantitation of rate constants. PNAS, 93(3):1125-1129

32. Nanga R. P. R., J. R. Brender, J. Xu, K. Hartman, V. Subramanian, A. Ramamoorthy. 2009. Three-Dimensional Structure and Orientation of Rat Islet Amyloid Polypeptide Protein in a Membrane Environment by Solution NMR Spectroscopy. J. Am. Chem. Soc., 131 (23):8252–8261

STOICHIOMETRY AND AFFINITY OF THE HUMAN SERUM ALBUMIN – ALZHEIMER'S Aβ PEPTIDE INTERACTIONS

CHAPTER 5

Chapter Five Preface

This work has been published:

Milojevic, J. and G. Melacini 2011. Stoichiometry and affinity of the human serum albumin-alzheimer's A beta peptide interactions. Biophys. J. 100, 183-192.

Permission has been granted by the publisher to reproduce the material here.

I conducted all the experiment and data analysis described in this chapter. G. Melacini modeled the dependence of the Aβ saturation transfer on the concentration of abumin.

STOICHIOMETRY AND AFFINITY OF THE HUMAN SERUM ALBUMIN – ALZHEIMER'S Aβ PEPTIDE INTERACTIONS

Milojevic, J. and G. Melacini 2011 Biophys. J. 100, 183-192.

ABSTRACT: A promising strategy to control the aggregation of the Alzheimer's Aβ peptide in the brain is the clearance of Aβ from the central nervous system into the peripheral blood plasma. Among plasma proteins, human serum albumin plays a critical role in the Aβ clearance to the peripheral sink by binding to Aβ oligomers and preventing further growth into fibrils. However, the stoichiometry and the affinities of the albumin – Aβ oligomer interactions are still to be fully characterized. For this purpose, here we investigate the Aβ oligomer - albumin complexes through a novel and generally applicable experimental strategy combining saturation transfer and off-relaxation NMR experiments with ultra-filtration, domain deletions and dynamic light scattering. Our results show that the Aβ oligomers are recognized by albumin through sites that are evenly partitioned across the three albumin domains and that bind the Aβ oligomers with similar dissociation constants in the 1-100 nM range, as assessed based on a Scatchard-like model of the albumin inhibition isotherms. Our data not only explain why albumin is able to inhibit amyloid formation at physiological nM Aβ concentrations, but are also consistent with the presence of a single high affinity albumin-binding site per Aβ protofibril, which avoids the formation of extended insoluble aggregates.

INTRODUCTION

The Alzheimer's Aβ peptide is produced not only in the central nervous system (CNS) but also in most cells of peripheral tissues (1). Removal of the Aβ peptide from the CNS to the periphery through the blood brain barrier (BBB) has been proposed as an effective strategy to prevent the Aβ accumulation in the brain (1). Specifically, according to the peripheral sink hypothesis, blood plasma proteins, such as human serum albumin (HSA), control Aβ aggregation within the brain from the periphery, by regulating the equilibrium of Aβ peptide across the BBB. Therefore, it is likely that plasma protein dysfunctions affect the clearance of Aβ from the CNS and consequently Aβ plaque deposition within the brain. For instance, recent clinical studies show that low albumin levels are associated with increased odds of cognitive impairment and moreover indicate the use of albumin in plasma exchange therapies as a promising avenue in the treatment of mild to moderate Alzheimer's disease (AD) (2,3). Furthermore, HSA is also an effective inhibitor of Aβ fibrillization (4-7).

Despite the clinical relevance of albumin in the context of AD, several fundamental questions about the nature of the HSA – Aβ interactions are still open. While it has been suggested that albumin preferentially targets Aβ oligomers rather than monomers through capping of exposed hydrophobic sites (4), considerable uncertainty remains on the stoichiometries and on the affinities of HSA – Aβ binding (5-9). Here we

report both the prevailing binding stoichiometries and the domain-specific binding affinities for the Aβ / HSA system.

HSA is composed of three domains (Fig. 1a) and the distribution of binding sites across the three HSA domains varies widely for different albumin ligands (10). For instance, non-esterified fatty acids (FAs) are one of the primary physiological HSA ligands and their binding involves up to seven binding sites, three of which are confined within domain 3 whereas the other four are in domains 1 and 2 (Figure 1a) (10, 11). Unlike FAs, exogenous amphiphilic drugs bind HSA at sites that do not involve all three domains (10). Specifically, ibuprofen-like drugs with aromatic carboxylates in an extended conformation display a marked selectivity for Sudlow's site II in domain 3, whereas warfarin-like drugs with a bulky heterocyclic anion bind preferentially Sudlow's site I in domain 2. Within this range of possible binding stoichiometries, it is currently unknown whether the recognition of Aβ oligomers by HSA approaches more closely the three-domain binding pattern of fatty acids or the domain-selective interactions displayed by several drugs.

Furthermore, only partial characterizations are available for the binding affinities of the HSA - Aβ assembly complexes (4, 7, 8). Based on measured IC_{50} values for the competitive inhibition by HSA of the incorporation of Aβ monomers into pre-formed fibrils, a broad upper limit of ~10 μM for the Aβ assembly-HSA dissociation constants has been proposed (7, 8). It is therefore still unclear whether the Aβ oligomer-HSA K_D values are in the μM or in the nM range, which would be more comparable to the

physiological nM concentration of the Aβ peptide in human plasma (1). In addition, due to the presence of a distribution of Aβ oligomer sizes and possibly of binding stoichiometries (12), it is also unknown if and how the Aβ oligomer-HSA K_D values vary among the three domains of HSA.

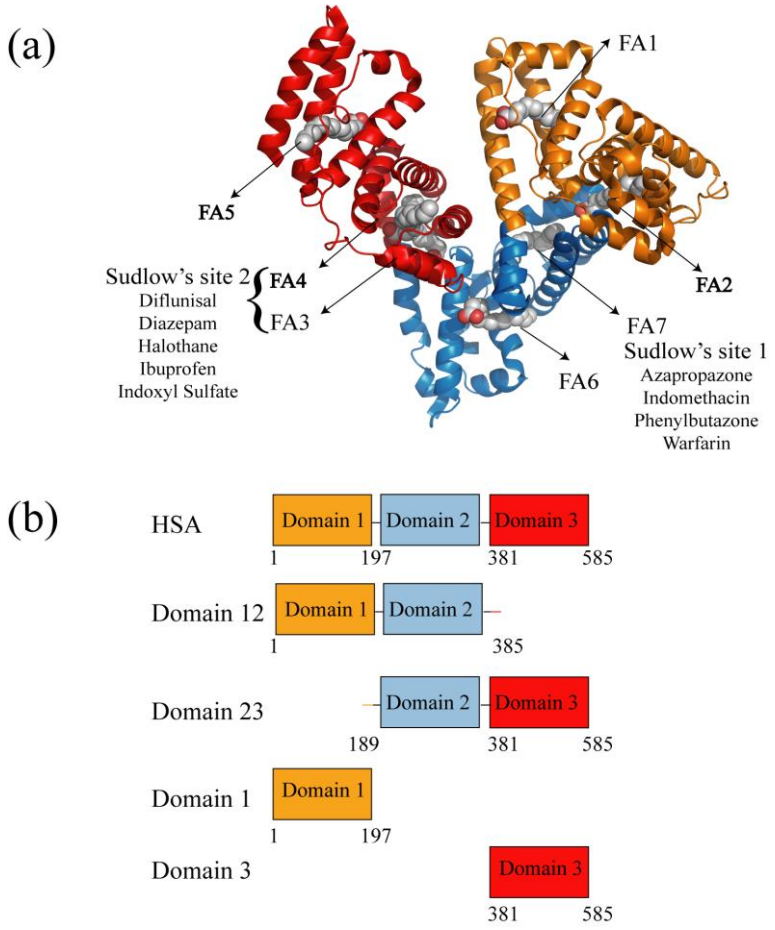

Figure 1. Domain organization of HSA and design of the HSA constructs used in this investigation. Panel (a) depicts a ribbon diagram of the HSA structure (PDB file1E7H) (11). The HSA domains 1, 2 and 3 are colored orange, blue and red, respectively. Palmitate molecules are shown in space-filling representation to indicate fatty acid binding sites and are colored by atom: carbon (gray), oxygen (red). Drug binding sites are indicated as Sudlow sites 1 and 2, and their representative drug ligands are listed (10). Panel (b) depicts the constructs used in this study.

In order to investigate the Aβ oligomer-HSA binding stoichoimetries and domain-specific binding affinities, we have developed an integrated experimental strategy based on saturation transfer difference (STD) (4, 13, 14) and off-resonance relaxation (ORR) (15, 16) NMR experiments aimed at quantitatively comparing the Aβ oligomerization inhibitory potencies of different HSA deletion constructs. Our comparative NMR analyses have primarily focused on the Aβ (12-28) peptide, which not only spans the central hydrophobic core of the Aβ peptide ($L_{17}VFFA_{21}$) and key HSA binding sites (5), but it is also known to provide a reliable and stable model for the Aβ oligomers (17, 18, 19). However, whenever possible the results obtained for Aβ (12-28) were validated using the longer Aβ (1-42) peptide.

Our data indicate an even partitioning of largely independent Aβ oligomer binding sites across the three HSA domains, with similar affinities in the sub μM range. In addition, the presence of a single high affinity albumin binding site per Aβ oligomer/protofibril was established through dynamic light scattering (DLS) measurements, which, unlike NMR, are sensitive to small populations of high MW species. We anticipate that the experimental strategies proposed here will be useful for the characterization of complex stoichiometries and relative affinities in other systems involving oligomerization inhibitory proteins and amyloidogenic peptides that self-associate into a distribution of oligomers with heterogenous sizes (12).

RESULTS

HSA Domain Dissection Approach. Our experimental design aimed at defining the partitioning of the Aβ oligomer binding sites across the three HSA domains and at dissecting the HSA domain contributions to the inhibition of the Aβ oligomerization relies on five protein constructs (Figure 1b). Besides full length HSA, these include two one-domain and two-domain HSA deletion mutants (Figure 1b). The one-domain segments include domains 1 and 3, which are soluble in isolation. However, domain 2 is only marginally soluble when isolated from HSA (20) and therefore it was expressed and purified as part of a pair of two-domain constructs (*i.e.* 12 and 23, Figure 1b), in which the fusion to either domain 1 or 3 ensures the required solubility. The inhibitory efficiency of domain 2 with respect to the Aβ oligomerization can then be assessed through the comparative analysis of the one- and two-domain constructs. The structural integrity of the five HSA constructs in Figure 1b was confirmed by CD spectroscopy (Supp. Mat. p. S2, Figure S1, Table S1).

All Three HSA Domains Contain Aβ Oligomer Binding Sites and Inhibit Aβ Oligomer Formation. The oligomerization inhibitory properties of the five HSA constructs shown in Figure 1b were initially qualitatively evaluated through simple 1D NMR spectra of the model peptide Aβ (12-28), as illustrated in Figure 2. The reference spectrum of the filtered Aβ (12-28) (Figure 2a) was acquired first and is characterized by narrow line-widths as expected for a largely monomeric Aβ peptide (4). As previously

indicated (4), addition of 25 mM NaCl to the filtered Aβ (12-28) results in signal broadening of most resonances (Figure 2b) (4) due to screening of repulsive inter-molecular electrostatic interactions and hydrophobic-collapse driven oligomerization.

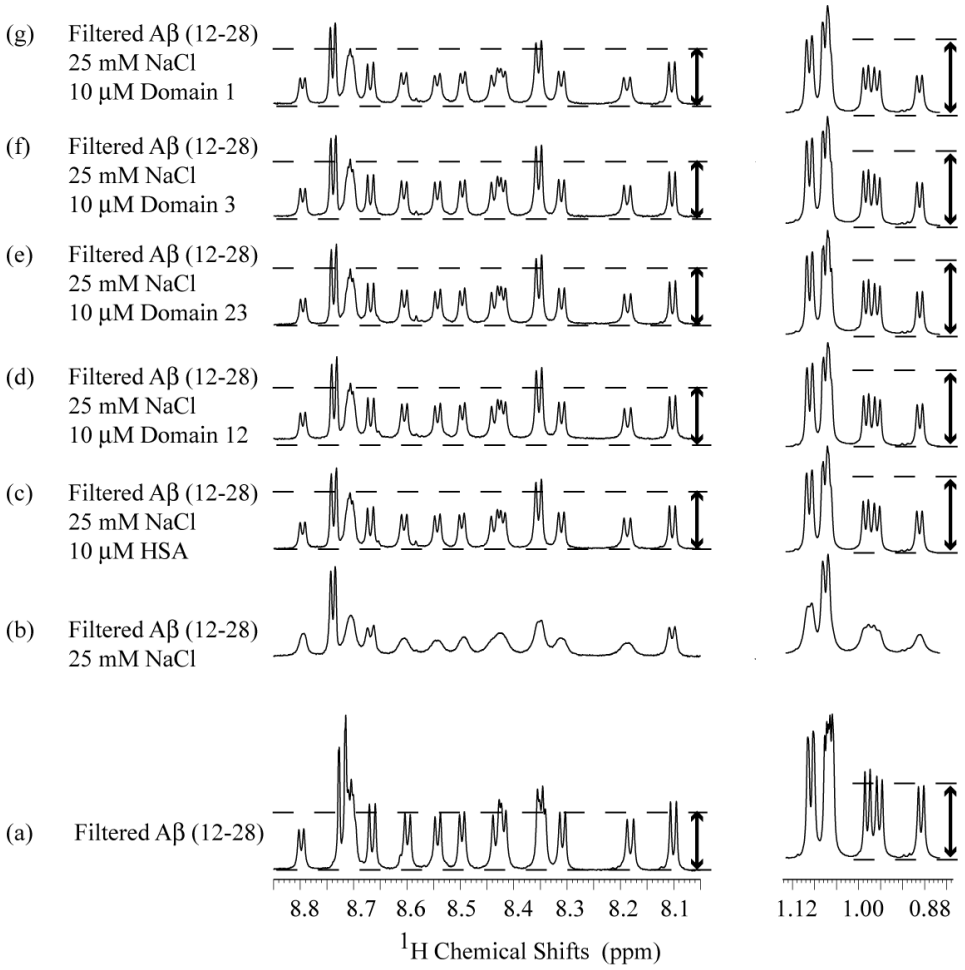

Figure 2. Effect of wt HSA and its deletion mutants on the 1D–NMR spectra of the Aβ (12-28) peptide. Panel (a) reports the spectrum of 30 kDa filtered 1 mM Aβ (12-28). Addition of 25 mM NaCl causes significant aggregation as indicated by line broadening and intensity losses (panel (b)). Panels (c-g) show the effect of the addition of HSA and its deletion mutants: domains 1-2 and 2-3 and domain 3 and 1, respectively. A similar line sharpening is obtained upon addition of all protein constructs. Dotted lines and arrows were added to facilitate the comparison of the 1D intensities between different spectra and to show that although protein addition results in line sharpening, it does not result in the restoration of the starting signal intensity. Spectra (a-c) were previously published elsewhere (4) and are reported here only for comparison purposes.

The signal broadening observed in Figure 2b is therefore a result of the exchange of polypeptide chains between the monomeric and the oligomeric states of Aβ (12-28). Albumin interferes with this chemical exchange phenomenon and results in a marked line sharpening (Figure 2c). The Aβ (12-28) line sharpening observed upon albumin addition is not caused by non-specific Aβ interactions with HSA, because control proteins (*i.e.* insulin and lysozyme) did not result in any detectable line-width change (Figure S2). A closer inspection to the spectra in Figure 2a-c indicates that, although HSA sharpens several peaks to line-widths comparable with those of the filtered sample, HSA is unable to restore the NMR signal intensities to those of the original filtered Aβ (12-28) sample before the salt-induced oligomer formation (Figure 2a). This observation points to a significantly lower population of the monomeric states in the samples with HSA relative to the filtrated solution and has been rationalized in terms of a "Aβ monomer competitor" inhibitory mechanism, whereby HSA does not revert the oligomerization equilibria back to the monomeric peptide, but binds the Aβ oligomers and blocks their growth (4).

When similar experiments are repeated with the HSA deletion mutants, *i.e.* corresponding to domains 1, 3, 12 and 23 (Figure 1b), a line sharpening comparable to that observed after the addition of wt HSA is observed (Figure 2d-g). These observations indicate that both domains 1 and 3 contain Aβ oligomer binding sites and they are able to inhibit Aβ oligomerization through the "Aβ monomer competitor" inhibitory mechanism. Nonetheless, based on these data alone no firm conclusions can be inferred about the inhibitory function of domain 2, because at this point we cannot rule out that the line-

sharpening effect detected for the two-domain constructs (Figure 2d,e) is mainly due to domains 1 and 3.

The results obtained in Figure 2 for the Aβ (12-28) peptide are in full agreement with the inhibitory profiles measured for the full-length Aβ peptide spanning residues 1-42, for which self-association was monitored both in the absence and presence of wild-type HSA and of several HSA deletion mutants. The self-assembly of Aβ (1-42) into NMR-undetectable oligomers, protofibrils and fibrils was followed over time through the simple loss in 1D NMR signal intensity (Figure S3). Figure S3a shows that in the absence of oligomerization inhibitors more that 50 % of the original 1D signal is lost already after 11 hours from sample preparation. Conversely, in the presence of sub-stoichiometric amounts of HSA this decay is dramatically quenched (Figure S3b) and a similar effect is observed for sub-stoichiometric amounts of the HSA deletion mutants (Figure S3c-e), confirming that domains 1 and 3 include Aβ binding sites and preserve significant Aβ oligomerization inhibitory functions even for the full-length Aβ peptide. Therefore, overall the results on the Aβ (1-42) peptide (Figure S3) corroborate the relevance of the Aβ (12-28) construct and of the related 1D line-width analysis (Figure 2).

Furthermore, the Aβ 1D NMR spectra acquired immediately after addition of the HSA constructs do not differ significantly from the spectra of the Aβ peptide alone (Figure S4), confirming that inhibition of Aβ fibril formation in the presence of HSA is not due to interactions with monomeric but with oligomeric Aβ (1-42). However, it is still

not possible based on these data alone to reach a definitive conclusion on the role of domain 2 in the Aβ oligomer inhibition, or to obtain information on the dissociation constants of the albumin - Aβ oligomer interactions. In order to dissect the contributions of the single domains more quantitative estimations of the oligomerization inhibitory potencies of the different HSA constructs is required. For this purpose 1D saturation transfer difference (STD) data were acquired at increasing protein concentrations (Figure 3b-f), starting from filtered Aβ (12-28) samples in which stable oligomers were induced by salt addition, as in Figure 2b. These STD experiments are less suitable for the longer Aβ (1-42) peptide as in this case the soluble oligomers in exchange with the NMR-detectable low-MW species appear only transiently (4, 21).

The STD monitored titration data (Figure 3b-f) display a typical dose-response pattern, in which the I_{STD}/I_{STR} ratios decrease progressively as the protein concentration increases, until a plateau is reached. This dose-response pattern is observed for full length HSA as well as for all four HSA deletion mutants (Figure 3b-e). While no major differences were observed among the HSA constructs in the plateau heights, which cluster around a residual basal STD effect corresponding to ~15 - 18 % of the original value measured in the absence of protein (Figure 3b-f), significant domain-dependent variations were observed in the slope of the initial I_{STD}/I_{STR} decay (Figure 3b-f). The latter is quantified in terms of half-maximal inhibitory protein concentration (*i.e.* IC_{50}), corresponding to the midpoint between the maximum (*i.e.* initial) I_{STD}/I_{STR} value and the plateau region (Figure 3b-f).

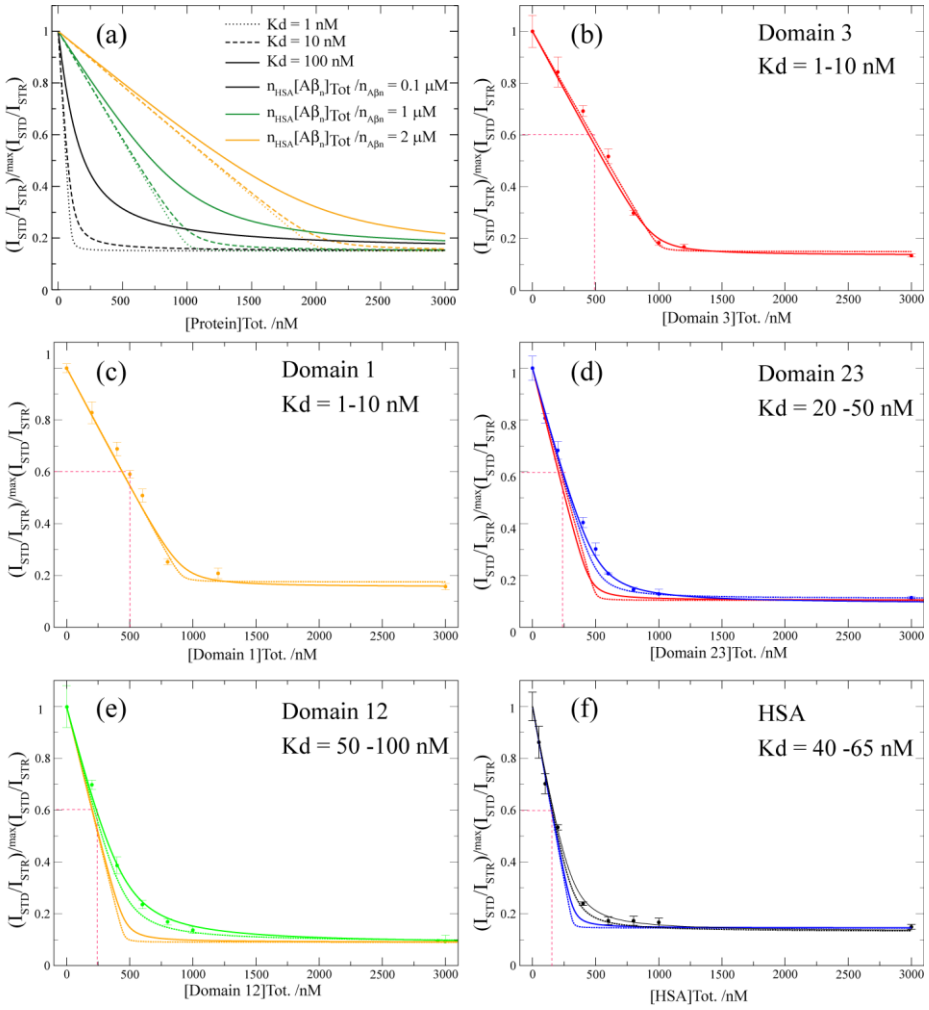

Figure 3. Dose-response STD-based profiles for the inhibition of the Aβ (12-28) self-association by HSA and its deletion mutants. Panel (a) illustrates the effect of different K_D values and of different HSA-binding competent Aβ oligomer concentrations on dose-response STD curves simulated according to a Scatchard-like model. This model assumes full equivalence and independence of all sites in HSA that can bind Aβ oligomers. Further details on this model are available in the text. Panels (b-f): Effect of HSA deletion mutants (*i.e.* domain 3, domain 1, domains 23, domains 13) and wt HSA, respectively, on the relative I_{STD}/I_{STR} ratios measured for the filtered Aβ (12-28) peptide aggregated through the addition of 25 mM NaCl. All ratios were normalized to their maximum value measured before protein addition. In panels (b) and (c), dashed and full lines correspond to back-calculated dose-response curves using the Scatchard-like model and K_D values of 1 and 10 nM, respectively. In panel (d), dashed and full blue lines correspond to back-calculated dose-response curves using the Scatchard-like model and K_D values of 20 and 50 nM, respectively. This range of K_D values is in good agreement with the experimental data measured for the domain 23 construct. The red lines in panel (d) are obtained based on the single domain constructs K_D values (1 and 10 nM), assuming that individual domains bind independently, *i.e.* simply down-scaling the one-domain curves of panel (b) by a factor of two. Similarly, in panels (e) and (f) the green and black

curves were computed using the K_D values that fit the experimental data, while the orange and blue lines in panels (e) and (f) were obtained based on the one-domain curves of panel (c) assuming fully independent binding of Aβ oligomers to two and three domains, *i.e.* simply down-scaling the curves of panel (c) by a factor of two or three, respectively.

Notably, Figure 3b-f shows that the measured IC_{50} values decrease in an almost linear progression as the number of domains in the inhibitory HSA constructs increases. Specifically, for both domains 1 and 3 the IC_{50} values are about 500 nM (Figure 3b,c), while the IC_{50} decreases by ~50% (*i.e.* ~250 nM) for the two domain constructs (Figure 3d,e) and by ~67 % *(i.e.* ~160 nM) for full length HSA with all three domains (Figure 3f). These observations point to the presence of Aβ oligomer binding sites also within the second HSA domain and to the equivalence of the three HSA domains in their efficiency as self-assembly inhibitors under our experimental conditions.

The even partitioning across the three albumin domains of binding sites for the Aβ oligomers revealed by the IC_{50} analysis suggests the existence of a common oligomer recognition mode shared by all three HSA domains. To test this hypothesis the effect of the HSA deletion mutants on the oligomeric equilibria of Aβ (12-28) was monitored also through nonselective 2D-off-resonance relaxation experiments with a 35.5^{o} tilt angle, which provide a sensitive probe of the involvement of each Aβ residue in self-recognition (15,16). Specifically, the residue-specific variations in H_{α}-$R_{35.5^{o},ns}$ rates induced by each HSA deletion mutant were correlated with the corresponding changes in H_{α}-$R_{35.5^{o},ns}$ rates caused by full length HSA (Figure 4).

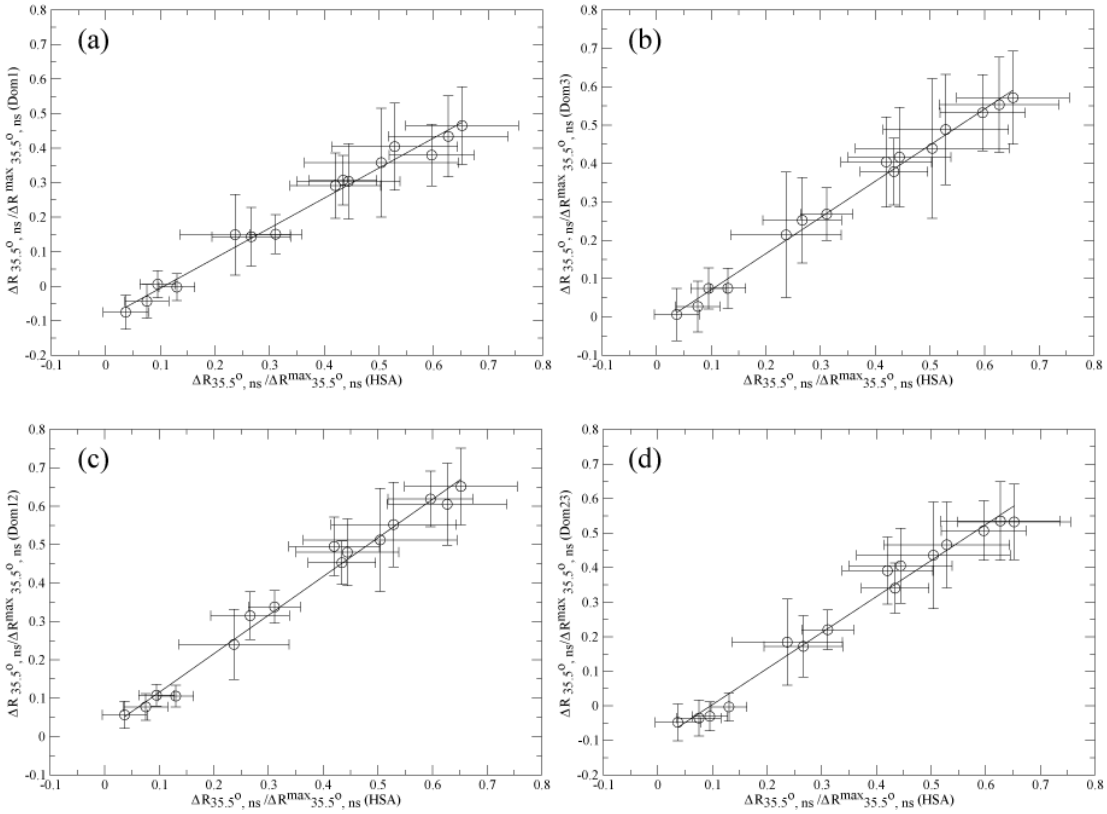

Figure 4. Correlations between the non-selective off-resonance relaxation data of full length HSA and those measured for the four HSA deletion mutants shown in Figure 1b. In all panels the horizontal axes report the differences in residue specific H_α non-selective off-resonance relaxation rates measured for the aggregated 1 mM Aβ(12-28) sample before and after addition of 10 μM full length HSA. The vertical axes of panels (a-d) report the corresponding variations caused by the addition to the aggregated sample of 10 μM of the four HSA deletion mutants (domain 1, 3, domains 12 and 23, respectively).

As shown in Figure 4, the nonselective 2D-off-resonance relaxation profiles of both one-domain and two-domain constructs correlate well with that of full length HSA supporting the hypothesis that all three domains share a similar Aβ (12-28) oligomer recognition mode.

While the equivalent self-assembly inhibitory efficiency of the three HSA domains is independently supported by both the off-resonance relaxation experiments (Figure 4) and the relationship between the IC_{50} values and the number of domains in the HSA constructs (Figure 3b-f), it is important to note that the IC_{50} values or the data in Figure 4 do not provide any strict quantification of the affinity between the HSA domains and the Aβ oligomers. For instance, the IC_{50} values derived from the STD titration curves depend on the oligomer concentrations, which in turn depend on the concentrations of Aβ peptide and salt (Figure S5), and therefore can be used only to provide an upper limit for the dissociation constants (K_D) of the Aβ oligomer – albumin complexes. The determination of these K_D values requires a more quantitative modeling of the dose-response inhibitory profiles in Figure 3b-f.

Modeling the Dependence of the Aβ Saturation Transfer on the Concentration of Albumin. The dissociation constant, unlike the IC_{50} value, is independent of the Aβ oligomer concentration and therefore provides a more meaningful descriptor of the affinity of HSA for the Aβ oligomers. To obtain dissociation constant values for the Aβ oligomer - HSA complex, the titration data of Figure 3b-f were analyzed according to a simple model of the binding isotherms. The first assumption of this model is that in the absence of albumin, the NMR saturation transfer difference (STD) signal observed for the monomeric Aβ peptide arises from the saturation of Aβ oligomers, here denoted as $A\beta_n$ (4). Therefore, the STD/STR ratio can be expressed as:

$$(STD/STR)_{[HSA]=0} \propto [A\beta] / (K_{D,A\beta} + [A\beta]) \quad (1)$$

where [Aβ] is the concentration of monomeric free Aβ and $K_{D, A\beta}$ is the dissociation constant of a single polypeptide chain of Aβ from the $A\beta_{n+1}$ oligomers. It should be emphasized that $K_{D, A\beta}$ represents just an effective dissociation constant that captures only the average STD effects of the heterogeneous distribution of $A\beta_n$ sizes present in solution. In this respect, the use of a single effective $K_{D, A\beta}$ constant as opposed to several $A\beta_n$ MW-dependent dissociation constants is a major over-simplification. However, equation (1) is still useful for the interpretation of the data in Figure 3b-f to the extent that it represents one of the simplest possible models still able to reproduce the key trends observed in the experimental data, avoiding over-parameterization and the consequent risk of making line fitting an underdetermined problem. Similar considerations apply for the other dissociations constants defined below.

Since albumin competes with the Aβ monomers for binding to the $A\beta_n$ oligomers (4), HSA is effectively modeled as a competitive inhibitor of the interaction between Aβ monomers and oligomers. For the sake of simplicity we assume that HSA and the Aβ oligomers bind in a 1:1 ratio with an effective dissociation constant: $K_{D,HSA} = [HSA][A\beta_n]/[HSA: A\beta_n]$. The STD/STR ratio is then modeled as:

$$(STD/STR)_{[HSA]>0} \propto [A\beta]/K_{D, A\beta} / (1 + [A\beta]/K_{D, A\beta} + [HSA]/K_{D,HSA}) \quad (2)$$

Equation (2), however, does not take into account that only a fraction of the oligomers in solution is HSA-binding competent (4, 5). It has been shown that only Aβ oligomers larger than a critical MW are able to bind albumin (4, 5). While the exact MW cut-off for the size of the Aβ oligomers that bind HSA is still unknown, it is possible to model this effect into equation (2) by introducing the fraction "f" of Aβ oligomers that are not HSA-binding competent. These smaller Aβ oligomers are not bound by HSA (5) and therefore equation (2) becomes:

$$(STD/STR)_{[HSA]>0} \propto$$

$$(1\text{-}f)\ \{[\ A\beta]/K_{D,\ A\beta}\ /\ (\ 1 + [A\beta]/K_{D,\ A\beta} + [HSA]/K_{D,HSA}\ )\} + f\ \{[\ A\beta]/K_{D,\ A\beta}\ /\ (\ 1 + [A\beta]/K_{D,\ A\beta})\} \quad (3)$$

Equation (3) essentially combines equations (1) and (2) and it can be further simplified by defining the effective apparent dissociation constant:

$$K_{D,HSA,app.} = K_{D,HSA}\ (1 + [A\beta]/K_{D,\ A\beta}\ ) \quad (4)$$

$K_{D,HSA,app.}$ *as defined in equation (4) is an effective equilibrium constant because* the monomeric Aβ concentration (*i.e. [Aβ]*) *is not significantly affected by [HSA], as shown by the 1D NMR spectra of Aβ (12-28) acquired at different concentrations of albumin (Figure S6).* Using equation (4) and normalizing the $(STD/STR)_{[HSA]>0}$ ratio through $(STD/STR)_{[HSA]=0}$ as expressed in equation (1), equation (3) is simplified to:

$$(STD/STR)_{[HSA]>0}/(STD/STR)_{[HSA]=0} = f + (1-f)\, K_{D,HSA,app.} / (K_{D,HSA,app.} + [HSA]) \quad (5)$$

This equation was used to model the inhibition curves shown in Figure 3. In the absence of HSA, equation (5) correctly predicts $(STD/STR)_{[HSA]>0}/(STD/STR)_{[HSA]=0} = 1$, while at saturating concentrations of HSA, i.e. $[HSA] >> K_{D,HSA,app.}$, equation (5) reduces to:

$$(STD/STR)_{[HSA]>0}/(STD/STR)_{[HSA]=0} = f \qquad \text{for } [HSA] >> K_{D,HSA,app} \quad (6)$$

The fraction f of oligomers that are HSA-binding incompetent is therefore directly 'readable' from the plateau height of the dose-response inhibition plots of Figure 3. For intermediate concentrations of albumin, it is important to note that in Figure 3 the $(STD/STR)_{[HSA]>0}/(STD/STR)_{[HSA]=0}$ ratios are reported as a function of the total HSA concentration ($[HSA]_{Tot}$) as opposed to the free HSA concentration ([HSA]) used in equation (5). However, [HSA] can be easily estimated starting from $[HSA]_{Tot}$ since equation (5) indicates that the normalized STD/STR ratios of Figure 3 are effectively modeled by the binding of HSA to the $A\beta_n$ oligomer with an apparent dissociation constant $K_{D,HSA,app.}$. [HSA] can then be computed from $[HSA]_{Tot.}$ using $K_{D,HSA,app.}$ as a parameter, provided that the total concentration of HSA-binding competent oligomers (*i.e.* $[A\beta_n]_{Tot}$) is known. $[A\beta_n]_{Tot}$ is determined experimentally from the transition point between the binding and saturation regions of the HSA titrations curves of Figure 3, *i.e.* from the beginning of the plateau region. Using the experimentally determined $[A\beta_n]_{Tot}$

value and $K_{D,HSA,app}$ as a fitting parameter, it is possible to compute [HSA] for each $[HSA]_{Tot.}$ based on equation (S1) (Supp. Mat. p. S2). Once [HSA] is known, the value of $(STD/STR)_{[HSA]>0}/(STD/STR)_{[HSA]=0}$ is then calculated through equation (5), and compared to the experimental data reported in Figure 3.

In conclusion, for the case of a 1:1 HSA: $A\beta_n$ oligomer binding stoichiometry, the inhibitory dose-response titration curves of $(STD/STR)_{[HSA]>0}/(STD/STR)_{[HSA]=0}$ *vs.* $[HSA]_{Total}$ provide three distinct parameters: (1) The height of the plateau represents the fraction f of $A\beta_n$ oligomers that are not HSA binding competent (*i.e.* f); (2) The $[HSA]_{Tot}$ concentration at which the plateau starts (*i.e.* crossing point of binding and saturation regions) provides the total concentration of $A\beta_n$ oligomers that are HSA-binding competent (*i.e.* $[A\beta_n]_{Tot.}$); (3) Through fitting it is possible to obtain the average apparent dissociation constant of the HSA: $A\beta_n$ oligomer complexes, $K_{D,HSA,app}$, which is highly sensitive to the curvature of the plot in the transition zone between the binding and saturation regions (Figure 3a). Once the $K_{D,HSA,app}$ value is determined, the actual non-apparent $K_{D,HSA}$ can be computed using equation (4). However, it should be noted that in our case the monomer concentration [Aβ] is in the sub-mM range and under our experimental conditions $K_{D,\ A\beta}$ is expected to be of the order of mM (17). We therefore expect that, within error, $K_{D,HSA,app}$ and $K_{D,HSA}$ are in the same concentration range.

If the number of $A\beta_n$ oligomers bound per HSA molecule ($n_{A\beta n}$) is higher than one, the simplest possible model that accounts for our experimental data assumes that the multiple $A\beta_n$ oligomer binding sites within HSA are all equivalent and independent of

each other (*i.e.* Scatchard-like model). In this case, it is still possible to employ the formalism developed above leading to equations (5) and (S1) provided that the $[HSA]_{Tot}$ used in equation (S1) is scaled up according to the number of $A\beta_n$ oligomers bound per HSA molecule (*i.e.* it is multiplied by $n_{A\beta n}$). This is easily appreciated considering that, if the multiple binding sites are equivalent and independent of each other, an increase in $n_{A\beta n}$ is indistinguishable from a corresponding increase in the number of HSA molecules, which are also equivalent and independent from each other. In other words, an increase in $n_{A\beta n}$ results mainly in a rescaling of the horizontal axes of the plots of Figure 3, explaining also the linear relationship between the observed IC_{50} values and the reciprocal of the number of domains in each HSA construct used in Figure 3.

In the case the number of HSA molecules bound per $A\beta_n$ oligomer (n_{HSA}) is higher than one, we find that the simplest possible model that accounts for our experimental data assumes, again in a Scatchard-like manner, that the multiple HSA binding sites within each $A\beta_n$ oligomer are all equivalent and independent of each other. Also in this case, similarly to what was mentioned for $n_{A\beta n} > 1$, it is still possible to use equations (5) and (S1), but only after re-scaling by an n_{HSA} factor the total concentration of HSA-binding competent $A\beta_n$ oligomers (*i.e.* $[A\beta_n]_{Tot.}$). Therefore, an increase in n_{HSA} results mainly in a rescaling of the horizontal axes of the plots of Figure 3, similarly to the effect of decreased $n_{A\beta n}$. This means that in general terms the transition point between the binding and the saturation regions in the titration curves of Figure 3 provides only the

$n_{HSA}[A\beta_n]_{Tot.}/n_{A\beta n}$ product and based on the inhibition data of Figure 3 alone is not possible to dissect further the stoichiometric ratio, $n_{HSA.}/n_{A\beta n}$, from $[A\beta_n]_{Tot.}$.

Figure 3 shows that the experimental $(STD/STR)_{[HSA]>0}/(STD/STR)_{[HSA]=0}$ *vs.* $[HSA]_{tot}$ profiles are well reproduced by equations (5) and (S1) of our model. Specifically, K_D values of 1-10 nM modeled well the experimental data measured for the single domain constructs (*i.e.* domain 1 and domain 3) (Figure 3b,c), while for the two domains constructs, *i.e.* domain 12 and domain 23, the experimental STD data is in good agreement with K_D values in the range of 50-100 and 20-50 nM, respectively (Figure 3d,e). Interestingly, these dissociation constant values obtained for the two domain constructs are higher than the K_D values measured for the single domain constructs (blue *vs.* red and green *vs.* orange curves in Figure 3d, e, respectively). A possible interpretation of the increased K_D values observed for the two *vs.* one domain constructs is that binding of Aβ oligomers to two domain constructs is at least partially inhibited by steric hindrance imposed by binding of other Aβ oligomers to the adjacent domain. No major changes in the fitted K_D values were observed in going from the two domain constructs to full length has (Figure 3d-f), confirming that, apart from the partial steric hindrance between adjacent domains, the three domains of albumin bind Aβ oligomers independently of each other and all in the 1-100 nM range.

Aβ Oligomers/Protofibrils Contain a Single High Affinity Albumin Binding Site. While the previous analyses clearly support the presence of several Aβ -oligomer binding

domains within HSA, they cannot unambiguously define the number of albumin molecules bound per Aβ oligomers/protofibrils. However, the observation that all three domains of HSA bind $A\beta_n$ oligomers with comparable affinities implies that, if the $A\beta_n$ assemblies bind more than one albumin molecule, albumin is expected to function as an effective cross linker of $A\beta_n$ oligomers, resulting in the formation of large web-like networks and possibly in sample precipitation. We did not observe any visible precipitation upon addition of albumin, suggesting that polymer-like networks do not form upon mixing of Aβ and HSA. In order to confirm this initial qualitative assessment, we performed dynamic light scattering (DLS) measurements, which are ideally suited to detect large molecular assemblies because the DLS sensitivity increases for larger particle sizes, allowing the detection of minor populations of high MW aggregates (22, 23).

Figure 5 illustrates the main results obtained through DLS. Specifically, a solution of 0.1 mM Aβ freshly prepared (*i.e.* without incubation) in the absence of albumin displays an oligomer size distribution with two main peaks (Figure 5a). The first peak is centered at 17 nm and is assigned to Aβ pentamers/hexamers, which have been proposed as main building block of high MW assemblies (22, 23). The second peak is centered at 178 nm and it corresponds to high MW assemblies (23). After 48 h. incubation, the oligomer size distribution of Aβ in the absence of albumin evolves to result in two peaks in the 10-100 nm region and still a single peak in the 100-1000 nm window, but shifted towards sizes larger than the original 178 nm (Figure 5b).

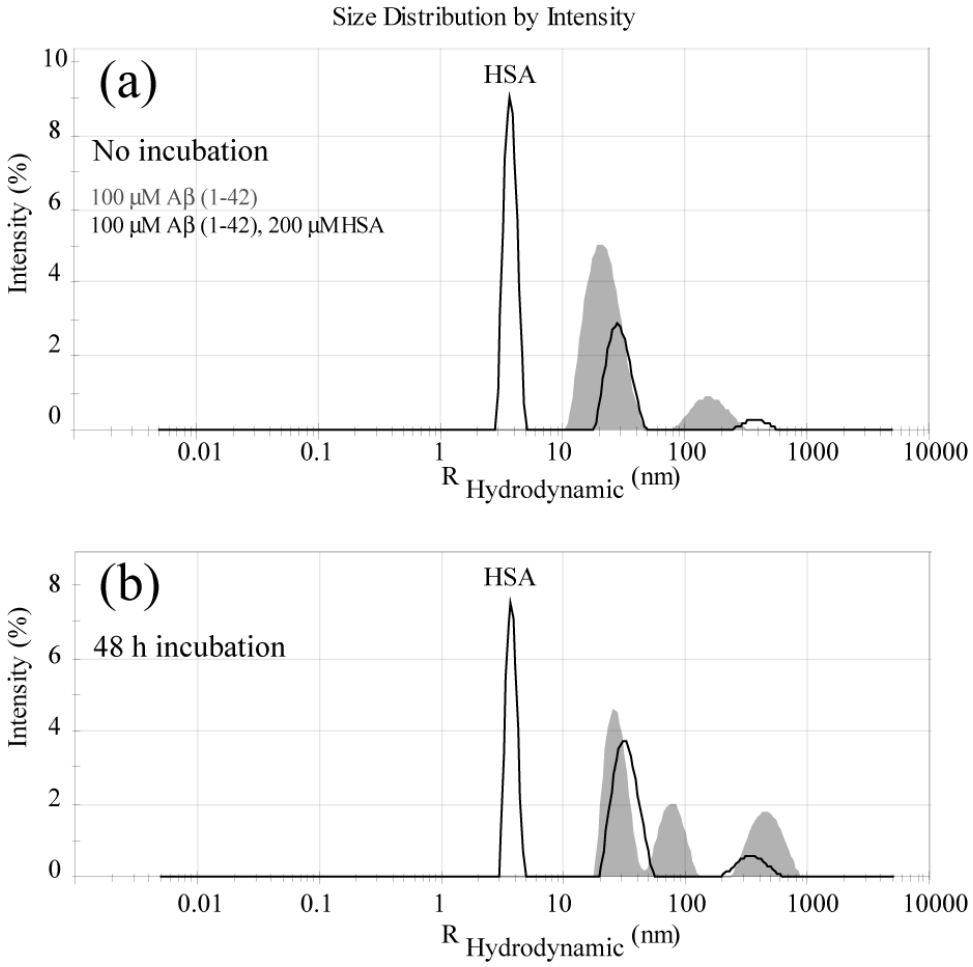

Figure 5. Intensity *vs.* size distribution obtained from dynamic light scattering (DLS) measurements of 0.1 mM Aβ (1-42) in the presence and absence of 200 μM of HSA. Measurements collected immediately after samples were prepared are reported in panel (a), while measurements on the same samples incubated for 48 hour at 37 ^{o}C after preparation are reported in panel (b). The DLS profiles in the absence and presence of HSA are depicted in gray and black, respectively. All measurements were performed using a 12 μL volume cells and a Zetasizer Nano S system at 25 ^{o}C.

When the DLS experiments are repeated in the presence of albumin, the main difference observed without incubation (Figure 5a) is a new peak with a ~ 3.8 nm radius, which belongs to excess apo albumin. The two main peaks in the 10-100 nm and 100-1000 nm regions detected for Aβ in the absence of albumin are also observed in the

presence of HSA (Figure 5a). After 48 h. incubation, a similar pattern with two main peaks in the 10-100 nm and 100-1000 nm regions is still preserved in the presence of albumin (Figure 5b). This observation supports the absence of the above-mentioned large polymer-like networks expected if the Aβ assemblies bound more than one HSA molecule, suggesting that the Aβ oligomers/protofibrils contain only a single high affinity albumin-binding site. These results are also in agreement with previous electron microscopy (EM) images of Aβ (1-42) recorded at different time intervals after the addition of HSA (24). In these EM images no large MW aggregates were detected in the presence of albumin (24). The DLS and EM data therefore consistently support the presence of a unique high affinity albumin-binding site per $A\beta_n$ oligomers/protofibrils.

DISCUSSION

The combined analysis of our STD, ORR and DLS data is consistent with a general model whereby each domain of HSA binds at least one Aβ oligomer with dissociation constants in the 1-100 nM range (Figure 6). In agreement with a previously proposed 'monomer-competition' model (4), each albumin domain binds the Aβ oligomers with a similar recognition mode targeting sites within the Aβ oligomers that would otherwise accept additional Aβ monomers, thus inhibiting further growth of the Aβ assemblies.

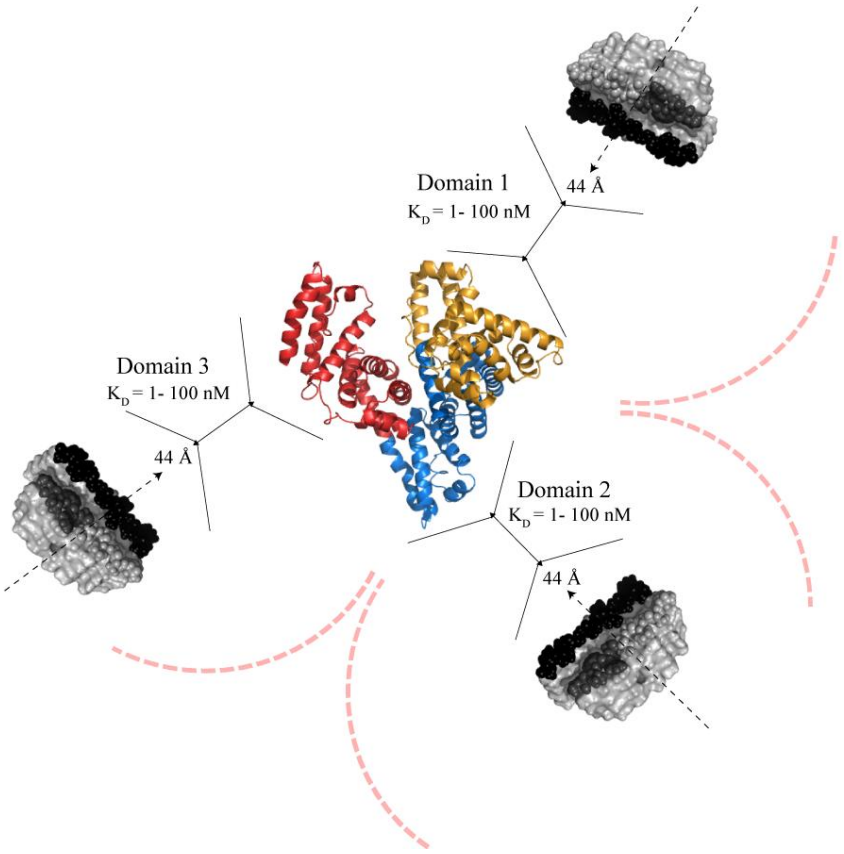

Figure 6. Schematic model to summarize the prevailing stoichiometries and affinities for the complexes between HSA and the Aβ protofibrils. The structures of apo albumin (PDB file 1AO6) and of the Aβ protofibrils (PDB file 2BEG) were used to generate a model with reliable relative scales. Albumin domains 1, 2 and 3 are depicted in orange, blue and red, respectively. The red dashed lines indicate possible steric hindrance between Aβ protofibrils binding to different domains. The black solid lines are used as an aid in the comparison of the sizes of the albumin domains and of Aβ protofibril. The dashed arrows indicate the direction of protofibril growth, while 44 Å indicate protofibril width. The C-terminal hydrophobic residues are depicted in red, while hydrophobic residues in the central hydrophobic core (CHC) are indicated in yellow. Although a single Aβ protofibril is shown per albumin domain, we cannot rule out based on our data the presence of additional Aβ protofibrils.

The interactions of the Aβ oligomers with different HSA domains appear to be to a large extent independent of each other, as the experimental STD based dose-response curves of Figure 3 are in good agreement with a Scatchard-like model assuming full

equivalence and independence for the multiple albumin sites that bind Aβ oligomers. However, the slight but significant increase in K_D values observed in going from the one- to the two-domain constructs (Figure 3b-e) is consistent with some degree of cross-talk arising from steric hindrance between adjacent domains. Despite its simplicity, this model leads to three notable implications.

First, the even partitioning of the Aβ oligomer binding sites across the three domains of albumin suggests that HSA recognizes the Aβ assemblies quite differently from most drugs, which either target Sudlow's site I or II of HSA (Figure 1a). The presence of Aβ oligomer binding sites in all three HSA domains is instead more reminiscent of the binding of fatty acids, for which the binding sites are spread over all three albumin domains (Figure 1a). This observation suggests that albumin may target hydrophobic residues in Aβ and also provides a possible explanation for the marked selectivity of albumin towards the Aβ oligomers (*i.e.* $K_D < \mu M$) relative to the Aβ monomers (*i.e.* $K_D \geq$ mM) (4). In the monomeric Aβ peptide the central hydrophobic residues are shielded by intra-molecular hydrophobic contacts (25, 26), which compete with inter-molecular interactions with HSA. However, it has been shown (27) that in the Aβ protofibrils several hydrophobic residues of Aβ become solvent exposed and therefore potentially available to interact with HSA. It is also possible that the Aβ protofibrils pre-organize these hydrophobic side chains for their recognition by albumin. This protofibril-specific pre-organization would significantly minimize the entropic loss that would otherwise occur if HSA bound Aβ monomers, which unlike protofibrils

populate a structurally diverse ensemble of conformations in dynamic equilibrium (25, 26).

A second notable feature of our model (Figure 6) is that the HSA domains bind Aβ oligomers with an affinity in the 1-100 nM range, which is higher than that reported for most low MW HSA ligands (10). This marked difference in affinity is fully consistent with the different physiological functions of the HSA interactions with Aβ as opposed to other ligands. Albumin functions as a delivery reservoir for FAs and exogenous ligands and therefore the binding of these molecules to HSA requires reversibility. This is why the carrier function of albumin is optimally implemented through affinities in the μM range. On the contrary, when HSA functions as an Aβ fibrilization inhibitor, no binding reversibility is warranted. As a consequence albumin binds Aβ oligomers with K_D < μM, minimizing Aβ oligomer release and ensuring an effective inhibition of Aβ fibril deposition. Furthermore, the nM affinity observed here between HSA and the Aβ assemblies explains also why the majority of Aβ in blood plasma is bound to albumin (6). The Aβ peptide is present in human plasma at ~nM concentrations (6, 28) and the previously reported IC_{50} value of ~10 μM for the Aβ fibrillization inhibition by HSA (7) cannot explain alone why the large majority (89%) of Aβ in plasma is bound to albumin (6). It is possible that the previously reported IC_{50} measurement was limited by the amount of Aβ fibrils used in the experiments and therefore it provides only a broad upper limit for the actual affinity of albumin towards Aβ assemblies.

The third key implication of our proposed model (Figure 6) is that, while each HSA molecule can bind multiple Aβ oligomers, each Aβ oligomer binds only a single HSA molecule in the prevailing stoichiometry. This DLS- and EM-based conclusion is independently supported by the structure of Aβ protofibril proposed by Luhrs *et.al.* (27)**.** Based on this structure, only a single extended patch of exposed hydrophobic residues is present in the Aβ protofibril and it is located at a site referred to as the "odd" protofibril edge (27). The protofibril "odd edge" is not only a locus for monomer recognition, and therefore a protofibril growing site, but it is also a site available for interactions with possible inhibitors (27), such as HSA. The presence of a single albumin binding site within each Aβ protofibril *in vitro* is therefore supported by our DLS data and by independent structural evidence. Furthermore, this conclusion is expected to be relevant *in vivo* as well, because if more than a single albumin binding site was present within each Aβ protofibril, then the albumin – Aβ interactions could easily lead to the formation of extended polymer-like aggregates and actually promote the formation of insoluble deposits.

Overall, we conclude that the affinities and the stoichiometric ratios of the proposed model for the albumin – Aβ interactions (Figure 6) appear to be functional to the effective inhibition by HSA of Aβ fibrillization. In addition, the experimental strategies integrating NMR, DLS, ultrafiltration and deletion mutagenesis as well as the Scatchard-like modeling of inhibition outlined here are expected to be of general

applicability to other systems composed of amyloid inhibitors and amyloidogenic peptides (32, 33).

ACKNOWLEDGEMENTS: We thank NSERC for financial support to G.M. G.M. is also grateful to the Heart and Stroke Foundation of Canada for a Maureen Andrew New Investigator award. We thank Elle Dunitz, Annie Raditis, Rajeevan Selvaratnam, Madoka Akimoto, Bryan Vanschouwen, Dr. J. Ortega and Dr. Rahul Das for helpful discussions. J.M. is funded by an NSERC graduate fellowship.

REFERENCES

1. Deane, R., Z.H. Wu and B.V. Zlokovic 2004. RAGE (yin) versus LRP (yang) balance regulates alzheimer amyloid beta-peptide clearance through transport across the blood-brain barrier. Stroke. 35, 2628-2631.

2. Llewellyn, D. J., K.M. Langa, R.P. Friedland and I.A. Lang 2010. Serum albumin concentration and cognitive impairment. Current Alzheimer Research. 7, 91-96.

3. Boada, M., P. Ortiz, F. Anaya, I. Hernandez, J. Munoz, L. Nunez, J. Olazaran, I. Roca, G. Cuberas, L. Tarraga, M. Buendia, R.P. Pla, I. Ferrer and A. Paez 2009. AMYLOID-TARGETED THERAPEUTICS IN ALZHEIMER'S DISEASE: USE OF HUMAN ALBUMIN IN PLASMA EXCHANGE AS A NOVEL APPROACH FOR A beta MOBILIZATION. Drug News & Perspectives. 22, 325-339.

4. Milojevic, J., A. Raditsis and G. Melacini 2009. Human serum albumin inhibits A beta fibrillization through a "monomer-competitor" mechanism. Biophys. J. 97, 2585-2594.

5. Milojevic, J., V. Esposito, R. Das and G. Melacini 2007. Understanding the molecular basis for the inhibition of the alzheimer's A beta-peptide oligomerization

by human serum albumin using saturation transfer difference and off-resonance relaxation NMR spectroscopy. J. Am. Chem. Soc. 129, 4282-4290.

6. Biere, A. L., B.L. Ostaszewski, E.R. Stimson, B.T. Hyman, J.E. Maggio and D.J. Selkoe 1996. Amyloid-beta peptide is transported on lipoproteins and albumin in human plasma. J. Biol. Chem. 271, 32916-32922.

7. Bohrmann, B., L. Tjernberg, P. Kuner, S. Poli, B. Levet-Trafit, J. Naslund, G. Richards, W. Huber, H. Dobeli and C. Nordstedt 1999. Endogenous proteins controlling amyloid beta-peptide polymerization - possible implications for beta-amyloid formation in the central nervous system and in peripheral tissues. J. Biol. Chem. 274, 15990-15995.

8. Rozga, M., M. Kloniecki, A. Jablonowska, M. Dandlez and W. Bal 2007. The binding constant for amyloid A beta 40 peptide interaction with human serum albumin. Biochem. Biophys. Res. Commun. 364, 714-718.

9. Reyes Barcelo, A. A., F.J. Gonzalez-Velasquez and M.A. Moss 2009. Soluble aggregates of the amyloid-beta peptide are trapped by serum albumin to enhance amyloid-beta activation of endothelial cells. J Biol Eng. 3, 5.

10. Varshney, A., P. Sen, E. Ahmad, M. Rehan, N. Subbarao and R.H. Khan 2010. Ligand binding strategies of human serum albumin: How can the cargo be utilized? Chirality. 22, 77-87.

11. Bhattacharya, A. A., T. Grune and S. Curry 2000. Crystallographic analysis reveals common modes of binding of medium and long-chain fatty acids to human serum albumin. J. Mol. Biol. 303, 721-732.

12. Yan, Y. L., Y.Z. Liu, M. Sorci, G. Belfort, J.W. Lustbader, S.S. Yan and C.Y. Wang 2007. Surface plasmon resonance and nuclear magnetic resonance studies of ABAD-A beta interaction. Biochemistry (N. Y.). 46, 1724-1731.

13. Mayer, M. and B. Meyer 2001. Group epitope mapping by saturation transfer difference NMR to identify segments of a ligand in direct contact with a protein receptor. J. Am. Chem. Soc. 123, 6108-6117.

14. Huang, H., J. Milojevic and G. Melacini 2008. Analysis and optimization of saturation transfer difference NMR experiments designed to map early self-association events in amyloidogenic peptides. J Phys Chem B. 112, 5795-5802.

15. Esposito, V., R. Das and G. Melacini 2005. Mapping polypeptide self-recognition through H-1 off-resonance relaxation. J. Am. Chem. Soc. 127, 9358-9359.

16. Milojevic, J., V. Esposito, R. Das and G. Melacini 2006. Analysis and parametric optimization of H-1 off-resonance relaxation NMR experiments designed to map polypeptide self-recognition and other noncovalent interactions. J Phys Chem B. 110, 20664-20670.

17. Mansfield, S. L., D.A. Jayawickrama, J.S. Timmons and C.K. Larive 1998. Measurement of peptide aggregation with pulsed-field gradient nuclear magnetic resonance spectroscopy. Biochimica Et Biophysica Acta-Protein Structure and Molecular Enzymology. 1382, 257-265.

18. Zhang, S. S., N. Casey and J.P. Lee 1998. Residual structure in the alzheimer's disease peptide: Probing the origin of a central hydrophobic cluster. Fold. Des. 3, 413-422.

19. Jarvet, J., P. Damberg, K. Bodell, L.E.G. Eriksson and A. Graslund 2000. Reversible random coil to beta-sheet transition and the early stage of aggregation of the A beta(12-28) fragment from the alzheimer peptide. J. Am. Chem. Soc. 122, 4261-4268.

20. Mao, H. Y., A.H. Gunasekera and S.W. Fesik 2000. Expression, refolding, and isotopic labeling of human serum albumin domains for NMR spectroscopy. Protein Expr. Purif. 20, 492-499.

21. Hou, L. M., H.Y. Shao, Y.B. Zhang, H. Li, N.K. Menon, E.B. Neuhaus, J.M. Brewer, I.J.L. Byeon, D.G. Ray, M.P. Vitek, T. Iwashita, R.A. Makula, A.B. Przybyla and M.G. Zagorski 2004. Solution NMR studies of the A beta(1-40) and A beta(1-42) peptides establish that the met35 oxidation state affects the mechanism of amyloid formation. J. Am. Chem. Soc. 126, 1992-2005.

22. Ahmed, M., J. Davis, D. Aucoin, T. Sato, S. Ahuja, S. Aimoto, J.I. Elliott, W.E. Van Nostrand and S.O. Smith 2010. Structural conversion of neurotoxic amyloid-beta(1-42) oligomers to fibrils. Nature Structural & Molecular Biology. 17, 561-U56.

23. Bitan, G., M.D. Kirkitadze, A. Lomakin, S.S. Vollers, G.B. Benedek and D.B. Teplow 2003. Amyloid beta-protein (A beta) assembly: A beta 40 and A beta 42 oligomerize through distinct pathways. Proc. Natl. Acad. Sci. U. S. A. 100, 330-335.

24. Kooistra, J., J. Milojevic, G. Melacini and J. Ortega 2009. A new function of human HtrA2 as an amyloid-beta oligomerization inhibitor. Journal of Alzheimers Disease. 17, 281-294.

25. Sgourakis, N. G., Y.L. Yan, S.A. McCallum, C.Y. Wang and A.E. Garcia 2007. The alzheimer's peptides A beta 40 and 42 adopt distinct conformations in water: A combined MD/NMR study. J. Mol. Biol. 368, 1448-1457.

26. Triguero, L., R. Singh and R. Prabhakar 2008. Comparative molecular dynamics studies of wild-type and oxidized forms of full-length alzheimer amyloid beta-peptides A beta(1-40) and A beta(1-42). J Phys Chem B. 112, 7123-7131.

27. Luhrs, T., C. Ritter, M. Adrian, D. Riek-Loher, B. Bohrmann, H. Doeli, D. Schubert and R. Riek 2005. 3D structure of alzheimer's amyloid-beta(1-42) fibrils. Proc. Natl. Acad. Sci. U. S. A. 102, 17342-17347.

28. Cavani, S., A. Tamaoka, A. Moretti, L. Marinelli, G. Angelini, S. Di Stefano, G. Piombo, V. Cazzulo, S. Matsuno, S. Shoji, Y. Furiya, D. Zaccheo, F. Dagna-Bricarelli, M. Tabaton and H. Mori 2000. Plasma levels of amyloid beta 40 and 42 are independent from ApoE genotype and mental retardation in down syndrome. Am. J. Med. Genet. 95, 224-228.

29. Hindo, S. S., A.M. Mancino, J.J. Braymer, Y.H. Liu, S. Vivekanandan, A. Ramamoorthy and M.H. Lim 2009. Small molecule modulators of copper-induced A beta aggregation. J. Am. Chem. Soc. 131, 16663-16665.

30. Nanga, R. P. R., J.R. Brender, J.D. Xu, K. Hartman, V. Subramanian and A. Ramamoorthy 2009. Three-dimensional structure and orientation of rat islet amyloid polypeptide protein in a membrane environment by solution NMR spectroscopy. J. Am. Chem. Soc. 131, 8252-8261.

SUPPORTING INFORMATION:

Confirmation of the structural integrity of the HSA constructs. The refolding and secondary structure elements of the HSA mutants prepared through bacterial expression were validated by acquiring far-UV CD spectra (Figure S1). Based on the measured molar ellipticities at 222 nm (20), the α-helical content of full length wt HSA as well as of domains 1 and 3 are calculated to be 68 %, 45 % and 56 %, respectively (Table S1). These values are in good agreement with those previously published for corresponding HSA mutants purified from yeast *P. Pastoris* cells (Table S1) (S1). However, no reference data is available for the two domains constructs and therefore for these deletion

mutants a lower limit to the α-helical content was calculated as a weighted average of the α-helical percentages reported for the individual domains (Table S1). The experimental α-helical percentages measured for the two-domain constructs are slightly higher relative to the values calculated using the single domain constructs (Table S1). These minor differences of about 7-8 % units are expected based on the structure of HSA (Figure 1a) and are rationalized in terms of partial local unfolding of inter-domain helices due to the elimination of domain 2 from the two-domain constructs. Overall, the CD data (Figure S1) support a successful refolding of all the prepared HSA constructs (Figure 1b).

Equation S1: The concentration of free HSA is derived from $[HSA]_{Tot.}$, $[A\square_n]_{Tot}$ and $K_{D,HSA,app.}$ according to equation S1:

$$[HSA] = [HSA]_{Tot} - 0.5\{ b - \sqrt{(b^2 - 4[A\beta_n]_{Tot}[HSA]_{Tot.})}\} \quad (S1)$$

where $b = [HSA]_{Tot.} + [A\beta_n]_{Tot} + K_{D,HSA,app.}$.

MATERIAL AND METHODS

Aβ (12-28) Peptide Sample Preparation. Samples of 0.65 and 1 mM Aβ (12-28) were prepared as previously described (4,5) by dissolving a lyophilized powder in 50 mM acetate buffer–d_4 at pH 4.7, with 10% D_2O. At this pH, Aβ (12-28) undergoes chemical exchange between the monomeric and oligomeric states. This exchange is detectable by

NMR through line-broadening, STD and ORR, while at higher pH this exchange is significantly reduced. This pH is also relevant for HSA, since at this pH albumin is still present in the physiologically relevant N form as previously reported (4). The Aβ (12-28) peptide used in this investigation was purchased from Genscript Corp., Piscataway, NJ with a purity of 98 %. After the peptide was dissolved, the solution was filtered through a Ultrafree-MC Millipore with a 30 kDa cutoff filter in 5 min intervals at 3,000 rpm to remove aggregates possibly serendipitously formed during the peptide lyophilization and dissolution processes. To induce aggregation in a controlled manner, a 1 M NaCl solution prepared in 50 mM acetate buffer at pH 4.7 was then added to the filtered peptide sample up to a final concentration of 25 or 40 mM NaCl. The resulting aggregated Aβ (12-28) solutions were allowed to equilibrate for seven days. This equilibration time was determined to be sufficient for sample stability, as assessed through line width analysis and through 1D-STD NMR experiments. Care was taken to ensure that all the Aβ (12-28) samples used in the titrations came from the same peptide stock solution, so that any difference observed in the protein titrations cannot be attributed to differences in the peptide preparations. For this reason we prepared an aggregated peptide stock solution, from which 500 µL aliquots were obtained and used for each titration.

Aβ (1-42) Peptide Sample Preparation. The Alzheimer's peptide Aβ(1-42) was purchased from EZBiolab Inc., with a purity greater than 95 %. Soluble 90 µM Aβ(1-42) samples were prepared by dissolving 1 mg of the Aβ (1-42) peptide in 500 µL of 10 mM

NaOH. After sonication for 1 min, the peptide sample was then placed on ice for a two minute interval, after which it was sonicated again for another minute. This solution was then diluted with 2 mL of a 15 mM potassium phosphate buffer at pH 7.4, with 10 % D_2O and 0.02 % NaN_3. The final peptide concentration was 90 µM at a pH of 7.4. Immediately after preparation, the 90 µM Aβ(1-42) solution was divided into several fractions to which wild-type HSA or HSA deletion mutants, dialyzed in the same buffer, were added prior to the acquisition of NMR data at 37 ^oC. During the time between NMR data acquisition sessions, the NMR samples were stored in water bath at 37 ^oC without stirring or mixing.

Protein Sample Preparations – Sub-Cloning. The HSA gene in the pUC19 vector was purchased from ATCC (Cat. number 61356). Sequencing results indicated that the HSA gene has an internal NdeI restriction enzyme site (5'- ACA TAT G-3') located in domain 2 of HSA. This site was mutated using PCR to 5'- ACT TAT G-3', which does not change protein amino acid sequence but prevents NdeI digestion at domain 2. The NdeI restriction enzyme site was instead introduced in the pUC19 vector at the beginning of domain 1 of full length HSA. This vector was then digested with the NdeI and BamH1 (pUC19 cloning site) enzymes to release the HSA gene. The isolated HSA gene was purified from a 1% agarose gel and was ligated into the pET 15B vector, which encodes for a His-tag used in the protein purification. While the his-tag is always removed by thrombin cleavage, it leaves behind four residues (Gly-Ser-His-Met), which are present at

the beginning of the HSA constructs. Sequencing confirmed the correct insertion of the HSA gene into the pet15B vector. Individual domains and HSA gene constructs were then obtained as follows. The domain 1 gene (Figure 1b) was obtained by introducing two stop codons at the end of the domain 1 through PCR mutagenesis. The construct for domains 12 (Figure 1b) was obtained by introducing a stop codon at the end of domain 2, while the domain 23 fragment (Figure 1b) was obtained by introducing an NdeI restriction enzyme site at the end of domain 1. This mutated DNA was then digested with the NdeI enzyme, which resulted in the removal of domain 1. Ligation of the purified vector resulted in the domain 23 construct (Figure 1b). Similarly, the DNA sequence of domain 3 (Figure 1b) was generated by introducing an Nde1 restriction enzyme site at the end of domain 2. Digestion with the Nde1 enzyme resulted in the removal of the sequences of domains 1 and 2 and subsequent ligation generated the domain 3 construct. The sequence of each constructs was confirmed through PCR based sequencing. The exact positions of the domain boundaries are indicated in Figure 1b.

Protein Sample Preparations – Expression and Purification. The main protocol for the expression and purification of our albumin constructs was adapted from reference (20). In brief, each construct was expressed in BL21-CodonPlus (DE3) cells. Protein expression was induced with 1 mM IPTG at 37 ^{o}C for 3 hours after the optical density reading at 600 nm reached a 0.9 value. After induction cells where collected and re-suspended in 20 mM Tris HCl buffer at pH 7.9 with 150 mM NaCl. Cells where then lysed using a French press/emulsifier (EmulsiFlex-C5). Protein inclusion bodies were

collected by centrifugation at the 13,000 rpm. Protein pellets were solubilized using a 6M guanidine hydrochloride solution (20 mM TrisHCl, 2 mM beta mercaptoethanol (BME), 6M guanidine HCl, pH 7.9) and were loaded onto Nickel beads for 16 hours at 4 °C. Non-specifically bound proteins were washed from the beads using a 20 mM imidazole buffer (20 mM imidazole, 8M urea, 20 mM Tris, 2 mM BME, pH 7.9). The target protein was then eluted using a 1 M imidazole solution (8M urea and 20 mM Tris, 2 mM BME, pH 7.9). Nickel ions where removed by dialyzing the protein in water and then 0.5 % acetic acid. The precipitated protein was solubilized in 8M urea and reduced with 50 mM DTT at 37 °C for 30 minutes. The protein was then diluted to a 0.5 mg/mL concentration with a solution of 8M urea, 50 mM sodium bicarbonate at pH 10. Removal of urea and subsequent protein refolding was performed by dialyzing the solution in 50 mM sodium bicarbonate, 1 mM EDTA buffer at pH 10. The pH of the final solution was adjusted to the 7.0 and the properly folded protein was collected using a HiTrap Blue Sepharose column (GE Healthcare). The protein was then digested with thrombin and further purified using a Superdex 75 preparation grade XK26/60 column (GE Healthcare) pre-equilibrated with 50 mM sodium phosphate buffer (pH 6.5) containing 150 mM NaCl, 0.1 mM EDTA, and 0.02 % NaN_3. The thrombin digested monomeric protein construct was collected and delipidated using a hydroxyalkoxypropyl dextran type VI resin (Sigma Chemical) at pH 3 for 90 min at room temperature. The collected protein was then dialyzed in 50 mM sodium phosphate buffer, pH 6.5, 150 mM NaCl, 0.02 % NaN_3. Fatty acid free and essentially globulin free full length HSA was purchased from Sigma with a 99% purity. All final protein samples were dialyzed either in a 20 mM acetic acid, 25

mM NaCl solution to be used for the Aβ (12-28) titration experiments or in a 15 mM potassium phosphate buffer (pH 7.4) to match the conditions of the Aβ (1-42) samples. 20 mM acetic acid, 25 mM NaCl buffer was used as opposed to 50 mM acetic-d_4 buffer, 25 mM NaCl in peptide solution to avoid excessive acetic acid signal in the NMR spectrum during peptide titration at high protein concentrations. The final protein concentrations were measured using the absorbance at 280 nm on a Hewlett Packard 8453 UV–vis spectrophotometer and in a 6 M guanidine hydrochloride solution. The extinction coefficient used to calculate protein concentrations was obtained using the biology workbench software (http://workbench.sdsc.edu/). All HSA constructs were run through SDS-PAGE and in addition their secondary structure was probed by far-UV circular dichroism (CD) measurements performed between 195 nm and 260 nm on an AVIV Circular dichroism (model 215) spectrometer at 25°C after dilution in 50 mM sodium phosphate buffer (pH 6.5) containing 150 mM NaCl, and 0.02% NaN_3.

NMR Spectroscopy – Saturation Transfer Difference (STD) Experiments. 1D-STD experiments were used to monitor the effect of HSA and its constructs on the Aβ(12-28) samples. All STD experiments were acquired using previously described pulse sequences (13,14) and a Bruker Avance 700 MHz spectrometer equipped with 5 mm TCI Cyroprobe at 20 ^{o}C. Selective saturation was achieved using a train of 40 Gaussian-shaped pulses of 50 ms each and separated by a 1 ms inter pulse delay, resulting in total saturation time of ~2 seconds which was preceded by a 100 ms inter-scan delay. The

strength of each saturating Gaussian pulse was 110.23 Hz with a 1 % truncation and 1000 digitization points. On-resonance saturation was achieved by setting the carrier frequency of the Gaussian pulse train at 0.75 ppm, while off-resonance saturation was obtained by saturating at 30 ppm. The saturation transfer difference spectra were obtained by subtracting on-resonance and off-resonance spectra through phase cycling. In all experiments the water magnetization was suppressed using the 3-9-19 Watergate gradient spin-echo (S2). A 30 ms spin lock pulse with strength of 2.6 kHz was applied to suppress the residual protein signal in all STD and saturation transfer reference (STR) experiments. For the STD experiments 128 scans and 8 dummy scans were acquired, which were reduced to 32 scans and 32 dummy scans for the more sensitive STR spectra. For each titration point two STR and four STD replica spectra were collected. All STD and STR replicas were then added to increase the S/N ratios. The 6.88-7.25 ppm spectral region was used to determine the I_{STD}/I_{STR} ratios and the related errors were evaluated as standard deviations of the signal/noise ratios of the individual replicas. Before each titration, STD experiments were preformed on a control aggregated Aβ(12-28) sample without protein to confirm sample stability, and to ensure differences observed in the titration profiles for different proteins are not due to the different oligomer populations in different Aβ samples. The titration curves were fitted using a Scatchard-like model as outlined in the Results section. Due to the transient nature of the oligomers formed by the longer Aβ (1-42) peptide, the STD experiments were not performed for this longer peptide. However, the Aβ (1-42) self-association was monitored through the signal loss occurring over time after sample preparation in a 1D Watergate experiment incorporating

a 30 ms long spin lock pulse with a 2.6 kHz strength prior to acquisition to suppress the residual protein signal. These 1D time-profiles for Aβ (1-42) were acquired at 600 MHz using 128 scans and 64 dummy scans. All 1D spectra were processed using an exponential multiplication window function prior to zero filling.

NMR Spectroscopy – Off-Resonance Relaxation (ORR) Experiments. Nonselective off-resonance relaxation 2D-TOCSY experiments (15,16) were acquired at 700 MHz with an off-resonance trapezoidal spin-lock including two adiabatic pulses of 4 ms duration and applied at the angle of 35.5° for 13 ms and 88 ms. The strength of the off-resonance and TOCSY spin locks were 8.25 and 10 kHz, respectively. The spectral widths for both dimensions were 8389.26 Hz with 256 and 1024 t_1 and t_2 complex points, respectively. The interscan delay was 2 seconds long. The water magnetization was suppressed using the binomial 3-9-19 Watergate gradient spin-echo (WG) (S2). Each experiment was collected with 8 scans and 128 dummy scans. For each spin-lock duration two data sets were acquired. 2D replica sets were then added to increase the S/N ratios and processed with Xwinnmr (Bruker Inc.) using a 90^o phase shifted squared sine bell window function for both dimensions prior to zero filling. The 2D cross-peak intensities were measured with Sparky 3.11126 (S3) by Gaussian line fitting using the fit peak heights. The standard deviation of the differences in fit heights between two copies was used to estimate the error of the individual spectra. The error of the sum was scaled up proportionally to the square root of the total number of scans. For all residues, the $H_{\alpha,i}$-$H_{N,i}$ cross-peaks were

used for data analysis, with the exception of G25 and of the N-terminal V12 (15,16). G25 was omitted from the analysis due to the overlap of its degenerate H_α protons, while for V12, the $H_{\alpha,12}$-$H_{Me,12}$ cross-peak was used to probe Hα relaxation rates. The non-selective off-resonance relaxation rates were related to the experimental fit heights as previously explained (15,16). The measured rates and the related errors were normalized with respect to the maximum observed rate.

Dynamic Light Scattering (DLS) Measurements. DLS measurements were preformed on a Zetasizer Nano S (Malvern Instruments, Malvern UK) using a detection angle of 173° at a temperature of 25 °C and with a 4 mW He-Ne laser operating at a wavelength of 633 nm. All measurements were performed using a 12 μL (ZEN2112) quartz cell. The particle diameter detection limit is 0.6 – 6 μm. The viscosity value for water was used in the analysis of all measurements. The intensity size distributions were obtained from the analysis of the correlation functions using the cumulant algorithm in the Zetasizer Nano S software. A stock 1 mM albumin sample was filtered using a 0.1 μm filter, while a 0.1 mM Aβ (1-42) stock solution was centrifuged for 10 minutes at 5,000 rpm prior to protein addition to remove possible dust particles. Measurements were preformed on a 0.1 mM Aβ (1-42) samples in the absence of and in the presence of 200 μM HSA, immediately after sample preparation and 48 hour after incubation at 37 ^oC. For each sample condition three measurements were collected to ensure reproducibility of the intensity distribution.

Table S1. Comparison of α-Helical Content in Different HSA Constructs

Constructs	Residue Ranges	Reference Values[a]	Calculated Values[b]	Measured Values[c]
Wt full length HSA[d]	1-585	66 +/- 0.6%	N/A	68 %
Domain 1	1-197	46 +/- 0.5%	N/A	45 %
Domain 3	381-585	53 +/- 1.5%	N/A	56 %
Domain 2	189-385	37 +/- 0.5%	N/A	N/A
Domain 23	189-585	N/A	45 %	52 %
Domain 12	1-385	N/A	41 %	49 %

[a]From (S1) based on constructs expressed in yeast.

[b]Weighted average of the reference values reported for the isolated domains.

[c]All data was recorded at 25°C on an AVIV Circular Dichroism spectrometer. The percentages of the α-helical structures were calculated from the molar ellipticities at 222 nm.

[d]The protein concentrations were 15, 30, 7, 5.5, and 28.7 μM for HSA (commercial), domain 3, domain 23, domain 12 and domain 1, respectively. All proteins samples were in 50 mM sodium phosphate buffer (pH 6.5) containing 150 mM NaCl, and 0.02% NaN_3.

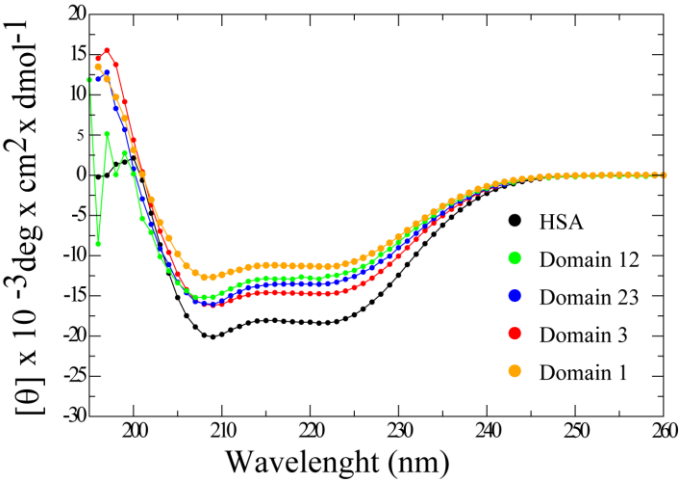

Figure S1: CD spectra of all protein constructs used in this study. Spectra were collected on an AVIV Circular Dichroism spectrometer at 25°C and were used to validate the protein fold, as indicated in Table 1. Measurements were preformed in 50 mM sodium phosphate buffer (pH 6.5) containing 150 mM NaCl, and 0.02% NaN_3.

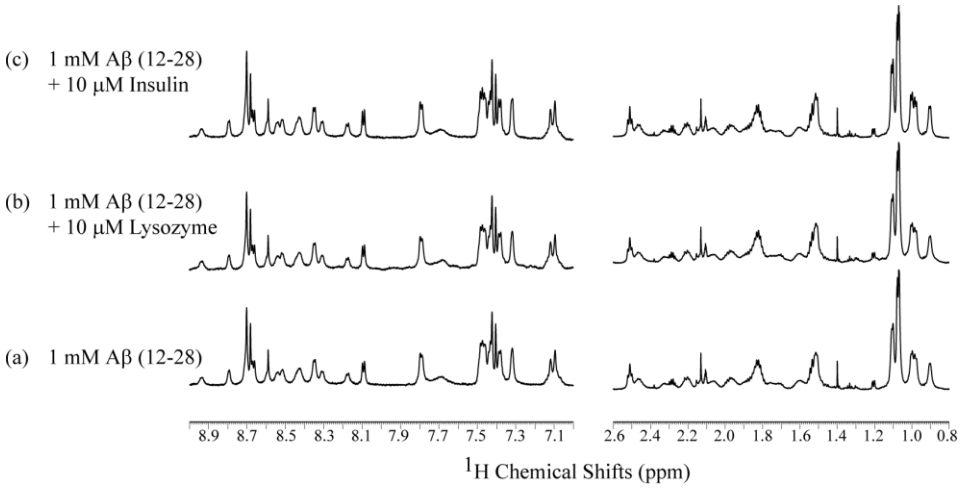

Figure S2: Effect of insulin and lysozyme on the aggregated 1 mM Aβ (12-28) sample. Panel (a) reports aggregated 1 mM Aβ (12-28). Effect of the lysozyme and insulin addition is shown in panel (b) and (c), respectively. Contrary to the HSA these proteins do not interact with Aβ and therefore have no effect on the line widths of the 1D spectrum as it was observed in Figure 2 upon addition of HSA and HSA constructs. All samples were prepared in 50 mM deuterated acetate buffer with 10% D_2O at pH 4.7. Experiments were recorded at 700 MHz using a TCI CryoProbe and at 293K.

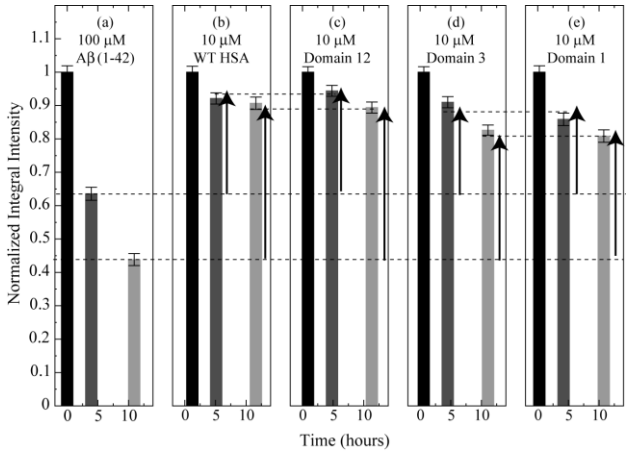

Figure S3: Effect of HSA and of the HSA deletion mutants on the early aggregation of the Aβ (1-42) peptide. Changes in the intensity of the 1D spectra were used to monitor the Aβ(1-42) aggregation state in the absence (a) and presence of 10 μM of HSA (b), the domain 12 construct (c), domain 3 (d) and domain 1 (e), respectively. Experiments were recorded at 600 MHz and 37 ^{o}C using a 30 ms spin lock to suppress protein signals. The integrals reported in this Figure as a function of time are for the methyl spectral region (0.6–1.1 ppm). The error was estimated from the spectral noise. All integrals were normalized to their starting values. In between acquisition sessions, NMR samples were stored in a water bath at 37 ^{o}C.

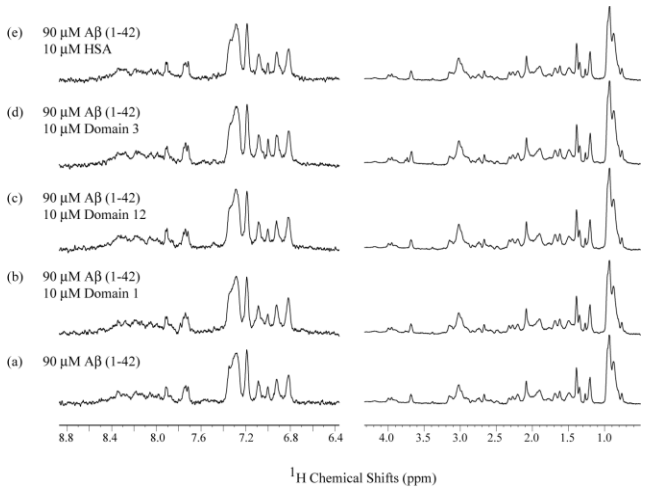

Figure S4: 1D-WG NMR spectra comparisons to show that the HSA deletion mutants do not interact with the monomeric Aβ(1-42) peptide. All samples used for this Figure contain 90 μM Aβ(1-42) either in the absence or in the presence of 10 μM HSA or its deletion constructs indicated in the Figure. These 1D-WG experiments were obtained with a 30 ms spin lock filter to suppress the protein signal and were recorded at 600 MHz at 37 ^{o}C. All spectra were processed using an exponential multiplication window function with a line-broadening coefficient of 3 Hz. Samples were prepared in 15 mM potassium phosphate buffer with 10% D_2O at pH 7.4.

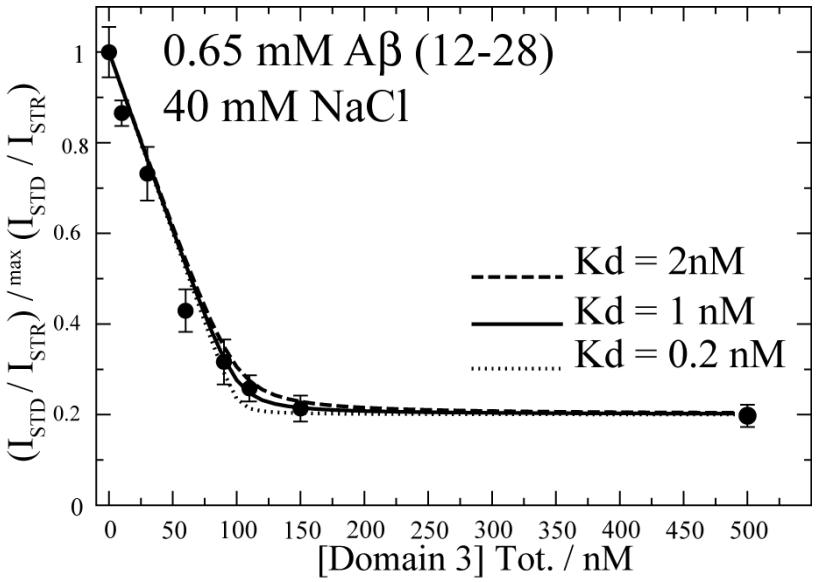

Figure S5: Effect of domain 3 on the relative I_{STD}/I_{STR} ratios measured for the filtered 0.65 mM Aβ (12-28) peptide aggregated through addition of 40 mM NaCl. Experiments were recorded at 700 MHz using a TCI CryoProbe and at 20 ^{o}C. All ratios were normalized to their maximum value measured before domain 3 additiosn. Dotted lines were used to model dissociation constants in the 2-0.2 nM range.

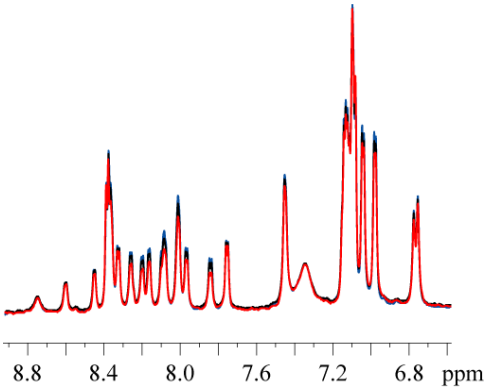

Figure S6: 1D –STR NMR spectra of the Aβ(12-28) peptide in the absence and presence of HSA domain 3 processed using an exponential multiplication window function with a line broadening coefficient of 5 Hz. This line broadening coefficient ensures that the linewidth is approximately independent of the amount of HSA domain 3 added. The spectral intensity can therefore be used to estimate the relative concentrations of monomeric Aβ(12-28). These 1D-WG experiments used a 30 ms spin lock filter to suppress the protein signal and were recorded at 700 MHz at 293K. The spectrum of 0.65 mM Aβ(12-28) in the absence of domain 3 is shown in red, while samples with 60 and 500 nM of domain 3 are shown in black and blue respectively. While addition of the domain 3 affects significantly the STD signal, no major intensity or chemical shift changes were observed in the Aβ STR spectra. All samples were prepared in 50 mM acetic acid-d_4, 40 mM NaCl buffer with 10% D_2O at pH 4.7.

REFERENCES FOR SUPLEMETARY MATERIAL

S1. Dockal, M., D.C. Carter and F. Ruker 1999. The Three Recombinant Domains of Human Serum Albumin. J. Biol. Chem. 274, 29303-29310.

S2. Piotto, M., V. Saudek and V. Sklenar 1992. Gradient-tailored excitation for single-quantum nmr-spectroscopy of aqueous-solutions. J. Biomol. NMR. 2, 661-665.

S3. Sparky 3.111 Goddard, T. D. and Kneller, D. G., SPARKY 3, University of California, San Francisco

INVESTIGATING THE DETERMINANTS OF THE ALZHEIMER'S Aβ PEPTIDE BINDING TO HUMAN SERUM ALBUMIN: NMR STUDY OF THE HUMAN SERUM ALBUMIN DOMAIN 3: Aβ INTERACTIONS

CHAPTER 6

INVESTIGATING THE DETERMINANTS OF THE ALZHEIMER'S Aβ PEPTIDE BIDING TO HUMAN SERUM ALBUMIN: NMR STUDY OF THE HSA DOMAIN 3: Aβ INTERACTIONS

Julijana Milojevic, Giuseppe Melacini

ABSTRACT

Human serum albumin (HSA) binds Aβ oligomers through binding sites that are characterized by similar affinities and are evenly partitioned across the three albumin domains, effectively preventing Aβ development into amyloid fibrils. Although the binding stoichiometry and affinities of the Aβ-albumin complexes were recently investigated, it is not currently known how Aβ binding compares to the recognition of other endogenous ligands (*i.e.* fatty acids (FA)). We have addressed this question through the comparative NMR and fluorescence analysis of several mutants of the HSA domain 3, which is a model system also for the other homologous domains of HSA. In particular, here we show that, similarly to the FA binding sites, the Aβ binding sites are located in both 3A and 3B sub-domains. However, our analyses indicated that the Aβ and the FA recognition sites don't fully overlap as multiple domain 3 mutants show that residues forming hydrogen bonds with FAs are not significantly involved in Aβ binding. Moreover, ^{15}N-^{1}H HSQC experiments were used to identify specific peptide regions of domain 3 with significant Aβ-self association inhibition potency. We show that Aβ is specifically recognized by partially unstructured, hydrophobic and aggregation prone domain 3 regions and we propose these as the main Aβ binding determinants.

INTRODUCTION

Recent studies show that late-onset Alzheimer's disease (AD) is associated with impairment in the clearance of Aβ, suggesting that Aβ clearance mechanisms are critically important in the development of AD (1). The majority of Aβ is cleared from the brain via transport through the blood brain barrier (BBB) mediated by the low-density lipoprotein receptor-related protein (LRP) (2). In addition, agents that do not penetrate the BBB but bind Aβ in the plasma promote an equilibrium shift of soluble Aβ from the brain toward the periphery reducing amyloid formation within the brain, as posited by the 'peripheral sink' hypothesis (3). About 90% of the circulating plasma Aβ is bound to albumin, suggesting that albumin is a key mediator of the Aβ clearance, as confirmed by recent clinical investigations showing that low concentrations of albumin in plasma are associated with cognitive impairment (4, 5). Moreover albumin replacement through plasma dialysis was proposed as a promising strategy for the treatment of mild AD (6).

The binding mechanism, stoichiometry and affinity of the Aβ-albumin complexes were recently investigated (7). Currently it is understood that albumin specifically targets Aβ oligomers through binding sites evenly partitioned across three albumin domains and with dissociation constants in the sub nM range (7). Such degeneracy of the Aβ binding sites within albumin implies that each single albumin domain can be used as a model system to further probe the HSA/*Aβ* interactions. Therefore, to further dissect the albumin determinants of Aβ oligomer binding, we have specifically investigated

Aβ interactions involving albumin domain 3, which remains well structured and soluble even when in isolation (7, 8).

Here, we use domain 3 and several related constructs to address three main questions. First, it is not understood how Aβ binding compares to the binding of other endogenous ligands (*i.e.* fatty acids). The fatty acid binding sites are distributed through the three HSA domains (Fig. 1), similarly to Aβ binding sites. In addition, while extensive hydrophobic interactions are common for all fatty acid binding sites, it is the number of hydrogen bonds formed between the albumin amino acid side chains and the fatty acid carboxylate groups that determines the binding affinities (9, 10). It is currently not clear if residues involved in fatty acid H-bonding are also involved in the Aβ binding. Therefore to answer this question we have investigated the interactions of Aβ with several domain 3 mutants. Specifically, the R410AY411A, R485AS489A and K525A domain 3 mutants were selected, as these mutations were previously shown to affect FA binding affinities (11). Using a combination of NMR experiments and Scatchard-like models, we show that these domain 3 mutations had no significant effects on the Aβ binding, suggesting that the FA binding determinants are at least partially different from those for Aβ binding.

The second open question addressed here pertains to the sub-domain distribution of the Aβ binding sites in albumin. Although helices 2-4 in the 3A sub-domain are structurally homologous to the helices 8-10 in the 3B sub-domain, the 3A sub-domain cavity is enclosed by several helices (helix 1, 2, 5 and 6) to form a wide hydrophobic

cavity (Figure 1). Unlike 3A, 3B sub-domain is enclosed only by a 3_{10} helix 7 and a long hydrophobic loop (10). Moreover opposed to the 3A which is lined mainly with leucine and valine residues, the 3B sub-domain is mainly lined with phenylalanine residues which make it more constricted significantly reducing the number of ligands that bind to this sub-domain (10). Although binding of albumin to small molecules has been extensively studied and well understood, the contribution of each sub-domain to Aβ binding is still unknown.

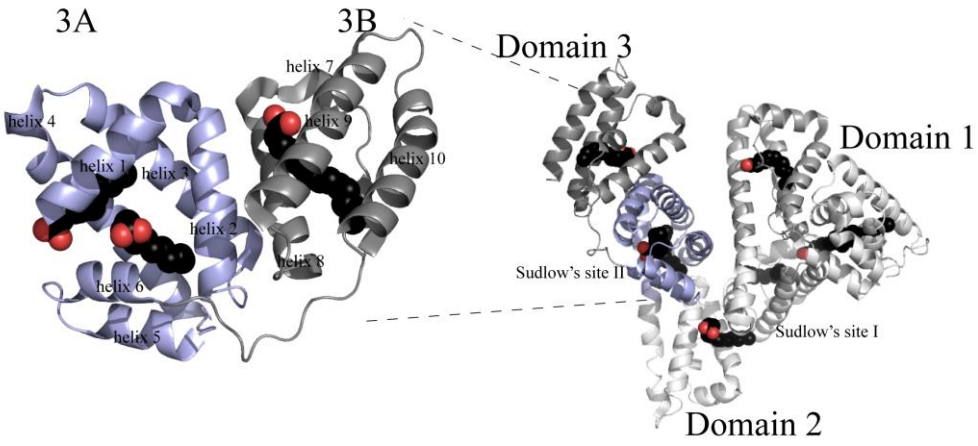

Figure 1. Distribution of the ligand binding sites within human serum albumin (PDB file1E7H) (12). Palmitate molecules are shown in space-filling representation and are colored by atom: carbon (black), oxygen (red). Major drug binding sites are labeled as Sudlow's sites I and II and their location in the 2A and 3A sub-domains, respectively, is indicated. We mainly focused on the interactions of the Aβ with domain 3, whose structure is shown in separate insert. Helix 1- 6 are located in sub-domain 3A, while helices 7-10 are located in 3B as indicated in the Figure.

In order to understand if Aβ displays sub-domain selectivity, we have probed the binding of Aβ to two domain 3 deletion mutants, *i.e.* sub-domains 3A and 3B. Our results show that both sub-domains 3A and 3B are involved in Aβ self-recognition inhibition.

The third question we have been focusing on the identification of the Aβ binding determinants within the domain 3 sub-domains. For this purpose, we have assigned the ^{15}N-^{1}H HSQC spectrum of apo HSA domain 3 (23.1 kDa, 205 residues) and we have mapped the domain 3 chemical shifts changes caused by the Aβ oligomers. Using this approach, we have identified a putative Aβ interaction site in subdomain 3B. The domain 3 peptide spanning the identified Aβ interaction site was designed and tested against both Aβ (12-28) and Aβ (1-40) peptides. The corresponding peptide displays significant potency in the inhibition of Aβ self-association and matches well with a region of albumin prone to self-association. These results suggest that sites of inter-molecular contact in the self-association of proteins may also serve as possible Aβ recognition sites.

MATERIALS AND METHODS

Aβ (12-28) Peptide Sample Preparation. The Aβ (12-28) peptide used in this investigation was purchased from Pepnome Limited with a purity of 98 %. Lyophilized peptide was dissolved in 50 mM acetate buffer–d_4 at pH 4.7, with 10% D_2O to a concentration of 1 mM. After the peptide was dissolved, the solution was filtered through a Ultrafree-MC Millipore with a 30 kDa cutoff filter in 5 min intervals at 3,000 rpm to remove aggregates formed during the peptide lyophilization and dissolution processes (7, 13, 14). To induce aggregation a 1 M NaCl solution prepared in 50 mM acetate buffer at

pH 4.7 was then added to the filtered peptide sample up to a final concentration of 40 mM NaCl followed by a 7 day incubation period at room temperature (7, 13).

Aβ (1-42) Peptide Sample Preparation. The Alzheimer's peptide Aβ(1-42) was purchased from EZBiolab Inc., with a purity greater than 95 %. A stock Aβ(1-42) solution was prepared by dissolving 1 mg of the Aβ (1-42) peptide in 500 µL of 10 mM NaOH (7, 14). This stock solution was sonicated twice using 1 minute intervals followed by two minute incubation on ice. 500 µL of the stock solution were then diluted with 2 mL of a 20 mM sodium phosphate buffer at pH 7.4, with 10 % D_2O and 0.05 % NaN_3 to a final peptide concentration of 90 µM. Immediately after preparation, the 90 µM Aβ(1-42) solution was divided into several fractions to which wild type and domain 3 mutant proteins in the 20 mM sodium phosphate buffer at pH 7.4 were added for collection of NMR spectra at 700 MHz with a cyroprobe and at 37 ^{o}C. During the time between NMR data acquisition sessions, the NMR samples were stored in a water bath at 37 ^{o}C and were not stirred or mixed.

TFA Removal from the Aβ Samples. Although all peptides were commercially obtained with > 95% purity, they all contained residual TFA (trifluoroacetic acid), which is routinely used in the final stage of the peptide purification. This poses a problem since TFA specifically binds to domain 3 of human serum albumin. Therefore TFA was removed from the Aβ samples prior to the addition of the domain 3 using at least three lyophilization steps in the presence of 50-100 mM HCl (15). 1D-^{19}F NMR was used to insure complete TFA removal (Figure S2).

Aβ (1-40) Peptide Sample Preparation for ^{15}N-^{1}H HSQC Experiments. To obtain complete control of the buffer conditions, the Aβ: Domain 3 samples were prepared as shown in the Figure S3. For this purpose 2 mM Aβ (1-40) was diluted in the 5 mM NaOH followed by two cycles of one minute sonication. 0.1 mL of the stock solution was dissolved in 0.4 mL of the 20 mM sodium phosphate, 80 mM NaCl, 10% D2O, 0.05% NaN3, 0.1 mM EDTA at pH 6.5. To this solution 100 μL of 0.5 mM stock ^{15}N Domain 3 in an identical buffer was immediately added (Figure S3-sample I). ^{15}N-^{1}H HSQC experiments were then collected immediately after this sample was prepared. After data acquisition, the sample was concentrated to 100 μL using a 10 kDa filter. A control protein solution was then prepared by dissolving 100 μL of the 0.5 mM stock of Domain 3 in 400 μL of the filtrate solution (Figure S3- sample IV).

Protein Sub-Cloning, Expression and Purification. The domain 3 gene flanked by the NdeI restriction enzyme site and six hystidines at the N–terminus was generated in the pet15B vector as previously published (7). The Y411AR410A, R485AS489A and K525A mutants were generated following standard PCR protocols for generating point mutants. The 3A subdomain was generated by mutating T496 into a stop codon using as a primer 5’ GCTCTGGAAGTCGATGAATAATACGTTCCC 3’. The 3B construct was generated by mutating D494 and E495 into an NdeI restriction enzyme site. This was done using the 5’ CAGCTCTGGAAGTCCATATGACATACGTTCCC 3’ primer. Since the 3A sub-domain was flanked by the NdeI site, digestion of this mutated DNA resulted in the excision of the 3A sub-domain from the domain 3 sequence. Subsequent ligation

generated a 3B sub-domain DNA construct. The sequence of each constructs was confirmed through PCR based sequencing. All proteins samples were expressed and purified as previously published (7, 8).

NMR Spectroscopy –Saturation Transfer Difference (STD) and 1D-WG Experiments. 1D-STD experiments were used to monitor the effect of domain 3 mutants and deletion constructs on the Aβ(12-28) samples. The same experimental set up as previously published was used (7) and therefore will not be discussed here. The titration curves were fitted using a Scatchard-like model as previously published (7). Due to the transient nature of the oligomers formed by the longer Aβ (1-42) peptide, the STD experiments were not performed for this longer peptide, however the intensities of 1D Watergate experiments were previously shown to be effective in probing the protein inhibited aggregation of Aβ (1-42) (7, 14). These experiments rely on the incorporation of a 30 ms long spin lock pulse with a 2.6 kHz strength prior to acquisition to suppress the residual protein signal and selectively observe the monomeric and low MW Aβ signal. All experiments were acquired on a Bruker Avance 700 MHz spectrometer equipped with a 5 mm TCI Cyroprobe. The STD experiments were performed at 20 ^{o}C, while 1D-WG experiments were performed at 37^{o}C.

NMR Spectroscopy – ^{15}N-^{1}H HSQC Experiments. Gradient and sensitivity enhanced [^{15}N-^{1}H] heteronuclear single quantum coherence (HSQC) spectra were collected with 128 (t1) and 1,024 (t2) complex points. Spectral widths of 31.82 and 14.06 ppm for the ^{15}N and ^{1}H dimensions, respectively, were employed with 8 scans and a

recycle delay of 1 s. All HSQC spectra were processed with NMRPipe (16) employing linear prediction in the ^{15}N dimension, and a resolution-enhancing 60° shifted sine-squared bell window function for both dimension. All ^{15}N-^{1}H HSQC cross-peaks were analyzed with Sparky using Gaussian line-fitting (17). Errors in the chemical shifts were calculated as standard deviations of the chemical shifts obtained for three replica spectra of the apo Domain 3. Errors in intensities were calculated from the Signal/Noise ratios. Compounded chemical shift differences between the Apo Domain 3 and Domain 3 in the presence of Aβ were defined as follows: $\Delta\delta_{N,H\ comp} = \sqrt{(\Delta^1 H)^2 + (\frac{\Delta^{15} N}{6.5})^2}$ (18).

NMR Spectroscopy – Triple Resonance Experiments for the Assignment of the HSA Domain 3. The ^{15}N-^{1}H HSCQ spectrum of Domain 3 was assigned using a combination of triple resonance Trosy based experiments: HNCO, HNCA, HNCACO, CBCA(CO)NH, HNCACB. The spectra were recorded on a 0.5 mM deuterated, ^{15}N, ^{13}C labeled domain 3 sample. For this purpose the protein was expressed using 1 L of M9 media in D_2O. To achieve complete deuteration $^{13}C_6$-1,2,3,4,5,6,6, -d_7 D-glucose was used. The protein sample was purified and refolded as previously published (7). Refolding was performed in H_2O based buffer, which ensured complete exchange of the backbone amide deuterium into NMR detectable protons. Tripe resonance experiments were acquired using 128 complex t1 increments of 1024 (t3), 100 (t2) data planes with 16 (HNCA, CBCA(CO)NH, HNCACB) or 8 (HNCO, HN(CO)CA) transients. Only non-overlapped cross-peaks were used in the chemical shift analysis. ^{15}N-NOESY-HSQC spectra were used to confirm the assignments and were acquired using a 0.5 mM ^{15}N labeled sample

with 32 scans and a 1024 (t3) x 100 (t2) x 96 (t1) point matrix. The assigned NMR chemical shifts were used as input for the program PECAN (19) in order to determine the secondary structure elements of domain 3 and to confirm proper protein folding.

ThT Fluorescence. ThT fluorescence spectra were recorded using a Tecan Safire fluorescence spectrometer and 96 well plates with 80 μL sample volumes and 50 (14, 20). The concentration of Aβ (1-40) in all samples was 10 μM, while the concentration of inhibitory and control peptides, *i.e.* HSA (495-526) and HSA (530-550), respectively, and HSA was set to 50 μM. Measurements were performed in 20 mM sodium phosphate buffer, pH 7.4, 0.05% NaN_3. As a control, individual ThT fluorescence spectra were collected for HSA and HSA peptides samples. These values were subtracted from the values obtained from the HSA:Aβ or the HSA peptides:Aβ mixtures. For each sample at least three measurements were performed and averaged values are reported. The error was calculated as the standard deviation of all measurements.

Bioinformatics analysis. The Waltz algorithm (http://waltz.switchlab.org/) was used to predict domain 3 regions prone to amyloid formation (21). For the Waltz profile the output with high sensitivity and pH 7 were chosen. The Waltz score was plotted against the residue number to show the residue-specific propensity of amyloid formation.

RESULTS

Comparison of Aβ and Fatty Acid Binding Modes: Effects of the R410A/Y411A, R485A/S489A and K525A Mutations. We have previously shown that the HSA binding site distribution of Aβ oligomers and of fatty acids (FAs) are similar (*i.e.* binding sites for both Aβ and FA are located in all three albumin domains) (7). Based on this observation, we have hypothesized that Aβ and FA might share common binding determinants. In order to test this hypothesis we have investigated the interaction between Aβ and HSA mutants that abrogate FA binding. For instance, the R410A/Y411A double mutation completely prevents fatty acid binding within the 3A sub-domain of HSA (Figure 2(b)), while K525A abolishes FA binding within the 3B sub-domain (Figure 2(f)) (11). Moreover, as indicated in Figure 2(d), both S489 and R485 further contribute to the FA stabilization within 3A sub-domain. Therefore we have engineered these three sets of mutants (*i.e.* R410A/Y411A, R485A/S489A and K525A) in a construct of domain 3 and tested their interactions with Aβ oligomers. The domain 3 construct (381-585) is significantly representative of HSA because the three albumin domains bind the Aβ oligomers with similar affinities and to a large extent independently of each other, suggesting that any single domain provides a useful model system to investigate the Aβ interactions in further detail. In addition, domain 3 is highly soluble and properly folded in isolation as indicated by the high degree of overlap between the secondary structure elements predicted based on the NMR chemical shifts (19) and those identified based on the albumin crystal structure (22) (Figure S1). Moreover, domain 3 contains binding sites for exogenous and other endogenous ligands, including fatty acids (FAs) (Figure 1).

Therefore, Domain 3 is ideally suited to test whether the Aβ oligomers and FAs interact with albumin at common interaction sites.

The Aβ oligomers are efficiently trapped by the Aβ (12-28) construct, which spans the central hydrophobic core of the Aβ peptide and key residues involved in HSA binding (7, 13, 14). Furthermore, the binding of Aβ (12-28) oligomers to albumin can be monitored by STD NMR experiments, resulting in albumin inhibition isotherms from which effective but quantitative K_D values for the Aβ oligomer: HSA complexes are obtained based on Scatchard-like models (7). Therefore, we have investigated the binding of Aβ (12-28) to the R10A/Y411A, R485A/S489A and K525A domain 3 mutants using STD monitored titrations, as shown in Figure 2. The STD-monitored titration data (Figure 2 (a), (c) and (e)) displays a typical dose-response pattern in which the I_{STD}/I_{STR} ratios decrease progressively as the protein concentration increases, until a saturation plateau point is reached. These observations indicate that all three domain 3 mutants are active inhibitors of Aβ (12-28) self-association. Furthermore, no significant differences are observed when the titration profile of each mutant is compared to the corresponding profile of the WT domain 3 using an identical Aβ (12-28) stock solution (Figure 2(a, c, e), red dots). These results point to the presence of marked differences between the binding determinants for fatty acids and those for the Aβ oligomers formed by Aβ (12-28). In order to confirm the validity of this conclusion for longer and more physiologically relevant Aβ peptides, we also tested the interactions between the three domain 3 mutants and Aβ (1-42).

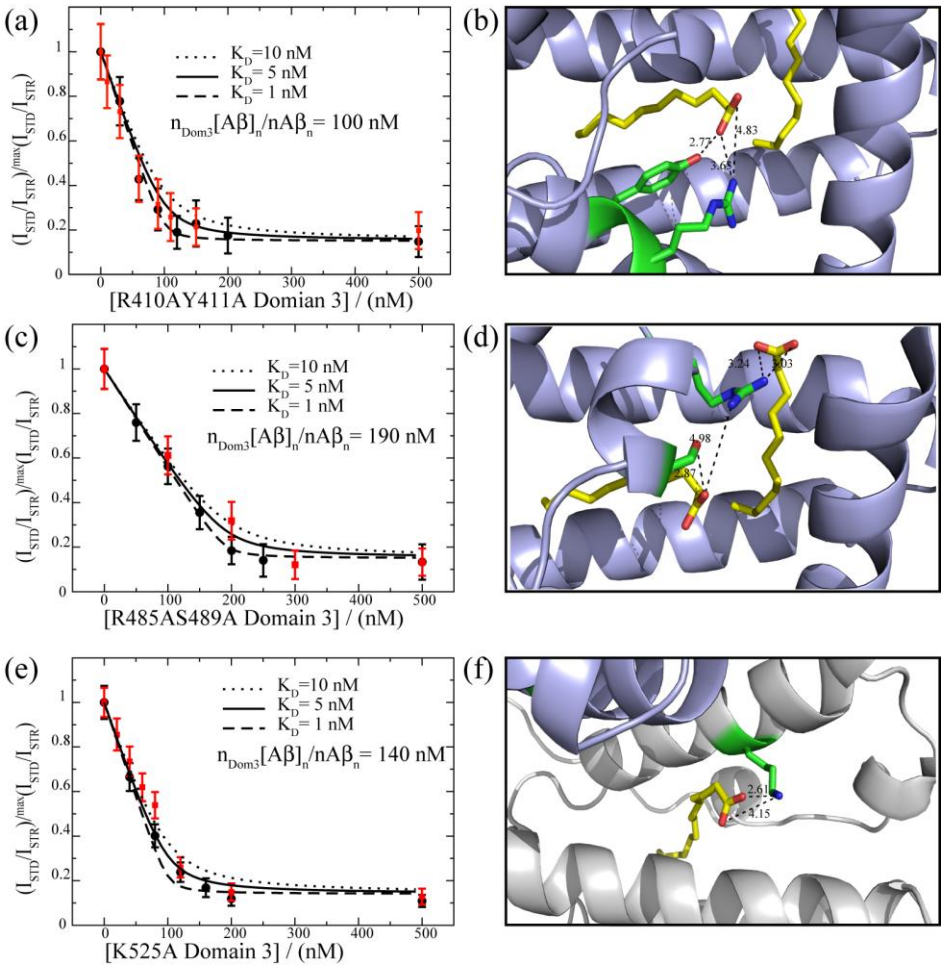

Figure 2. Effect of domain 3 mutants on the relative I_{STD}/I_{STR} ratios measured for filtered 1 mM Aβ (12-28) peptide aggregated through the addition of 40 mM NaCl. All ratios were normalized to their maximum value measured before protein addition. In panels (a), (c) and (e), dashed, full lines and dotted correspond to dose-response curves back-calculated using a Scatchard-like model and K_D values of 1, 5 and 10 nM, respectively. For reference purposes, the titration profile of wild-type domain 3 is shown in each panel in red color. In panels (b), (d) and (f), the side chains of the mutated residues interacting with fatty acids are shown in green and the fatty acids in yellow (12). Hydrogen bonds to the palmitate molecule are indicated by dashed lines and lengths are reported in Å.

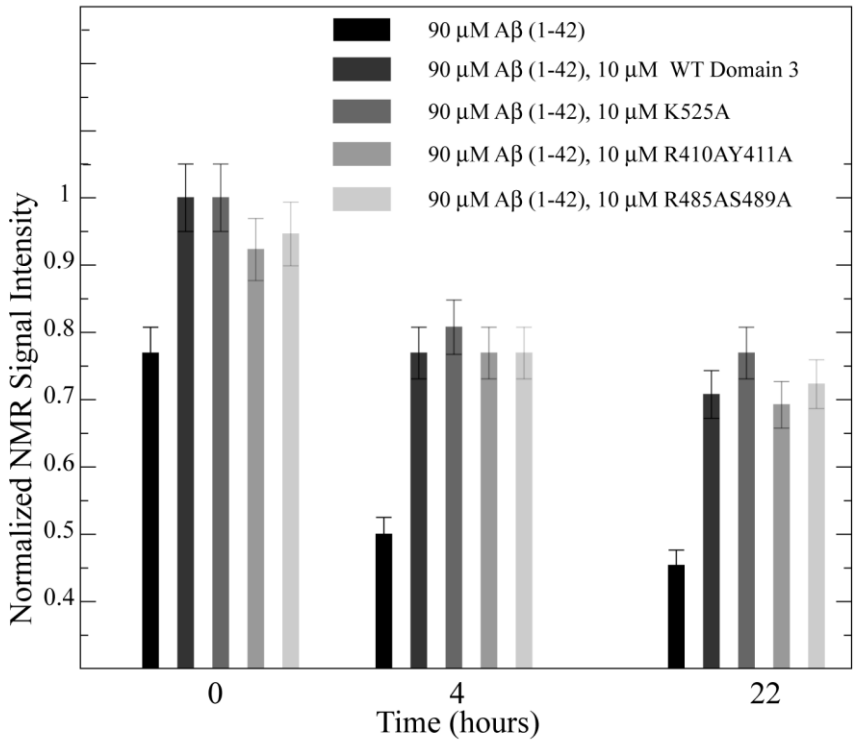

Figure 3. Interaction of domain 3 and its point mutants with Aβ (1-42) probed by 1D-NMR. Experiments were acquired at the 700 MHz at 310 K in 20 mM potassium phosphate, pH 7.4, 10% D_2O, 0.05% NaN_3. A 50 ms long spin lock was used to suppress residual protein signal. All spectra were processed using an exponential multiplication window function with a line broadening coefficient of 3 Hz. Color coding is as per the legend in the figure.

The experiments on the physiologically relevant Aβ (1-42) peptide at physiological pH (Figure 3) confirmed the differences between the Aβ and FA binding modes already emerged from Figure 2. Specifically, Figure 3 indicates that the incubation of Aβ (1-42) at 37 ^oC results in peptide aggregation and consequent significant losses of the Aβ NMR signal over time. These signal losses are significantly reduced in the presence of WT domain 3. A similar reduction in aggregation is observed for all

domain 3 constructs, suggesting that the mutations did not significantly perturb binding of the Aβ oligomers to domain 3, although they had a marked effect on FA binding. We conclude that the mutated residues (*i.e.* R410, Y411, S489, R485 and K525), although donors of hydrogen-bonds to albumin-bound FAs, are not part of the domain 3 determinants for Aβ binding. This result opens then the question as to whether Aβ binds both domain 3 sub-domains, as FAs, or it is selective for a single sub-domain. In order, to address this second question, we have sub-cloned, expressed and purified separate sub-domains 3A and 3B and tested their interactions with both Aβ peptides, Aβ (12-28) and Aβ (1-42).

Both A and B Sub-Domains in Domain 3 are Involved in the Inhibition of Aβ Self-Association. As depicted in Figure 4, the clear dose-response pattern of the STD monitored Scatchard-like curves observed for the 3A and 3B constructs indicate that both 3A and 3B sub-domains span Aβ binding sites. Moreover, since identical Aβ stock solution were utilized for all experiments in Figure 4, the STD profiles in panels (a-c) are directly comparable and demonstrate that in the case of the sub-domains the protein concentration necessary to reach the initial STD saturation point is twice that required for the integral domain 3. This observation further confirms that in domain 3 both 3A and 3B sub-domains are involved in the Aβ oligomer binding and suggests that the 3A:$A\beta_n$ and 3B:$A\beta_n$ interactions are to large extent independent of each other.

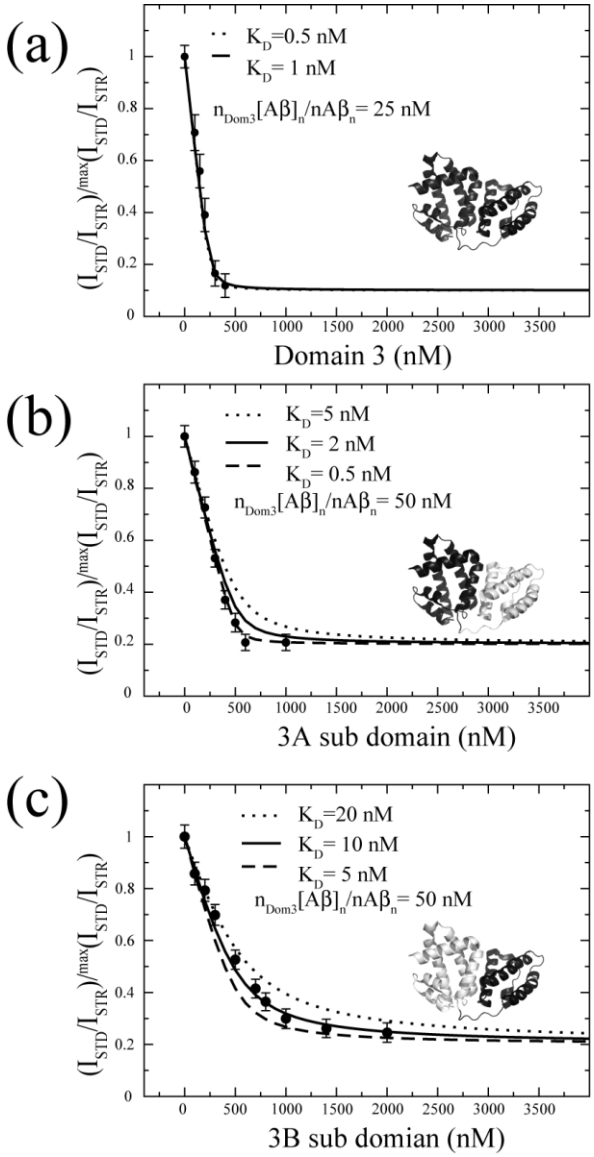

Figure 4. Dose-response STD-based profiles for the inhibition of the Aβ (12-28) self-association by domain 3 and its sub-domain deletion mutants. Panels (a)-(c) illustrate the effect of domain 3 and its deletion mutants (*i.e.* sub-domain 3A, sub-domain 3B), respectively, on the relative I_{STD}/I_{STR} ratios measured for a filtered 1 mM Aβ (12-28) peptide sample aggregated through addition of 40 mM of NaCl. In panels (a)-(c), dashed and full lines correspond to back-calculated dose-response curves using a Scatchard-like model. In each panel structure of domain 3 is shown (PDB: 1A06) and the sub-domains used in the titration are shown in the black.

It should also be noted that, based on Figure 4, the affinity of the 3A sub-domain for the Aβ oligomers is slightly higher than that of sub-domain 3B. However this difference could also be due to different degrees of unfolding experienced by these two protein constructs upon isolation into individual sub-domains. Furthermore, a similar sub-domain partitioning of binding sites was obtained for the Aβ (1-42) as indicated in Figure 5.

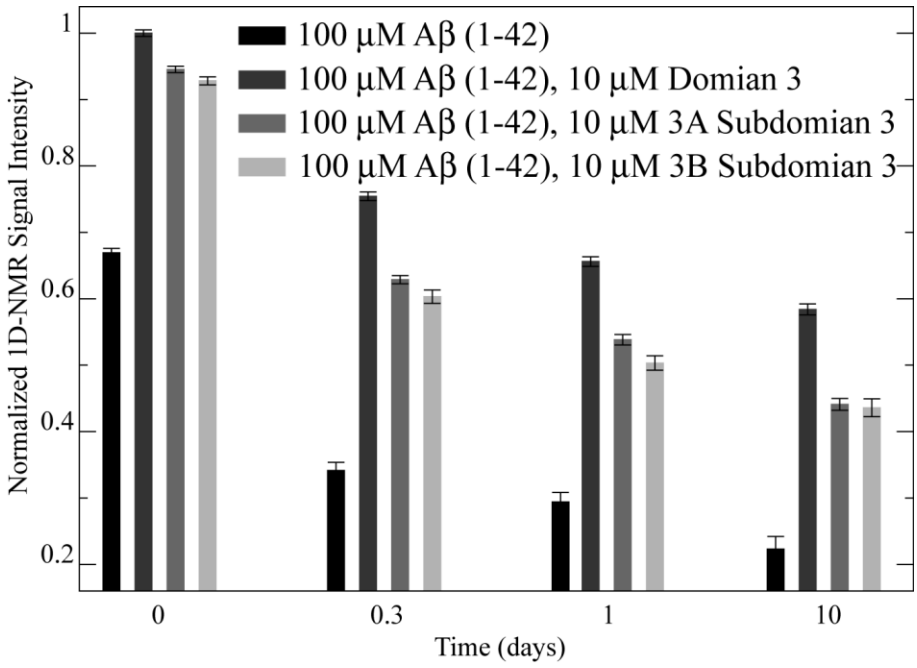

Figure 5. Interaction of domain 3 and its sub-domain deletion mutants with Aβ (1-42) probed by 1D-NMR. 0.1 mM Aβ (1-42) samples were incubated with 10 μM of domain 3 constructs. Changes in the methyl region of 1D-WG spectra with time are reported. All intensities were normalized to the 0.1 mM Aβ (1-42) sample in the presence of the 10 μM of domain 3 acquired for the first incubation time point. Spectra were processed as stated in Figure 3 captions.

As shown in Figure 5, domain 3 showed higher inhibition potency than the individual sub-domains corroborating that both sub-domains, A and B, in domain 3 are involved in the Aβ oligomer binding. Given that each sub-domain interacts with $A\beta_n$, the next open question we focused on pertains to the specific $A\beta_n$ contact sites with each HSA sub-domain.

Towards Defining the HSA Domain 3:Aβ_n Interaction Determinants at Residue Resolution. To further understand the Aβ binding determinants of albumin, we decided to map the domain 3:$A\beta_n$ interactions by the NMR chemical shifts changes observed in the ^{15}N-^{1}H HSQC spectrum of domain 3 in the presence of unlabeled Aβ peptide. For this purpose we assigned first the HSQC spectrum of apo domain 3 using standard TROSY triple-resonance methods. Once the assignment is obtained, the chemical shift mapping by HSQC spectra is in principle a simple comparative experiment. However, several experimental challenges have to be addressed before reliable interaction data are obtained for the domain 3:$A\beta_n$.

First, it is essential to consider that, although all Aβ samples utilized were obtained with > 95% purity, the Aβ batches contained residual trifluoroacetic acid (TFA), which is routinely used in the final stage of peptide purification. This poses a problem since we have observed that TFA specifically binds to sub-domain 3A (Figure S4). Moreover TFA was estimated to be in ~6x molar excess relative to the Aβ peptide (Figure

S2). This means that, although the affinity of domain 3 for TFA is much lower than that for Aβ oligomers (*i.e.* ~mM vs. nM), the effective Aβ oligomers/domain 3 stoichiometric ratio is significantly lower than the TFA/domain 3 stoichiometric ratio and therefore the domain 3 chemical shifts induced by Aβ binding can easily be masked by the chemical shift changes induced by TFA (Figure S2). Therefore TFA removal from the Aβ samples prior to the addition of the domain 3 is necessary. TFA was removed using at least three lyophilization steps in the presence of 50-100 mM HCl (15) and ^{19}F NMR was used as control to verify that the concentration of TFA in all samples was significantly lower than the 0.1 mM (Figure S2).

A second critical challenge in mapping the domain 3:Aβ interactions arise from the selective recognition by domain 3 of Aβ oligomers as opposed to Aβ monomers. The domain 3 selectivity for Aβ oligomers *vs.* monomers makes the detection of Aβ: domain 3 complexes by NMR challenging for two main reasons. First, only a minor population of the Aβ oligomers competent to bind albumin falls within the typical low MW detection window of solution NMR, as illustrated in Figure 6. Second, domain 3 binds only to selected oligomers loci (*i.e.* growing sites) (7, 13, 14) thus further decreasing the effective concentration of $A\beta_n$ sites in solution available to bind domain 3 to levels that are significantly lower than the total peptide concentration (Figure 6). This effect explains why the average HSQC intensity loss is only ~20 % (Figure 7(b)), although the ratio between the concentrations of the ^{15}N-labeled domain 3 and the unlabeled Aβ (1-40) is 1:4.

A third challenge posed by the domain 3:Aβ interactions is in sensitivity of the HSQC spectra of albumin to minimal variation in experimental conditions, a complete control of buffer conditions is necessary.

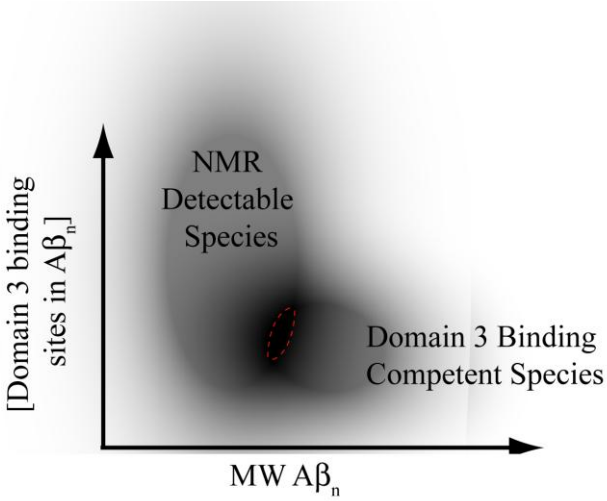

Figure 6. Narrow overlap between the NMR detection window and the albumin/Domain 3 binding competent window is indicated by dashed red lines.

For this purpose, we have devised the sample preparation protocol depicted in Figure S3 which described in detail in the Material and Method section. The main feature of this protocol is that a control domain 3 sample was prepared by diluting the stock domain 3 solution in the Aβ filtrate (sample IV, Figure S3)). This means that differences in the ^{15}N-^{1}H HSQC spectra of domain 3 in the absence and presence of Aβ arise mainly from the binding of Aβ oligomers. This protocol not only insures optimal control over the buffer conditions, but it also prevents the complete Aβ peptide precipitation and formation of large MW, and thus NMR undetectable, Aβ assemblies by adding domain 3 immediately after the Aβ peptide dissolution.

Using the protocol of Figure S3 we measured the combined ^{15}N-^{1}H chemical shifts changes of domain 3 caused by Aβ (1-40) (Figure 7 (a)). Consistent with the results of our sub-domain dissection study (Figure 4 and Figure 5), the ppm variations reported in Figure 7(a) are located in both 3A and 3B subdomain (Figure 7(e)). Specifically, minor changes are observed in helices 1, 2 as well as in helix 6 of the 3A sub-domain (Figure 7 (a)) and more significant and localized chemical shift changes are detected in helix 7 and in the hydrophobic loop of the 3B sub-domain (Figure 7 (a)). However, chemical shift changes have to be interpreted with caution since they might arise not only from direct contacts with the Aβ oligomers, but also from Aβ induced conformational changes. In this respect, it should be considered that albumin inhibits Aβ self-association by targeting the same sites within the Aβ oligomers where Aβ monomers bind. We therefore expect that HSA segments involved in direct contacts with the Aβ assemblies should closely mimic the Aβ peptide to ensure optimal complementarity with the available interface at the $A\beta_n$ growing locus. Based on this notion, we aligned the sequences of the HSA sub-domain 3B and 3A sub-domains with the sequence of the Aβ (12-28), which includes key albumin binding residues (Figure 7(d)).

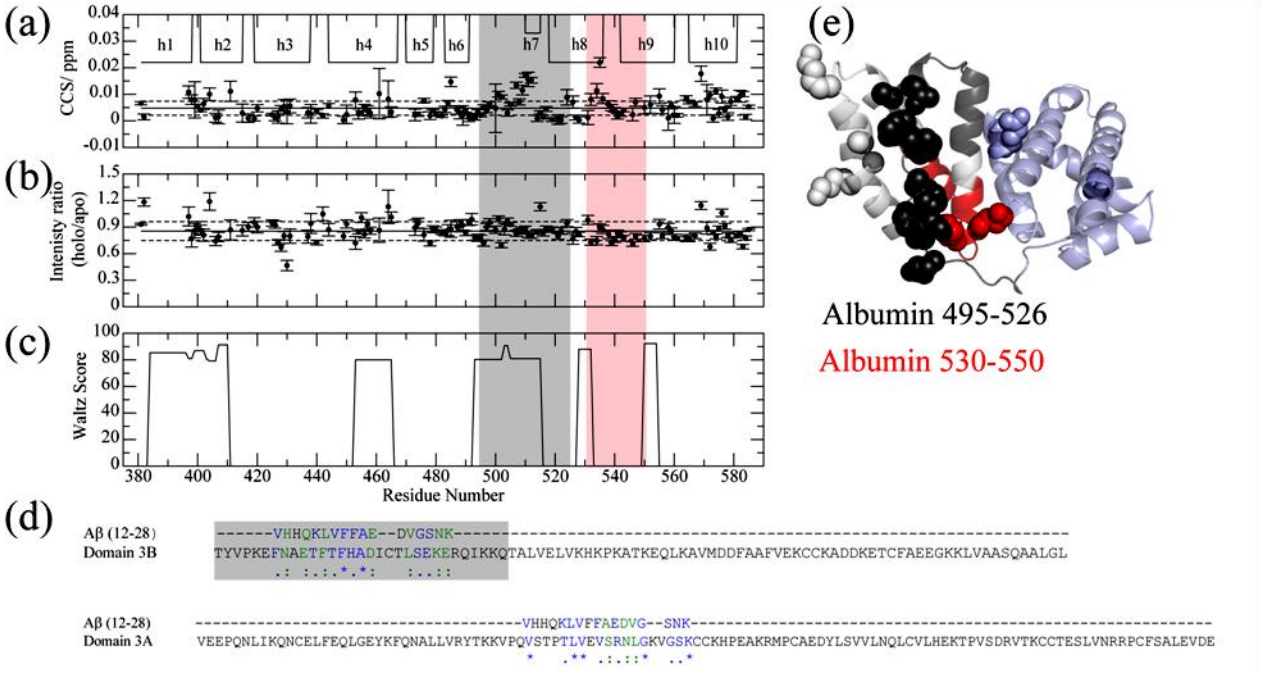

Figure 7. (a) ^{1}H-^{15}N compound chemical shifts of 0.1 mM domain 3 caused by 0.4 Aβ (1-40). The horizontal lines correspond to the 10% trimmed mean compound chemical shift and ±1 standard deviations. The secondary structure according to the apo albumin crystal structure (PBD ID: 1AO6) (22) is shown with solid lines. In this structure helix 7 is a 3^{10} helix. Sub-domain 3A spans residues 381-495, while sub-domain 3B spans residues 496-585. Panel (b) depicts the effect of the Aβ (1-40) peptide on the intensities of the protein HSQC spectrum. Panel (c) depicts the amyloid forming regions as predicted by the Waltz algorithm (21) based on the domain 3 sequence. Panel (d) reports Clustaw sequence alignment of 3A and 3B sub-domains and Aβ (12-28). The domain 3 region used to design Aβ self-association inhibitory peptide is highlighted in gray. Residues of no consensus are indicated as black dash, single, fully conserved residues are indicated in blue star, while strong and weak conserved residues are indicated as green semicolon and blue dot respectively. Panel (e) depicts domain 3 structure. Residues experiencing chemical shift changes are shown as spheres. Inhibitory peptide sequences 495-526 and control peptide sequence 530-550 are highlighted in the black and red color, respectively.

The V418-K436 protein region of the 3A sub-domain shows the highest complementarity with the CHC spanned by the Aβ (12-28) peptide. While in the presence of Aβ we could not assign all residues the residues in the V418-K436 HSA region, we did observe significant losses of signal intensity for R428 and L430 suggesting this protein region might be involved in Aβ binding. However the sequence alignment of 3B sub-domain and Aβ (12-28) identifies the HSA residues 502-522, which match well also with a major cluster of significant chemical shift variations (Figure 7(a), grey region). These results consistently point to the 502-522 loop region as a putative site for direct contacts between albumin and the Aβ oligomers. In order to confirm this result, we tested as an inhibitor of Aβ self-association a synthetic peptide that spans the 502-522 segment as well additional flanking residues to minimize truncation end-effects and to enhance the solubility (*i.e.* peptide 'Albumin 495-526'). As a control, we also checked a peptide mimicking the HSA residues 530-550, a region which does not align with the Aβ sequence (*i.e.* peptide 'Albumin 530-550').

The Albumin 495-526 Peptide Inhibits Aβ Self-Association. To further confirm that region spanning residues 502-522 of HSA is directly involved in Aβ oligomer binding we tested the peptide spanning albumin residues 495-526 for the inhibition of Aβ (12-28) and Aβ (1-40) self-association. As indicated in Figure 8(a), the selected peptide resulted in an STD dose-response profile with a clear plateau region, indicating that the albumin 495-526 construct is effective in inhibiting the self-association of Aβ (12-28) through specific interactions, although with a binding affinity for the Aβ (12-28)

assemblies reduced by ~two order of magnitudes relative to the integral domain 3 (Figure 4(a)). Moreover the control peptide spanning albumin residues 530-550 did not inhibit Aβ self-association (Figure 8(a), red dots). These results suggest that the chemical shift changes observed in the 530-550 region (Figure 7(a)) are due to the close spatial proximity to the residues located in the 502-522 region, which interacts directly with the Aβ assemblies, as illustrated in Figure 7(e).

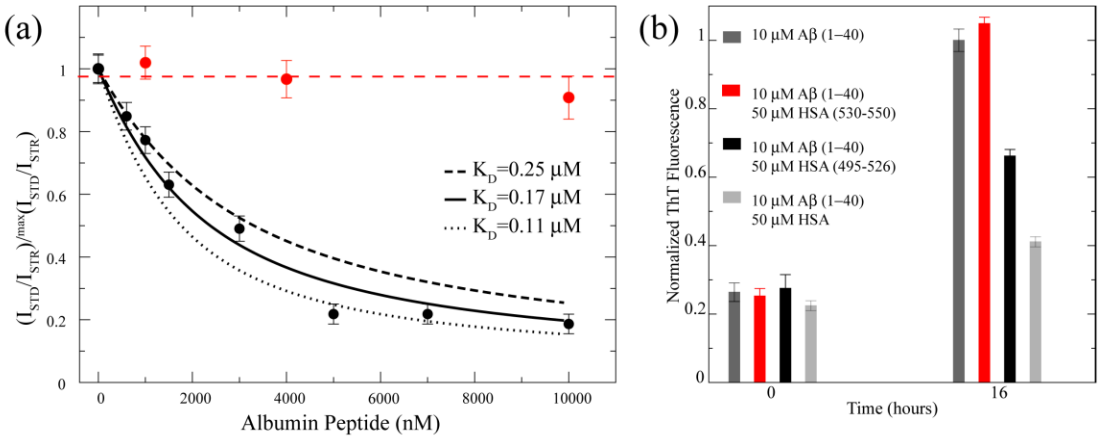

Figure 8. Panel (a) reports the dose-response STD-based profiles for the inhibition of the Aβ (12-28) self-association by the domain 3-derived peptides, *i.e.* albumin 495-526 and 530-550. The latter peptide serves as a negative control. Panel (b) reports the inhibition of Aβ(1-42) aggregation by the albumin 495-526 (black bars) and albumin 530-550 (red bars) peptides, as monitored by ThT fluorescence. The effect of wild-type full length three-domain albumin is also shown for comparison purposes.

The effect of the albumin peptides on the Aβ (1-40) self-association was monitored by ThT fluorescence experiments, because 1D NMR experiments could not be used for this purpose due to the overlap between the Aβ spectra and the resonances of the albumin-derived peptides. As indicated in Figure 8(b), incubation of Aβ (1-40) with time

results in a significant ThT fluorescence increase due to the formation of cross–β sheet aggregates. Under our experimental conditions, after 16 hours Aβ (1-40) is completely aggregated and no further changes in fluorescence intensity are observed (data not shown). Similar results were obtained in the presence of the control albumin peptide spanning residues 530-550 (Figure 8(b)), indicating that it does not inhibit Aβ (1-40) aggregation and confirming the results obtained for Aβ (12-28) (Figure 8(a)). However, in the presence of albumin or of the albumin 495-526 peptide the ThT fluorescence at 16 hours increases by 20% and 50%, respectively, confirming that both, full length HSA and HSA 495-526, effectively block Aβ self-association into cross-β strand structured aggregates. Interestingly, the 495-526 region matches quite well with a segment of HSA prone to adopt a β-strand conformation and predicted to form amyloid structures (21) with high propensity (Figure 7(c)). We conclude therefore that regions prone to β-strand structures and amyloid formation might also serve as Aβ recognition sites.

DISCUSSION

The data presented here (Figure 4 and Figure 5) consistently support that both 3A and 3B sub-domains of albumin domain 3 are involved in the inhibition of Aβ self-recognition. Although this partitioning of the Aβ binding sites is reminiscent of the FA binding site distribution within domain 3 (Figure 1), significant differences in the binding determinants are observed between FAs and Aβ. For example, mutations involving the

polar amino acids located close to the protein hydrophobic cavities significantly affect the FA binding affinities, but had no detectable effect on Aβ binding (Figure 2 and Figure 3). This result is consistent with the notion that binding of Aβ to albumin is mainly determined by hydrophobic interactions, as opposed to FA binding affinities that are to a large extent dictated by hydrogen bonding to their carboxylate head groups (Figure 2(b, d, f)). This conclusion is in full agreement with the cluster of chemical shift changes and with the significant potency in the inhibition of Aβ self-association observed for the HSA (495-526) segment (Figure 8), which aligns well with the sequence of Aβ (12-28) spanning the Aβ central hydrophobic core (Figure 7(d)). Interestingly, the albumin 495-526 region corresponds to a loop of the 3B sub-domain that is predicted to be highly prone to adopt a β-strand structure and to form amyloids. Overall, we therefore propose that binding of the Aβ oligomers to albumin is reminiscent of Aβ self-association in two ways. First the Aβ: albumin association is driven by hydrophobic interactions. Second, partially folded segments and flexible loops prone to β-strands and self-association into amyloid deposits of the inhibitory protein are also putative regions for binding Aβ oligomers at their growing sites where Aβ monomers would others bind.

The notion that hydrophobic interactions are key determinants for the binding of Aβ oligomers is also supported by the observation that several other Aβ binding proteins besides albumin, such as sLRP(23), clusterin (24,25) and ApoE (26), are also involved in lipid binding. Additionally, it was recently shown that binding of Aβ to proteins not involved in lipid metabolism, such as ABAD and affibody $Z_{Aβ3}$, is mainly driven by a

favorable entropic change, consistent with hydrophobic effect driving the protein:Aβ interactions (27- 29). Furthermore, the solution structure of the complex between Aβ and the affibody $Z_{Aβ3}$ dimer shows a large hydrophobic cavity that is required for high Aβ affinity (27).

The notion that flexible loop regions are key sites for the recognition of Aβ oligomers is independently corroborated by the observation that the binding of Aβ by several other proteins is mediated by flexible protein segments. For example, in the alcohol dehydrogenase ABAD the Aβ binding sites span the flexible L_D loop regions. In addition, the structure of the affibody $Z_{Aβ3}$ bound to Aβ revealed a series of hydrogen bonds between the Aβ β-strands and a $Z_{Aβ3}$ β-strand spanning a region that forms a partially unstructured helix 1 in apo $Z_{Aβ3}$. Furthermore, in other fibrillization inhibitory systems, flexible Aβ interacting loops are either inherently present similarly to albumin and ABAD (*e.g.* the ATC and TC proteins (30)) or are similarly to $Z_{Aβ}$ generated through protein unfolding and/or structural changes (*e.g.* ApoE) (31- 35). The proposed Aβ binding determinants discovered here for albumin are likely to be relevant also for other Aβ fibril binding proteins. The methods and experimental approaches utilized for albumin are also expected to be transferable to other amyloid inhibitory systems.

REFERENCES:

1. Mawuenyega, K. G., W. Sigurdson, V. Ovod, L. Munsell, T. Kasten, J.C. Morris, K.E. Yarasheski and R.J. Bateman 2010. Decreased clearance of CNS beta-amyloid in alzheimer's disease. Science. 330, 1774-1774.

2. Zlokovic, B. V. 2004. Clearing amyloid through the blood-brain barrier. J. Neurochem. 89, 807-811.

3. DeMattos, R. B., K.R. Bales, D. J. Cummins, J.-C. Dodart, S. M.Paul and D. M. Holtzman 2001. Peripheral anti-Aβ antibody alters CNS and plasma Aβ clearance and decreases brain Aβ burden in a mouse model of Alzheimer's disease. Proc. Natl. Acad. Sci. U. S. A. 98:8850–8855.

4. Biere, A. L., B. Ostaszewski, E.R. Stimson, B.T. Hyman, J.E. Maggio and D.J. Selkoe 1996. Amyloid beta-peptide is transported on lipoproteins and albumin in human plasma. J. Biol. Chem. 271, 32916-32922.

5. Llewellyn, D. J., K.M. Langa, R.P. Friedland and I.A. Lang 2010. Serum albumin concentration and cognitive impairment. Current Alzheimer Research. 7, 91-96.

6. Boada, M., P. Ortiz, F. Anaya, I. Hernandez, J. Munoz, L. Nunez, J. Olazaran, I. Roca, G. Cuberas, L. Tarraga, M. Buendia, R.P. Pla, I. Ferrer and A. Paez 2009. AMYLOID-TARGETED THERAPEUTICS IN ALZHEIMER'S DISEASE: USE OF HUMAN ALBUMIN IN PLASMA EXCHANGE AS A NOVEL APPROACH FOR A beta MOBILIZATION. Drug News & Perspectives. 22, 325-339.

7. Milojevic, J. and G. Melacini 2011. Stoichiometry and affinity of the human serum albumin-alzheimer's A beta peptide interactions. Biophys. J. 100, 183-192.

8. Mao, H. Y., A.H. Gunasekera and S.W. Fesik 2000. Expression, refolding, and isotopic labeling of human serum albumin domains for NMR spectroscopy. Protein Expr. Purif. 20, 492-499.

9. Petitpas, I., T. Grune, A.A. Bhattacharya and S. Curry 2001. Crystal structures of human serum albumin complexed with monounsaturated and polyunsaturated fatty acids. J. Mol. Biol. 314, 955-960.

10. Curry, S., H. Mandelkow, P. Brick and N. Franks 1998. Crystal structure of human serum albumin complexed with fatty acid reveals an asymmetric distribution of binding sites. Nat. Struct. Biol. 5, 827-835.

11. Simard, J. R., P.A. Zunszain, C.E. Ha, J.S. Yang, N.V. Bhagavan, I. Petitpas, S. Curry and J.A. Hamilton 2005. Locating high-affinity fatty acid-binding sites on albumin by x-ray crystallography and NMR spectroscopy. Proc. Natl. Acad. Sci. U. S. A. 102, 17958-17963.

12. Bhattacharya, A. A., T. Grune and S. Curry 2000. Crystallographic analysis reveals common modes of binding of medium and long-chain fatty acids to human serum albumin. J. Mol. Biol. 303, 721-732.

13. Milojevic, J., V. Esposito, R. Das and G. Melacini 2007. Understanding the molecular basis for the inhibition of the alzheimer's A beta-peptide oligomerization by human serum albumin using saturation transfer difference and off-resonance relaxation NMR spectroscopy. J. Am. Chem. Soc. 129, 4282-4290.

14. Milojevic, J., A. Raditsis and G. Melacini 2009. Human serum albumin inhibits A beta fibrillization through a "monomer-competitor" mechanism. Biophys. J. 97, 2585-2594.

15. Andrushchenko, V. V., H.J. Vogel and E.J. Prenner 2007. Optimization of the hydrochloric acid concentration used for trifluoroacetate removal from synthetic peptides. Journal of Peptide Science. 13, 37-43.

16. Delaglio, F., S. Grzesiek, G.W. Vuister, G. Zhu, J. Pfeifer and A. Bax 1995. Nmrpipe - a multidimensional spectral processing system based on unix pipes. J. Biomol. NMR. 6, 277-293.

17. Goddard, T. D., D.G. Kneller 2006. SPARKY—NMR Assignment and Integration Software, Univ of California, San Francisco.

18. Mulder, F. A. A., D. Schipper, R. Bott and R. Boelens 1999. Altered flexibility in the substrate-binding site of related native and engineered high-alkaline bacillus subtilisins. J. Mol. Biol. 292, 111-123.

19. Eghbalnia, H. R., L.Y. Wang, A. Bahrami, A. Assadi and J.L. Markley 2005. Protein energetic conformational analysis from NMR chemical shifts (PECAN) and its use in determining secondary structural elements. J. Biomol. NMR. 32, 71-81.

20. Benseny-Cases,N., M. Cocera, J. Cladera. 2007. Conversion of non-fibrillar beta-sheet oligomers into amyloid fibrils in Alzheimer's disease amyloid peptide aggregation. Biochemical and Biophysical Research Communications. 361: 916–921

21. Maurer-Stroh, S., M. Debulpaep, N. Kuemmerer, M.L. de la Paz, I.C. Martins, J. Reumers, K.L. Morris, A. Copland, L. Serpell, L. Serrano, J.W.H. Schymkowitz and

F. Rousseau 2010. Exploring the sequence determinants of amyloid structure using position-specific scoring matrices. Nature Methods. 7, 237-U109.

22. Sugio, S., A. Kashima, S. Mochizuki, M. Noda and K. Kobayashi 1999. Crystal structure of human serum albumin at 2.5 angstrom resolution. Protein Eng. 12, 439-446.

23. Sagare, A., R. Deane, R.D. Bell, B. Johnson, K. Hamm, R. Pendu, A. Marky, P.J. Lenting, Z. Wu, T. Zarcone, A. Goate, K. Mayo, D. Perlmutter, M. Coma, Z. Zhong and B.V. Zlokovic 2007. Clearance of amyloid-beta by circulating lipoprotein receptors. Nat. Med. 13, 1029-1031.

24. Matsubara, E., B. Frangione and J. Ghiso 1995. Characterization of apolipoprotein J-alzheimers A-beta interaction. J. Biol. Chem. 270, 7563-7567.

25. Calero, M., A. Rostagno, E. Matsubara, B. Zlokovic, B. Frangione and J. Ghiso 2000. Apolipoprotein J (clusterin) and alzheimer's disease. Microsc. Res. Tech. 50, 305-315.

26. Petrlova, J., H. Hong, D.A. Bricarello, G. Harishchandra, G.A. Lorigan, L. Jin and J.C. Voss 2011. A differential association of apolipoprotein E isoforms with the amyloid-beta oligomer in solution. Proteins-Structure Function and Bioinformatics. 79, 402-416.

27. Lustbader, J. W., M. Cirilli, C. Lin, H.W. Xu, K. Takuma, N. Wang, C. Caspersen, X. Chen, S. Pollak, M. Chaney, F. Trinchese, S.M. Liu, F. Gunn-Moore, L.F. Lue, D.G. Walker, P. Kuppusamy, Z.L. Zewier, O. Arancio, D. Stern, S.S.D. Yan and H. Wu 2004. ABAD directly links A beta to mitochondrial toxicity in alzheimer's disease. Science. 304, 448-452.

28. Hoyer, W., C. Gronwall, A. Jonsson, S. Stahl and T. Hard 2008. Stabilization of a beta-hairpin in monomeric alzheimer's amyloid-beta peptide inhibits amyloid formation. Proc. Natl. Acad. Sci. U. S. A. 105, 5099-5104.

29. Hoyer, W. and T. Hard 2008. Interaction of alzheimer's A beta peptide with an engineered binding protein - thermodynamics and kinetics of coupled folding-binding. J. Mol. Biol. 378, 398-411.

30. Elliott, P. R., D.A. Lomas, R.W. Carrell and J.P. Abrahams 1996. Inhibitory conformation of the reactive loop of alpha(1)-antitrypsin. Nat. Struct. Biol. 3, 676-681.

31. Hatters, D. M., N. Zhong, E. Rutenber and K.H. Weisgraber 2006. Amino-terminal domain stability mediates apolipoprotein E aggregation into neurotoxic fibrils. J. Mol. Biol. 361, 932-944.

32. Luo, J., J. Marechal, S. Warmlander, A. Graslund and A. Peralvarez-Marin 2010. In silico analysis of the apolipoprotein E and the amyloid beta peptide interaction: Misfolding induced by frustration of the salt bridge network. Plos Computational Biology. 6, 1-7.

33. Taboada, P., S. Barbosa, E. Castro and V. Mosquera 2006. Amyloid fibril formation and other aggregate species formed by human serum albumin association. J Phys Chem B. 110, 20733-20736.

34. Mettenburg, J. M. and S.L. Gonias 2005. Beta-amyloid peptide binds equivalently to binary and ternary alpha(2)-macroglobulin-protease complexes. Protein Journal. 24, 89-93.

35. Mettenburg, J. M., D.J. Webb and S.L. Gonias 2002. Distinct binding sites in the structure of alpha(2)-macroglobulin mediate the interaction with beta-amyloid peptide and growth factors. J. Biol. Chem. 277, 13338-13345.

SUPPORTING INFORMATION:

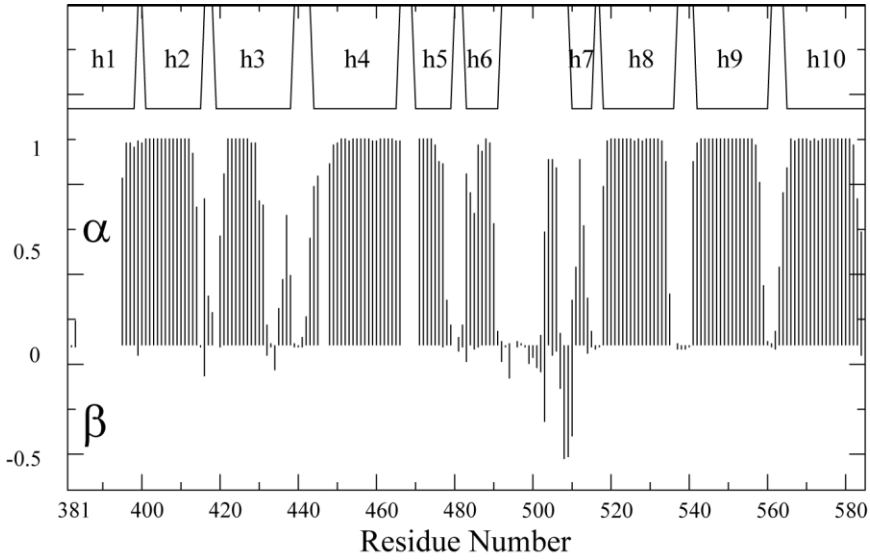

Figure S1. The NMR derived structure probabilitie obtained by PECAN analysis using Hα, Cα, Cβ and C0 chemical shifts (19). The probability of α-helical (positive values) and β-strands (negative values) are plotted per residue. Secondary structure based on the albumin crystal structure (pdb: 1AO6) (22) are depicted and labeled. The overall good correlation between the two structures is obtained.

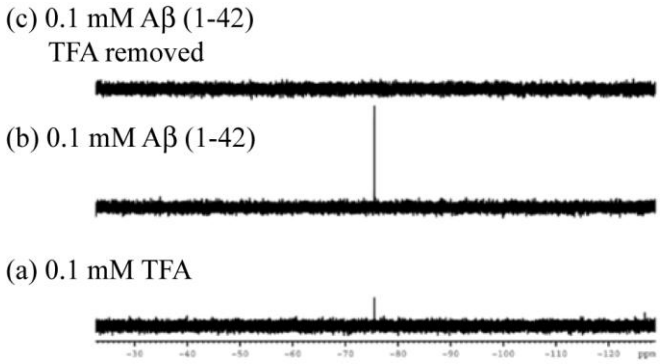

Figure S2. ^{19}F spectra were used to estimate TFA concentration in the samples. Panel (a) reports spectra of TFA at 0.1 mM concentraiton. Panel (b) reports spectum of the 0.1 mM Aβ (1-42) prior TFA removal. Panel (c) depicts ^{19}F spectrum of Aβ (1-42) followed by TFA removal protocol and indicates complete removal of TFA upon HCl treatment. Spectra in all panels were acquired and processed using identical parameters and intensities are directly comparable.

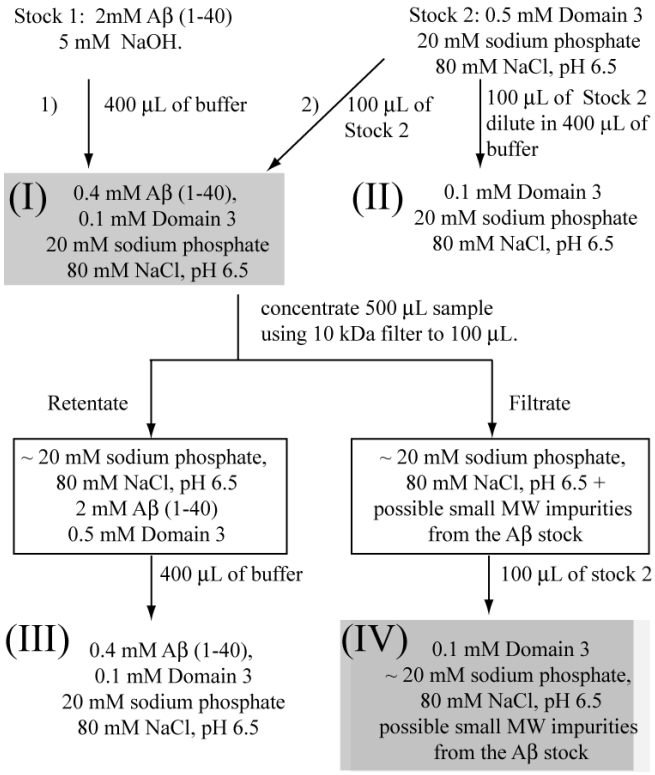

Figure S3. **S**ample preparation protocol. The ^{15}N-^{1}H HSQC spectra of the domain 3 samples (I) and (IV) (highlighted in gray) are compared to identify Aβ oligomer binding sites in domain 3 as explained in material and method section.

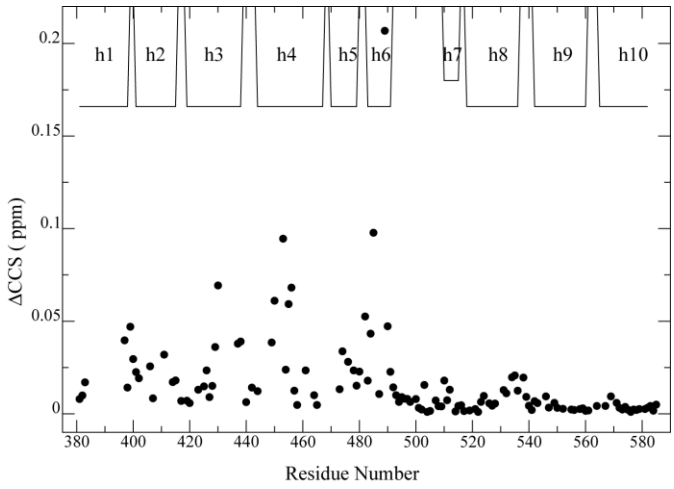

Figure S4. ^{1}H-^{15}N compound chemical shifts of 0.1 mM domain 3 caused by 1 mM TFA. Chemical shift changes mainly cluster in sub-domain 3A, with highest chemical shift observed for S489 in helix 6.

CONCLUDING REMARKS AND OUTLOOK ON FUTURE DEVELOPMENTS

CHAPTER 7

CONCLUDING REMARKS AND OUTLOOK ON FUTURE DEVELOPMENTS

A summary of this thesis has already been included in Chapter 1. This chapter will therefore focus on the questions that still remain open and on possible future developments of the HSA/Aβ project based on research leads that were generated during the course of this thesis. These can be partitioned in two major groups. The first group of leads pertains to additional approaches to refine our understating of the HSA/Aβ interactions. The second group focuses on how to capitalize on the work carried out on the HSA/Aβ complexes to start exploring other systems that involve amyloid inhibitory proteins different from albumin or amyloidogenic peptides different from Aβ. The first group includes three sections, *i.e.* approaches towards the definition of the albumin binding determinants in Aβ, refinement of the Aβ binding determinants in albumin through competition binding experiments with FAs, correlations between HSA dynamics and Aβ binding. The second set of leads focuses on two main topics, *i.e.* identification of Aβ interacting sequences in proteins that inhibit Aβ amyloid formation and the effect of albumin on amyloidogenic peptides different from Aβ. These sections are discussed in greater detail in the remaining part of this Chapter.

7.1. Towards the Definition of the Albumin Binding Determinants in Aβ.

Our work mainly focused so far on identifying the key Aβ binding determinants within HSA, however the albumin binding determinants in Aβ are still poorly understood.

Therefore our next goal is to identify key residues within Aβ involved in the albumin binding and also to understand the source of the specificity we observed in albumin preferential binding to Aβ oligomers as opposed to Aβ monomers. Albumin inhibits self-association of Aβ (1-42), Aβ (1-40) and Aβ (12-28) peptides. As the central hydrophobic core (CHC) is a common feature of these peptides and albumin is known to bind hydrophobic ligands, we have hypothesized that the CHC region might be an albumin recognition site. To test this hypothesis and to quantitatively estimate the effect of each Aβ amino acid on domain 3 binding we have used the structural descriptors (*i.e.* weighting coefficients) of the chemometric methodology developed by Hajduk *et. al*. to predict binding the HSA domain 3 potential of chemical moieties (1). As indicated in Figure 1 (a), the CHC residues (i.e. Phe19 and Phe20) and the negatively charged C-terminus, are key Aβ regions that promote interaction with Domain 3. Therefore we propose that small peptide containing mainly the CHC (i.e. K_{16}-F_{20}) would bind albumin in the monomeric form. To test this initial hypothesis we have investigated binding of the $K_{16}LVVFF_{20}$ peptide to domain 3 by using STD NMR experiments. Figure 1(b) indicates that in the absence of the protein no STD signal is observed, as expected for the purely monomeric Aβ sample. However, upon addition of 50 μM of HSA significant STD signal was observed, indicative of interactions between the K_{16}-F_{20} peptide and HSA (Figure 1(c)). Moreover, we mainly observe STD signal buildup for the Phe aromatic side chains indicating these are key domain 3 recognition sites. This is also supported by the F20A and F19A single mutants, which show that single Phe to Ala mutation (*i.e.* F19A, F20A) significantly reduces binding of the K_{16}-F_{20} peptide to HSA (Figure 1(d-e)).

Consistently, no STD signal is observed for the F19AF20A double mutant (Figure 1 (f)), proving that F19 and F20 are the key domain 3 recognition residues. These results are consistent with the notion that aromatic ligands with localized negative charge mainly bind to the Sudlow's site I located in domain 3 of HSA. However, these results don't explain why albumin preferentially binds oligomeric *vs.* monomeric Aβ peptides.

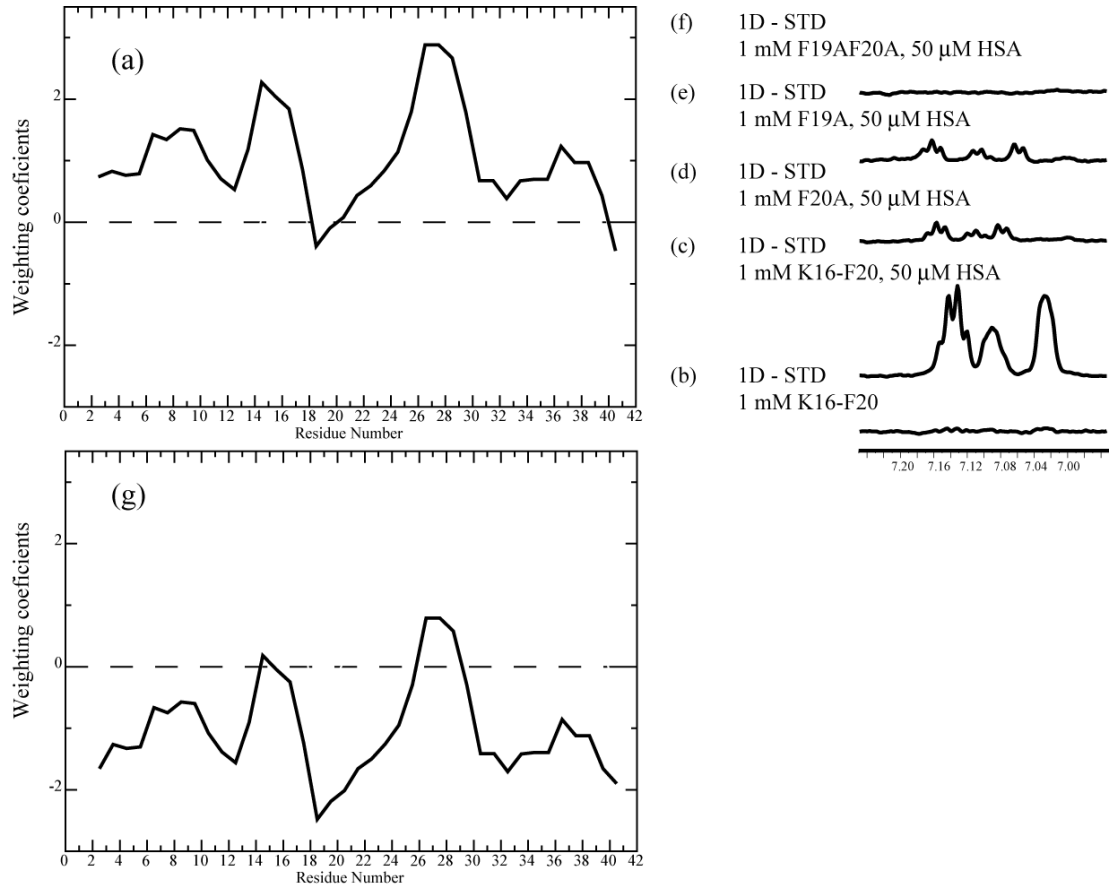

Figure 1. Panel (a) depicts contribution of the Aβ (1-42) structural descriptors (weighting coefficients) for each amino acid (1). Both, backbone amide and side chains, are included in the calculations. Panel (b) depicts STD signal of the 1 mM K16-F20 peptide in the absence of the albumin. Panels (c), (d), (e), and (f) report STD signal of the K16-F20 WT, F20A, F19, and F19AF20A, respectively in the presence of the 50 µM of albumin. All samples were prepared in 20 mM sodium phosphate, 80 mM NaCl, pH 6.5, 105 D_2O and were acquired at 700 MHz at 293K. Panel (g) depicts contribution of the Aβ (1-42) structural descriptors (weighting coefficients) for each amino acid, however in these calculations only side chains were considered (1). For both panels (a) and (g) 4 point average was used to smooth data.

Initially we have proposed several hypotheses as to why albumin selectively interacts with the aggregated Aβ as opposed to monomers. Those include shielding of the CHC residues through intra-molecular interactions within the Aβ monomer and/or significant entropy losses associated with the highly flexible Aβ monomer binding to HSA. In addition, a recent structure of the Aβ protofibrils (2) indicates that the CHC residues at the protofibril axial edges are solvent exposed and available for interaction with potential binders, suggesting that the Aβ oligomer:HSA interactions are hydrophobically driven, *i.e.* they are driven by a large entropy gain associated with the release of the structured water molecules from the exposed Aβ protofibril hydrophobic sites. Furthermore, the chemometric analysis of the Aβ structural descriptors contributing to albumin binding (Figure 1(a and g)) provides an additional plausible insight into the Aβ/HSA interactions. Specifically, the comparison of the Aβ structural descriptors depicted in Figures 1(a) and (g) suggests that the peptide backbone amides negatively contribute to albumin binding. This observation is relevant to the selectivity of albumin towards the Aβ oligomers, because the Aβ peptide backbone is exposed in the monomeric peptide, while in the oligomers, protofibrils and fibrils the backbone amides are involved in inter-Aβ peptide hydrogen bonds and therefore are shielded from albumin minimizing their disruptive effect on the Aβ binding to albumin.

7.2 Refinement of the Aβ Binding Determinants in Albumin Through Competition Binding Experiments Between FAs and Aβ.

Although the albumin:Aβ oligomer binding affinities can be significantly higher than the μM affinities measured for several exogenous ligands that require high binding reversibility, Aβ binding affinities are comparable to those observed for high affinity fatty acid binding sites, which are in the 2-10 nM range (3, 4). Under normal physiological conditions only 0.2-1 mol of fatty acid is bound per HSA and therefore FA interferences in the binding of Aβ oligomers are expected to be negligible. However, under diseased states the FA/HSA ratio can increase up to a value of six (5), making the competition for the Aβ binding site more likely, which could potentially reduce the effectiveness of albumin as an Aβ self-association inhibitor. In addition, the competitive binding of FAs and Aβ provides further insight into the mode of binding of Aβ oligomers.

In order to investigate the possible interferences between FA and Aβ binding, we have preformed NMR STD monitored titrations of Aβ (12-28) using apo albumin and albumin saturated with the one of the most common albumin endogenous ligands, linoleic acid (3). Fatty acid saturation was achieved by dissolving 10 mg of the linoleic acid in 100 μL of 1.5 mM albumin in 25 mM sodium phosphate buffer, pH 7.4, resulting in a final 100:1 ratio of FA to albumin. After 24 hour incubation at room temperature, the HSA sample was centrifuged for 10 min at 7, 000 rpm to remove excess FA and then diluted in water to 10 μM concentration which was used as a titration stock. 1D-WG spectra of the apo albumin and albumin saturated with the linoleic acid were acquired to

confirm successful lipidation as indicated in Figure2. Figure 2 shows some differences in the chemical shifts in the 0-1 ppm region between the FA saturated and FA free HSA, consistent with lipid binding. However as depicted in Figure 3, the STD monitored titration profiles display only a minor increase in K_D values and a minor increase in the final I_{STD}/I_{STR} ratio. This preliminary data suggests FA binding to HSA does not completely abolish Aβ binding.

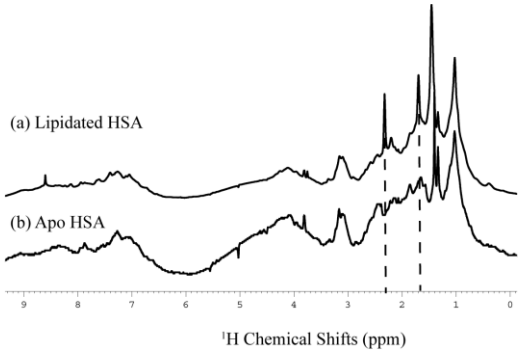

Figure 2. 1D-WG spectra of the apo albumin (panel (a)) and linoleic acid saturated albumin (panel (b)). Spectra were collected at 306K in 90% H_2O, 10% D_2O. Dashed lines indicate linoleic acid signal.

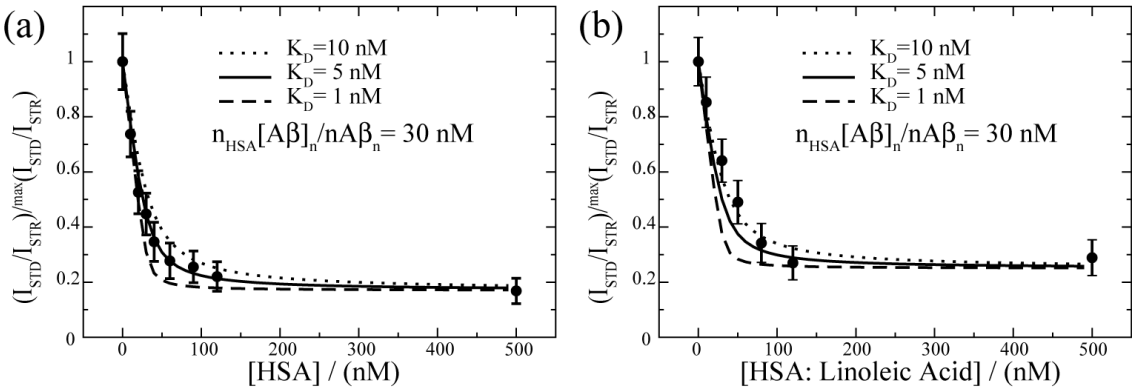

Figure 3. Dose-response STD-based profiles for the inhibition of the Aβ (12-28) self-association by apo albumin (a) and albumin saturated with linoleic acid (b). Dashed and full lines correspond to back-calculated dose-response curves using a Scatchard-like model.

To some extent these data were surprising since we have previously hypothesized that both Aβ oligomers and FA are recognized by the hydrophobic albumin residues. However, it has to be considered that, while the FA carboxylate head is strongly anchored to the HSA through an extensive network of hydrogen bonds, the FA hydrophobic tails maintain a certain degree of flexibility within the hydrophobic sites (4), which undergoes an expansion of 1-2 Å upon FA binding (4)). Moreover it is unlikely that the bulky Aβ oligomers are completely inserted within the HSA cavities that bind FAs and it is possible that bound FAs might to some extent provide further hydrophobic contacts with Aβ in the ternary complex between HSA, Aβ oligomers and FAs. This model also explains how albumin maintains its Aβ amyloid inhibitory properties even during diseased states that increase the FA/HSA molar ratio.

7.3 Correlating the Aβ Binding Determinants of Domain 3 with Domain 3 Dynamics

In order to understand the role of dynamics in the Aβ binding to albumin, the dynamics of domain 3 were investigated by ^{15}N relaxation NMR experiments and summarized as shown in Figure 4. The ps-ns and μs-ms backbone dynamics of domain 3 were characterized through the measurement of the ^{15}N R_1 and R_2 relaxation rates and of the HNNOE data shown in Figure 4. Panels (a) and (e) of Figure 4 point to protein truncation causing unfolding of helix 1 and fast ps-ns time scale dynamics at the N-terminus of domain 3 (Figure 4(a) and (c)). In addition, panels (c) and (e) indicate that the truncation of the protein at the N-terminus does not affect only helix 1, but it also

significantly affects helix 4 in 3A sub-domain, which is located at the domain 1: domain 3 interface in the full length HSA. However unlike helix 1, helix 4 mainly experiences an increase in the ms–μs time scale dynamics, which are usually associated with larger "breathing motions" of the protein. Moreover, helix 1 was only partially assigned possibly due to the fast exchange with water or line broadening caused by conformational exchange in intermediate time-scales. Overall, extensive μs-ms motions in sub-domain 3A as opposed to sub-domain 3B suggest the exposure of 3A sub-domain hydrophobic cavity to the solvent upon isolation of domain 3 from the other domains of HSA. Unlike the slower μs-ms motions, fast time scale (ps –ns) dynamics are present in loops connecting helices and are especially evident in the 3B loop, a protein region involved in Aβ binding based on our studies of Chapter 6. This observation suggests that flexibility might be a requirement for Aβ oligomer binding regions. Moreover since albumin selectively recognizes exposed hydrophobic residues of the Aβ, we propose dynamics of hydrophobic residues are of particular importance in understanding of Aβ binding to HSA.

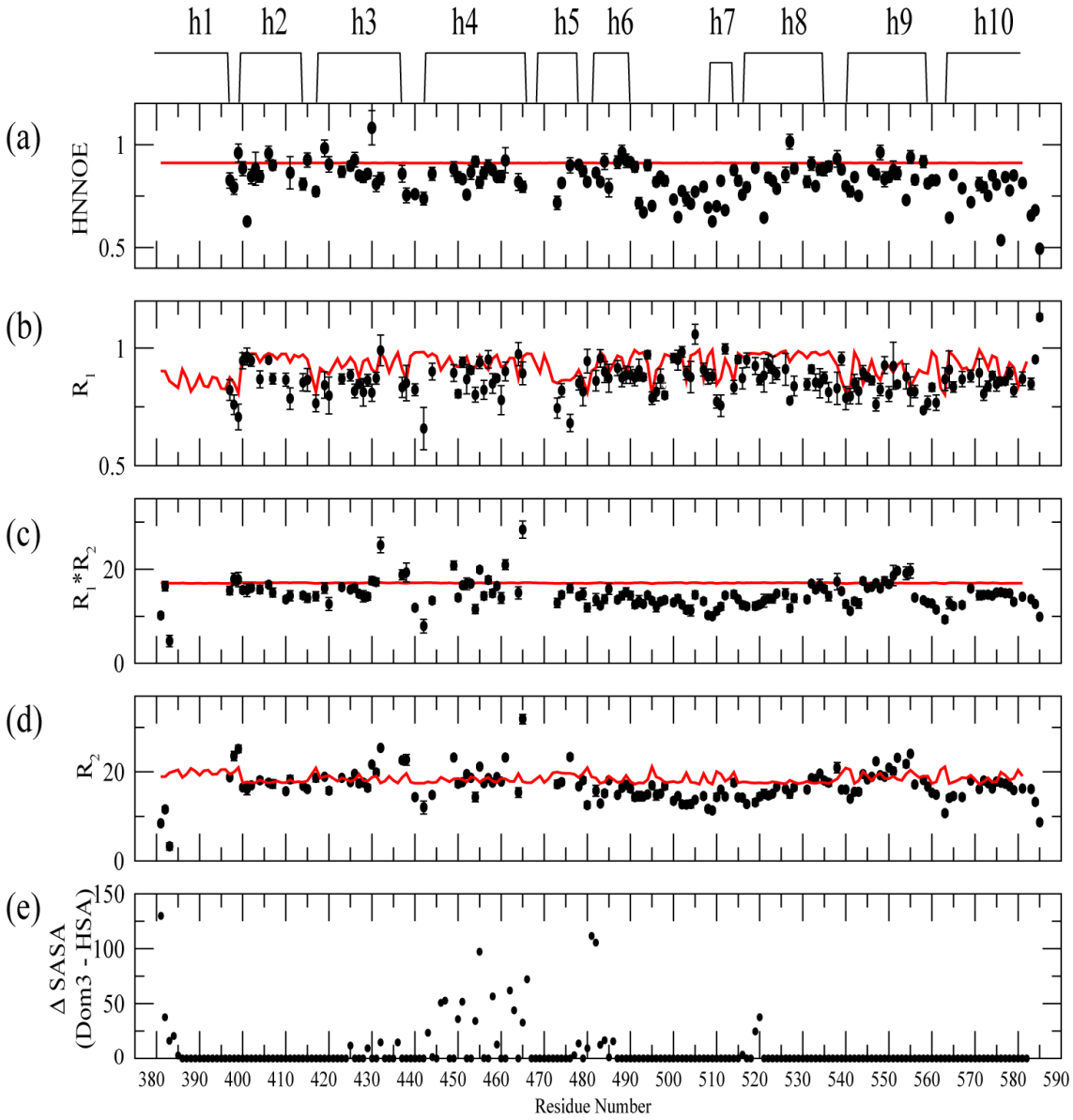

Figure 4. Plot of backbone ^{15}N relaxation rates of HSA domain 3 *vs.* residue number. All data were measured at a field of 700 MHz at 306 K and in 20 mM sodium phosphate, 80 mM NaCl, pH 6.5, 0.05% NaN3, 10% D_2O.The *red lines* in *a–d* denote rates computed based on hydrodynamic bead model (HYDRONMR) (6) of domain 3 with an atomic element radius of 3.3 Å. Panel *a* reports $^{15}N\{^1H\}$NOE computed as I_{sat}/I_{nonsat}, panel (b) reports the spin-lattice relaxation rates (R_1); (c) reports the R_1R_2 product, which minimizes the effects of motional anisotropy, (d) the spin-spin relaxation rates (R_2)corrected for the R_1 contribution (8). Panel (e) reports the difference in the solvent accessible surface area (SASA) (7) between the full length HSA and domain 3.

7.4 Development of a Methodology to Identify Aβ Binding Sequences in Aβ Self-Association Inhibitory Proteins.

Using human serum albumin domain 3 as a model system we have investigated the determinants for Aβ binding for the purpose of indentifying Aβ contact sites in other Aβ amyloid inhibitory proteins. We propose that Aβ self-association inhibitory proteins require several features to bind Aβ. Those include the presence of unstructured protein regions prone to amyloid formation with hydrophobic character and possibly with complementarity to the CHC region of the Aβ. Based on the ^{15}N-^{1}H HSQC chemical shifts and the above requirements, we have identified a potent Aβ self-association inhibitory sequence within the 3B sub-domain. Therefore we hypothesize that a similar approach can be applied not only to the other HSA domains, but also to other Aβ inhibitory proteins. The difficulty of testing this hypothesis lies in the limited number of proteins that bind Aβ and for which the structure and/or the Aβ binding sequences are available. Among the Aβ binding proteins reviewed in Chapter 1, the ABAD and the affibody $Z_{Aβ3}$ systems meet this criterion and will be used here as models to provide an initial test of our hypothesis on the identification of Aβ inhibitory peptides.

The WALTZ analysis of ABAD sequence indicates a large number of amyloid prone regions and possibly the presence of several Aβ binding sites (Figure 5 (a)). To further narrow down the location of the Aβ binding sites, only solvent accessible regions were considered (Figure 5(b)). This resulted in the identification of the two regions spanning residues, 92-120 and 210-230, respectively. According to our hypothesis only

unstructured protein regions or regions with isolated β-strands (*i.e.* not part of a β-sheet) (Figure 5(c)) are involved in Aβ binding and were considered here. Using this sequential approach the correct Aβ binding sequence (92-120) within the ABAD was identified.

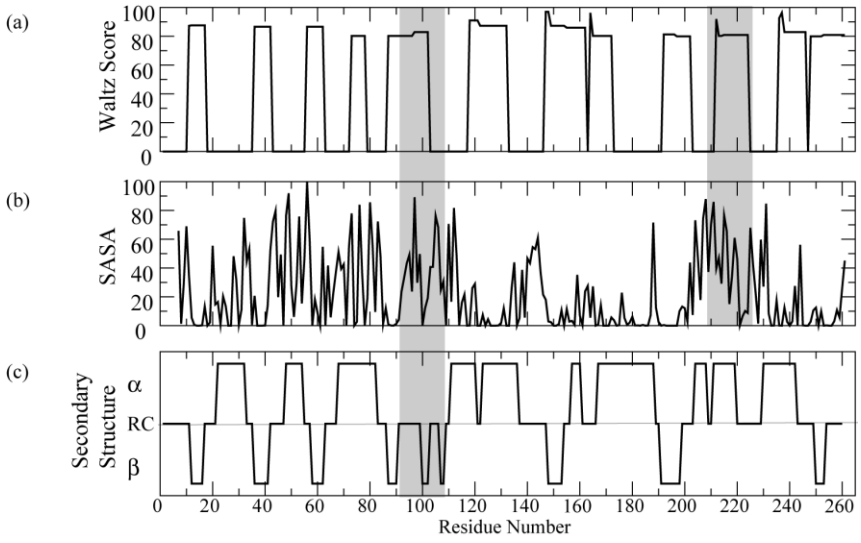

Figure 5. Proposed scheme to identify the Aβ binding sequence within the Aβ inhibitory proteins. Panel (a) depicts WALTZ scores, which predict amyloid propensity. Panel (b) reports the solvent exposed surface area (7). Panel (c) depicts the ABAD secondary structure elements. Since the structure of apo ABAD is not available, for all panels the structure of the ABAD bound to the NAD(+) and an inhibitory compound (pdb: 1U7T) was used (9).

We have also proposed that the Aβ binding sequences should exhibit complementarity to the Aβ CHC. This hypothesis was inspired by the work of Sato et al., who showed that CHC pentapeptide analogues can effectively inhibit fibril formation (10, 11). However, in the case of ABAD the sequence that aligns with the Aβ CHC, *i.e.* 210-232 (Figure 6 (b)), does not interact with the Aβ, suggesting that secondary structure preferences are more important for Aβ binding than Aβ complementarity.

(a)

```
KLVFF              ----------KL------VF--F------
ABAD (92-120)      AGIAVASKTYNLKKGQTHTLEDFQRVLDV
                             :*      .:  *
```

(b)

```
KLVFF                    --KLV-FF--------------
ABAD (210-232)           PEKVRNFLASQVPFPSKLGDPA
                           *:  *:
```

Figure 6. Sequence alignment of the Aβ CHC pentapeptide inhibitory sequence (11) and the Aβ binding sites within ABAD, proposed based on the combination of the WALTZ and SASA analysis.

A similar approach was used to confirm the correct identification of the Aβ binding sequence within the affibody $Z_{Aβ3}$. The apo $Z_{Aβ3}$ structure was not available and therefore for the analysis the Aβ bound $Z_{Aβ3}$ structure (pdb: 2OTK) (12) was used.

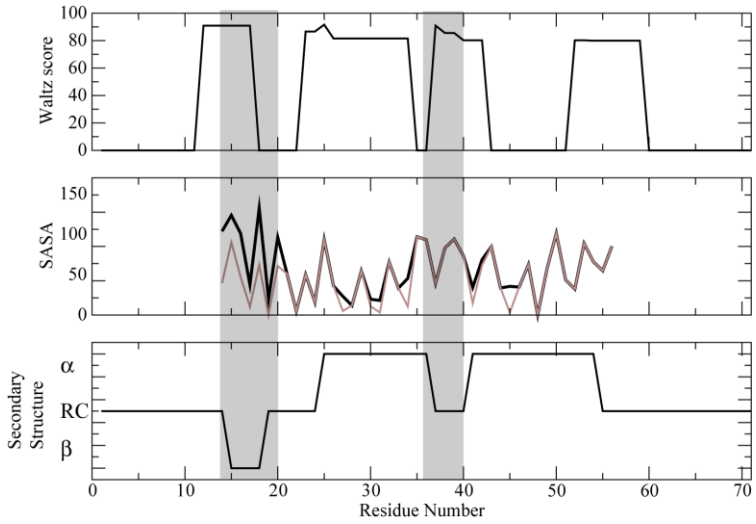

Figure 7. Panel (a) depicts WALTZ scores, which predict amyloid propensity of selected regions. Panel (b) reports the solvent exposed surface area of the $Z_{Aβ3}$ bound to Aβ (brown line), and $Z_{Aβ3}$ from which Aβ has been removed (black line) (7). Panel (c) depicts the $Z_{Aβ3}$ secondary structure elements. Since the structure of apo $Z_{Aβ3}$ is not available, for all panels the structure of the $Z_{Aβ3}$ bound to Aβ (pdb: 2OTK) was used (12).

The combination of the WALTZ, SASA and secondary structure elements identified two possible regions for the interaction, (14-20) and (35-40), respectively

(Figure 7). However the residues 35-40 (*i.e.* DDPAQS) are not significantly involved in Aβ binding. This could be explained by the absence of the hydrophobic residues needed for the recognition of the hydrophobic Aβ growing sites. These observations seem therefore to suggest that only when all four requirements are satisfied (*i.e.* amyloid propensity, exposure to the solvent, no secondary structure or isolated β-strand, hydrophobicity) the proposed sequence is effective in Aβ binding.

7.5 Albumin is a general peptide self-association inhibitor.

We propose albumin is not only involved in the clearance of Aβ, but might be involved in interactions with other amyloidogenic peptides as well. To test this hypothesis, the ability of albumin to inhibit the self association of other amyloidogenic peptides, such as the transthyretin (Ttr) fragment (105-115), with the YTIAALLSPYS sequence, and the human amylin fragment hIAPP (20-29), with the SNNFGAILSS sequence, should be tested (13,14). Preliminary results suggest that albumin inhibits aggregation of Ttr (105-115) (Figure 8 and Figure 9) and support the proposed hypothesis of albumin being a general self-association inhibitor. hIAPP did not aggregate at pH 4.7, and currently we are investigating conditions that promote aggregation of both peptides.

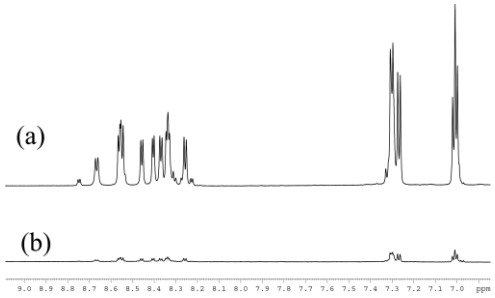

Figure 8. ^{1}H 1D-NMR spectra of 1 mM Ttr (105-115) in 50 mM acetic acid –d4, pH 4.7 acquired at 293K at 700MHz. Panel (a) report spectrum of the Ttr sample immediately after sample was prepared while panel (b) reports Ttr sample after 2 weeks of incubation at RT. In both spectra an identical number of scans was acquired.

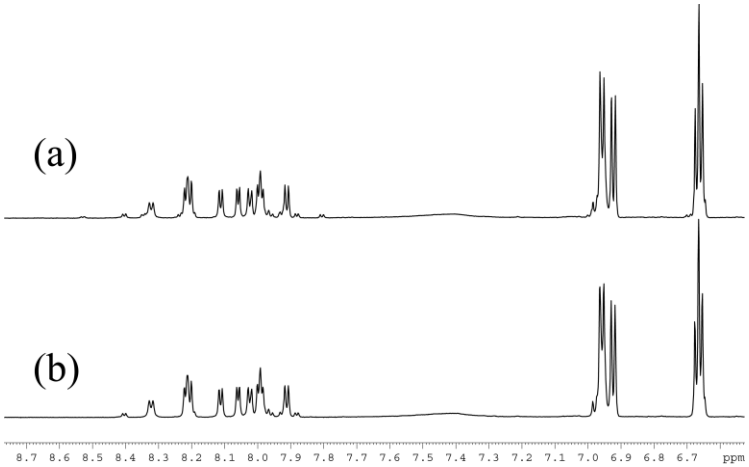

Figure 9. ^{1}H 1D-NMR spectra of 1 mM Ttr (105-115) in the presence of 100 μM HSA. Samples were prepared in 50 mM acetic acid –d4, pH 4.7. Spectra were acquired at 293K at 700MHz. Panel (a) report spectrum of the Ttr in the presence of 100 μM of HSA immediately after sample was prepared while panel (b) reports identical sample 2 week after incubation at RT. In both spectra identical number of scans was used. No change in the signal intensity with time was observed in the presence of albumin.

REFERENCES:

1. Hajduk, P. J., R. Mendoza, A.M. Petros, J.R. Huth, M. Bures, S.W. Fesik and Y.C. Martin 2003. Ligand binding to domain-3 of human serum albumin: A chemometric analysis. J. Comput. Aided Mol. Des. 17, 93-102.

2. Luhrs, T., C. Ritter, M. Adrian, D. Riek-Loher, B. Bohrmann, H. Doeli, D. Schubert and R. Riek 2005. 3D structure of alzheimer's amyloid-beta(1-42) fibrils. Proc. Natl. Acad. Sci. U. S. A. 102, 17342-17347.

3. Petitpas, I., T. Grune, A.A. Bhattacharya and S. Curry 2001. Crystal structures of human serum albumin complexed with monounsaturated and polyunsaturated fatty acids. J. Mol. Biol. 314, 955-960.

4. Curry, S., H. Mandelkow, P. Brick and N. Franks 1998. Crystal structure of human serum albumin complexed with fatty acid reveals an asymmetric distribution of binding sites. Nat. Struct. Biol. 5, 827-835.

5. Simard, J. R., P.A. Zunszain, C.E. Ha, J.S. Yang, N.V. Bhagavan, I. Petitpas, S. Curry and J.A. Hamilton 2005. Locating high-affinity fatty acid-binding sites on albumin by x-ray crystallography and NMR spectroscopy. Proc. Natl. Acad. Sci. U. S. A. 102, 17958-17963.

6. de la Torre, J. G., M.L. Huertas and B. Carrasco 2000. HYDRONMR: Prediction of NMR relaxation of globular proteins from atomic-level structures and hydrodynamic calculations. Journal of Magnetic Resonance. 147, 138-146.

7. Fraczkiewicz, R. and Braun, W. (1998) "Exact and Efficient Analytical Calculation of the Accessible Surface Areas and Their Gradients for Macromolecules" *J. Comp. Chem.*, **19**, 319-333.

8. Yip, G. N. B. and E.R.P. Zuiderweg 2004. A phase cycle scheme that significantly suppresses offset-dependent artifacts in the R-2-CPMG N-15 relaxation experiment. Journal of Magnetic Resonance. 171, 25-36.

9. Lustbader, J. W., M. Cirilli, C. Lin, H.W. Xu, K. Takuma, N. Wang, C. Caspersen, X. Chen, S. Pollak, M. Chaney, F. Trinchese, S.M. Liu, F. Gunn-Moore, L.F. Lue, D.G. Walker, P. Kuppusamy, Z.L. Zewier, O. Arancio, D. Stern, S.S.D. Yan and H. Wu 2004. ABAD directly links A beta to mitochondrial toxicity in alzheimer's disease. Science. 304, 448-452.

10. Sato, T., P. Kienlen-Campard, M. Ahmed, W. Liu, H.L. Li, J.I. Elliott, S. Aimoto, S.N. Constantinescu, J.N. Octave and S.O. Smith 2006. Inhibitors of amyloid toxicity based on beta-sheet packing of A beta 40 and A beta 42. Biochemistry (N. Y.). 45, 5503-5516.

11. Tjernberg, L. O., J. Naslund, F. Lindqvist, J. Johansson, A.R. Karlstrom, J. Thyberg, L. Terenius and C. Nordstedt 1996. Arrest of beta-amyloid fibril formation by a pentapeptide ligand. J. Biol. Chem. 271, 8545-8548.

12. Hoyer, W., C. Gronwall, A. Jonsson, S. Stahl and T. Hard 2008. Stabilization of a beta-hairpin in monomeric alzheimer's amyloid-beta peptide inhibits amyloid formation. Proc. Natl. Acad. Sci. U. S. A. 105, 5099-5104.

13. Liang, Y., S.Z. Jasbi, S. Haftchenary, S. Morin and D.J. Wilson 2009. Binding interactions in early- and late-stage amyloid aggregates of TTR(105-115). Biophys. Chem. 144, 1-8.

14. Nielsen, J. T., M. Bjerring, M.D. Jeppesen, R.O. Pedersen, J.M. Pedersen, K.L. Hein, T. Vosegaard, T. Skrydstrup, D.E. Otzen and N.C. Nielsen 2009. Unique identification of supramolecular structures in amyloid fibrils by solid-state NMR spectroscopy. Angewandte Chemie-International Edition. 48, 2118-2121.